Analysis and Optimization of a Dual-Load Vapor Compression Cycle Using Non-Azeotropic Refrigerant Mixtures

M. K. Smith and T. A. Newell

ACRC CR-3 November 1993

For additional information:

Air Conditioning and Refrigeration Center
University of Illinois
Mechanical & Industrial Engineering Dept.
1206 West Green Street
Urbana, IL 61801

(217) 333-3115

The Air Conditioning and Refrigeration Center was founded in 1988 with a grant from the estate of Richard W. Kritzer, the founder of Peerless of America Inc. A State of Illinois Technology Challenge Grant helped build the laboratory facilities. The ACRC receives continuing support from the Richard W. Kritzer Endowment and the National Science Foundation. The following organizations have also become sponsors of the Center.

Acustar Division of Chrysler
Allied-Signal, Inc.
Amana Refrigeration, Inc.
Carrier Corporation
Caterpillar, Inc.
E. I. du Pont de Nemours & Co.
Electric Power Research Institute
Ford Motor Company
General Electric Company
Harrison Division of GM
ICI Americas, Inc.
Johnson Controls, Inc.
Modine Manufacturing Co.
Peerless of America, Inc.
Environmental Protection Agency
U. S. Army CERL
Whirlpool Corporation

For additional information:

Air Conditioning & Refrigeration Center
Mechanical & Industrial Engineering Dept.
University of Illinois
1206 West Green Street
Urbana IL 61801

217 333 3115

ANALYSIS AND OPTIMIZATION OF A DUAL-LOAD VAPOR COMPRESSION CYCLE USING NON-AZEOTROPIC REFRIGERANT MIXTURES

Mark Kennedy Smith, Ph.D.
Department of Mechanical Engineering
University of Illinois at Urbana-Champaign, 1994
Ty A. Newell, Advisor

Some Non-Azeotropic Refrigerant Mixtures (NARMs) have been identified as potential replacements for R12 because of their low ozone depletion potential, low global warming potential and promising thermodynamic characteristics which could improve cycle efficiency. A NARM experiences a variable temperature glide during a constant-pressure phase change process, making it a logical candidate for the two-temperature level cooling found in refrigerators. There are two fundamental thermodynamic benefits to using a NARM over a pure refrigerant: 1) mixture and air-temperature glides can be better matched to improve the system performance, and 2) lower refrigerant temperatures can be achieved through the use of intercooling with no decrease in evaporating pressure. The objective of this research was to investigate optimal pure refrigerant (R12 and R134a) and NARM (65% R22/35% R123 and 80% R22/20% R141b) refrigerator system configurations that minimized life-cycle cost.

A two-evaporator flow loop was constructed to help develop an evaporator heat transfer model and take NARM heat transfer data. For the mass flux range of 25-45 kg/m^2-s, the mixture heat transfer coefficients were on the order of 50% less than those of R12. For higher mass fluxes, the mixture coefficients rose rapidly, and approached the R12 values.

A steady-state optimization model was used to minimize the life-cycle cost of each system configuration studied. The optimized system configuration with the lowest life-cycle cost was a R22/R123 system with both high and low-temperature intercoolers. This system used 5.7% less energy, 23% more evaporator area, and its life-cycle cost was 2.1% less than that of an optimized R134a single-evaporator system. Furthermore, this system used 10.5% less energy, 46% more evaporator area, and its life-cycle cost was 4.5% less than that of a modeled R12 base-case system. The optimized R22/R123 systems performed better than the equivalent R22/R141b systems. The high-temperature intercooler mixture systems performed as well as the two intercooler systems. Mixture heat transfer coefficient enhancement had a limited impact on life-cycle cost.

TABLE OF CONTENTS

NOMENCLATURE

English:

A	area (m^2)
C	Celsius or heat capacity (W/K)
c_p	constant-pressure specific heat (J/g-K)
c_v	constant volume specific heat (J/g-K)
D	tube inside diameter (m) or (mm)
g	gram or acceleration of gravity (m/s^2)
G	mass flux (kg/m^2-s)
h	enthalpy (kJ/kg)
h_{lg}	latent heat of vaporization (kJ/kg)
k	thermal conductivity (W/m-K)
len	length (m)
m	mass (kg) or (g)
$\dot{m}$	mass-flow rate (g/s) or (g/min) or (kg/s)
mdot	mass-flow rate (g/s) or (g/min) or (kg/s)
mol	also mole - defined as 6.022×10^{23} atoms
MW	molecular weight (g/mol)
p	pressure (kPa)
P	perimeter (m)
q	heat load (W)
q"	heat flux (kW/m^2)
Q	volumetric flow rate (ml/min) or (m^3/s)
R	gas constant = 8.314 (kJ/kmol-K)
R_a	air-side resistance (K/W)
R_r	refrigerant-side resistance (K/W)

T	temperature (K or °C)
temp.	temperature (K or °C)
U	overall heat transfer coefficient (W/m^2-K)
v	velocity (m/s)
w	weight fraction or specific work (J/g)
W	work energy (W)
x	mass-flow fraction or quality
X	mass concentration of component A
XM	mole composition fraction
z	length in axial direction (m)

Greek:

α	heat transfer coefficient (W/m^2-K)
ε	effectiveness
η	efficiency
μ	viscosity (g/m-s or kg/m-s)
ν	specific volume (m^3/g) or (m^3/kg)
ρ	density (g/m^3 or kg/m^3)
σ	surface tension (dynes/cm) or standard deviation
υ	kinematic viscosity (m^2/s)

Subscripts:

a	air
act	actual
amb	ambient
bs	bubble suppression
c	critical or cold or chiller
cb	convective boiling

cond	condenser
cros	cross sectional
cur	current
D	based on diameter
duct	ducting
evap	evaporator
f	freezer
ff	fresh-food
g	gas
h	hydraulic or hot
hp	high pressure
i	increment or section
id	ideal
in	inlet
l	liquid
lg	liquid-gas
lo	liquid only
lp	low pressure
m	mean
max	maximum
min	minimum
mul	mullion
NARM	Non-Azeotropic Refrigerant Mixture
nb	nucleate boiling
nbp	normal boiling point
o	initial

opt	optimum
out	outlet
ov	overall
p	pump
r	reduced or refrigerant
s	isentropic
sat	saturation
std	standard
sum	summation
tot	total
tpl	two-phase liquid
v	vapor
vt	liquid laminar - vapor turbulent
w	with
w/o	without

Other:

$	cost in dollars
$\bar{x}$	average value of variable x
Δx	change in variable x
dx	differential of variable x
%Dev	percentage deviation
1E	single-evaporator system
2E	dual-evaporator system
ACRC	Air Conditioning and Refrigeration Center
AHAM	Association of Home Appliance Manufacturers

ASHRAE	American Society of Heating, Refrigerating and Air Conditioning Engineers
ASME	American Society of Mechanical Engineers
BC	base-case system
cfanf	cost of the freezer evaporator fan ($)
cfanff	cost of the fresh-food evaporator fan ($)
CFC	chlorofluorocarbon
CFM	cubic feet per minute (ft^3/min)
coeff.	coefficient
cof	cost to manufacture freezer evaporator ($)
coff	cost to manufacture fresh-food evaporator ($)
cohi	cost to manufacture high-temp. intercooler ($)
coli	cost to manufacture low-temp. intercooler ($)
comp.	compressor
conc.	concentration
cond.	condenser
cons.	consumer
COP	coefficient of performance
CSD	Carnahan-Starling-DeSantis
dc	duty-cycle
dev.	device
diff.	difference
DOE	Department of Energy
EES	Engineering Equation Solver
ene$	energy consumption cost relative to the base-case system ($)
EOS	equation of state

exp.	expansion
ft	foot
fn	function
gal	gallon
GWP	global warming potential
HEF	high-efficiency fan
HI	high-temperature intercooler
hp	horse power
hr	hour or hours/year (hr/yr)
HTC	heat transfer coefficient
HTE	high-temperature evaporator
HTIC	high-temperature intercooler
hxer	heat exchanger
H_2O	water
IC	intercooler
IMSL	Mathematical and Statistical Library
in.	inch
IP	interaction parameter
irrev.	irreversibility
K	Kelvin
kg	kilogram
L	liter
lbs.	pounds
LCC	life-cycle cost
lhi	load on the high-temperature intercooler (W)
LI	low-temperature intercooler

lli	load on the low-temperature intercooler (W)
LMTD	log mean-temperature difference
LTE	low-temperature evaporator
LTIC	low-temperature intercooler
mA	milli-ampere
man$	manufacturing cost relative to the base-case system ($)
min	minute
mu	markup factor
mul	mullion
NARB	Non-Azeotropic Refrigerant Blends
NARM	Non-Azeotropic Refrigerant Mixture
NBP	normal boiling point
NBS	National Bureau of Standards
NIST	National Institute of Standards and Technology
NTU	number of transfer units
obj.	objective
ODP	ozone depletion potential
ORNL	Oak Ridge National Laboratory
OV	occupied volume
ovf	occupied volume of freezer evaporator (m^3)
ovff	occupied volume of fresh-food evaporator (m^3)
ovhi	occupied volume of high-temp. intercooler (m^3)
ovli	occupied volume of low-temp. intercooler (m^3)
pa	present worth factor
pass#	number of tube passes
pc	compressor power (W)

pcd	power of condenser fan (W)
pf	freezer fan power (W)
pff	fresh-food fan power (W)
PID	proportional-integral-derivative
pow.	power
psi	pounds per square inch
psia	pounds per square inch absolute
psig	pounds per square inch gauge
RC	resistor-capacitor
RPM	revolutions per minute
Re	Reynolds number
R_{sp}	intercooler spiral ratio
R12	dichlorodifluoromethane, CCl_2F_2
R22	chlorodifluoromethane, $CHClF_2$
R123	dichlorotrifluoroethane, $CHCl_2CF_3$
R141b	fluorodichloroethane, CH_3CCl_2F
s	second
sfin	distance between each fin (m)
sh	superheat
SH	superheat
SH8	superheat at state point 8
SLH	suction-line heat exchanger
SPM	sequential perturbation method
tot.	total
UIUC	University of Illinois at Urbana-Champaign
uncert.	uncertainty

up	power cost ($/kW-hr)
USEPA	United States Environmental Protection Agency
uv	cost/volume ($/m^3)
velf	velocity of air over freezer evaporator (m/s)
velff	velocity of air over fresh-food evaporator (m/s)
yr	year

Dimensionless Numbers:

Bo	Boiling number $Bo = \frac{q''}{Gh_{lg}}$
Co	Convection number $Co = \left(\frac{1-x}{x}\right)^{0.8}\left(\frac{\rho_g}{\rho_l}\right)^{0.5}$
ε	heat exchanger effectiveness $\varepsilon = q/q_{max}$
Fr	Froude number of liquid $Fr_l = \frac{G^2}{\rho_l^2 gD}$
NTU	Number of Transfer Units $NTU = \frac{UA}{C_{min}}$
Pr_l	Prandtl number of liquid $Pr_l = \frac{c_{p_l}\mu_l}{k_l}$
Re_l	Reynolds number of liquid $Re_l = \frac{GD(1-x)}{\mu_l}$
Re_{lo}	Reynolds number of liquid only $Re_{lo} = \frac{GD}{\mu_l}$
X_{vt}	Martinelli parameter for laminar liquid flow and turbulent gas flow $X_{vt} = \left[\frac{(dp/dz)_l}{(dp/dz)_g}\right]^{1/2}$

CHAPTER 1: INTRODUCTION

This project was undertaken as part of a coordinated research effort headed by the United States Environmental Protection Agency. The goal of the program was to explore alternative refrigerants and refrigeration cycles in an attempt to replace dichlorodifluoromethane (CCl_2F_2, R12) in domestic refrigerators. The first part of this chapter addresses the need to replace R12 and describes potential substitutes. The balance of the chapter focuses on the specific objectives of this research and describes the content and format of the subsequent chapters.

1.1 Why Replace R12?

When R12 is released into the atmosphere, it causes destruction of the ozone layer and contributes to the greenhouse effect. In September 1987, the Montreal Protocol was signed by 24 countries and the European Community to phase out ozone-depleting, global-warming refrigerants and to identify alternate substances.[1] The Protocol indirectly requires improved energy efficiency for alternative refrigerant systems. Poor system performance causes secondary greenhouse effects. Additional combustion of fossil fuel is required to compensate for decreased energy efficiency which releases more carbon dioxide into the atmosphere. The alternate refrigerant system performance therefore must equal or exceed that of current systems. In November 1989, the United States Government announced not only the phase-out of R12, but also stricter energy standards for domestic refrigerators.[2]

Due to alarming new reports, environmental concern over the use of chlorofluorocarbons has greatly increased. In October 1991, the National Aeronautics and Space Administration reported that the erosion of the ozone layer over Antarctica had reached record levels.[3] The erosion now extends over the southern portions of South America, exposing people and crops in the more moderate climates to the harmful effect of increased ultra-violet radiation. Fortunately, in August 1993, the National Oceanic and Atmospheric Administration reported that the emissions of R11 and R12 have slowed sooner than researchers had expected, and the gradual repair of Earth's battered ozone layer could begin by the year 2000.[4] Researchers said that it will still be a century before the ozone layer returns to normal. It was further reported that the emissions of R11 and R12 slowed to a growth rate of about 1% per year, down from a peak of 5% per year in the 1980s.

1.2 Potential Replacements for R12

Some Non-Azeotropic Refrigerant Mixtures (NARMs) have been identified as potential replacements for R12 because of their low ozone depletion potential (ODP), low global warming

potential (GWP) and promising thermodynamic characteristics which could improve cycle efficiency. A NARM experiences a variable temperature *glide* during a constant-pressure phase change process, making it a logical candidate for the two-temperature level cooling found in refrigerators. A better match between the refrigerant temperatures and circulating air temperatures is possible, theoretically allowing substantial improvement in system performance. In selecting NARMs, the hope is that the improved thermodynamic performance will allow for more flexibility in selecting environmentally safe components, while still being able to meet new energy efficiency standards.

1.3 Objective of Research

The major objective of this research was to investigate a NARM refrigerator evaporator module for a specific mixture combination and range of operating conditions that minimize the life-cycle cost of the system. Both government and industry must know if these mixtures are capable of being economically competitive with azeotropes and pure refrigerants for the same applications. Chapters 6 and 7 cover the optimization study and attempt to answer this question.

Two NARM pairs were investigated for this study, 65% R22/35% R123 and 80% R22/20% R141b. Both of these NARMs have a temperature glide of approximately 30°C at typical refrigerator operating conditions in keeping with the recommendations of Lorenz and Meutzner[5] for two-temperature level cooling (domestic refrigerator) applications. These mixtures are *representative* of the NARMs that could be used in domestic refrigerators. Since the selection of these fluids in 1989, the phase out of R22 has been agreed upon; therefore, the results of this study cannot *directly* apply to NARMs under consideration currently. However, the performance and economic *trends* from this study could be extended to include these newer mixtures.

A NARM vapor compression system is shown in Figure 1.1. The major components of the module are high and low-temperature evaporators (HTE and LTE), high and low-temperature intercoolers (HTIC and LTIC) and an expansion valve. The NARM evaporator module is enclosed within the dotted lines. The life-cycle cost optimization sizes the four module exchangers, determines the optimal evaporator air-flow rates, and determines the optimal superheat level required to meet a given load distribution.

Another objective of this research was to investigate the basic thermodynamics of the NARM vapor compression cycle. Understanding the thermodynamic advantages of using mixtures, and under what conditions they provide significant thermodynamic gains, is

fundamental to this study. These concepts are covered in Chapter 2. The magnitude of the heat source glide influences the performance of a mixture system versus the performance of a pure-refrigerant system. Intercooling can significantly enhance the performance of a NARM system. The relative thermodynamic merits of using a pure-refrigerant system versus a NARM system will also be covered in Chapter 2.

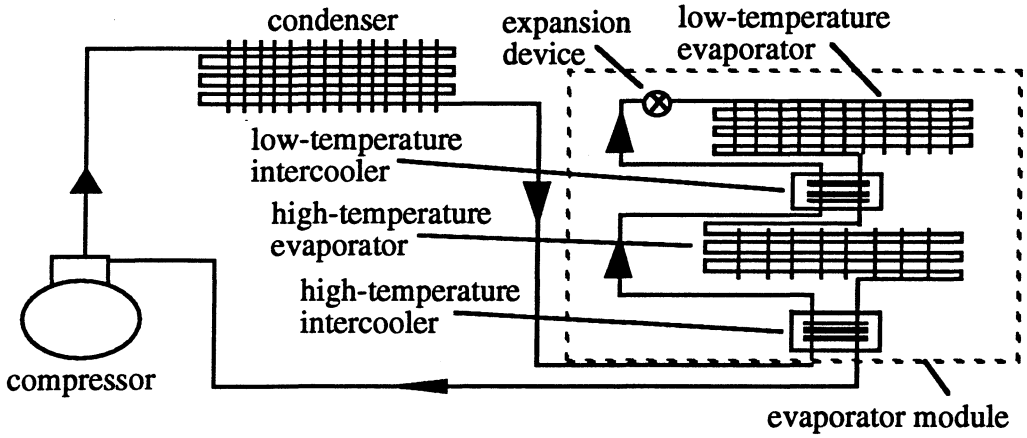

Figure 1.1: NARM vapor compression refrigeration system

To accomplish the primary objective of this research, a heat transfer correlation for mixtures in the stratified/wavy regime had to be developed. This is the focus of Chapter 5. In the literature there are a limited number of mixture correlations, but none exclusively covering the low-mass flux and heat flux range found in domestic refrigerators. In order to develop the mixture correlations, heat transfer data needed to gathered. It was decided that the data was to be gathered from the evaporator module since no horizontal tube facility was available at the time. Performing an energy balance on each evaporator allowed refrigerant-side resistance to be calculated as a function of flow conditions and loading for two different quality levels. On the basis of this information, a refrigerant heat transfer coefficient was calculated for each exchanger. In the future, when horizontal tube data becomes available, the magnitude of the two sets of data can be compared to assess the relative effect of the evaporator tube bends and the non-uniformity of the applied heat flux from the evaporator air flow.

Before the mixture tests were run, the heat transfer characteristics of the two evaporators in the evaporator module had to be determined from energy balance information taken from the system charged with R12. Chapter 4 covers the calculation of the air-side heat transfer coefficient as a function of air velocity for each evaporator. A refrigerant correlation had to be selected to permit the calculation of the air-side heat transfer coefficient. Fortunately, Wattelet *et*

al. were developing an R12 correlation for the stratified/wavy flow regime from horizontal tube measurements as reported by Smith *et al.*[6]

For the optimization work, a fan model was developed and cost relationships were established for the required components. The development of the optimization model is presented in Chapter 6. Using the correlation described in Chapter 5 and the air-side information from Chapter 4, a complete evaporator module optimization was developed. The life-cycle cost results for various run conditions are presented in Chapter 7.

This work will answer many of the questions, fully or in part, surrounding the use of mixtures for a refrigerator application. Hopefully, many more useful questions will be raised in the future as a result of this work.

1.4 References

---

[1] United Nations Environmental Programme, "Montreal Protocol on substances that deplete the Ozone Layer. Final Act.", 1987, New York : United Nations.

[2] *Federal Register*, Friday November 17, 1989, Part III, Department of Energy, Office of Conservation and Renewable Energy, 10 CFR Part 430, "Energy Conservation Program for Consumer Products: Energy Conservation Standards for Two Types of Consumer Products", Vol. 54, No. 221.

[3] "Ozone Loss Hits Us Where We Live", *News & Comment*, November 1, 1991, p. 645.

[4] "Ozone-destroying Chemicals' Buildup Slowing, Study Shows", *Champaign-Urbana News Gazette,* August, 26, 1993.

[5] Lorenz, A. and K. Meutzner, "On Application of Non-Azeotropic Two-Component Refrigerants in Domestic Refrigerators and Home Freezers", XIV International Congress of Refrigeration, Paper B2.42, 1975 Moscow.

[6] Smith, M. K., J. P. Wattelet and T. A. Newell, "A study of evaporation heat transfer coefficient correlations at low heat and mass fluxes for pure refrigerants and refrigerant mixtures", *Heat Transfer with Alternate Refrigerants*, ASME HTD-Vol. 243, August, 1993, pp. 19-26.

CHAPTER 2: BACKGROUND

This chapter is broken down into three sections. The first section will cover the basic thermodynamics of NARMs and the NARM vapor compression cycle. The second section will explain the origin of the thermodynamic gains for the NARM cycle. The last section will examine the mixture literature and cover applicable correlations and system performance results. This chapter provides crucial background information for the rest of this study.

2.1 Basic Thermodynamics and the NARM Vapor Compression Cycle

2.1.1 An Azeotrope versus a Non-Azeotrope (Zeotrope)

Nearly all refrigerants in use today are pure fluids, such as R12, or *azeotropic mixtures* of pure refrigerants, such as R502, which is an azeotropic mixture of 48.8% R22 and 51.2% R115. Azeotropic mixtures and pure refrigerants are characterized by constant fluid temperature during constant-pressure phase change. Some refrigerants, however, are non-azeotropic refrigerant mixtures (NARMs) or *zeotropic mixtures*. A zeotrope, which is a specific blend or mixture of two or more refrigerants of differing boiling points, is characterized by a temperature glide during constant-pressure phase change.

An arbitrary, temperature versus concentration, binary-phase diagram with a maximum boiling-point azeotrope is shown in Figure 2.1. This diagram shows the difference between a zeotropic mixture of bulk concentration X_Z, and an azeotropic mixture of concentration X_A at constant pressure for a mixture of A and B. For the zeotrope, the magnitude of the temperature glide is shown in the liquid and vapor envelope. As the temperature of mixture X_Z is varied within the range of the liquid/vapor envelope (two-phase region), the concentration of the liquid and vapor vary while the bulk concentration remains at X_Z.

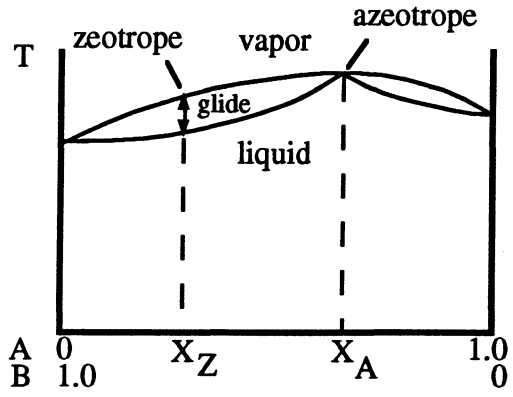

Figure 2.1: Temperature versus concentration diagram for a mixture of refrigerants A and B at constant pressure

Note the characteristic temperature glide for the zeotrope mixture. The magnitude of the glide is dictated by the mixture composition, or how much of component A is in B, and the component selection. During the evaporation process from the lower saturated liquid line to the upper saturated vapor line, the more volatile component, A, will evaporate more readily, increasing its concentration in the vapor phase. As a result, the less volatile component, B, will be enriched in the liquid phase, thus increasing the liquid's boiling point. This shifting boiling point is the temperature glide for the mixture.

During the course of this discussion much mention will be made of the performances of pure-refrigerant systems and NARM systems. "Pure refrigerant," unless otherwise specified, indicates a no-glide fluid. As just mentioned, a no-glide fluid can be either a pure refrigerant or an azeotropic mixture of two or more refrigerant components.

2.1.2 Carnot vs. Lorenz Cycle: Ideal Reversible Thermodynamic Cycles

To begin the discussion of thermodynamics, the fundamental ideal cycles upon which mixture and pure refrigerant performance are judged must be addressed. The ideal cycle used to evaluate the performance of a zeotropic mixture as a working fluid in an ideal vapor-compression refrigeration system is the *Lorenz cycle*. The corresponding cycle for a pure refrigerant is known as the *Carnot cycle*. The Lorenz cycle is the ideal reversible thermodynamic cycle operating between non-isothermal reservoirs, and the Carnot Cycle is the ideal reversible thermodynamic cycle operating between isothermal reservoirs. The Lorenz cycle is named after a German scientist from the late 1800's.[1] Figure 2.2 shows the temperature entropy diagrams for the two cycles.

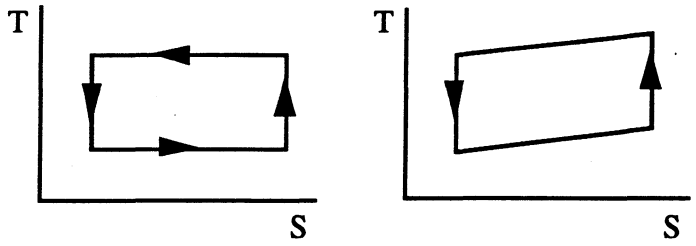

Figure 2.2: The Carnot Cycle (left) and the Lorenz Cycle (right)

From basic thermodynamics it is known that the area under the low-temperature path is the heat absorbed by the cycle, and the area under the high-temperature path is the heat rejected by the cycle. The difference in the heat rejected and the heat absorbed, or the area enclosed by the cycle, is the work required to drive the cycle. Comparing the performance of the Lorenz cycle and the Carnot cycle is difficult. The performance comparison is dependent upon what

temperature level is required at a particular location in the Lorenz cycle to meet the *application* need. McLinden and Radermacher essentially came to this conclusion, reporting that "the results (of the comparison) depend entirely on how the characteristic temperatures are defined."[2]

For the Carnot cycle, the entire heat exchange process with the low and high-temperature reservoirs is at a constant temperature. The Carnot cycle must operate between the lowest and highest temperature required by the application, regardless of where this constraint is placed in the cycle.

For the Lorenz cycle, the heat exchange with the low and high-temperature reservoirs is at a variable temperature. Depending on what portion of the cycle the temperature restraint is placed, the Lorenz cycle could outperform or under-perform the Carnot cycle. Performance is judged by the Coefficient of Performance, or COP, for the cycle. COP is defined in Equation 2.1.

$$COP = \frac{\text{cooling load}}{\text{work}} = \frac{\text{area under low temperature path}}{\text{enclosed area by cycle}} \qquad (2.1)$$

For the Lorenz and Carnot cycles, there are no irreversibilities for the heat exchange process between the thermodynamic fluid and the reservoirs and the advantage of the NARM temperature glide is not apparent. For these cycles, the heat exchange occurs at a zero temperature difference between the fluid and the reservoir. In a real vapor compression cycle, the effect of the finite heat exchangers and irreversible heat transfer must be considered.

2.1.3 Ideal Performance Limit for Two-Temperature Level Cooling

The Carnot cycle is the best performing cycle operating between two constant-temperature reservoirs. Two Carnot cycles would provide the best performing means of extracting heat from two, constant low-temperature reservoirs. One cycle would operate between the lowest temperature reservoir and the high-temperature reservoir and the other cycle would operate between the intermediate temperature reservoir and the high-temperature reservoir. The combined COP would be a function of the demand placed on each cycle, as shown in Equation 2.2, where x is defined as the low-temperature cycle demand fraction.

$$COP = (x)COP_{low} + (1-x)COP_{intermediate} \quad \text{where } 0 < x < 1 \qquad (2.2)$$

Figure 2.3, right scale, is a plot of the ideal performance *limit* for two-temperature level cooling as a function of low-temperature cycle demand fraction for the reservoir temperatures of

-15°C, 5°C and 30°C. No COP can exceed the COP in Figure 2.3 for the same demand fraction and reservoir temperatures.

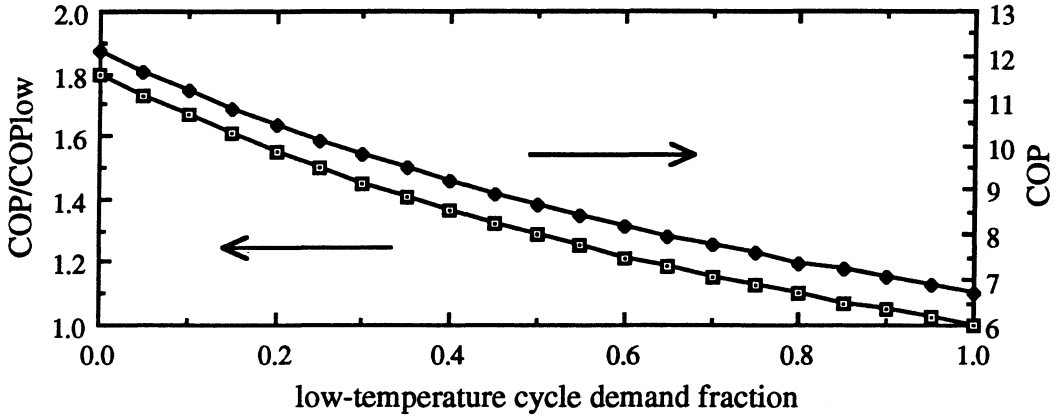

Figure 2.3: Ideal performance limit ratio (left) and ideal performance limit (right) for two-temperature level cooling as a function of the low-temperature cycle demand fraction for low-temperature reservoirs of -15°C and 5°C and a high-temperature reservoir of 30°C

The real world application for this situation is to provide two-temperature leveling cooling with a *dual compressor, dual-evaporator system* for a domestic refrigerator. Figure 2.3, left scale, shows the ratio of the performance of the dual compressor/evaporator system relative to a *single compressor/evaporator system.* The single compressor system would have to operate at the lowest temperature requirement, the freezer temperature, regardless of the load fraction between the two compartments. The graph presents the ideal performance improvement switching from a single compressor/evaporator system to a dual compressor/evaporator system if *both systems followed a Carnot cycle.*

If the low-temperature cycle demand fraction were 50%, the left scale indicates that the maximum COP improvement for a dual compressor, dual evaporator system is limited to 30% better than a single compressor/evaporator system. The 30% improvement is for the comparison of Carnot cycles with a low-temperature reservoirs of -15°C and 5°C and a high-temperature reservoir of 30°C.

This exercise is useful to help explore the ideal limits based solely on temperature levels and low-temperature cycle demand. In real heat transfer processes, the Carnot cycle is replaced with the vapor compression cycle. The performance now becomes a function of the specific fluid used in the cycle. Expansion and compression are no longer isentropic and the effect of real heat exchangers (finite area) must be taken into account.

2.1.4 NARM Vapor Compression Cycle for Two-Temperature Level Cooling

This section will explain the thermodynamics of the NARM vapor compression cycle for a domestic refrigerator application. The NARM vapor compression cycle for two-temperature level cooling includes two intercoolers and two evaporators. The two evaporators are required to meet the load demand for the low-temperature compartment (the freezer) and the load demand in the high-temperature compartment (the fresh-food section). The compressor and the condenser will be discussed, but they are not part of the actual test setup for this study, as explained in Chapter 3.

Figure 2.4 shows the components with the NARM evaporator module enclosed within the box. The refrigerant starts as a high-pressure liquid as it enters the evaporator module. It passes through the high-pressure side of both the high-temperature and low-temperature intercoolers. These intercoolers are exchanging heat with the two-phase vapor in the low-pressure portion of the cycle as shown in Figure 2.5's pressure/enthalpy diagram. After the expansion, the refrigerant enters the low-temperature evaporator which is located in the freezer compartment. As the refrigerant travels through the evaporator, the boiling point of the mixture increases. As explained previously, the more volatile component is driven off, enriching the liquid in the less-volatile component. Next, the refrigerant enters the low-temperature intercooler where it exchanges heat with the high-pressure liquid refrigerant. The refrigerant's boiling point continues to increase as more heat is added to the refrigerant. The refrigerant flows through the high-temperature evaporator, located in the fresh-food compartment, and finally through the high-temperature intercooler. The refrigerant vapor is compressed to a high-pressure gas. Finally, the refrigerant is condensed back to a liquid as it passes through the condenser. Notice

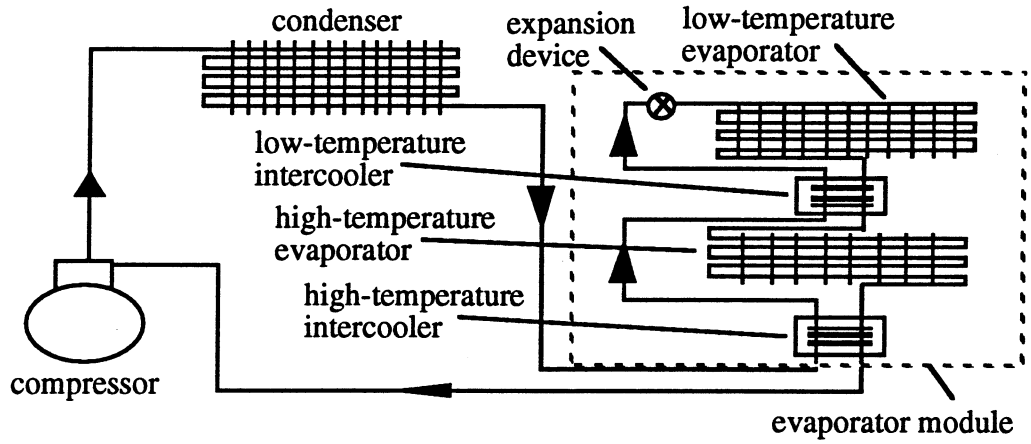

Figure 2.4: Schematic diagram of a NARM vapor compression system

that the opposite temperature-glide effect occurs in the condenser in the upper-right T-S diagram in Figure 2.5. The less-volatile component condenses out first, leaving the vapor enriched in the more volatile component. The condensation point of the vapor progressively drops.

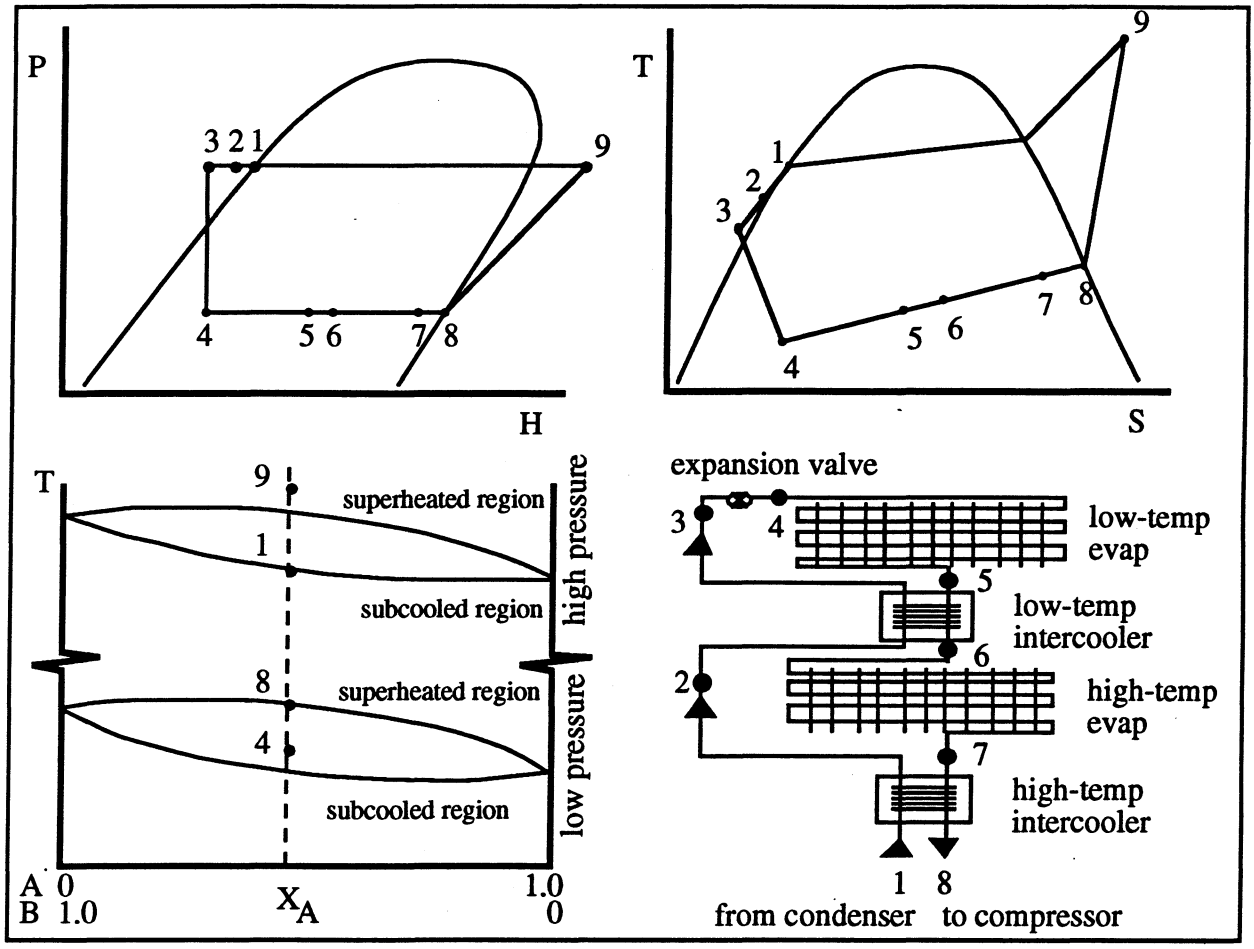

Figure 2.5: Pressure/enthalpy diagram (top left), temp./entropy diagram (top right), temp./concentration diagram (bottom left) and the NARM evaporator module schematic (bottom right) components: 1-2,7-8 high-temp. intercooler; 2-3, 5-6 low-temp. intercooler; 3-4 expansion device; 4-5 low-temp. evaporator; 6-7 high-temp. evaporator; 8-9 compressor

2.2 Advantages and Disadvantages of Using NARMs

2.2.1 Thermodynamic Advantages of a NARM Vapor Compression Cycle

There are two main thermodynamic advantages to using a NARM over a pure refrigerant. (An extended discussion of these advantages can be found in a paper by Smith *et al.*[3]) The first advantage of NARMs is that the refrigerant and air-temperature glides can be better matched. The magnitude of this advantage is dictated by the goodness of the fit. Assuming that the

refrigerant-temperature glide is fixed, the fit becomes a function of the air velocity through the evaporator. This matching thermodynamically reduces the irreversibility of the heat exchange process, thereby increasing performance. Practically speaking, the better temperature matching allows for a higher low-side pressure in the evaporator module, reducing the compressor work required for the system; however, the required evaporator area increases. The second advantage of using a NARM is that intercooling can be added to the system to increase system performance by relieving heat exchanger 'pinch-points'. (A pinch-point occurs when temperature difference between the two fluids in a heat exchanger is small or negative and the heat transfer is stopped or flows in the opposite direction than was intended.) The heat transfer process is shifted further back into the saturation dome, allowing the low-side pressure to be raised. Both of these advantages assume non-isothermal heat sinks and sources (*moderate* air-flow rates over the evaporators).

Advantage 1: A Better Match of Heat Source and Working Fluid Temperature Glides

Theoretically, NARMs can provide improvements in the COP for a specified range of evaporator air-flow rates and reasonable load splits between the low and high-temperature evaporators as shown in Figure 2.6. The high air-flow rate graphs on the left show that there is no significant drop in air temperature across the evaporators. (The evaporators are idealized counter-flow exchangers for the sake of illustration.) The air temperature forces the NARM refrigerant system to operate at a lower pressure to avoid an air-refrigerant pinch-point at the low-temperature evaporator outlet. A pinch-point could occur at the exit of the high-temperature evaporator depending on the slope of the NARM temperature glide and the fraction of energy exchange allocated to the evaporators. Since, the pure-refrigerant system does not experience a singular pinch-point and is able to operate at a higher pressure than the NARM system, its performance is better.

The lower air-flow rate graphs on the right show that there is significant air-temperature variation across the evaporators. The air-temperature variation forces the pure-refrigerant system to operate at a lower pressure to avoid a pinch-point at the low-temperature evaporator inlet. However, the NARM system will not take a performance penalty as long as the slope of the air-temperature line does not exceed the mixture's temperature glide. The performance penalty between a low and high air-flow rate case for a pure system is shown between the top two graphs.

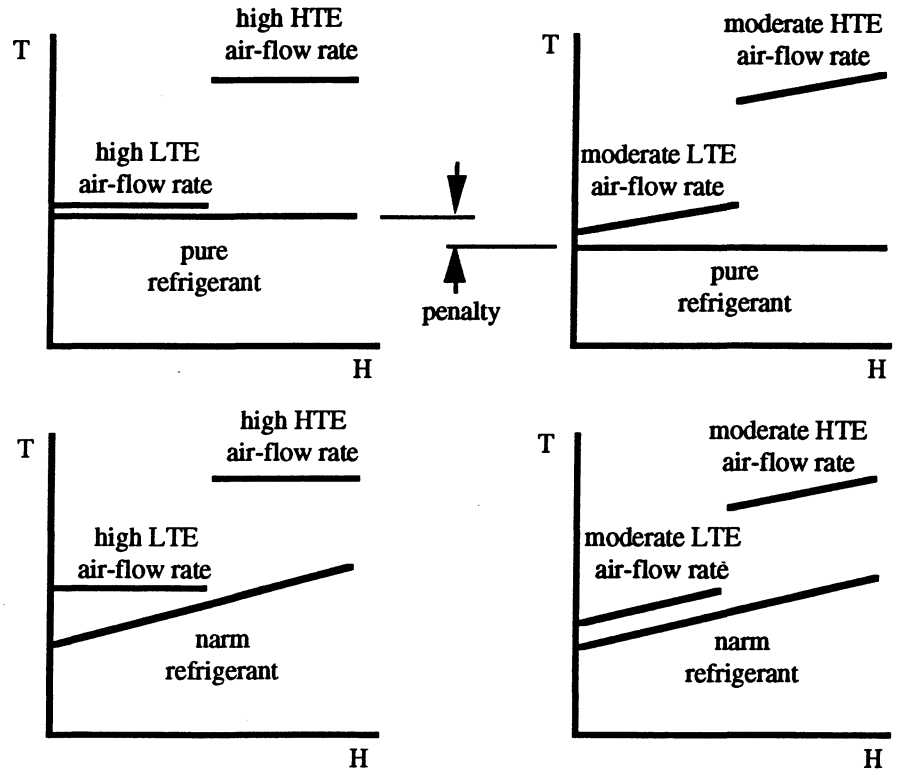

Figure 2.6: Performance change for different air-flow rates: a comparison between mixtures and pure refrigerants for constant air-inlet temperature

Figure 2.7 shows the effect of a changing air-glide temperature on the relative system performance for a pure refrigerant and a *specific* NARM system with the assumption of a constant air inlet temperature. Summarizing, for low air-glides (high air-flow rates), the NARM system is restricted to operate at a lower evaporating pressure than a pure-refrigerant system to avoid a heat exchanger pinch-point. This penalizes system performance. As the air-glide is

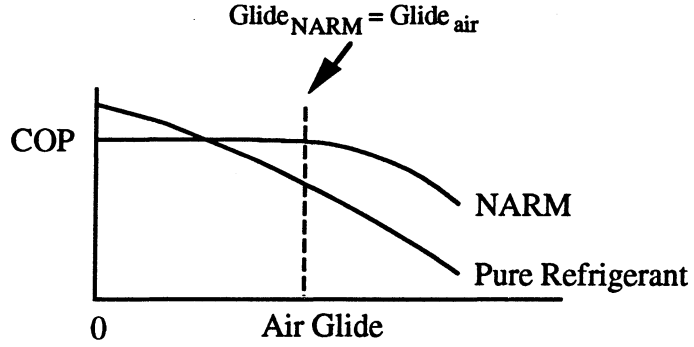

Figure 2.7: The overall effect of air-flow rate on system performance for a *specific* NARM versus a pure refrigerant (this assumes that the NARM glide through the evaporator and condenser are equal and the air glide is adjusted in an equivalent manner for the evaporator and condenser)

continually increased, the pure-refrigerant system is restricted to operate at lower and lower evaporating pressures to avoid a heat exchanger pinch-point and system performance steadily deteriorates. As the air-glide increases, the NARM system does take a performance penalty until the air-glide matches the NARM glide. If the air-glide is increased beyond the NARM glide, the NARM system performance will begin to deteriorate because of a pinch-point in the opposite end of the heat exchanger and the system is forced to operate at a lower evaporating pressure.

Figure 2.8 presents simulation results for a R22/R123 NARM for various concentrations and air-glides (air-flow rates). The pure R123 (0.0% R22) system has the best COP for the 0.0°C air-glide. There are no other concentrations that yield a higher COP for the system at this air-glide. At an air-glide of 2.5°C, there are two concentrations that yield the best system COP, 0.0% and 65.0% R22. This corresponds to the performance cross-over point in Figure 2.7. The pure-refrigerant R123 system's COP equals that of the 65% R22/R123 NARM. Between the 2.5°C and 5.0°C air-glides, the 65% R22/R123 NARM system's COP exceeds all other COPs including the COP of the R123 pure-refrigerant system. At a 10.0°C air-glide, the best system COP still holds for a NARM, but the R22 concentration has shifted to 60%. This simulation example illustrates the general performance trends shown in Figure 2.7.

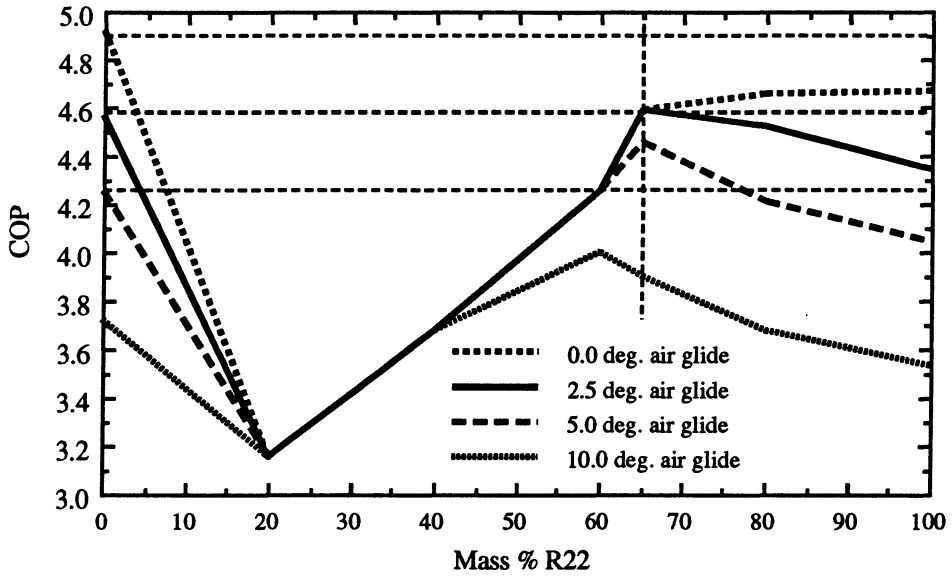

Figure 2.8: Simulation results for a R22/R123 system with two evaporators and two intercoolers with equal load distribution on each evaporator - COP versus concentration at different air glides

Advantage 2 : Intercooling - Lower Evaporating Temperatures with no Work Increase

Figure 2.9 is similar to Figure 2.6, with the addition of intercooling between the high and low-temperature evaporators. We will assume for the sake of discussion that the refrigerant at the exit of the high-temperature evaporator is fixed at a quality of 1. Intercooling has the effect of moving the heat transfer process of the low-temperature evaporator back further into the saturation dome, freeing up heat exchanger pinch-points and allowing the low-side pressure of the system to be raised, thus increasing overall system performance.

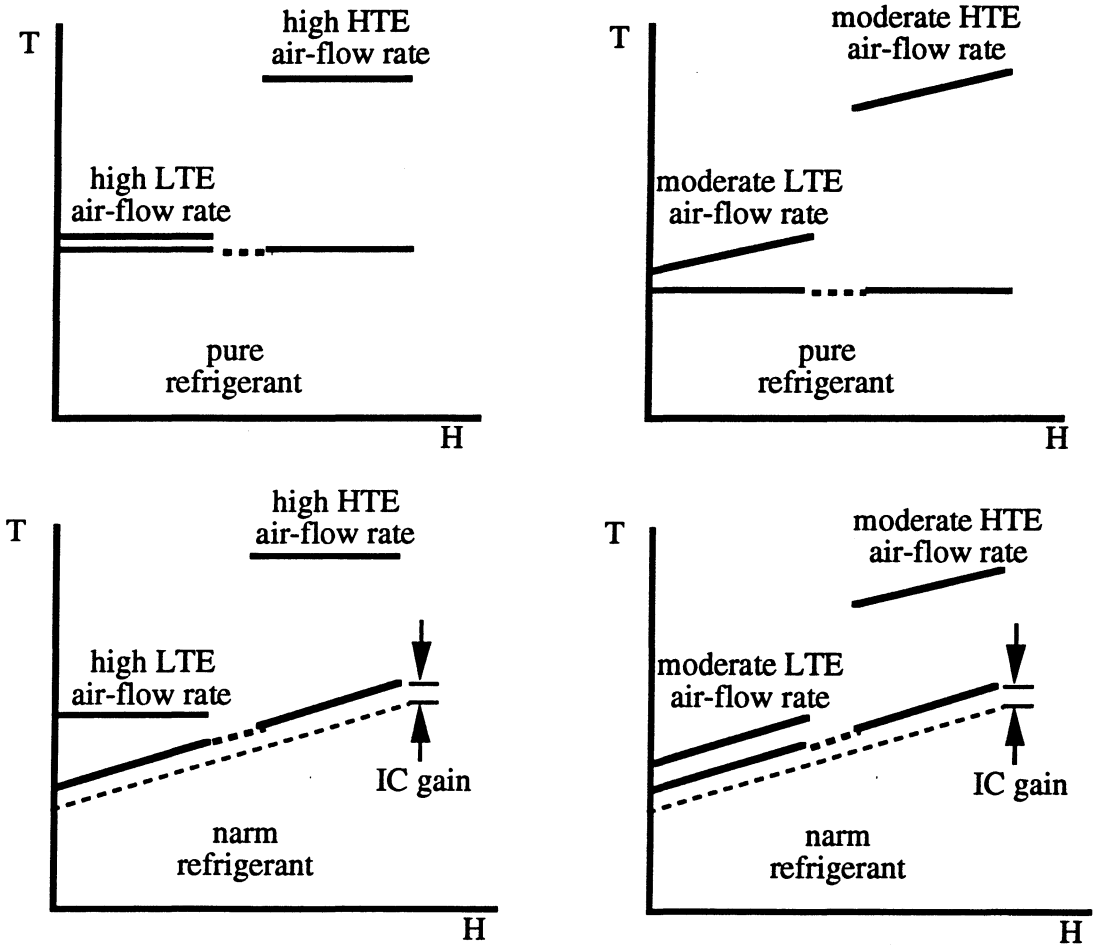

Figure 2.9: Performance change for different air-flow rates: a comparison of mixture and pure refrigerants with intercooling

The top two graphs illustrate the effect of intercooling on the pure-refrigerant system. Intercooling has no effect other than to re-circulate energy within the system. No advantage can be gained with intercooling for a pure-refrigerant system with no superheating. Pure-refrigerant system intercooling may improve the efficiency if the system is operating in superheat and the

increase in capacity is greater than the increase in the compressor work. More compressor work is required because the compression starts further out in the superheat region.

The lower two graphs show that intercooling with a NARM system allows the shifting of the low-temperature evaporator heat transfer process as explained above. Notice that performance improvements for the NARM system are not limited to the moderate air-flow rate case. Even the high air-flow rate case shows a performance improvement. The performance gain for adding an intercooler between the low and high-temperature evaporators is shown on two lower graphs for NARMs.

Figure 2.10 attempts to further clarify the advantage of intercooling with refrigerant mixtures. The graphs are pressure versus enthalpy plots showing the effect of inserting an intercooler at the exit of the evaporator. The lines of constant temperature slope down and to the right. At constant pressure, the temperature of the refrigerant rises from left to right (low quality to high quality). When the intercooler is inserted, as shown in the right graph, the average temperature of the refrigerant in the evaporator falls from (5 + -15)/2 = -5 to (0 + -20)/2 = -10 without having to reduce the evaporating pressure. Assuming that a designer desires to maintain the heat load removed by the evaporator, two benefits may be realized. The evaporating pressure can be raised to restore the previous average refrigerant temperature, or the evaporating pressure can remain the same and the evaporator area can be reduced. (This is an idealized representation of a mixture P-h diagram. The constant-temperature lines are not necessarily straight.)

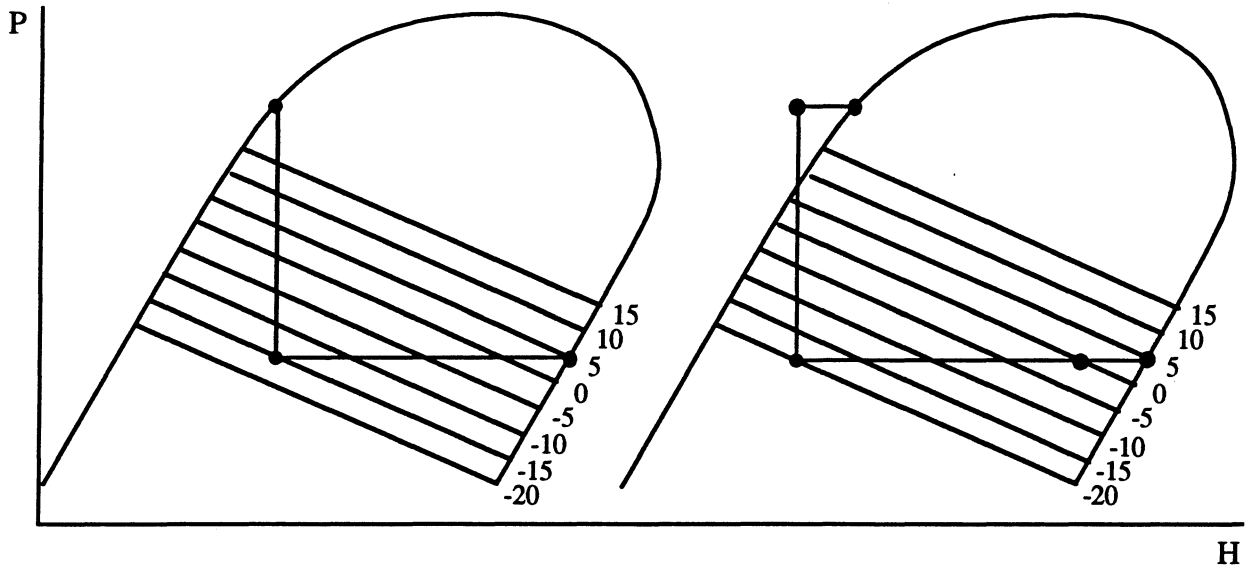

Figure 2.10: Pressure versus enthalpy showing the average lowering of evaporator temperature with insertion of an intercooler from -5 to -10

Intercooling may be justified in some cases but not in others, depending on the NARM glide and the load distribution between the freezer and the fresh-food compartments as shown in Figure 2.11. These are some ideal R22/R123 system simulation results from an infinite area and air-flow rate ideal study with an isentropic compressor. The heat transfer area is infinite because the temperature difference between the air and the refrigerant can be driven to zero. Infinite air flow is shown by the horizontal air-temperature profiles. As before, the refrigerant at the exit of the NARM module is fixed at a quality of 1. The top left graph is the base case for the NARM with no intercooling at all, case 00. The COP is 3.853. The top right graph shows the insertion of an intercooler between the low and high-temperature evaporators, case 10. The COP remains unchanged. The exit of the high-temperature evaporator has remained the pinch-point in the system. The addition of the intercooler was *not* able to relieve the system pinch-point.

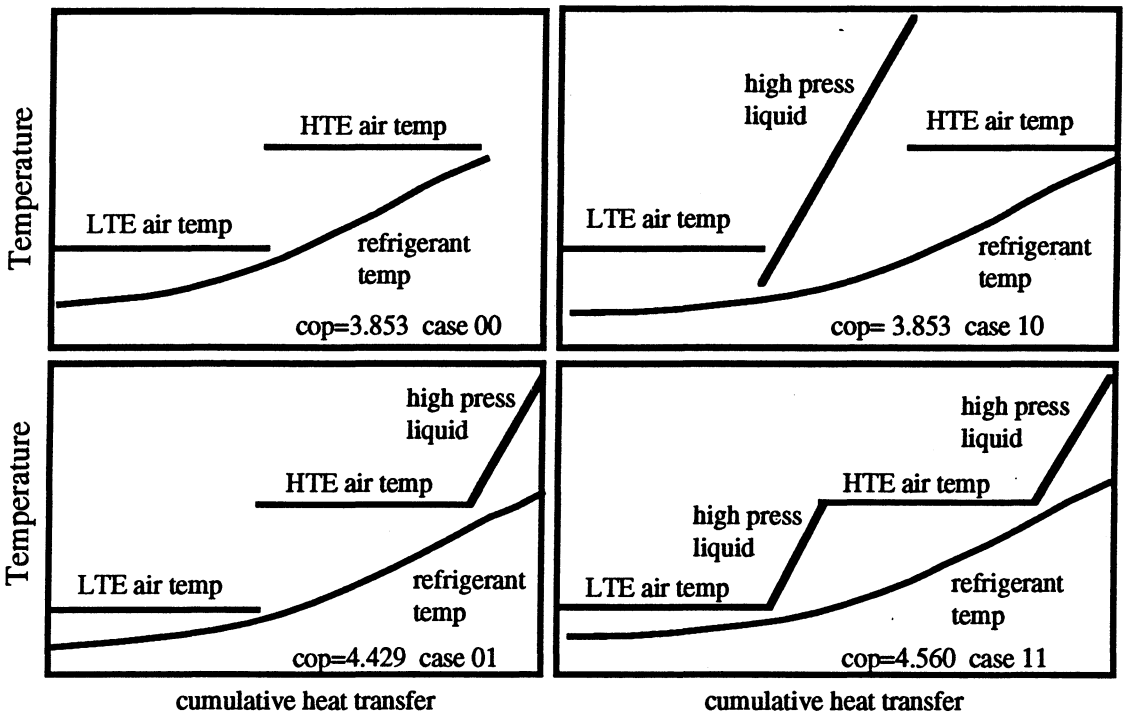

Figure 2.11: System simulation for 65% R22/35% R123 for a 50% load split between the two evaporators, plotting temperature versus cumulative heat transfer

The bottom left graph shows the case when an intercooler is added to the exit of the high-temperature evaporator, case 01. The addition of the intercooler is *able* to relieve the system pinch-point at the exit of the high-temperature evaporator. The refrigerant low-side pressure is raised, resulting in a increase in the COP to 4.429. The bottom right graph shows the two intercooler case, case 11. Very little improvement in COP is seen, leading to the conclusion that the additional intercooler is not justified on a performance basis and can be left out of the system.

For an interesting discussion on Figure 2.11 which explains the simulation results in terms of component irreversibility, see Appendix K.

2.2.2 Other Advantages of NARMs

As shown above, NARM systems have the thermodynamic potential for improved energy efficiency. Depending on the slope of the temperature glide, lower evaporator temperatures with moderate pressure ratios are possible for a single stage compression NARM system. In addition, capacity may be controlled for a NARM system by selectively shifting the composition of the circulating refrigerant and reducing energy consumption by reducing cycling losses. The composition of the mixture could be shifted by selectively withdrawing liquid or vapor during the phase change process, thereby changing the thermodynamic characteristics of the mixture.

2.2.3 Disadvantages of NARMs

General

Very little intensive industrial research has been published on the NARM cycle, and there are problems that have not yet been addressed. For example, the temperature glide of the mixture is a characteristic of the mixture percentage; therefore, each system requires 'tuning' to load conditions and air-flow rates. The refrigerant for each application would have to be optimized by selecting a specific composition.

Experimental results have also shown a tendency to have liquid carry over even at high levels of apparent superheat.[4] Liquid in the compressor suction line would require the compressor inlet state point to be farther out into the superheat region to avoid slugging, but additional superheat can penalize system performance.

Low Heat Transfer Coefficients

One major disadvantage of NARMs is that they are characterized by a lower heat transfer coefficient than pure refrigerants, especially under the low heat and mass flux flow conditions typical of refrigerators. Wattelet *et al.*[5] found that the heat transfer coefficients of a slight zeotropic mixture of R22, R124 and R152a under-performed R12's heat transfer coefficients by 20% in the wavy-stratified regime. The current study, as discussed in Chapter 5, found that the heat transfer coefficients of the NARM mixtures of R22/R123 and R22/R141b under-performed R12's heat transfer coefficients by an average of 50% in a specific region of the wavy-stratified regime.

The lower mixture heat transfer coefficients are believed to be caused by a diffusion gradient effect.[6] [7] [8] The diffusion of the more volatile component away from the tube wall enriches the remaining liquid in the higher boiling point component. This reduces the amount of effective superheat at the wall which may delay or totally suppress the onset of nucleate boiling. In addition, convective boiling is decreased under low-mass flux flow conditions (as compared to high-mass flux flow conditions) because of decreased turbulence and reduced refrigerant-to-tube contact from the refrigerant flowing in the bottom of the tube. Decreased flow turbulence also allows concentration gradients to be set up in the liquid and the vapor.

Jung *et al.*[9] reported that for annular flow conditions, nucleate boiling was suppressed for mixtures, due to loss of wall superheat and mass transfer resistance. Wattelet *et al.*[10] confirmed these results with the slight zeotropic mixture of R22, R124 and R152a. Wattelet further reported that at low heat fluxes, as mass flux was increased to cause a flow transition from stratified/wavy to annular flow, the tested mixture's heat transfer coefficient increased relative to the R12's heat transfer coefficient and eventually surpassed it. This transition occurred between 100 and 150 kg/m^2-s for small tube diameters, 8.0 to 12.0 mm. This range of diameters is typical for refrigerator heat exchangers.

2.2.4 Challenges of NARMs

The use of NARMs will pose many challenges. Leakage may be a problem for large non-hermetic systems; however, Blaise and Dutto[11] reported that a preferential leak caused only a minor composition change for a specific ternary NARM system. The fear is that if preferential leaking were to occur, it would be difficult to return the system to its original composition in the field.

Furthermore, some mixtures might be extremely sensitive to small changes in composition. A small change in composition could severely penalize performance. Methods for accurately sensing superheat must be developed for applications in which expansion valves are controlled by superheat. The temperature glide of the NARM makes the traditional method of sensing superheat by temperature less reliable, because the temperature glide masks the onset of superheat.

The negative effect of heat transfer coefficient degradation could be overcome by installing turbulators in the heat exchangers and/or increasing the refrigerant velocity by using smaller diameter tubes at the expense of additional pressure drop. However, pressure drop must be minimized because it offsets the NARM temperature glide.

Several factors need to be considered when evaluating a NARM, including its ozone depleting and global warming potentials, flammability, reactivity with oils and materials, toxicity and thermal stability. Commercial availability must also be considered, since some of the NARM components being considered are in limited production.

Efficient counter-flow heat exchangers, evaporators and intercoolers must be designed and built to exploit the NARM temperature glide and help offset lower boiling heat transfer coefficients. Many researchers have noted the need for better heat exchanger design to ensure the success of NARMs. Ted Atwood of Allied Signal said that "the primary efforts for cycle enhancement [for NARMs] need to be on the heat exchangers, where increased area must be provided and counter-flow principles applied."[12] P. S. Burr summarized his work with G. G. Haselden with these words:

> "The design of the evaporator will pose a greater challenge due to the need to keep the refrigerant pressure drop low whilst ensuring that the generated vapor remains closely in phase equilibrium with the liquid throughout the boiling process. In addition, there is a control problem involved in ensuring that liquid is not carried forward from the evaporator outlet. However, in view of the increasing cost of power, it is considered that further work on the development of the mixed refrigerant circuit is justified."[13]

2.3 Literature Review

When the project began, the emphasis was upon overall performance of the NARM cycle. It became clear that the first area to explore were the existing pure-refrigerant and refrigerant-mixture heat transfer correlations. As explained in Chapter 4, pure-refrigerant correlations were required to characterize the air-side performance of the evaporators. Mixture correlations and the air-side performance data required for the NARM cycle optimization are explained in Chapter 6. This section is divided into three parts: a discussion of classical flow maps used to predict flow regimes, a discussion of existing correlations in the literature for azeotropes and zeotropes and a discussion of overall system performance results from various researchers from the last thirty years.

2.3.1 Flow Regimes

Flow regimes are of particular interest when predicting flow boiling heat transfer coefficients. Depending on the flow regime and the heat flux level, the relative contribution of

convective and nucleate boiling can be different at various quality levels. If the dominate mode of boiling is known, it can influence the form of the proposed correlation. At certain levels of mass and heat flux, the heat transfer coefficient may or may not vary with quality. When correlating data, if the heat transfer coefficient is expected to vary with quality, then a local correlation form might be fitted first. If the heat transfer coefficient is not expected to vary with quality, then an average correlation form may provide the best fit to the data.

There are two classic papers that stand out in flow regime prediction: Baker[14] and Taitel & Dukler.[15] In 1954, Baker published a flow map based on water-air and oil-air data. The x and y axis of the Baker map are the gas- and liquid-phase mass fluxes multiplied by ratios of their fluid properties to those of air and water. In 1976, Taitel and Dukler published a flow-pattern map. This map predicts flow-pattern transitions on the basis of physically-grounded models rather than the experimental observations of Baker's map. The x-axis of the map is the Lockhart-Martinelli parameter, a measure of the local liquid content. The individual transition lines are predicted with different models; therefore, the y-axis value depends on the transition line of interest. If there is no optical access to the flow which is being studied, then the use of a flow map may be a good place to start the process of developing a correlation.

Most refrigerant correlations in the literature span two different flow regimes: the wavy/stratified and the annular flow. Stratified flow is generally found in low-load applications such as domestic refrigerators and freezers. Annular flow is generally found in high-load applications such as room air conditioners, heat pumps and stationary air conditioners. Worsoe-Schmidt[16] found that the flow transition for R12 in a 10.8 mm diameter tube occurred around 100 kg/m^2-s.

Stratified Flow

In stratified/wavy flow, the mass flux is generally less than 100 kg/m^2-s and the liquid flows in the bottom of the tube. The liquid is stratified, devoid of turbulence and churning, with small wave formation on the liquid's surface. The liquid is flowing slowly enough for the inertia effects of the liquid to be less than the effects of gravity and viscous forces. The ratio of inertia force to gravity force is captured by the non-dimensional Froude number and the ratio of the inertial to viscous force is captured by the Reynolds number. Thus, stratified wavy flows have comparatively lower Froude and Reynolds numbers.

Stratified flow is characterized by a small component of convective boiling. Nucleate boiling does not appear to be suppressed at higher qualities or lower heat fluxes. There is no

major effect of quality on the heat transfer coefficients which varies only with heat flux. For this regime, part of the tube wall remains dry, reducing the convective heat transfer area and thereby decreasing its contribution to the overall heat transfer coefficient. Convective boiling is also decreased by the reduced turbulence of the flow.

The tendency for nucleate boiling to be present can be accounted for by the boiling number. (The boiling number is the heat flux divided by the mass flux and the latent heat of evaporation across the entire saturation dome.) As the boiling number increases, nucleate boiling is more likely to be present. The boiling number can be increased by increasing the heat flux (holding mass flux constant) or by decreasing the mass flux (holding the heat flux constant). The boiling number can have the same value for a high mass and heat flux flow as it does for a low-mass and heat flux flow. If mass and heat flux are reduced, the lower value of mass flux in the denominator keeps the boiling number from decreasing. Thus, nucleate boiling does not appear to be suppressed for stratified flow (low-mass fluxes) at low heat fluxes.

Nucleate boiling does not appear to be suppressed at higher qualities for stratified flow because the flow never transitions to annular flow at the higher qualities. The lack of transition to annular flow is caused by the decrease in slip ratio at the lower mass fluxes between the vapor and liquid streams. With a lower slip ratio there is less chance of slug/annular flow initiation from a high vapor core velocity. There is greater chance of nucleate boiling when there is a thick liquid layer present. (For stratified flow, a thicker liquid layer flows in the bottom of the tube, as opposed to annular flow, where a thinner liquid annulus flows around the circumference of the tube). For the thicker liquid layer, there is more liquid conductive resistance and an increased chance of superheat at the tube wall; therefore, nucleation and nucleate boiling are more likely to occur.

Annular Flow

Annular flow can occur at mass fluxes greater than 100 kg/m^2-s. For annular flow, the Reynolds and Froude numbers and the slip ratio increase. The inertia forces begin to dominate the gravity and viscous forces. The liquid is carried up on the tube wall by the higher velocity gas core and forms an annulus covering the entire wall.

Convective boiling is greatly enhanced for the higher mass flux annular flows in two ways: (1) the heat transfer area is increased because the entire wall is covered with liquid and (2) flow turbulence is enhanced because of the high velocity vapor core.

For low heat fluxes, the heat transfer coefficient increases with quality. Nucleate boiling is suppressed because there is not enough heat flux to start nucleation at the higher mass fluxes (lower boiling number). The variation with quality is predominately due to convective boiling. At higher qualities, the liquid layer thins and vapor velocity increases, enhancing convective boiling.

For high heat flux cases, nucleate boiling is present at low qualities because the thicker liquid annulus increases the chance of superheat formation at the wall. At higher qualities, the liquid layer thins and nucleate boiling is diminished. Therefore, for the high heat flux cases, there may be no variation of the heat transfer coefficient with quality.

2.3.2 Pure-Refrigerant Correlations

Several mixture and pure-refrigerant correlations were examined in the course of this study. Pierre's correlation, as presented in a 1956 paper,[17] is an excellent R12 correlation that has stood the test of time. Pierre did an extensive study covering the mass flux range from 16 to 340 kg/m^2-s and the heat flux range of 1 to 23 kW/m^2. The evaporating temperatures varied from -20 to 10°C and oil concentration was varied from 0 to 18% by volume. Pierre's correlation form is simple. It will be presented in Chapter 4.

Another widely used correlation is Shah's.[18] His correlation was converted from a graphical form to equation form because of its widespread use. It is a generalized local correlation, based on 780 data points from 19 experimental studies. A total of eight fluids were used covering a wide operating range. The mean deviation of the correlation is 14%. Shah's correlation does a good job of predicting heat transfer coefficient values at higher values of heat and mass flux but not at the lower values of heat and mass flux, as discussed in Chapter 4. The correlation was based on a mass flux range of 13 to 580 kg/m^2-s and a heat flux range of 1.5 to 35 kW/m^2. His correlation broke flow boiling into three distinct regimes: a nucleate boiling dominated regime; a bubble suppression regime, where nucleate boiling and convective boiling are important, and a convective boiling dominated regime. The correlation is evaluated by taking the largest heat transfer coefficient calculated for the three regimes. The boiling number is a component of the nucleate boiling term, and the convection number is a component of the convective boiling term. Shah introduced a Froude number-based correction factor for the convective boiling term. (The Froude number can be used to predict the transition between stratified/wavy and annular flow). The Froude number accounts for the loss of tube wetting in horizontal flow for low-mass fluxes. Shah's correlation will be presented in Chapter 4.

Kandlikar[19] developed another generalized local correlation. The correlation was based on a mass flux range of 104 to 4480 kg/m^2-s and a heat flux range of 0.3 to 35 kW/m^2. Since it is a general correlation, it incorporates a fluid-dependent parameter in the nucleate boiling term to account for the different nucleate boiling effects that occur from fluid to fluid. As with Shah's correlation, Kandlikar included a Froude-dependent term to enhance the convective boiling term. The correlation is based on 5246 data points from 24 experimental studies. A total of ten fluids were used. The correlation has a mean deviation of 18.8%. The R22/R123 mixture correlation, as discussed in Chapter 5, is modeled after the form of Kandlikar's correlation. The Kandlikar correlation is presented in Equation 2.3.

$$\frac{\alpha}{\alpha_l} = C_1 Co^{C_2} (25Fr)^{C_5} + C_3 Bo^{C_4} F_{fl} \quad \text{where} \quad \alpha_l = 0.023 Re_l^{0.8} Pr_l^{0.4} (k_l / D) \qquad (2.3)$$

Table 2.1 lists the applicable constants for either the convective or nucleate boiling regions. The correlation is to be evaluated with both sets of constants, and the higher of the two values is the predicted correlation value. This method provides continuity between the convective and nucleate boiling regions. Table 2.2 presents the values of the fluid dependent parameter, F_{fl}.

Table 2.1: Constants for the Kandlikar correlation

constant	convective region	nucleate boiling region
C_1	1.136	0.6683
C_2	-0.9	-0.2
C_3	667.2	1058.0
C4	0.7	0.7
C_5*	0.3	0.3

* C_5=0 for vertical tubes, and for horizontal tubes with $Fr_l > 0.04$.

Table 2.2: Fluid dependent parameters for the Kandlikar correlation

fluid	F_{fl}
Water	1.00
R11	1.30
R12	1.50
R13b1	1.31
R22	2.20
R113	1.30
R114	1.24
R152a	1.10
Nitrogen	4.70
Neon	3.50

The last pure-refrigerant correlation that has gained some acceptance over the last several years is the Jung and Radermacher correlation.[20] This correlation is reported to have a mean deviation of 7.2% based on experimental data obtained with R22, R12, R152a and R114. The correlation is based on over 3000 data points. Jung and Radermacher's correlation follows Chen's[21] supposition that the two-phase heat transfer coefficients can be predicted by superimposing the convective boiling and nucleate boiling components as shown in Equation 2.4.

$$\alpha = \alpha_{nb} + \alpha_{cb} \tag{2.4}$$

The correlation covers a mass flux range of 250 to 720 kg/m^2-s and a heat flux range of 10 to 45 kW/m^2. The Jung and Radermacher correlation is presented in Equations 2.5 to 2.12. N is a boiling suppression factor, α_{sa} is a pool boiling coefficient obtained by Stephan and Abdelsalam's[22] correlation, F is a two-phase enhancement factor and α_l is a single-phase heat transfer coefficient obtained by the Dittus-Boelter[23] correlation.

$$\alpha = N\alpha_{sa} + F\alpha_l \tag{2.5}$$

$$N = 4048 X_{tt}^{1.22} Bo^{1.13} \text{ for } X_{tt} \le 1 \tag{2.6}$$

$$N = 2.0 - 0.1 X_{tt}^{-0.28} Bo^{-0.33} \text{ for } 1 < X_{tt} \le 5 \tag{2.7}$$

$$\alpha_{sa} = 207 \frac{k_l}{bd} \left(\frac{q'' bd}{k_l T_{sat}} \right)^{0.745} \left(\frac{\rho_v}{\rho_l} \right)^{0.581} Pr_l^{0.533} \tag{2.8}$$

where

$$bd = 0.0146\, \beta \left[\frac{2\sigma}{g(\rho_l - \rho_v)} \right]^{0.5} \text{ with a contact angle of } \beta = 35^\circ \tag{2.9}$$

$$F = 2.37 \left(0.29 + \frac{1}{X_{tt}} \right)^{0.85} \tag{2.10}$$

$$X_{tt} = \left(\frac{1-x}{x} \right)^{0.9} \left(\frac{\rho_v}{\rho_l} \right)^{0.5} \left(\frac{\mu_l}{\mu_v} \right)^{0.1} \tag{2.11}$$

$$\alpha_l = 0.023\frac{k_l}{d}Re^{0.8}\,Pr^{0.4} \tag{2.12}$$

The final pure-refrigerant correlation examined here was developed at the University of Illinois Air Conditioning and Refrigeration Center by Wattelet reported in a paper by Smith *et al.*[24] This correlation proved most useful because of its dedicated formulation from low heat and mass flux range data typical of domestic refrigerators and freezers. The correlation is based on a mass flux range of 25 to 100 kg/m^2-s and a heat flux range of 2 to 10 kW/m^2. The correlation is based on 140 R12 and R134a data points with a mean deviation of 10%. The Wattelet correlation is presented in Chapter 4.

An expanded version of the Wattelet *et al.* correlation has since been developed.[25] This correlation covers a much wider range of heat and mass fluxes. The mass flux range is from 25 to 500 kg/m^2-s and the heat flux range is from 2 to 30 kW/m^2. The correlation is fitted from over 600 R12 and R134a data points. The correlation is based on Kutateladze's[26] form, presented in Equation 2.13, which is an asymptotic, power-type-addition model for the nucleate and convective boiling components.

$$\alpha_{tp} = \left[\alpha_{nb}^n + \alpha_{cb}^n\right]^{1/n} \tag{2.13}$$

The significant feature of the correlation form is the smooth (asymptotic) suppression of the weaker boiling term. The Wattelet correlation is presented in Equations 2.14 to 2.21.

$$\alpha_{tp} = \left[\alpha_{nb}^n + \alpha_{cb}^n\right]^{1/n} \quad n = 2.5 \tag{2.14}$$

$$\alpha_{nb} = 55M^{-0.5}q^{0.67}P_r^{0.12}[-\log P_r]^{-0.55} \tag{2.15}$$

$$\alpha_{cb} = F\alpha_l R \tag{2.16}$$

$$F = 1 + 1.925X_{tt}^{-0.83} \tag{2.17}$$

$$\alpha_l = 0.023\frac{k_l}{D}Re_l^{0.8}\,Pr_l^{0.4} \tag{2.18}$$

$$X_{tt} = 0.551P_r^{0.492}\left(\frac{1-x}{x}\right)^{0.9} \tag{2.19}$$

$$R = 1.32 Fr_l^{0.2} \text{ if } Fr_l < 0.25 \quad (2.20)$$

$$R = 1 \text{ if } Fr_l \geq 0.25 \quad (2.21)$$

2.3.3 Refrigerant-Mixture Correlations

There were two mixture correlations in the literature that were examined for potential use for this project. The first correlation, by Jung *et al.*,[27] is a modification of their pure-refrigerant correlation. More than 2000 local heat transfer coefficients were obtained with a mixture of R12 and R152a. The mass flux varied from 250 to 720 kg/m^2-s and the heat flux varied from 10 to 45 kW/m^2. The mixture correlation has a mean deviation of 9.6%. This correlation was evaluated as a basis of comparison for the heat transfer data taken in Chapter 5, but the mass and heat flux range were not compatible.

An extensive study was performed by Wattelet *et al.*[28] on the differences between heat transfer coefficients at low heat and mass flux conditions and those at higher mass and heat fluxes for both pure refrigerants and refrigerant mixtures. The findings show that mixtures under-perform pure fluids at low heat and mass fluxes. As the mass and heat fluxes increase, the mixture heat transfer coefficients increase to a level comparable with pure-refrigerant heat transfer coefficients. Application of the high mass and heat flux correlation of Jung and Radermacher to the low mass and heat fluxes in this experiment would have given incorrect results.

Kandlikar's[29] mixture correlation was also examined. This correlation is a modification of the Kandlikar pure-refrigerant correlation previously described. The modifications take into account the mass diffusion in the liquid phase during nucleate boiling, changes in the liquid film concentration, local saturation temperature and liquid phase properties along the evaporator tube. Kandlikar used Jung and Radermacher's mixture data (described above) and reported a mean deviation of 15%.

Kandlikar's mixture correlation was not able to be evaluated as a basis of comparison for this study due to the lack of several fluid dependent parameters and diffusivity data. The correlation required knowledge of mutual diffusivity of component A in component B and the mutual diffusivity of component B in component A. The correlation also required a fluid dependent parameter for R123 and R141b for flow in aluminum tubes. Parameter information is currently only available for R12, R22, R114 and R152a for flow in copper and stainless steel

tubes. Even if these values were available, the heat and mass flux range is similar to the Jung mixture correlation, which is not in the same range as the Chapter 5 data.

2.3.4 System Performance

This last section explores the NARM system work from the past 30 years. Most source and sink glides (air glides) for refrigerator applications are between 5 and 10°C. Examining Figure 2.8 gives an indication of the ideal performance gains that can be expected for these air glides. The maximum R22/R123 COP for the 10°C air-glide case occurs a concentration of 60% R22. The COP at 60% R22 is 8% greater than the best pure-refrigerant (R123) system's COP.

Only a few researchers have reported significant experimental gains in efficiency. Most reports found little or no improvement in the COP of a NARM compared to pure-refrigerant performance. The following list outlines the most significant work done on refrigerant mixtures for two-temperature level cooling in the last 30 years:

- *Tschaikovsky and Knuznetsov (1963)*[30] - Tschaikovsky and Knuznetsov were the first team to suggest the use of NARMs in domestic refrigeration and tested mixtures of R12/R22 and R12/R13. No pure-refrigerant results were given in the paper to judge the relative performance of the mixture systems.

- *Lorenz and Meutzner (1975)*[31] - This is the classic work most often cited by people in the NARM field. Lorenz and Meutzner's work was based on a two-evaporator, two-intercooler, vapor-compression cycle that was specifically intended for use in domestic refrigerators. They were the first to use intercooling to further enhance energy efficiency. They suggested for a two-temperature level refrigerator application that the best mixture combination would have a 65°C normal boiling point difference.

  For their study, an existing refrigerator was modified with two evaporators and two intercoolers as shown in Figure 2.4. They reported, "power savings up to 20% were obtained as compared with R12 (for a 50% R22/R11 mixture)." The *transient* tests were carried out at ambient temperatures of 32, 25, 16 and 10°C where the duty cycle of the compressor was controlled by a thermostat in the freezer compartment. *No* other details were given for *any* the test runs; especially details on the pure R12 runs which formed the basis of their claim.

- *Stoecker (1978)*[32] - Stoecker *modeled* a non-optimized two-evaporator, two-intercooler domestic refrigerator using a 50% mixture of R12/R114. The model showed

an energy savings of 12% (COP increase of 13.6%) compared to a pure R12 model. An 100% efficient isentropic compressor model was used to calculate the required pumping power for the systems.

- *Lunay and Stoecker (1981)*[33] - Lunay and Stoecker *optimized* a two-evaporator, two-intercooler refrigerator system using a 75% efficient isentropic compressor model. A 30% R12/R114 optimized mixture system showed an energy savings of 9% (COP increase of 9.9%) over a pure R12 optimized system with the same loads and total heat exchanger area. For the 30% R12/R114 optimized system, their optimization work found that the low-temperature intercooler area was driven to zero. For the pure R12 optimized system, both of the intercooler areas were driven to zero even with 5°C of fixed superheat at the compressor inlet.

- *Arthur D. Little, Inc.(1984)*[34] - Drop-in 90°F closed-door tests were performed using two mixtures of 40 and 60% R22/R114 in a modified Amana 18 ft^3, a two-evaporator, high-temperature intercooler only refrigerator. The freezer evaporator was forced convection, and the fresh-food evaporator and condenser were natural convection. They found a 2.7% increase in COP (a 7.1% decrease in energy consumption - the evaporator loads were not similar) for the system charged with the 40% R22/R114 mixture compared to the best R12 COP run at the same conditions. The COPs (not including fan power) for the 40% R22/R114 and the R12 runs were 0.927 and 0.952 respectively. They observed that the 40% R22/R114 system had higher condensing pressures that resulted in *lower* condenser inlet and outlet temperatures as compared to the R12 system. This lowered the amount of effective temperature difference between the mixture in the condenser and the air.

- *Stoecker and McCarthy (1984)*[35] - Stoecker and McCarthy *simulated* a two-evaporator, two-intercooler domestic refrigerator using a 32% mixture of R12/R114 and showed a compressor energy savings of 8% as compared to a pure R12 cycle maintaining identical loads and temperatures (a 8.7% increase in COP). The model incorporated a more sophisticated isentropic compressor model that was a function of compressor speed. However, the model contained only an elementary heat transfer coefficient correlation that was a function of concentration only.

Experimental results from a two-evaporator, two-intercooler test setup revealed an approximate 2% reduction in power for mixtures between 85 and 90% R12/R114 for the same loads and temperatures. Stoecker reported that the discrepancy between simulation

and experiment was directly attributable to the reduction of the heat transfer coefficients in the condenser and evaporators. He reported that the condensing heat transfer coefficients were 10 to 30% lower depending on the position in the condenser. The maximum amount of degradation was in the stratified-flow regime. He observed that there was *no* decrease in the boiling heat transfer coefficients with the introduction of mixtures, but the magnitude of both the pure R12 and the R12/R114 heat transfer coefficients were lower than expected. The boiling heat transfer coefficients ranged from 160 to 390 kW/m^2 (G = 75 to 84.2 kg/m^2-s, q" = 1.87 to 3.75 kW/m^2) for 30% to 100% R12/R114 mixtures.

- *Stoecker and Boggs (1986)*[36] - Stoecker and Boggs *simulated* a two-evaporator, two-intercooler domestic refrigerator to quantify the effect of the degradation of boiling and condensing heat transfer coefficients on cycle performance. The R12/R114 system yielded a 2% savings in compressor power as compared to pure R12 consistent with the experimental results of Stoecker and McCarthy (1984).[37] If the same heat transfer coefficients as R12 could be maintained for a R12/R114 NARM system, a 3.5% energy saving could be realized, a difference of 1.5% additional energy savings for the R12/R114 systems as compared to the pure R12 system.

Experimental R12/R114 mixture results for this study from a two-evaporator, two-intercooler test setup revealed no reduction in compressor power in contrast to Stoecker and McCarthy's (1984)[38] previous study.

- *Kruse (1989)*[39] - Kruse modeled a steady-state two-evaporator, two-intercooler refrigerant system with a 45% mixture of R22/R142b, which showed an energy savings of 10% over pure R12. Steady-state experimental results using a 47.5% mixture of the same components showed a 1.9% improvement in COP over pure R12. Pull-down tests for 45% R22/R142b system showed an energy savings of 10% as compared to a pure R12 system.

Lorenz and Meutzner is the only work cited above that reported significant *experimental* gains with the use of refrigerant mixtures in a domestic refrigerator application, a 20% measured power savings for a 50% R22/R11 mixture system as compared to a pure R12 system. None of work cited above realized the experimental gains of Lorenz and Meutzner. The greatest *modeled* energy savings cited above were between 8 and 12% from work done by Stoecker which is consistent with our rough estimate from the beginning of this section. The steady-state

experimental energy savings reported Stoecker and Kruse were limited to 2% greater than an equivalent R12 system.

Why are experimental gains reported by Lorenz so much greater than others' experimental work? There are three possible explanations. First, the tests Lorenz performed were transient tests, not steady-state tests. Recall that Kruse reported a 10% energy savings for transient tests done with a R22/R142b mixture (relative to R12). A question that arises for these transient tests is, where was the thermostatic switch placed that controlled the duty cycle and at what temperature was it set to maintain? Lorenz mentioned that the compressor duty cycle was controlled by the "surface temperature of the cold storage compartment."[40] As discussed earlier, the definition of the heat-source temperature can strongly bias one cycle's performance relative to the other. Second, the compressor in the Lorenz system may have performed better for the R22/R11 mixture, reducing power consumption. The compressor design could not have been optimum for both R12 and the R22/R11 mixture. Third, whenever experimental results are presented that report measured energy savings, the results are questionable if no other information is given. There is no mention in Lorenz's paper about the loads or the 'equivalent' temperatures maintained in each compartment. (Recall the discussion from section 2.1.2.) To properly report energy savings for one system relative to another, each system should be operated with an optimized compressor for the specific fluid being tested, and identical loads and 'equivalent' temperatures must be maintain in each compartment. The next best method would be to use the system COP for the comparison.

It is believed that reduced heat transfer coefficients are one of the reasons why mixtures do not perform as well as pure refrigerants in the low heat and mass flux range. Wattelet *et al.*[41] found that a slight zeotropic mixture of R22, R124 and R152a under-performed R12 by 20% in the wavy-stratified regime. In Chapter 5, this study found that the NARM mixtures of R22/R123 and R22/R141b under-performed R12 by an average of 50%. (The average refrigerant-side resistance for these runs were 37.1%.) As mentioned earlier, Stoecker and McCarthy[42] reported that a discrepancy between experimental performance of an R12/R114 mixture and the simulated performance was directly attributable to reduced heat transfer coefficients in the stratified-flow regime.

2.4 References

---

[1] Lorenz, H., "Die Ausnutzung der Brennstoffe in den Kuhlmaschinen", Zeitschrift fur die gesammte Kalte Industrie, Vol. 1, 1894, pp. 10-15.

---

[2] McLinden, M. and R. Radermacher, "Methods for comparing the performance of pure and mixed refrigerants in the vapour compression cycle", *International Journal of Refrigeration*, Vol. 10, November, 1987, pp. 318-325.

[3] Smith, M. K., M. C. Heun, R. R. Crawford and T. A. Newell, "Thermodynamic performance limit considerations for dual-evaporator, non-azeotropic refrigerant mixture-based domestic refrigerator-freezer systems", *International Journal of Refrigeration*, Vol. 13, July, 1990, pp. 237-242.

[4] Atwood, T., Personal communication, April 1990.

[5] Wattelet, J. P., J. C. Chato, A. L. Souza and B. R. Christoffersen, "Evaporative Characteristics of R134a, MP39 and R12 at Low Mass Fluxes", ACRC TR-35, University of Illinois at Champaign Urbana, Air Conditioning and Refrigeration Center, May, 1993.

[6] Atwood, T. "NARBs - The Promise and the Problem", ASME Winter Annual Meeting, Paper 86-WA/HT-61, December, 1986.

[7] Wattelet, J. P., J. C. Chato, A. L. Souza and B. R. Christoffersen, "Evaporative Characteristics of R134a, MP39 and R12 at Low Mass Fluxes", ACRC TR-35, University of Illinois at Champaign Urbana, Air Conditioning and Refrigeration Center, May, 1993.

[8] Smith, M. K., J. P. Wattelet and T. A. Newell, "A study of evaporation heat transfer coefficient correlations at low heat and mass fluxes for pure refrigerants and refrigerant mixtures", *Heat Transfer with Alternate Refrigerants*, ASME HTD-Vol. 243, August, 1993, pp. 19-26.

[9] Jung, D. S., M. McLinden, R. Radermacher and D. Didion, "A study of flow boiling heat transfer with refrigerant mixtures", *International Journal of Heat and Mass Transfer*, Vol. 32, No. 9, 1989, pp. 1751-1764.

[10] Wattelet, J. P., J. C. Chato, A. L. Souza and B. R. Christoffersen, "Evaporative Characteristics of R134a, MP39 and R12 at Low Mass Fluxes", ACRC TR-35, University of Illinois at Champaign Urbana, Air Conditioning and Refrigeration Center, May, 1993.

[11] Blaise, J. C. and T. Dutto, "The First Industrial Application of Non-azeotropic Mixture", *Proceedings of the IIR*, Vol. 2, 1988.

[12] Atwood, T. "The ABCs of NARBs (Non-azeotropic Refrigerant Blends)", *ASHRAE Transactions*, Paper HI-85-18 No. 1, 1985, pp. 909-917.

[13] Burr, P. S. and G. G. Haselden, "A Non-isothermal Mixed Refrigerant Cycle for Air Conditioning Duties", *Proceedings of The Institute of Refrigeration*, Vol. 71, 1974-1975, pp. 18-23.

[14] Baker, O., "Designing for Simultaneous Flow of Oil and Gas", *Oil and Gas Journal*, 53, pp. 185-195, 1954.

---

[15] Taitel, Y. and A. E. Dukler, "A model for predicting flow regime transitions in horizontal and near-horizontal gas-liquid flow", *AIChE Journal*, 22(1), 47-55, 1976.

[16] Worsoe-Schmidt, P. "Some characteristics of flow pattern and heat transfer of Freon-12 evaporating in horizontal tubes", *Ingeniorne*-International Edition 3(3), 98-104, 1959.

[17] Pierre, B., "The Coefficient of Heat Transfer for Boiling Freon-12 in Horizontal Tubes", *Heating and Air Treatment Engineer*, December, 1956, pp. 302-310.

[18] Shah, M.M., "Chart Correlation for Saturated Boiling Heat Transfer: Equations and Further Study", *ASHRAE Transactions*, Vol. 88, Part 1, pp. 185-196.

[19] Kandlikar, S.G., "A General Correlation for Saturated Two-Phase Boiling Heat Transfer Inside Horizontal and Vertical Tubes", *Journal of Heat Transfer*, Vol. 112, February 1990, pp. 219-228.

[20] Jung, D.S. and R. Radermacher, "Prediction of Heat Transfer Coefficients of Various Refrigerants During Evaporation", *ASHRAE Transactions*, V. 97, Pt. 2.

[21] Chen, J. C. "A correlation for boiling heat transfer to saturated fluids in convective flow", *Industrial and Engineering Chemistry, Process Design and Development*, 5(3), 1966, 322-329.

[22] Stephan, K. and M. Abdelsalam, "Heat transfer correlations for natural convection boiling", *International Journal of Heat and Mass Transfer*, Volume 23, 1980, pp. 73-87.

[23] Dittus, F. W., and L. M. K. Boelter, *University of California Publications on Engineering*, Vol. 2, p. 443, Berkeley, 1930.

[24] Smith, M. K., J. P. Wattelet and T. A. Newell, "A study of evaporation heat transfer coefficient correlations at low heat and mass fluxes for pure refrigerants and refrigerant mixtures", *Heat Transfer with Alternate Refrigerants*, ASME HTD-Vol. 243, August, 1993, pp. 19-26.

[25] Wattelet, J. P., J. C. Chato, A. L. Souza and B. R. Christoffersen, "Evaporative Characteristics of R134a, MP39 and R12 at Low Mass Fluxes", ACRC TR-35, University of Illinois at Champaign Urbana, Air Conditioning and Refrigeration Center, May, 1993.

[26] Kutateladze, S. S., "Boiling heat transfer", *International Journal of Heat and Mass Transfer*, 4 : 1961, pp. 31-45.

[27] Jung, D. S., M. McLinden, R. Radermacher and D. Didion, "A study of flow boiling heat transfer with refrigerant mixtures", *International Journal of Heat and Mass Transfer*, Vol. 32, No. 9, 1989, pp. 1751-1764.

[28] Wattelet, J. P., J. C. Chato, A. L. Souza and B. R. Christoffersen, "Evaporative Characteristics of R134a, MP39 and R12 at Low Mass Fluxes", ACRC TR-35, University of Illinois at Champaign Urbana, Air Conditioning and Refrigeration Center, May, 1993.

[29] Kandlikar, S. G., "Correlating flow boiling heat transfer data in binary systems", HTD-Vol. 159, *Phase Change Heat Transfer*, ASME, 1991, pp. 163-169.

[30] Tschaikovsky, V. F., and A. P. Knuznetsov, "Utilization of Refrigerant Mixtures in Refrigeration Compression Machines", XI International Congress of Refrigeration, Munich, 1963.

[31] Lorenz, A. and K. Meutzner, "On Application of Non-Azeotropic Two-Component Refrigerants in Domestic Refrigerators and Home Freezers", XIV International Congress of Refrigeration, Paper B2.42, 1975 Moscow.

[32] Stoecker, W. F. , "Improving the Energy Effectiveness of Domestic Refrigerators by the Application of Mixed Refrigerants", ORNL Sub - 78/55463/1, September, 1978.

[33] Lunay, P. F., "Improving the Efficiency of Refrigerators and Heat Pumps by using a Non-azeotropic Mixture of Refrigerants", Master's Thesis, Department of Mechanical Engineering, University of Illinois, Urbana-Champaign, 1981.

[34] Report by Arthur D. Little, Inc., "An Evaluation of a Two-Evaporator Refrigerator-Freezer Using Non-azeotropic Refrigerant Mixtures", ORNL/ Sub - 82-47952/1, September, 1984.

[35] Stoecker, W. F. and C. I. McCarthy, "The Simulation and Performance of a System using an R12/R114 Refrigerant Mixture", ORNL Sub - 81-7762/3&01, May, 1984.

[36] Stoecker, W. F. and D. Boggs, "Performance and Simulation of Once-Through and Separating Cycles Using Non-azeotropic Refrigerant Mixtures", ORNL - Sub - 81-7762/5 & 01, June, 1986.

[37] Stoecker, W. F. and C. I. McCarthy, "The Simulation and Performance of a System using an R12/R114 Refrigerant Mixture", ORNL Sub - 81-7762/3&01, May, 1984.

[38] Stoecker, W. F. and C. I. McCarthy, "The Simulation and Performance of a System using an R12/R114 Refrigerant Mixture", ORNL Sub - 81-7762/3&01, May, 1984.

[39] Kruse, H., "Non-Azeotropic Refrigerant Mixture R22/R142b for a Two Temperature Refrigerator as Replacement for R12", presentation at USEPA Contractors Meeting, Washington, October, 1989.

[40] Lorenz, A. and K. Meutzner, "On Application of Non-Azeotropic Two-Component Refrigerants in Domestic Refrigerators and Home Freezers", XIV International Congress of Refrigeration, Paper B2.42, 1975 Moscow.

[41] Wattelet, J. P., J. C. Chato, A. L. Souza and B. R. Christoffersen, "Evaporative Characteristics of R134a, MP39 and R12 at Low Mass Fluxes", ACRC TR-35, University of Illinois at Champaign Urbana, Air Conditioning and Refrigeration Center, May, 1993.

[42] Stoecker, W. F. and C. I. McCarthy, "The Simulation and Performance of a System using an R12/R114 Refrigerant Mixture", ORNL Sub - 81-7762/3&01, May, 1984.

CHAPTER 3: EXPERIMENTAL APPARATUS

This chapter describes the test setup and its construction followed by a discussion of the flow loop instrumentation. The test loop was designed to operate without a condenser and without a compressor, eliminating the need for oil in the system. Oil in the refrigerant mixture would have changed the thermodynamic properties of the resultant refrigerant/oil mixture. A chiller, a gear pump, and a heater replaced the compressor and condenser. It was later determined that a diaphragm pump and a subcooler would be required for the system to reach the desired evaporating pressure and to help prevent gear pump cavitation.

Figure 3.1 shows a pressure-enthalpy diagram for the test loop. Note the superimposed refrigerant path that would exist if a compressor and a condenser were used in the system. Following this path, the refrigerant first passes through the evaporator module on the low-pressure side where heat is transferred to the refrigerant. The refrigerant starts in the low-temperature evaporator where it exchanges heat with the freezer compartment air. Next, the fluid passes through the low-temperature intercooler where it exchanges heat with the high-pressure liquid just prior to the expansion valve. The refrigerant then passes through the high-temperature

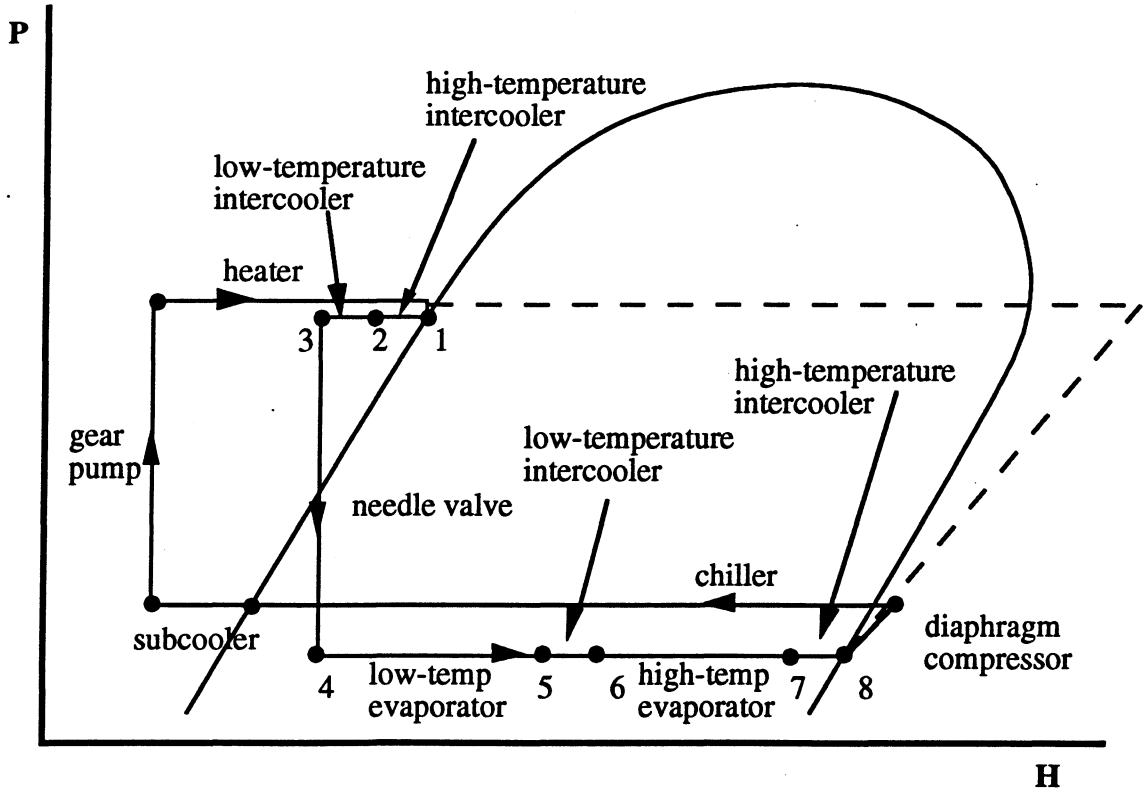

Figure 3.1: Test setup refrigerant path

evaporator where it exchanges heat with the fresh-food compartment air. Finally, the fluid passes through the high-temperature intercooler where it exchanges heat with the high-pressure liquid refrigerant entering the module.

After exiting the low-pressure side of the module, the refrigerant enters the diaphragm pump which pumps the exiting vapor up to a slightly higher pressure. The refrigerant then enters the chiller which cools and condenses the vaporized refrigerant to the point of a subcooled liquid. A subcooler further cools the refrigerant to prevent pump cavitation. The refrigerant is then pumped up to the high-side pressure by a positive-displacement, magnetically-coupled gear pump. The high-pressure liquid passes through a heated pipe section which heats the refrigerant to a desired 'condenser exit' condition. Next, the refrigerant passes through the high-pressure side of the refrigerant-to-refrigerant intercoolers to the expansion valve. The expansion valve throttles the high-pressure liquid to a low-pressure saturated condition.

3.1 Operational Range Defined

Pressure, mass-flow rate, chiller, and heater operational ranges had to be determined before sizing components for the test loop. When the test setup was designed, the test mixtures had not yet been selected, so the system was designed to accommodate the largest possible differential pressure based on an evaporating temperature of -17 °C and a condensing temperature of 37 °C from a potential list of ten *pure* refrigerants. A total evaporator load of 293 W was assumed. From this information, the mass-flow rate, chiller load, and heater load could be determined. The chiller load was calculated based on the assumption that the refrigerant exited as a saturated vapor from the evaporator module and had to be cooled to a saturated liquid. The heater load was calculated based on the assumption that the exit state of the refrigerant would be a saturated liquid. To ensure a conservative design, the maximum values of mass-flow

Table 3.1: Potential design conditions where T_{evap} = -17.7°C, T_{cond} = 37.7°C, load = 293 W

candidate	Δp (kPa)	plow (kPa)	phigh (kPa)	$\dot{m}$ (kg/s 10-3)	chiller (W)	heater (W)
R12	741.04	164.36	905.4	2.736	440	150
R22	1182.8	266.61	1449.4	1.921	420	130
R32	1927.36	441.74	2369.1	1.141	404	115
R123	131.3	14.56	145.86	2.255	412	120
R124	469.54	83.8	553.34	2.801	452	160
R125	1518.52	368.08	1886.6	3.697	540	250
R134a	810.8	146.2	957.01	2.137	454	160
R142b	423.13	73.57	496.7	1.839	402	115
R143a	1330.9	338.1	1669.0	2.439	503	212
R152a	720.6	135.76	856.39	1.280	414	122

rate, differential pressure, chiller load, and heater load were used as design values for the system components. Table 3.1 shows the results for the ten pure refrigerants.

3.2 Required Components

Figure 3.2 shows the component layout for the test setup. The components were attached to a 1.905 cm (0.75 in.) piece of plywood. The instrumentation cables were fed through holes to the back of the board and placed in a wire channel that ran the entire length of the board.

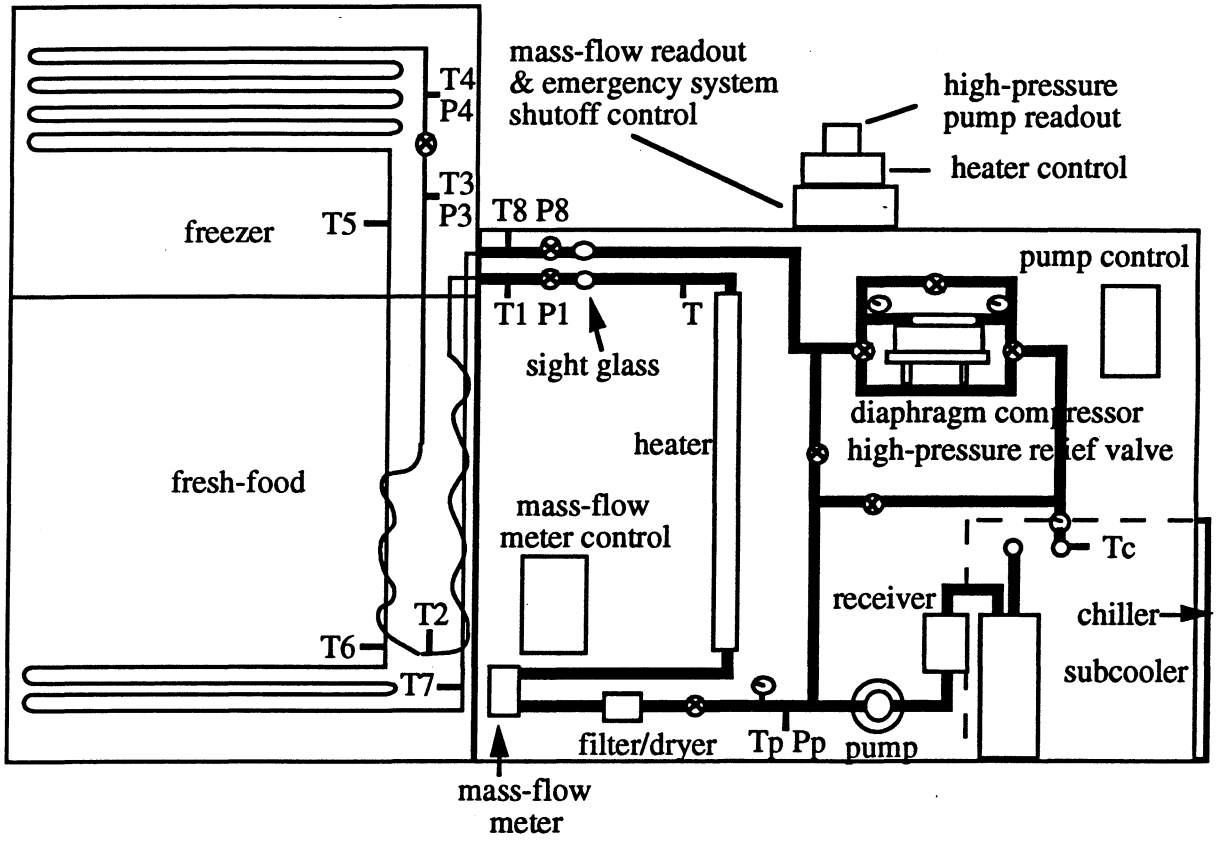

Figure 3.2: System component layout

3.2.1 Diaphragm Compressor

After the initial runs of the test loop, it was determined that a diaphragm compressor was needed to help the system reach the desired evaporating pressures and prevent gear pump cavitation. The diaphragm compressor, a Gast DOA-161-AA, was placed on a small shelf and connected to the test loop by two three-way valves. To prevent the compressor from overheating, two cooling fans were installed on either side of the unit. Special care was taken to seal the head of the compressor to prevent refrigerant leakage. Initially, it was not known how

the diaphragm material, a Nordel/Nomex sandwich, would react to the test refrigerants. Tests done by others showed that the diaphragm would not react to the presence of R12 but would react to R22 and R11.[1] Since R11 is similar to R123 and R141b, additional diaphragm service kits were purchased to be able to replace the diaphragm after each test refrigerant was run.

The three-way valves were used to isolate the compressor during shut down and startup. This reduced the chance of leaks and also enabled the unit to start. The compressor would not start unless the line pressure was less than 204.7 kPa (15 psig). During startup, the system was run until the low-side pressure was at or below this level, at which time the compressor was brought on-line. An additional valve was placed on the compressor bypass line. This valve was used to aid in the startup and control of the unit. Two mechanical low-pressure gauges were installed at the inlet and outlet of the compressor. During operation, the compressor would provide a differential pressure of 68.9 - 103.4 kPa (10 - 15 psi).

3.2.2 Chiller

An R502 chiller, FTS System RC-100B-L00, was chosen for the test loop. The unit contained a counter-flow tube-in-tube heat exchanger, which was connected to the test loop. The chiller could reduce the refrigerant temperature to approximately -25°C under normal loading conditions of 300 to 400 W. The refrigerant charge in the unit was adjusted to maximize the cooling capacity for this load range. The side panels were removed to maximize the air circulation over the internal chiller components because there was limited air space around the chiller. The refrigerant loop was connected to the chiller's heat exchanger to ensure a downward flow path for the refrigerant because the gear pump was initially gravity fed before the diaphragm compressor was added to the system.

3.2.3 Subcooler

A subcooler was added to the system because of cavitation problems in the gear pump. The subcooler lowered the refrigerant temperature from approximately -25°C to -50°C. The subcooler was a Dewar flask containing a bath of dry ice and isopropyl alcohol. The refrigerant lines were run directly into the bath. A crude heat exchanger was made by coiling the copper lines several times to increase the heat transfer surface in the bath. An insulated cap was placed over the Dewar flask. Dry ice was consumed at a rate of approximately 0.5 kg/hr during operation.

3.2.4 Receiver

A receiver was placed in the loop just prior to the gear pump to provide a reservoir of refrigerant to feed the gear pump. A standard refrigerant compressor exhaust muffler was used for this purpose. Great care was taken to insulate the receiver.

3.2.5 Gear Pump

The gear pump was sized to maintain a differential pressure of 1723.2 kPa (250 psi) and a flow rate of 3.15 cm^3/s (3 gal/hr). A modified Micropump 200 pumphead was selected with 1.6 mm gears. The pumphead was mounted to a 0.56 kW (3/4 hp) electric motor controlled by a Lancer GPD 402 variable speed drive. The drive was controllable by computer. The pumphead was sealed with a Viton o-ring. This o-ring had to be replaced because of compatibility problems between the o-ring material and the refrigerants used in the test. The best material for the o-ring was determined to be Neoprene.

Since the motor drive was capable of being computer controlled, an attempt was made to control the pump by using a small Omega CN4400 PID controller to maintain a constant system high-side pressure. Because the system would not settle to a stable operating condition, this method was abandoned after many attempts to tune the controller. A second attempt was made to control the pump by maintaining a constant mass-flow rate in the loop with the CN4400 controller. This setup also proved to be unstable even after many attempts to tune the controller. It was concluded that the gear pump speed and the mass-flow rate were too closely coupled to provide stable operation under a variety of conditions. The best way to operate the pump was to set the speed manually and adjust it during the test as needed. The drift of the pressure and mass-flow rate was minimal. The variable speed drive's manual control, a single-turn potentiometer, was replace by a ten-turn potentiometer to provide fine speed control.

3.2.6 Pump Bypass

A pump bypass line was installed to enable system startup. The bypass branched off from the main loop immediately after the pump and reconnected to the main loop at the input to the chiller. When the system was shut down, liquid refrigerant would be trapped in other parts of the system such as the fresh-food evaporator. At system startup, the bypass valve was opened, and the refrigerant left in the subcooler and receiver circulated through the chiller, allowing the refrigerant from other parts of the system to migrate to the chiller circulation loop. When there was an adequate amount of refrigerant in the chiller circulation loop, the bypass valve was

closed, and refrigerant would begin to circulate throughout the entire system. Without the bypass loop, system startup would have been *impossible*.

3.2.7 High-Pressure Relief Valve

Just prior to the pump bypass valve, a high-pressure relief valve was installed with a trip pressure of 2412.5 kPa (350 psi). The output of the relief valve was tied back into the low-pressure side of the system. If the pump pressure exceeded 2412.5 kPa (350 psi), the refrigerant would be exhausted back into the low-pressure side of the system and no refrigerant would be lost to the atmosphere. By preventing the discharge of refrigerant into the atmosphere, this valve also eliminated the necessity of recharging the entire mixture in the event of an unusually large high-side pressure. If the refrigerant were instead discharged into the atmosphere, it would not have been known what effect the discharge would have had on the overall mixture concentration in the system.

3.2.8 Filter/Dryer

A commercially available filter/dryer was installed in the loop just prior to the mass-flow meter. This was one of two in-line filters in the refrigerant loop. Another fine mesh filter was installed just prior to the expansion valve to prevent small debris from clogging it. The filter/dryer also served to remove moisture from the refrigerant. Moisture in the refrigerant would cause icing to occur at the expansion valve, resulting in erratic changes in the mass-flow rate.

3.2.9 Mass-Flow Meter

A Micro Motion D6 mass-flow meter, calibrated for full flow at 250 g/min, was used to measure mass-flow in the refrigerant loop. The remote electronics unit for the Micro Motion emitted a 4-20 mA signal that was read by the datalogger. An Omega CN4400 controller was used as a readout display and as an emergency shutdown device. The controller was programmed to shut off the refrigerant heater and the evaporator load systems in the insulated box if the mass-flow fell below a predetermined level. This prevented the potentially dangerous situation of having no refrigerant flowing over the refrigerant heater. The inlet and outlet connections to the mass-flow meter utilized Viton o-rings. These o-rings had to be replaced because of compatibility problems between the o-ring material and the refrigerants used in the test. The best material for the o-rings was found to be Neoprene.

The mass-flow meter worked well for the tests. The meter had to be placed carefully in the refrigeration loop. If the meter was oriented improperly, vapor could get trapped in the meter's U tube. If the flow was not single phase at the point of measurement, the meter would give erroneous results. To ensure single-phase flow through the meter, it was installed immediately after the gear pump just prior to the heater section (see Figure 3.1). The refrigerant was furthest from the saturation dome at this point, and the possibility of vapor at the measurement point was minimal.

The mass-flow meter's U tube developed a crack during the tests due to a manufacturing flaw. The crack had nothing to do with the compatibility of the stainless steel U tube with the refrigerants used in the tests. The U tube was replaced and no other problems were encountered with the Micro Motion meter.

3.2.10 Refrigerant Heater

A Watlow 400 W, 1.5875 mm (1/16 in.) diameter, 120-volt cable heater was used to heat the refrigerant in the heater section. The heater was mounted upside down to prevent dry out at the entry point fitting for the heater. Vapor could be trapped in the installation fitting if it were mounted at the top of the section. To prevent premature burnout of the heater, voltage spikes were dampened with a snubber circuit placed across the power input to the heater. The snubber circuit consisted of a 1.0 micro-farad capacitor and a 100 Ohm resistor as shown in Figure 3.3.

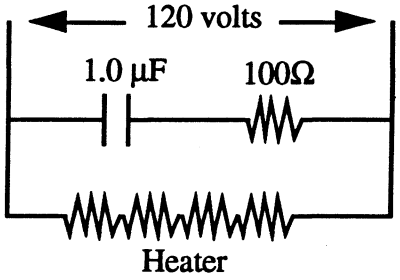

Figure 3.3: Snubber circuit for heater

The heater was driven by a Cole Parmer Digi-Sense temperature controller to maintain a predetermined temperature setting. A type-K thermocouple was placed approximately 10 cm downstream from the heater section's outlet.

3.2.11 Sight Glasses

Sight glasses were installed at the inlet and outlet to the evaporator module to enable visual checks of the refrigerant condition at these points. If bubbles were observed in the inlet

sight glass, the heater was bringing the refrigerant too close to the saturated liquid line. Under standard operating conditions, all refrigerant viewed in the inlet sight glass was in the liquid phase.

The refrigerant could be observed slipping into and out of superheat through the outlet sight glass. These sight glass observations also served to confirm the refrigerant state as calculated by the pressure and temperature readings at these points.

3.2.12 Fine Mesh Filter

As mentioned earlier, a fine mesh filter, 140 μm, was installed in the refrigeration loop just prior to the expansion valve. This filter prevented the expansion valve from being clogged with small particles. A 50 μm filter was initially used, but the pressure drop across the filter was too large. A 90 μm filter was also tried with the same result. A 140 μm filter was ultimately used. This size filter provided the best balance between filtering capability and pressure drop for the system.

3.2.13 Expansion Valve

A Nupro S series B-SS4 metering valve was selected to serve as the expansion valve. A larger valve was initially installed, but it did not provide adequate control in the desired mass-flow range of the system. The smaller B-SS4 valve was properly sized to provide excellent control of the refrigerant flow. Leakage problems were encountered with the seals in this valve. The standard Buna-N seals were replaced with Neoprene.

A rod connected to the metering valve through the wall of the insulated box permitted adjustments to the mass-flow rate during operation. During startup, the valve was full open. As the insulated box cooled to its operating temperature, the valve was slowly closed and the gear pump speed was adjusted simultaneously to achieve the desired system mass-flow rate and high-side pressure.

3.2.14 Heat Exchangers

The heat exchangers were designed and built by Heun.[2] An optimization was performed to determine the minimum mass design for the two evaporators and two intercoolers as well as the optimal fin/tube area ratio per segment of evaporator. The design conditions were as follows:

- Freezer and fresh-food loads: 100W
- Evaporator pressure: 180 kPa

- Condenser pressure: 1020 kPa
- Evaporator fan flow rates: 20 CFM (equivalent to 0.54 m/s air velocity)
- Refrigerant: 65% R22/35% R123

The minimum mass design under these conditions was:

- Freezer evaporator: eight 53.34 cm (21 in) passes
- Fresh-food evaporator: four 53.34 cm (21 in) passes
- Low-temperature intercooler: 0.40 m long
- High-temperature intercooler: 0.74 m long

The intercoolers were helically wrapped and soldered.

The air-side performance of the these evaporators were determined by Heun to be equivalent to a standard Peerless evaporator. Even if the air-side performance was significantly different from the standard evaporator there would have been no change in the results of this study. The air-side characteristics for these experimental evaporators built by Heun are determined in Chapter 4 and used through out the remainder of the study.

Evaporators

The two evaporators for the project were built in-house. One of the secondary objectives of the project was to experiment with new evaporator construction techniques that allowed flexibility in the design and construction of the evaporators.

The techniques centered around bonding the fin stock to the tubes with adhesive, as opposed to the current pressure-fit methods. Epoxying the fin stock provides two main advantages over pressure-fit designs:

1. ***Reduced fin stock thickness.*** Larger fin stock is required for the pressure-fit designs, since the fin stock must be thick enough to maintain its shape when the tube is forced through the tube opening.

2. ***Independent fin rows.*** Independent evaporator fin rows help minimize the thermal communication between neighboring tubes and preserve the refrigerant-mixture glide. Thermal communication may short circuit the refrigerant-temperature glide. For standard evaporators now used in domestic refrigerators, thermal communication

exists between adjacent tube passes because of the continuous fin plates. With epoxied fins, fin rows are independent, allowing the flexibility of staggering the application of the fins to the tube passes. This staggering improves the heat transfer efficiency of the exchanger by breaking the air's thermal and hydrodynamic boundary layer as it passes over the exchanger.

The tube circuiting was arranged in a cross counter-flow pattern. The heat exchangers should be a full counter-flow design to take full advantage of the refrigerant-mixture glide. Since this is not practical in the limited space of a refrigerator, a cross counter-flow design is the best exchanger flow configuration to use. The basic evaporator construction detail can be seen in Figure 3.4.

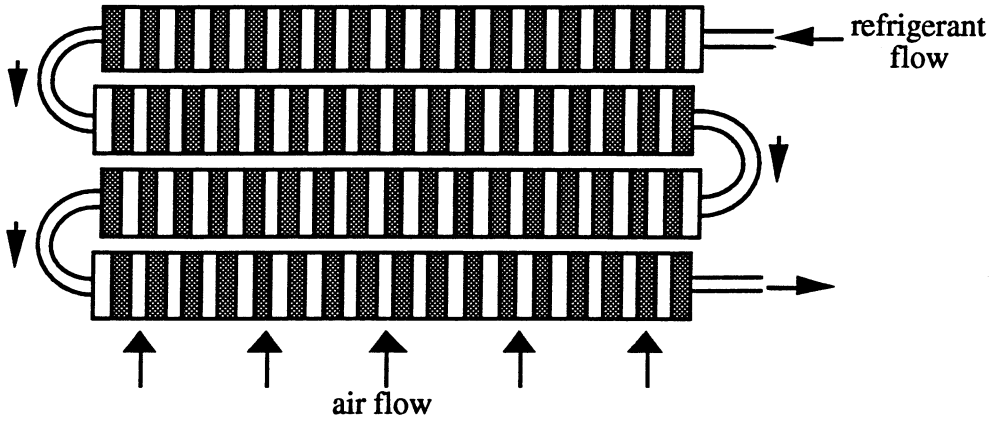

Figure 3.4: Basic evaporator construction

When the fins were bonded to the tubes, the thermally conductive epoxy was forced out from between the fin stock and tube forming a fillet at the interface. This was beneficial because it reduced the thermal resistance between the fin and the tube (more metal to metal contact) and helped strengthen the fin/tube bond. At the end of the experiments, the evaporators were examined for fin/tube separation possibly caused by the numerous thermal cyclings. Only an insignificant number of separations had occurred. It could not be determined if these separations had occurred because of exchanger handling.

Figure 3.5 shows the basic dimensions of the two evaporators. The freezer evaporator had eight passes, with a total height of 20.32 cm (8 in.). The fresh-food evaporator had only four passes and a height of 10.16 cm (4 in.). More construction details for the evaporators can be found in Heun's thesis.[3]

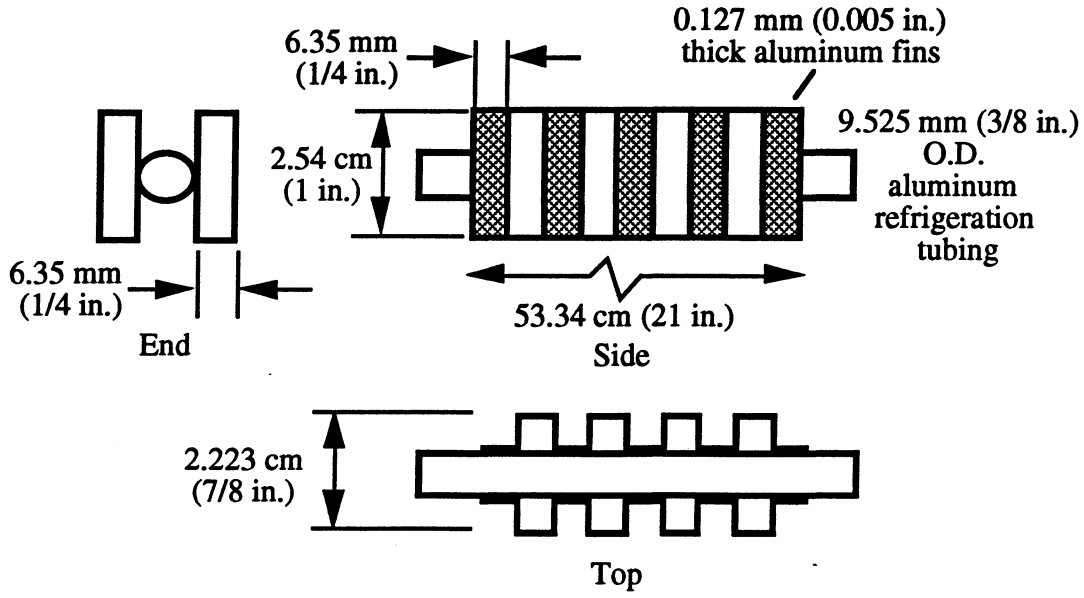

Figure 3.5: Basic evaporator dimensions

The evaporators were enclosed in a Plexiglas housing that served as an air duct over the exchanger. A hole was cut into the face of the Plexiglas to install the evaporator fan. As shown in Figure 3.6, a small air dam was installed inside the cavity just below the fan to prevent a high-velocity air core from developing at the center of the evaporator duct. The air-flow distribution was checked with an anemometer.

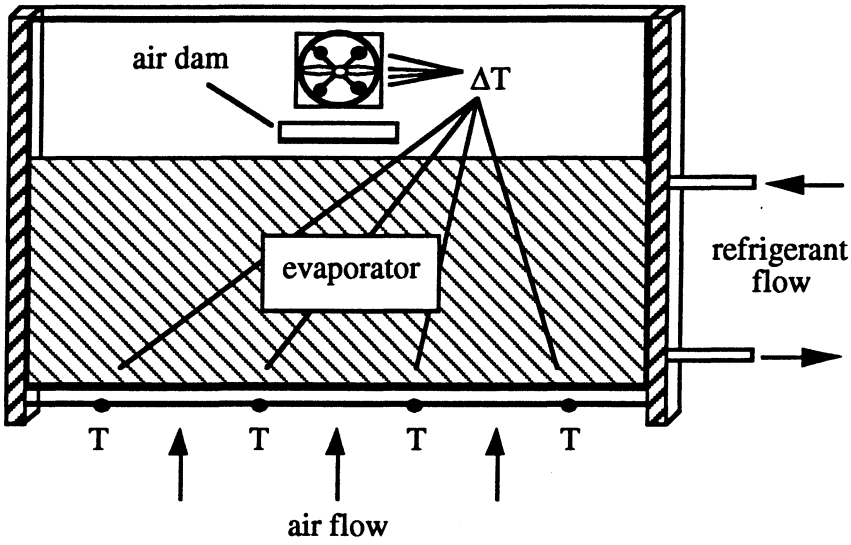

Figure 3.6: Mounted evaporator showing thermocouple locations

A ΔT thermocouple array was wired between the inlet and outlet to the case. Four inlet ΔT thermocouples were attached to a wire stretched across the inlet to the case. The

corresponding ΔT outlet thermocouples were attached to two wires stretched across the outlet of the case behind the evaporator fan.

The fan was mounted to the face of the case with screws and could easily be replaced with a higher or lower CFM model. There were two sets of fans used in the experiments. All four fans were commercially-available computer cooling fans. A three-bladed model was used for the air velocity range of 0.4 to 1.0 m/s. A five-bladed model was used for the air velocity range of 1.2 to 1.8 m/s. Both fans were controlled by variacs that were placed in each cabinet compartment. The power input to the variac was measured by a watt meter that was a part of the load control system explained in Appendix H.

The evaporator cases sat in the back of an insulated box on the two case support legs. The freezer evaporator case entirely covered the back of the freezer compartment. The fresh-food case was placed in the bottom of the fresh-food compartment. The ideal placement for the fresh-food evaporator would be in the top of the compartment where the air circulation and mixing could be aided by the relative density difference of the inlet and outlet air. For the experiments, the fresh-food case had to be placed in the bottom of the compartment to avoid the additional plumbing necessary to attach the intercoolers. Since a hair dryer was installed in the top of the compartment to ensure uniform air mixing, the placement of the case in the bottom of the fresh-food compartment was of no concern. Frosting of the evaporators was prevented by the placement of a desiccant in pans at the bottom of each compartment. The desiccant adsorbed any excess moisture in the compartment. The formation of frost would have complicated the heat transfer measurements performed in the experiment.

Thermocouples were installed in each compartment to measure the mixed air temperature. The thermocouples, along with the inlet and ΔT thermocouples, were attached to a terminal block located in each compartment. The evaporator was connected to the refrigeration loop with Gyrolok fittings. Care had to be taken to avoid damaging the aluminum tube by over-tightening the fittings.

Intercoolers

Two helically-wrapped and soldered intercoolers (see Figure 3.7) were built in-house. The high-temperature intercooler was 0.74 m long, and the low-temperature intercooler was 0.40 m long. The intercooler was constructed out of 9.525 mm (3/8 in.) and 3.175 mm (1/8 in.) diameter copper tubing. The smaller, high-pressure tubing was helically wrapped around the larger, low-pressure tubing. The two tubes were soldered together. Both intercoolers were well

insulated and placed vertically in the fresh-food compartment as shown in Figure 3.2. All tubing connections were Gyrolok fittings. Of several designs considered, the helically-wrapped and soldered intercooler was the best performing design.[4]

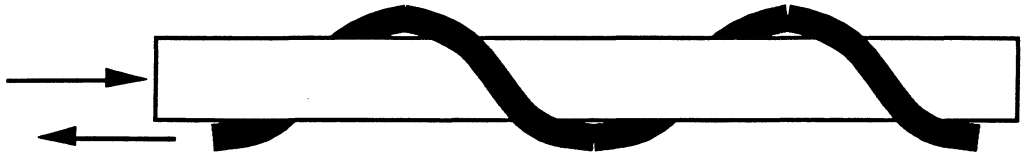

Figure 3.7: Intercooler design - 3.175 mm (1/8 in.) copper tubing soldered and helically wrapped around 9.525 mm (3/8 in.) copper tubing

The intercoolers were placed vertically in the refrigerator cabinet as shown in Figure 3.2. This was done because the high-temperature intercooler was too long the place horizontally in the cabinet. There was some concern that the vertical orientation of the intercoolers would cause slugging to occur in the entrance and exit of the fresh-food evaporator altering the measured results. (Slugging could enhance the convective boiling component of the boiling heat transfer coefficient.) The only place that slugging would have a tendency to occur would be at the exit of the evaporator because of the refrigerant having to travel up through the high-temperature intercooler. However, at this point, the quality of the refrigerant is high enough that there would not be enough liquid accumulation to back up into the fresh-food evaporator. There should be no slugging at the entrance of the evaporator because the quality of the refrigerant is reasonable high at this point and the flow continues *downward* through the evaporator from the low-temperature intercooler which prevents liquid from backing up and forming slugs at this point.

3.2.15 Refrigerator Cabinet

An integral part of the system was the refrigerator cabinet. The cabinet was constructed out of commercially available foam board and had the same internal dimensions as a top-mount 18 ft^3 (0.5097 m^3) refrigerator. A complete discussion on the construction and reverse heat-leak testing for the cabinet mockup can be found in Appendix G.

3.3 Instrumentation

The instrumentation inputs were read with a Fluke 2240A Datalogger. All inputs were scanned every six seconds. The data was downloaded to a Macintosh SE microcomputer through the serial port of the Fluke at 4800 baud. Table 3.2 lists the data measured in this experiment. A 24-volt power supply powered the 4-20 mA outputs of the pressure transducers and the mass-flow meter. The output voltage drop was provided by a 250 Ohm precision resistor at the input

terminal of the Fluke. Each resistance was measured and used in the conversion equation, Equation 3.1. Appendix I contains a detailed description of the data acquisition program, run on the Macintosh, and a program listing.

$$\text{value} = \left(\frac{\text{voltage}}{\text{resistance}} \times 1000 - 4\text{mA} \right) \left(\frac{\text{full scale output}}{20\text{mA} - 4\text{mA}} \right) \tag{3.1}$$

Table 3.2: Measured quantities and their Fluke channel number

measurement	Fluke channel number
ambient temperature	30
refrigerant temperature at chiller outlet (Tc)	46
refrigerant temperature at pump outlet (Tp)	47
T1*	31
T2	32
T3	33
T4	34
T5	35
T6	36
T7	37
T8	38
refrigerant pressure at pump outlet (Pp)	55
P1	56
P3	51
P4	57
P8	58
freezer evaporator air-inlet temperature	40
freezer evaporator air-temperature difference	41
freezer compartment air-temperature	42
fresh-food evaporator air-inlet temperature	43
fresh-food evaporator air-temperature difference	44
fresh-food compartment air-temperature	45
freezer evaporator load	53
fresh-food evaporator load	54
mass-flow meter	59

* refer to Figure 3.1 and 3.2 for definition of T# and P#

3.3.1 Thermocouples

Temperature measurements in the refrigeration loop were made with Omega type-T thermocouple probes. These probes were 1.5875 mm (1/16 in.) in diameter, 30.48 cm (12 in.) long and ungrounded. The location of the thermocouple probes in the refrigeration loop is shown in Figure 3.2. The probes were cut to custom lengths for each application. Care was taken to place each probe into the refrigerant flow as shown in Figure 3.8. All of the air-temperature measurements were made with welded type-T thermocouple wire placed in the insulated box compartments and in each evaporator case as shown in Figure 3.6.

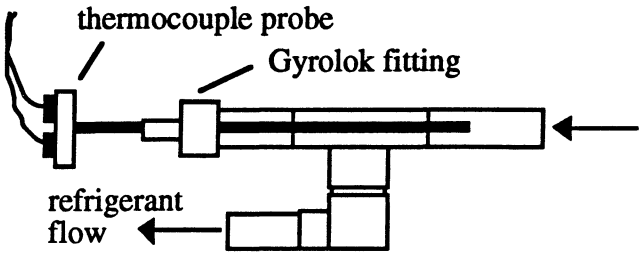

Figure 3.8: Thermocouple probe mounting in refrigeration loop

3.3.2 Pressure Transducers

Five Setra C-280E pressure transducers were used in the refrigeration loop, as shown in Figure 3.2. To prevent thermal transducer error, the transducers were not placed in the insulated box where the temperature was much lower than ambient. The transducers were connected to the loop with a copper tee and Gyrolok fittings. The pressure transducers were calibrated with a large mechanical gauge that had been calibrated on a dead weight pressure tester. Of the five transducers, two were low pressure, 0 - 689.3 kPa (0 - 100 psia), and the remaining three were high pressure, 0 - 3446.4 kPa (0 - 500 psia).

3.3.3 Watt Transducers

Two Scientific Columbus XL5C5A2 watt meters were used as a part of the evaporator load control system. The load control system is described in Appendix H. The outputs of the units were checked with a commercially available energy analyzer. The fresh-food watt transducer was found to read a consistent 2.4W higher than the actual value. The error was corrected by adjusting the fresh-food compartments power reading in the data acquisition software.

3.4 System Operation

The startup procedure for the refrigeration loop begins with the full opening of the expansion valve and the pump bypass valve. The heater control unit is switched off and the temperature set points in the load control systems are lowered. Lowering the set point on the load control system ultimately helps the compartment reach a steady-state more quickly. The heat control unit has no power because the emergency shut down system, as described in the mass-flow meter section, cuts the power off to the heater unit when the mass-flow drops below a preset value. The chiller and the gear pump are switched on, and dry ice is added to the subcooler. The pump is set to the highest rate to circulate as much refrigerant as possible back through the chiller. After the refrigerant has circulated for approximately five minutes, the pump

bypass valve is quickly closed allowing refrigerant to flow through the rest of the loop. The evaporator load systems are automatically switched on as soon as refrigerant flows through the mass-flow meter. (Only the evaporator fans and the circulation fans in the hair dryers are switched on. The temperatures in the compartments are not low enough to activate the load control heaters). The expansion valve is adjusted to achieve a high-side pressure of approximately 800-1000 kPa. As the compartments start to cool down, the mass-flow rate is lowered by slowing the pump, and the high-side pressure is maintained by closing the expansion valve. The operator has to balance the pressure rise and the mass-flow rate reduction when the expansion valve is closed with pump speed. As the mass-flow rate decreases, the evaporating pressure drops slightly, and the outlet state of the evaporator module starts moving towards the saturated vapor line and the superheat region. When the low-side pressure reaches approximately 170.3 - 204.7 kPa (10-15 psig) and the outlet state of the evaporator module has moved out into the superheat region, the diaphragm pump is brought on-line.

To bring the diaphragm pump on-line, the diaphragm pump bypass valve is opened, the pump and its cooling fans are switched on, the three-way valves are simultaneously turned to put the pump on-line, and finally, the bypass valve is closed. The system must be watched closely as the pump is brought on-line. Care must be taken not to slug the compressor by moving the outlet state of the evaporator module back into the two-phase region.

When the compartment temperatures drop below the desired temperatures, the load control set points are brought up to the desired set points. The refrigerant heater is switched on and the 'condenser outlet' temperature is set. The dry ice bath must be periodically checked and dry ice added as needed. The system is run for up to several hours while it achieves steady-state operation. The data acquisition screen output indicates when steady-state has been reached, as explained in Appendix I.

3.4.1 Air Velocities

The average air velocity over the evaporators were controlled by adjusting the voltage to the evaporator fans with the variacs. Once a change was made, it took up to ten minutes to reach a new steady state. The air velocities were obtained from an energy balance about the air, as shown in Equation 3.2.

$$\bar{v} = \frac{q}{\rho A c_p \Delta T} \tag{3.2}$$

Total evaporator load, q, is the sum of the load measured from the load control system and the heat-leak load from ambient into that compartment. The density, ρ, and specific heat, c_p, are calculated from air curve fits as functions of temperature. The temperature difference over the evaporator, ΔT, is measured. The cross sectional area, A, is known, so the velocity can be easily calculated.

3.4.2 Superheat

Superheat can be controlled in several different ways. Any system adjustment made that changes the location of state point 8, shown in Figure 3.1, could effect the amount of system superheat. Since the intercooler loads are internal and $h_3 = h_4$, the total refrigerant-side load on the evaporator module is the product of the mass-flow rate and the difference between the outlet and inlet enthalpy to the module as shown in Equation 3.3.

$$q_{tot} = q_f + q_{ff} = \dot{m}(h_8 - h_1) \tag{3.3}$$

Superheat was adjusted during the runs in three ways: (1) changing the heater input level, (2) changing the mass-flow rate or (3) changing the evaporator loading. The heater was used when it was necessary to change the superheat level within a local range of operating conditions. Turning the heater up moved state point 1 to the right and closer to the saturation dome. If the mass-flow rate and total load remained constant, then state point 8 was shifted proportionately further to the right to a higher level of superheat. Turning the heater down causes the exact opposite process to happen.

The superheat level at the exit of the evaporator module was sometimes varied by changing the mass-flow rate of refrigerant. Increasing the mass-flow rate moved state point 8 from the superheat region into the saturation dome. Decreasing the mass-flow rate caused the opposite effect. Maintaining a constant module load, q_{tot}, as mass-flow rate increased led to a decrease in the enthalpy difference. As mass-flow rate decreased, the enthalpy difference increased. If state point 1 is fixed, then state point 8 moves accordingly as the mass-flow rate is adjusted.

A third way to adjust superheat was to change q_{tot}, the sum of the freezer and fresh-food evaporator loads. The evaporator loads could be changed in two ways. The first way was to change the set-point temperature of the load controller. Increasing the temperature increased the evaporator load, moving state point 8 further out into the superheat region. The second way to change the evaporator loads was to increase the air velocity over the evaporator. Again, this

served to increase the evaporator load and move state point 8 further out into the superheat region. To reduce superheat, the opposite procedure would apply.

3.4.3 Subcooling

Subcooling can be adjusted in several ways. The primary way is to adjust the heater. This moves state point 1 but, as discussed in the previous section, state point 8 is also moved. A compensating adjustment is required to maintain the superheat level with one of the other methods described in the last section. Another method for adjusting subcooling would be to increase or decrease the high-side pressure in the system. Increased subcooling could be accomplished by increasing the pump speed and simultaneously closing the expansion valve to raise the high-side pressure.

3.4.4 Mass-Flow Rate

Mass-flow rate was primarily adjusted by changing the gear pump speed. An increase in pump speed led to an increase in the mass-flow rate. Opening the expansion valve would also increase mass-flow. In general, the best method for achieving a desired mass-flow rate involved adjusting both pump speed and the expansion valve to some degree.

3.4.5 High-Side Pressure

High-side pressure was adjusted in a similar fashion. The primary method for adjusting high-side pressure involved the expansion valve, although the pump speed could also be used. To raise the high-side pressure, the pump speed could be increased or the expansion valve could be closed.

3.4.6 Mass-Flow Rate and High-Side Pressure

Achieving the desired mass-flow rate and high-side pressure was an iterative process. Since the two conditions are coupled, adjusting one affects the other. If mass-flow is increased by increasing the pump speed, the high-side pressure also rises. The expansion valve must then be opened further to lower the high-side pressure back to the desired level. This in turn further increases the mass-flow rate, possibly beyond the desired setting. The pump speed, which is then slowed to lower the mass-flow rate, may lower the high-side pressure too much, necessitating closure of the expansion valve to bring the pressure back up. When the expansion valve is closed, the mass-flow rate drops. This entire process is continued until a satisfactory mass-flow rate and high-side pressure are achieved.

3.5 Test Mixtures

The research mixtures were chosen by the USEPA. The first pair, 65% R22/35% R123, was the best pair, based on previous testing in actual refrigerators. The second pair, 80% R22/20% R141b, was the best pair according to the EPA refrigerator model.[5] The less volatile components in each mixture, R123 and R141b, are potential replacements for R11. Both of these NARMs have a temperature glide of approximately 30°C at typical refrigerator operating conditions in keeping with the recommendations of Lorenz and Meutzner[6] for refrigerator applications. These mixtures are *representative* of the NARMs that could be used in domestic refrigerators. Since the selection of these fluids in 1989, the phase out of R22 has been agreed upon; therefore, the results of this study cannot *directly* apply to NARMs under consideration currently. However, the performance and economic *trends* from this study could be extended to include these newer mixtures.

Table 3.3 lists the mixture components and pure refrigerants used in this study. The manufacturing costs were estimated based on conversations in February, 1991 with the suppliers of the chemicals. The R123 was provided by Allied Signal, courtesy of Mr. Ted Atwood. The R141b was provided by Elf Atochem North America, courtesy of Mr. Dick Crooker.

Table 3.3: List of research chemicals used in this experiment

name	formula		MW(kg/kmol)	NBP (°C)	ODP	GWP	cost ($/kg)
CFC12	CCl_2F_2	Dichlorodifluoromethane	120.91	-29.79	1.0	3.0	8.60
HCFC22	$CHClF_2$	Chlorodifluoromethane	86.47	-40.76	0.051	0.47	4.23
HCFC123	$CHCl_2CF_3$	Dichlorotrifluoroethane	152.93	27.17	0.018	0.026	~16.00
HCFC141b	CH_3CCl_2F	Fluorodichloroethane	116.95	31.8	0.1	<0.087	~5.00

Also listed in Table 3.3 are the GWP and the ODP of the chemicals. Notice the low values of GWP and ODP for R123 and R141b. These are potential R11 replacements. R11 has a GWP of 1.0 and a ODP of 1.0. The GWP and ODP scales are based on R11. The manufacturing cost of R123 is much greater than R141b.

3.5.1 Thermodynamic and Physical Property Equations

The thermodynamic properties of these mixtures were calculated using the NIST CSD equations of state. Appendix J briefly explains the equations and lists the different fluids that can be simulated. The equations were incorporated into a FORTRAN subroutine library and were easily called by other FORTRAN programs. The physical properties for the mixtures were required for calculation of many of the relevant non-dimensional numbers. Appendix A

describes the physical property equations for the pure refrigerants R12, R22 and R134a and the refrigerant mixtures R22/R123 and R22/R141b.

3.5.2 Charging

The system charging procedure is covered in Appendix B.

3.6 References

---

[1] Personal communication with Dr. Don Bivens at DuPont Chemicals, Fluorochemicals Lab, March, 1992.

[2] Heun, M. K., "Thermal Performance Analysis of an Evaporator-Intercooler Module for a Lorenz Cycle", Master's Thesis, Department of Mechanical and Industrial Engineering, University of Illinois at Champaign-Urbana, 1991.

[3] Heun, M. K., "Thermal Performance Analysis of an Evaporator-Intercooler Module for a Lorenz Cycle", Master's Thesis, Department of Mechanical and Industrial Engineering, University of Illinois at Champaign-Urbana, 1991.

[4] Heun, M. K., "Thermal Performance Analysis of an Evaporator-Intercooler Module for a Lorenz Cycle", Master's Thesis, Department of Mechanical and Industrial Engineering, University of Illinois at Champaign-Urbana, 1991.

[5] Information received by Dr. Roy Crawford from Bob Hendriks at USEPA, Research Triangle Park, N. C., December, 4, 1990.

[6] Lorenz, A. and K. Meutzner, "On Application of Non-Azeotropic Two-Component Refrigerants in Domestic Refrigerators and Home Freezers", XIV International Congress of Refrigeration, Paper B2.42, 1975 Moscow.

CHAPTER 4: PURE-REFRIGERANT RUNS: R12 AND R22

This chapter explains how the air-side performance data were obtained for the freezer and fresh-food experimental evaporators. The test loop was charged with R12 and experiments were conducted over a defined range of air-flow rates and flow conditions. The R12 was removed and replaced with R22. The R22 experiments were conducted over a similar range of air-flow rates and flow conditions. Next, a proper refrigerant correlation was chosen which was equally valid for R12 and R22 at low heat and mass flux flow conditions. Utilizing the refrigerant correlation, the air-side resistance as a function of air velocity was calculated by performing an energy balance about each evaporator.

4.1 R12 Runs

Fifty-six experimental R12 runs yielding 112 data points were made over a range of conditions listed in Table 4.1. Six runs were rejected because the outlet state of the evaporator module had slipped into the saturation dome and there was no way to determine the state point location with only temperature and pressure measurements. Figure 4.1 shows the total energy balance error for the runs. All runs were within the error range of +2% to -7%. The error was calculated using Equation 4.1, which compared the heat-leak from the surroundings into the cabinet plus the energy supplied to the load control system from each compartment, $Load_f + Load_{ff}$, with the calculated energy absorbed by the refrigerant, $\dot{m}_r(h_g - h_l)$. The runs conditions were varied by adjusting the air-flow rate over each evaporator from approximately 0.4 m/s to 1.8 m/s in 0.2 m/s intervals (15 CFM to 67.5 CFM in 7.5 CFM intervals). The mass-flow rate and high-side pressure were adjusted to maintain reasonable values of subcooling and superheat. All valid runs had some degree of superheat at the evaporator module exit. As

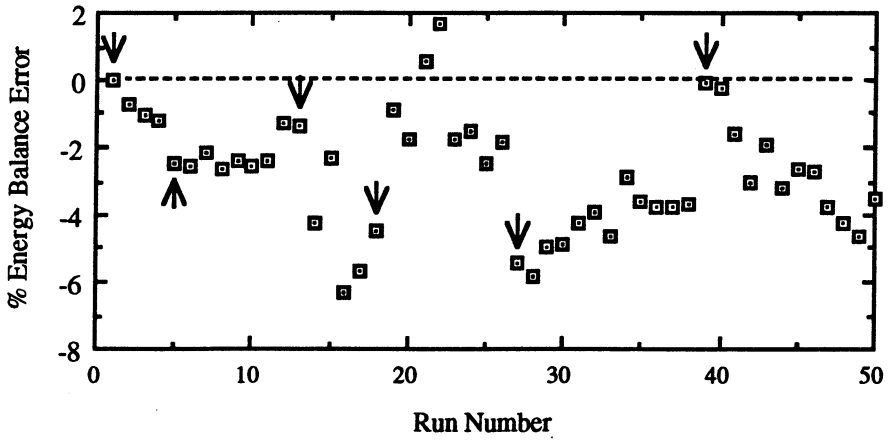

Figure 4.1: Total energy balance error for R12 runs

mentioned above, this technique allowed identification of the module outlet state point. Table 4.1 lists other pertinent conditions maintained or measured during the course of the R12 runs.

Table 4.1: Statistics on R12 runs

quantity	low	high	average
mass flux (kg/m^2-s)	38.9	65.1	53.4
heat flux, freezer evaporator (kW/m^2)	0.97	2.61	1.85
heat flux, fresh-food evaporator (kW/m^2)	1.89	3.94	3.12
evaporating temperature (°C)	-24.6	-12.4	-17.5
quality, freezer evaporator	0.01	0.48	0.25
quality, fresh-food evaporator	0.51	0.90	0.70
load, freezer evaporator (W)	103.0	276.5	193.4
load, fresh-food evaporator (W)	133.8	208.3	171.7
effectiveness, freezer evaporator	0.43	0.64	0.53
effectiveness, fresh-food evaporator	0.28	0.56	0.39
UA, freezer evaporator (W/K)	7.70	22.62	16.70
UA, fresh-food evaporator (W/K)	6.48	13.48	10.17
load, high-temp intercooler (W)	-	-	58.74
load, low-temp intercooler (W)	-	-	13.1
effectiveness, high-temp intercooler	-	-	0.82
effectiveness, low-temp intercooler	-	-	0.56
UA, high-temp intercooler (W/K)	-	-	4.35
UA, low-temp intercooler (W/K)	-	-	2.27
compartment temp., freezer section (°C)	-6.9	4.6	-0.6
compartment temp., fresh-food section (°C)	0.8	6.4	4.2
module subcooling (°C)	6.3	31.7	18.4
module superheat (°C)	2.1	29.4	12.7
module pressure drop (kPa)	1.31	6.15	4.48
air velocity, freezer evaporator (m/s)	0.39	1.75	1.00
air velocity, fresh-food evaporator (m/s)	0.38	1.80	0.95
refrigerant - side resistance, freezer evaporator (%)	15.0	31.9	23.2
refrigerant - side resistance, fresh-food evaporator (%)	18.8	26.4	23.0
refrigerant heat transfer coeff., freezer evaporator (W/m^2-K)	484.0	846.3	683.4
refrigerant heat transfer coeff., fresh-food evaporator (W/m^2-K)	650.3	962.8	835.1
air heat transfer coeff., freezer evaporator (W/m^2-K)	9.1	33.4	22.2
air heat transfer coeff., fresh-food evaporator (W/m^2-K)	16.1	36.9	26.8

$$\text{Error} = \frac{\dot{m}_r(h_8 - h_1) - (\text{Load}_f + \text{Load}_{ff})}{(\text{Load}_f + \text{Load}_{ff})} \qquad (4.1)$$

Figure 4.1 shows an apparent periodicity to the data. After examining the data, it was concluded that this is start-up error for the system. The arrows in Figure 4.1 are the first runs for that day. These data were taken over six separate days. Even though the system was run two to three hours before taking the first set of data, the system was not completely at steady-state. The final energy balance errors for each day tend toward the -2% to -4% range.

Several significant points about the information in Table 4.1:

- The average heat flux is higher in the fresh-food evaporator because of the decreased tube surface area. The fresh-food evaporator was four passes and the freezer evaporator was eight passes.

- The average freezer and fresh-food evaporator effectivenesses for these runs were 53% and 39% respectively. The UA values for the evaporators varied as the air velocity over them was varied. The average freezer and fresh-food evaporator UAs for these runs were 16.70 and 10.17 W/K respectively.

- The average high-temperature and low-temperature intercooler effectivenesses for these runs were 82% and 56% respectively. The average high-temperature and low-temperature intercooler UAs for these runs are 4.35 and 2.27 W/K respectively.

- It was originally intended to maintain an average freezer compartment temperature of -15 °C and an average fresh-food compartment temperature of 5°C. This proved to be impractical, particularly for the pure refrigerants. The -15°C freezer compartment temperature (-25 °C refrigerant temperature) was at the lower limit of what the test loop could supply to the evaporator module. If this compartment temperature was attempted, the freezer load would have had to be lowered significantly. Low loads on the evaporator were difficult to maintain due to load controller instabilities; furthermore, the time required for the freezer compartment to come to steady-state after a load change would have been prohibitively long.

- Positive values of subcooling were maintained at all times to prevent the cable heater from burning out due to surface dry-out.

- As mentioned above, all pure-refrigerant runs had superheat to enable the calculation of the module exit state point.

- The refrigerant's average pressure drop through the evaporator module was small at 4.48 kPa (0.65 psi).

- The average refrigerant-side resistance for the two evaporators was approximately 23%. The fresh-food evaporator experienced higher average refrigerant and air

heat transfer coefficients. The increase in both of the coefficients was such that the average refrigerant-side resistance stayed the same. The 23% refrigerant-side resistance is reasonable and in-line with values obtained by Admiraal and Bullard.[1]

- The refrigerant heat transfer coefficients were calculated from a correlation. This correlation is valid for R12, R22 and R134a in the low heat and mass flux range.
- The air heat transfer coefficients were obtained by performing an energy balance about each evaporator. The calculation method will be discussed later in this chapter.

4.2 R22 Runs

Similar sets of runs were made with R22. Thirty-nine experimental runs yielding 78 data points were made over a range of conditions listed in Table 4.2. Figure 4.2 shows the total energy balance error for the runs calculated from Equation 4.1 which consistently tended toward -2%. The startup and final energy balance error for the R22 runs is more predictable than the R12 error. For R22, a lower evaporating pressure was able to be maintained which improved load control stability provided by the load-control system. The start-up error is apparent for the data taken over four separate days. The run conditions were varied by adjusting the air-flow rate over each evaporator from approximately 0.4 m/s to 1.8 m/s in 0.2 m/s intervals (15 CFM to 67.5 CFM in 7.5 CFM intervals). The mass-flow rate and high-side pressure were adjusted to maintain reasonable values of subcooling and superheat. Table 4.2 lists other pertinent conditions maintained or measured during the course of the R12 runs.

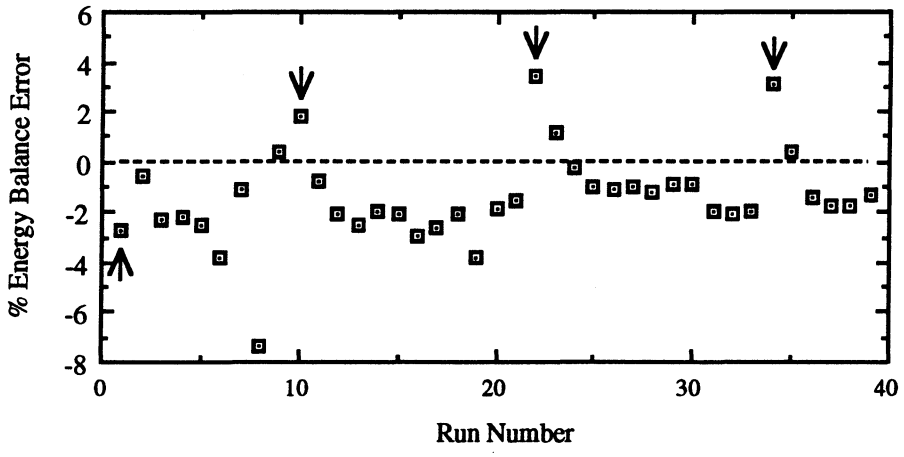

Figure 4.2: Total energy balance error for R22 runs

Table 4.2: Statistics on R22 runs

quantity	low	high	average
mass flux (kg/m^2-s)	34.7	51.9	46.2
heat flux, freezer evaporator (kW/m^2)	1.64	2.82	2.39
heat flux, fresh-food evaporator (kW/m^2)	2.37	4.3	3.45
evaporating temperature (°C)	-33.0	-22.3	-25.9
quality, freezer evaporator	0.01	0.51	0.26
quality, fresh-food evaporator	0.55	0.91	0.73
load, freezer evaporator (W)	173.8	298.8	253.0
load, fresh-food evaporator (W)	125.2	227.5	182.2
effectiveness, freezer evaporator	0.44	0.65	0.54
effectiveness, fresh-food evaporator	0.28	0.57	0.41
UA, freezer evaporator (W/K)	10.01	23.21	17.75
UA, fresh-food evaporator (W/K)	6.92	13.71	10.17
load, high-temp intercooler (W)	-	-	70.34
load, low-temp intercooler (W)	-	-	20.06
effectiveness, high-temp intercooler	-	-	0.75
effectiveness, low-temp intercooler	-	-	0.67
UA, high-temp intercooler (W/K)	-	-	4.96
UA, low-temp intercooler (W/K)	-	-	2.95
compartment temp., freezer section (°C)	-5.5	-4.3	-5.0
compartment temp., fresh-food section (°C)	-4.8	3.8	-2.4
module subcooling (°C)	3.0	22.8	13.1
module superheat (°C)	6.9	29.6	18.3
module pressure drop (kPa)	2.36	4.33	3.37
air velocity, freezer evaporator (m/s)	0.40	1.70	1.02
air velocity, fresh-food evaporator (m/s)	0.40	1.77	0.93
refrigerant - side resistance, freezer evaporator (%)	14.7	23.5	19.9
refrigerant - side resistance, fresh-food evaporator (%)	17.7	24.8	20.7
refrigerant heat transfer coeff., freezer evaporator (W/m^2-K)	638.7	932.7	823.4
refrigerant heat transfer coeff., fresh-food evaporator (W/m^2-K)	744.0	1050.0	955.9
air heat transfer coeff., freezer evaporator (W/m^2-K)	11.8	30.5	22.2
air heat transfer coeff., fresh-food evaporator (W/m^2-K)	16.9	36.6	26.9

Several significant points about the information in Table 4.2:

- The average freezer and fresh-food evaporator effectivenesses for these runs were 54% and 41% respectively. The average freezer and fresh-food evaporator UAs for these runs were 17.75 and 10.17 W/K respectively.

- The average high-temperature and low-temperature intercooler effectivenesses for these runs were 75% and 67% respectively. The average high-temperature and low-temperature intercooler UAs for these runs are 4.96 and 2.95 W/K respectively. Both the effectivenesses and the UAs for the evaporators and the intercoolers were very similar to the results from the R12 runs.

- The test loop was able to maintain a lower evaporating temperature for the R22 runs. As a result, the average freezer compartment temperature for the R22 runs was approximately 5°C lower than the R12 runs at -5°C.
- The refrigerant's average pressure drop through the evaporator module was small at 3.37 kPa (0.49 psi).
- The average refrigerant-side resistance is slightly lower than the R12 runs at approximately 20%. This is a consequence of the higher average refrigerant heat transfer coefficients of R22.
- The refrigerant heat transfer coefficients were calculated from a correlation as discussed in the next section.
- The air heat transfer coefficients were obtained by performing an energy balance about each evaporator.

4.3 Choosing the Pure-Refrigerant Correlation

Before the energy balances could be performed about each evaporator, a suitable pure-refrigerant correlation had to be selected. This section will cover the selection process. Many refrigerant correlations are developed primarily from data taken at mass and heat fluxes greater than 100 kg/m^2-s and 10 kW/m^2, respectively. The dominant flow regime at these conditions is annular, with nucleate boiling generally present at qualities less than 50 or 60%. (The quality at which nucleate boiling is totally suppressed is determined by the flow conditions, especially the level of heat flux. For nucleate boiling to be present for annular flows at a quality of 50% or greater, the heat flux would have to be extremely high - - greater than 25 kW/m^2.) These flow conditions typify those found in window air conditioners, heat pumps and stationary air conditioners. In domestic refrigerator evaporators, the mass fluxes are below 60 kg/m^2-s and heat fluxes are less than 2.5 kW/m^2. In this range, the flow pattern is predominately wavy/stratified. The question arises: are the correlations developed primarily from the annular flow data valid to use for wavy/stratified flow?

The section will begin with examining the flow regimes for the experimental data utilizing a flow map. The flow map will reveal that the flow regime for the data is predominately wavy/stratified. A correlation developed at the UIUC for R12 is examined as a potential candidate because of its development from wavy/stratified data. The UIUC R12 correlation is compared to two other well-known refrigerant correlations which were developed from data over

a much larger range, and included the wavy/stratified and annular flow regimes. The results of the three correlations are similar; therefore the UIUC R12 correlation is chosen to reduce the experimental data. (The UIUC R12 correlation was equally valid for R22 data as well.[2])

4.3.1 Flow Map

The R12 and R22 data were plotted on a modified Baker[3] flow map. The Baker map was modified by Scott[4] to include an uncertainty band between the flow regime regions. As shown in Figure 4.3, all the data fall within the uncertainty band about the wavy flow regime. The fresh-food data are to the left and the freezer data are to the right. The higher vapor velocity at higher qualities shifts the fresh-food data to the left. As described in Chapter 2, the x and y axis of the Baker (Scott) map are the gas- and liquid phase mass fluxes multiplied by ratios of their fluid properties to those of air and water. The Baker map is based on water-air and oil-air experimental data. Equations 4.2 to 4.5 show how the x and y coordinates are determined.

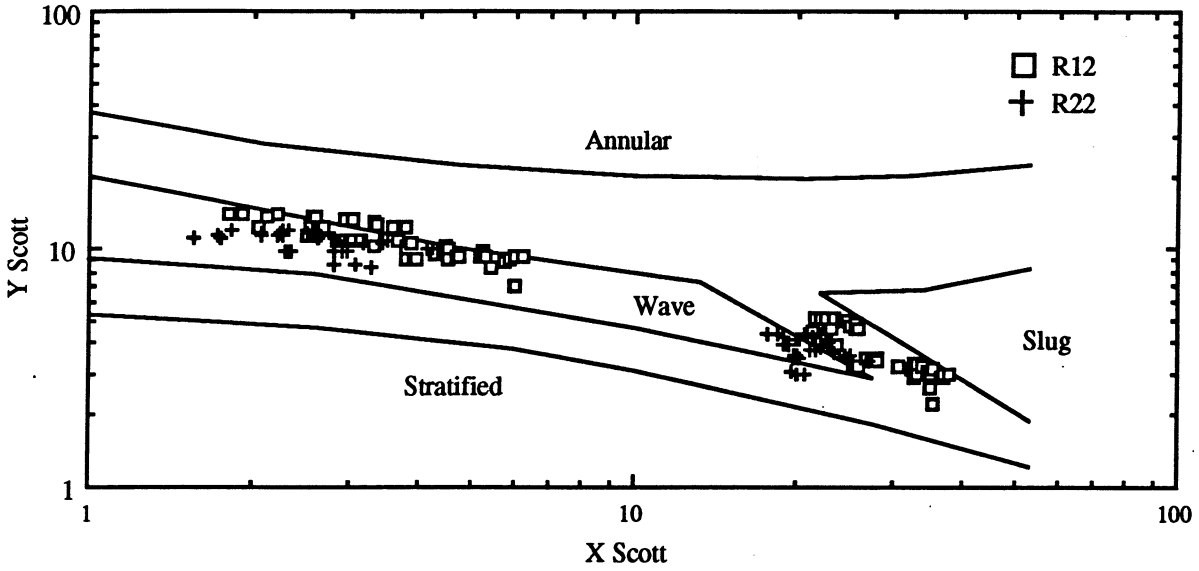

Figure 4.3: Scott flow map for predicting pure-refrigerant flow regimes

$$\text{Y Scott} = \frac{G_v}{\lambda} \tag{4.2}$$

$$\text{X Scott} = \left(\frac{G_l}{G_v}\right)\lambda\,\phi \tag{4.3}$$

where:

$$\lambda = \left(\frac{1}{16}\right)\left[\left(\frac{\rho_v}{0.075}\right)\left(\frac{\rho_l}{62.3}\right)\right]^{0.5} \tag{4.4}$$

$$\phi = \left(\frac{73.0}{\sigma}\right)\left((\mu_l)\left(\frac{16*62.3}{\rho_l}\right)^2\right)^{1/3} \tag{4.5}$$

4.3.2 Correlation Comparison

The use of a flow map is the first step in selecting a correlation for the experimental runs. The map indicates that the data are wavy/stratified; therefore, a suitable correlation would need to cover this flow regime. As mentioned above, the wavy/stratified-flow regime is characteristic of low heat and mass flux flow conditions. Several correlations from literature were examined, as well as a correlation developed at the University of Illinois (UIUC).[5] The UIUC R12 correlation is unique because it was developed specifically for the low heat and mass flux range. A comparison was made between the UIUC R12 correlation and existing correlations found in the literature. The correlations of Jung and Radermacher[6], Kandlikar[7], Pierre[8], and Shah[9] were examined. Table 4.3 lists the applicable heat and mass flux ranges for these correlations and the ranges for the pure-refrigerant experiments. A complete explanation of all the refrigerant correlations listed in Table 4.3 can be found in this section and in Chapter 2.

Table 4.3: Heat and mass flux ranges for 5 correlations and the pure-refrigerant experimental runs

Correlation	G (kg/m^2-s)	q" (kW/m^2)	Tube D.(mm)
Experiment R12	38.8-65.0	0.97-3.94	7.9
Experiment R22	34.7-51.9	1.64-4.30	7.9
UIUC 12	25.0-100.0	2.0-10.0	7.04
Jung	250.0-720.0	10.0-45.0	9.1
Kandlikar	104.0-4479.0	0.3-80.0	6.6, 18.9, 20.0
Pierre	16.4-343.9	0.93-34.9	12.0, 18.0
Shah	13.6-582.9	1.58-34.7	11.7, 14.5, 14.6

Figure 4.4 shows a map of heat flux versus mass flux with the ranges of each correlation represented as shaded boxes. Two additional boxes show the heat and mass flux ranges for typical operation of refrigerators and room air-conditioners. Jung's range is typical of heat pumps. The legend of the correlation map shows the increasing and decreasing directions for the boiling number and Froude number. By definition, the boiling number increases up and to the left as the heat flux increases and mass flux decreases. As the boiling number increases, the chance of nucleate boiling increases. The boiling number decreases down and to the right as

mass flux increases and heat flux decreases. The Froude number increases to the right as mass flux increases. Moving right, the flow transitions from stratified/wavy flow to annular flow. Moving left, the flow transitions from annular flow to stratified/wavy flow and the Froude number decreases.

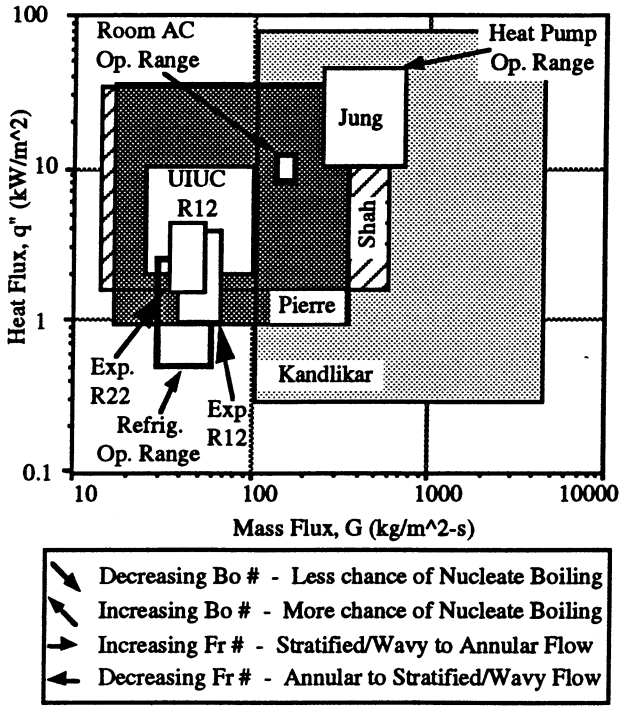

Figure 4.4: Map of heat flux versus mass flux showing the range of applicability of various correlations and the operation ranges of refrigerators, room air conditioners and heat pumps

UIUC R12 Correlation

The UIUC R12 correlation, Equation 4.6, is a function of the heat transfer coefficient of the liquid (from the Dittus-Boelter correlation[10]) and the boiling number. The heat transfer coefficient did not vary with quality in the low heat and mass flux regime; therefore, quality terms do not appear in the correlation. It has a mean deviation of +/- 10%. (Mean deviation is based on the absolute value of the error between the predicted and measured points.) As shown in Figure 4.4 and listed in Table 4.3, the heat flux and mass flux range for the UIUC R12 are much more limited than those of the other correlations. The correlation was developed specifically for low heat and mass-flux flow conditions. Two kW/m^2 was approximately the lower limit at which heat transfer coefficients could practically be determined because the small temperature differences between the refrigerant and the tube wall approached the temperature

measurement uncertainty. A description of the test setup used to obtain the data for this correlation can be found in a paper by Wattelet *et al.*[11]

$$\frac{\bar{\alpha}}{\alpha_{lo}} = 4.3 + 0.4\left(Bo \times 10^4\right)^{1.3} \quad \text{mean deviation} = \pm 10.0\% \tag{4.6}$$

where:

$$\alpha_{lo} = 0.023\frac{k_l}{D}Re_{lo}^{0.8}Pr_l^{0.4},\ 0.01 < Fr_l \le 0.1,\ Bo < 5.0 \times 10^{-4}$$

Pierre Correlation

Of the four correlations discussed above, only the Pierre and Shah correlations' heat and mass flux ranges overlap with the UIUC R12 correlation. Both of these correlations were developed with tubes at least 50% larger in diameter than those typically used for domestic refrigerator-evaporators. Pierre's correlation, Equation 4.7, is an average correlation developed specifically for R12 and covers the entire range of the UIUC correlation. K is a boiling number defined by Pierre.

$$\bar{\alpha} = 0.00097\frac{k_l}{D}Re_{lo}K^{0.5} \quad \text{where} \quad 10^9 < Re_{lo}^2K < 0.7 \times 10^{12} \quad \text{and} \quad K = \frac{\Delta x \cdot h_{lg}}{len \cdot g} \tag{4.7}$$

Shah Correlation

Shah's correlation is a generalized local correlation. For this correlation, data were gathered from nineteen independent experimental studies covering eight different fluids. For accurate comparison with the UIUC R12 average correlation, Shah's correlation was numerically integrated, as shown in Equation 4.8, over the quality range of 10-90% to obtain an average heat transfer coefficient.

$$\bar{\alpha} = \frac{1}{x - x_o}\int_{x_o}^{x} \alpha dx \tag{4.8}$$

Shah's correlation will be presented briefly here.[12] This correlation was originally a chart correlation, but due to great interest, Shah converted the chart correlation to a series of numerical correlations for ease of use. The Shah correlation is presented in Equations 4.9 through 4.20.

Define: $\Psi = \frac{\alpha}{\alpha_l}$: α_l is the Dittus – Boelter correlation[13] (4.9)

$$N = 0.38 Fr_l^{-0.3} \text{ for } CoFr_l \leq 0.04 \quad (4.10)$$

$$N = Co \text{ for } Fr_l > 0.04 \quad (4.11)$$

$$F = 14.7 \text{ for } Bo \geq 11 \times 10^{-4} \quad (4.12)$$

$$F = 15.43 \text{ for } Bo < 11 \times 10^{-4} \quad (4.13)$$

For $N > 1$:

$$\Psi_{nb} = 230.0 Bo^{0.5} \text{ for } Bo > 0.3 \times 10^{-4} \quad (4.14)$$

$$\Psi_{nb} = 1.0 + 46.0 Bo^{0.5} \text{ for } Bo < 0.3 \times 10^{-4} \quad (4.15)$$

$$\Psi_{cb} = \frac{1.8}{N^{0.8}} \quad (4.16)$$

take larger of Ψ_{nb} or Ψ_{cb}

For $0.1 < N \leq 1$:

$$\Psi_{bs} = FBo^{0.5} \exp(2.74 N^{-0.1}) \quad (4.17)$$

$$\Psi_{cb} = \frac{1.8}{N^{0.8}} \quad (4.18)$$

take larger of Ψ_{bs} or Ψ_{cb}

For $N \leq 0.1$:

$$\Psi_{bs} = FBo^{0.5} \exp(2.47 N^{-0.15}) \quad (4.19)$$

$$\Psi_{cb} = \frac{1.8}{N^{0.8}} \quad (4.20)$$

take larger of Ψ_{bs} or Ψ_{cb}

Comparison

As shown in Figure 4.4, the ranges of the Pierre and Shah correlations are large, encompassing at least a part of the operating ranges of refrigerators, room air conditioners and

heat pumps. It would be expected that these correlations would not be as accurate as a correlation specifically targeted for one of these ranges. There is a flow regime transition of stratified/wavy to annular flow from the low-mass flux refrigerator operating range to the high-mass flux heat pump operating range. Even within a specific range, there can be large differences in Bo number; therefore, the possibility of nucleate boiling exists at the wetted tube wall.

Figure 4.5 is a graph showing a comparison between the UIUC R12, Pierre's R12 correlation and Shah's correlation with UIUC experimental heat transfer coefficients. The mass flux and heat flux range over which the comparison was performed was that of the UIUC R12 correlation, G = 25-100 kg/m^2-s and q" = 2-10 kW/m^2. The saturation temperature was -10°C. The diameter was that of the UIUC R12 correlation data, D= 7.04 mm. The three lines on the graph are the +20%, 0% and -20% error bounds.

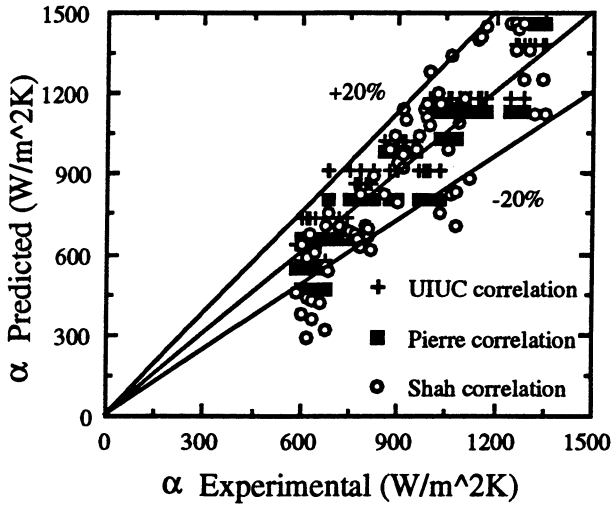

Figure 4.5: Shah and Pierre correlation heat transfer coefficients versus UIUC R12 correlation. G = 25-100 kg/m^2-s; q" = 2-10 kW/m^2; T_{sat} = 10°C; D= 7.04 mm

All three correlations predict R12 heat transfer coefficients with reasonable accuracy over the entire range of relatively low heat and mass flux flow conditions. Shah's correlation shows somewhat broader scatter, with deviations greater than 20% at the lower heat transfer coefficient range. However, given the relatively broad range of data used to derive the correlation, this is within acceptable accuracy.

The tendency for the Pierre and Shah correlations to under-predict at low heat and mass fluxes may be due to sparse data in this area. An investigation of the Re_{lo}^2K parameter reveals that Pierre's correlation is close to its lower limit. Shah believed[14] that if Bo<1x10^{-4} and

Fr_l<0.04, his correlation could under-predict by as much as 20% for 0.3<Co<1.0. For low qualities and low heat or mass fluxes, two of the three above-stated conditions are at their limits. As mentioned previously, both the Shah and Pierre correlations were developed with tubes at least 50% larger in diameter than the UIUC R12 correlation.

The UIUC R12 correlation was selected to reduce the R12 and R22 experimental data. The development of the correlation from similar data, low heat and mass flux flow conditions, and similar diameter tubes were the primary reasons for the selection. The fact that both the Pierre and Shah correlations were at limit conditions for use in the low heat and mass flux range also strengthen the argument to use the UIUC R12 correlation. Before the selection of the UIUC R12 correlation could be finalized, the non-over lapping ranges of the experimental data and the UIUC R12 correlation had to be addressed.

The experimental data collected for this experiment did not lie entirely within the heat flux range of the UIUC R12 correlation, as shown in Figure 4.6. Fortunately, only 34 points out of 178 (19%) are out of range. These low heat flux points are located in the freezer evaporator at low-load (low fan velocity) conditions. Since the percentage of the data outside the correlation range was small, the UIUC R12 correlation was chosen for use in this study to obtain the air-side heat transfer coefficients as a function of air velocity. The R12 correlation is equally valid for R22 and R134a; therefore, the R22 data were reduced with the same correlation. The next section explains how the air-side resistance was calculated for both evaporators.

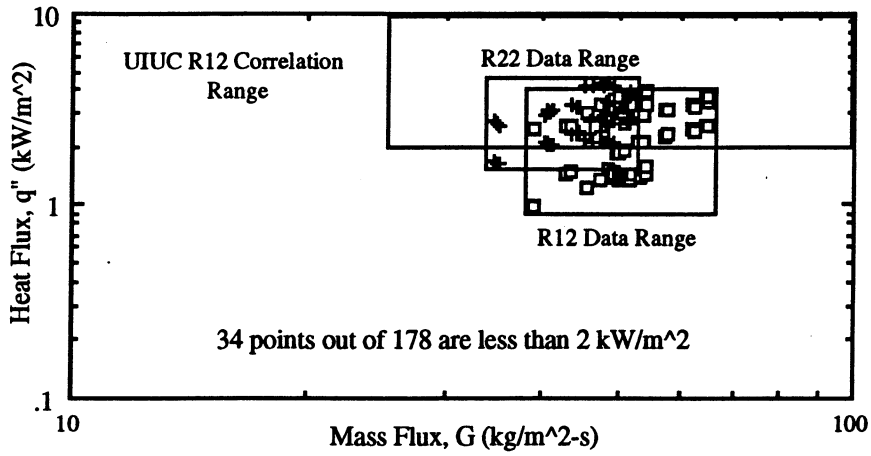

Figure 4.6: Map of heat flux versus mass flux showing the actual R12 and R22 data points with the UIUC R12 correlation range

4.4 Air-Side Characteristics of the Experimental Evaporators

This section explains how the air-side resistance values (air-side heat transfer coefficients) were calculated for both experimental evaporators. The UA/LMTD method was used to calculate the air-side resistances. The air-side resistances for both evaporators needed to be expressed as a function of air velocity for two reasons. First, the air-side resistances were needed to reduce the mixture experimental data in Chapter 5. Second, the resistance values for the eight-pass freezer evaporator, the four-pass fresh-food evaporator, and a single-pass fin/tube section (from Heun[15]) were used to develop a air-side resistance model which was a function of evaporator air velocity and the number of evaporator tube passes. The model was developed and verified by calculating the air-side resistance for the four-pass evaporator. There was a slight discrepancy between the modeled and measured results for the lower air velocities. A possible explanation is given for the difference. This model was required for the optimization which varied the size of each evaporator to minimize life-cycle cost of the system.

The UIUC R12 correlation was used to obtain air-side heat transfer coefficients as a function of air velocity for two sizes of refrigerator evaporators in the test facility. The test facility is described in Chapter 3. Controlled conditions were maintained in each compartment. Careful measurements of temperatures and mass-flow rates permitted an energy balance to be performed on each evaporator. Knowledge of the overall energy balance and the refrigerant heat transfer coefficient from the UIUC R12 correlation allowed direct calculation of an average air-side heat transfer coefficient at various air velocities.

The UA/LMTD method was used to calculate the air-side resistances. A heat exchanger such as an evaporator can be characterized by its UA value. Knowing the inlet/outlet air and refrigerant temperatures and the evaporator load, the UA value can be calculated from:

$$UA = \frac{q}{LMTD} \quad \text{where} \quad LMTD = \frac{\Delta T_2 - \Delta T_1}{\ln(\Delta T_2/\Delta T_1)} \tag{4.21}$$

Neglecting the small conductive tube resistance, an expression for UA can be written:

$$\frac{1}{UA} = \frac{1}{\alpha_a A_a} + \frac{1}{\alpha_r A_r} \tag{4.22}$$

Based on known values for the evaporator areas, UA and α_r, an average air-side heat transfer coefficient, α_a, could be calculated. There is no error when using the UA analysis for the cross

counter-flow arrangement of the four-pass and eight-pass experimental evaporators. The value of C_{min}/C_{max} is zero for a pure refrigerant in phase change; therefore, heat exchanger performance is independent of geometry.[16] The pressure drop is small through the evaporator module on the low-pressure side. The R12 runs had an average pressure drop of 4.48 kPa (0.65 psi) and the R22 runs had an average pressure drop of 3.37 kPa (0.49 psi). A large pressure drop would cause the temperature to change and C_{min}/C_{max} could no longer be considered zero. An extended discussion on the validity of using the UA/LMTD method for heat exchanger analysis is found in Appendix E.

The eight-pass freezer evaporator transferred heat in the quality range of approximately 0-50%, and the four-pass fresh-food evaporator transferred heat in the quality range of approximately 50-100%. With separate heat exchangers, the effect of quality change and heat flux could be studied independently. Figure 4.7 details the fin dimensions and air-flow direction of the UIUC evaporator design, which is also explained in Chapter 3.

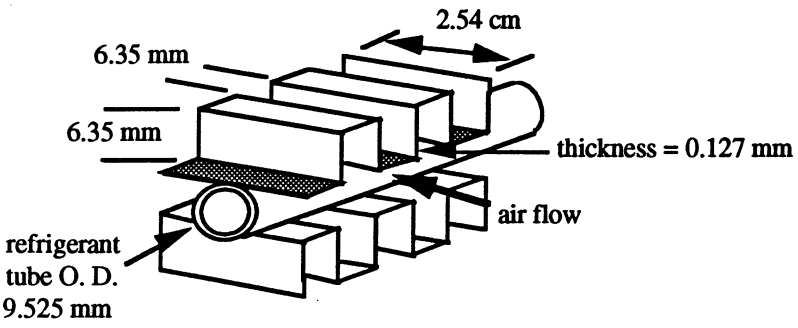

Figure 4.7: Fin dimensions and air-flow direction over the UIUC evaporator

Using the UIUC R12 correlation, the air-side heat transfer coefficients were calculated from Equation 4.22. Figure 4.8 shows a plot of the air-side heat transfer coefficients of the four- and eight-pass evaporators versus evaporator air velocity. The four-pass evaporator has greater air-side heat transfer coefficients over the tested velocity range than the eight-pass evaporator. This was expected because the shorter duct length of the four-pass evaporator prevents the bulk air flow from becoming as developed as the bulk flow over the eight-pass evaporator. The less-developed bulk flow maintains a steeper velocity profile along the air-side transfer surfaces, the fins, enhancing the heat transfer coefficient. The uncertainty associated with each point arises from the average deviation of the UIUC R12 correlation and the energy balance error for those runs.

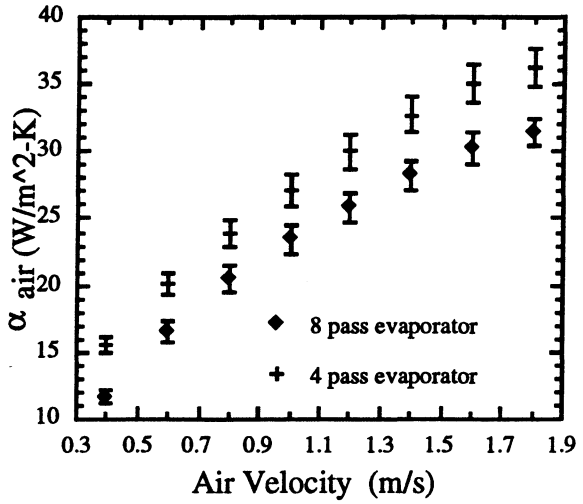

Figure 4.8: Air heat transfer coefficients for the UIUC eight-pass and four-pass evaporators versus air velocity

Figures 4.9 and 4.10 show the air-side resistance of the two evaporators for all the R12 and R22 data gathered and reduced using the UIUC R12 correlation. A best-fit line was drawn through the freezer evaporator data, as shown in Figure 4.9, because the freezer data showed the least scatter particularly for the low velocity points. The fit is very uniform and smooth. Using air-side resistance data from Heun[17] for a single-pass evaporator and the eight-pass freezer data, a linear model based on the number of passes accurately predicted the fresh-food air-side

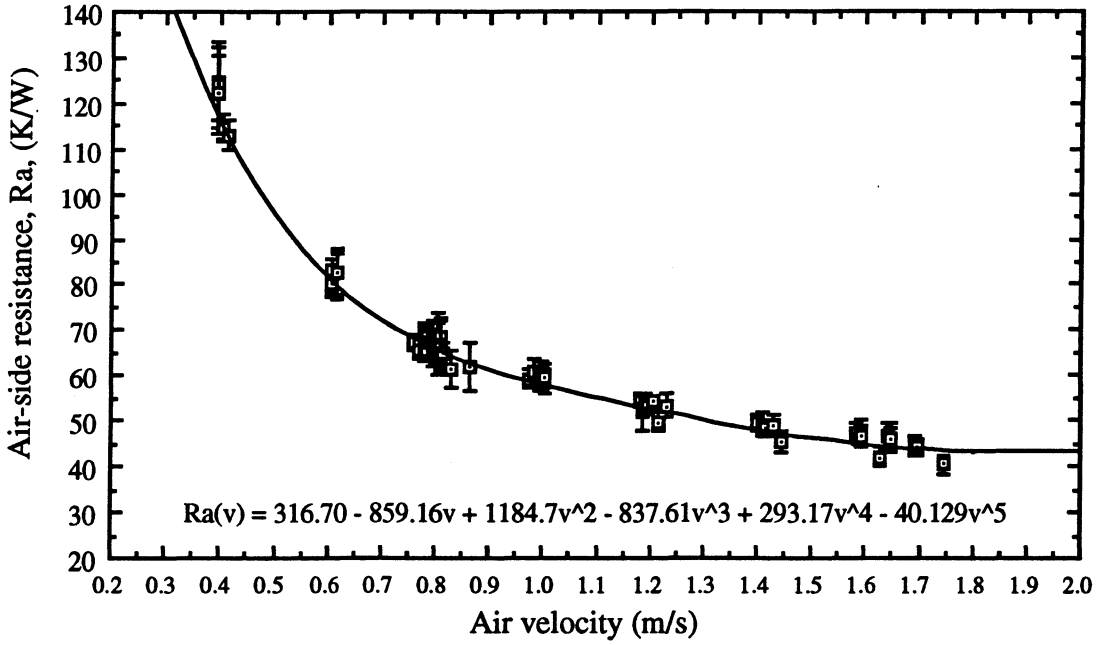

Figure 4.9: Air-side resistance as a function of air velocity for the eight-pass freezer evaporator - best fit line drawn through measured data

resistances for the higher air velocities. The model prediction is shown superimposed on Figure 4.10. This model needed to be developed for the system optimization presented in Chapters 6 and 7. The model is presented in Equation 4.23. The uncertainty bars in Figures 4.9 and 4.10 arise from the average deviation of the UIUC R12 correlation and the energy balance error for each run. See Appendix C for information. Figure 4.11 shows the eight-pass freezer evaporator best-fit line, the single-pass results provided by Heun, and the four-pass fresh-food evaporator model results.

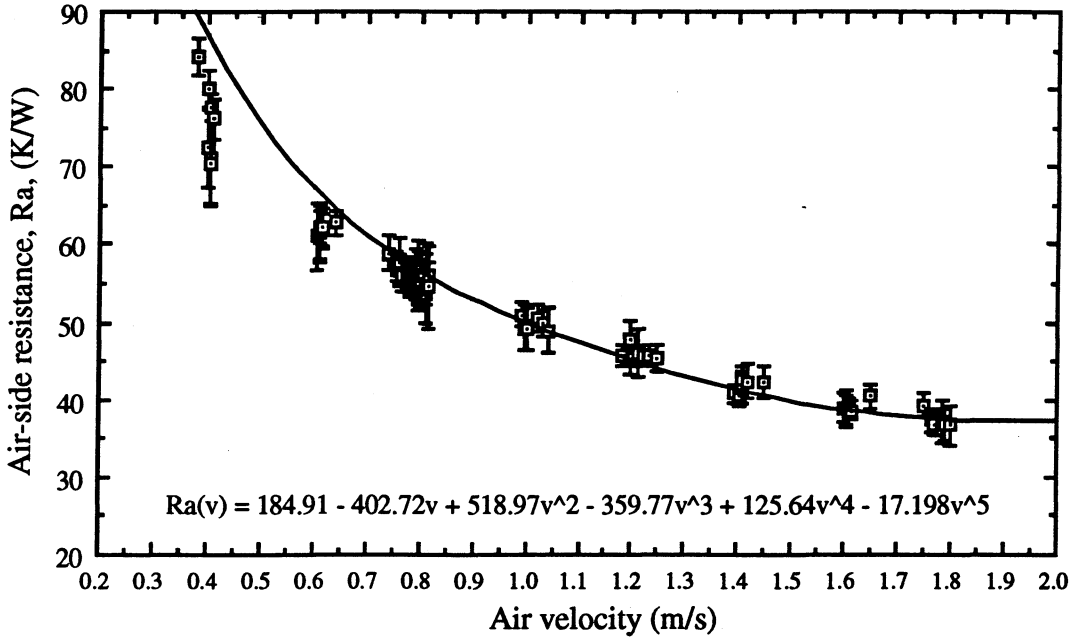

Figure 4.10: Air-side resistance as a function of air velocity for the four-pass fresh-food evaporator - comparison of the air-side resistance model with measured data

An examination of the fresh-food evaporator air-side resistance, Figure 4.10, reveals a slight drop in the air-side resistance at the lower air velocities relative to the model prediction. The scatter in the data can be attributed to the large measurement uncertainties associated with the reduced evaporator load at this point. The inconsistency between the data and the model may arise from the use of the UIUC R12 correlation at lower, out of range, heat fluxes when applied to the freezer evaporator conditions in the low air velocity range (recall Figure 4.6). It is in the larger freezer evaporator that the heat flux can fall below 2 kW/m^2 for low velocity (low load) conditions. The fresh-food results begin to deviate from the linear model at air velocities less than 0.6 m/s. This implies that the air-side resistance data less than 0.6 m/s for the freezer evaporator are incorrect and the model should be based on the air-side resistances from the fresh-food evaporator for this velocity range. Since the fresh-food model results fall almost within the

uncertainty bars for the fresh-food data and the scatter for the fresh-food data is large, the model based on the eight-pass data was kept. As will be seen in the next chapter, the experimental air velocities for the mixture data start at approximately 0.6 m/s. The inconsistency in the air-side resistance model does not effect the calculated values of the mixture heat transfer coefficients.

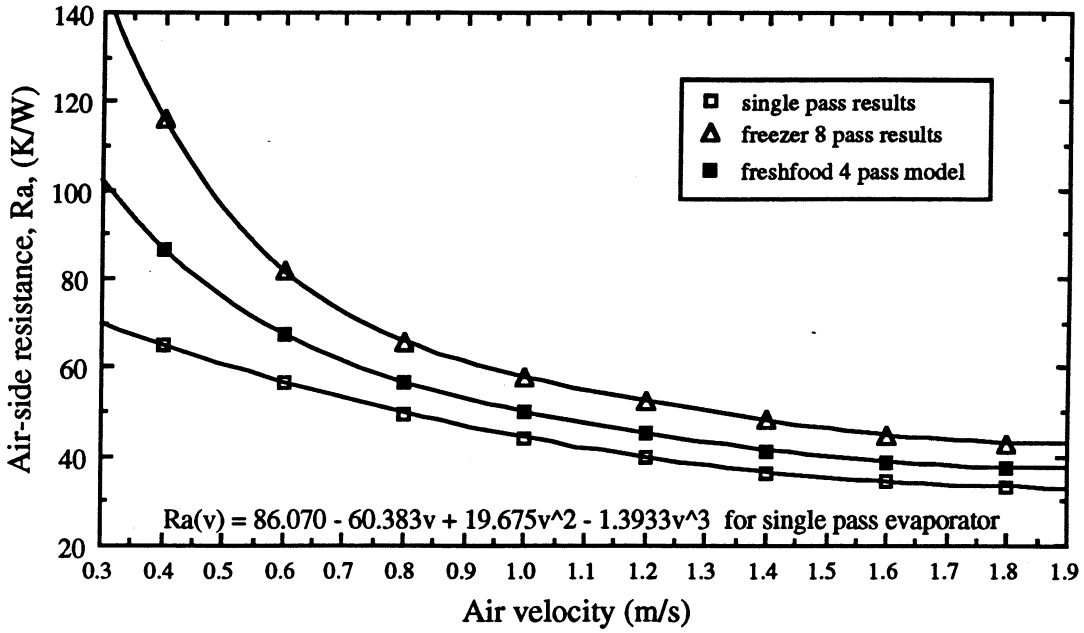

Figure 4.11: Air-side resistance results for a one-pass, four-pass and eight-pass evaporator as a function of air velocity - best fit line through the one-pass and eight-pass data, model prediction for the four-pass R_a

$$R_a(v,\text{pass\#}) = \left(\frac{R_{a,8pass}(v) - R_{a,1pass}(v)}{7}\right)(\text{pass\#}) + \left[R_{a,1pass}(v) - \left(\frac{R_{a,8pass}(v) - R_{a,1pass}(v)}{7}\right)\right] \quad (4.23)$$

4.5 References

---

[1] Admiraal, D. M. and C. W. Bullard, "Heat Transfer in Refrigerator Condensers and Evaporators", ACRC TR-48, University of Illinois at Champaign Urbana, Air Conditioning and Refrigeration Center, August, 1993, p. 35.

[2] Personal communication with Jon P. Wattelet, University of Illinois, Air-Conditioning and Refrigeration Center.

[3] Baker, O., "Designing for Simultaneous Flow of Oil and Gas", *Oil Gas Journal*, 53, pp. 185 - 195, 1954.

---

[4] Scott, D. S., "Properties of Co-Current Gas-Liquid Flow", *Advances in Chemical Engineering*, Vol. 4, pp. 199-277, Academic, New York, 1963.

[5] Wattelet, J. P., J. C. Chato, A. L. Souza and B. R. Christoffersen, unpublished correlation, University of Illinois at Champaign-Urbana, Department of Mechanical and Industrial Engineering, Fall, 1992.

[6] Jung, D.S. and R. Radermacher, "Prediction of Heat Transfer Coefficients of Various Refrigerants During Evaporation", *ASHRAE Transactions*, V. 97, Pt. 2.

[7] Kandlikar, S.G., "A General Correlation for Saturated Two-Phase Boiling Heat Transfer Inside Horizontal and Vertical Tubes", *Journal of Heat Transfer*, Vol. 112, February 1990, pp. 219-228.

[8] Pierre, B., "The Coefficient of Heat Transfer for Boiling Freon-12 in Horizontal Tubes", *Heating and Air Treatment Engineer*, December, 1956, pp. 302-310.

[9] Shah, M.M., "Chart Correlation for Saturated Boiling Heat Transfer: Equations and Further Study", *ASHRAE Transactions*, Vol. 88, Part 1, pp. 185-196.

[10] Dittus, F. W., and L. M. K. Boelter, *University of California Publications on Engineering*, Vol. 2, p. 443, Berkeley, 1930.

[11] Wattelet, J. P., J. C. Chato, A. L. Souza and B. R. Christoffersen, "Evaporative Characteristics of R134a, MP39 and R12 at Low Mass Fluxes", ACRC TR-35, University of Illinois at Champaign Urbana, Air Conditioning and Refrigeration Center, May, 1993.

[12] Shah, M. M., "A New Correlation for Heat Transfer During Boiling Flow Through Pipes", *ASHRAE Transactions*, Vol. 82, Part 2, 1976, pp. 66-86.

[13] Dittus, F. W., and L. M. K. Boelter, *University of California Publications on Engineering*, Vol. 2, p. 443, Berkeley, 1930.

[14] Shah, M.M., "Chart Correlation for Saturated Boiling Heat Transfer: Equations and Further Study", *ASHRAE Transactions*, Vol. 88, Part 1, pp. 185-196.

[15] Heun, M. K., "Thermal Performance Analysis of an Evaporator-Intercooler Module for a Lorenz Cycle", Master's Thesis, Department of Mechanical and Industrial Engineering, University of Illinois at Champaign-Urbana, 1991.

[16] Incropera, F. P. and D. P. DeWitt, Fundamentals of Heat and Mass Transfer, 2nd. ed., John Wiley & Sons, 1985, pp. 512-515.

[17] Heun, M. K., "Thermal Performance Analysis of an Evaporator-Intercooler Module for a Lorenz Cycle", Master's Thesis, Department of Mechanical and Industrial Engineering, University of Illinois at Champaign-Urbana, 1991, Chapter 6.

CHAPTER 5: REFRIGERANT-MIXTURE RUNS: R22/R123 AND R22/R141B

The purpose of this chapter is to explain how the mixture heat transfer coefficient data were obtained and calculated. The procedure involved running the two mixtures, 65% R22/35% R123 and 80% R22/20% R141b, in the test setup over a wide range of conditions and collecting the experimental data. The mixture's heat transfer coefficients were then calculated based on knowledge of the air-side resistance, from Chapter 4, and an energy balance about each evaporator. The heat transfer coefficient values obtained were fit to an appropriate correlation form. Several possible fits were explored. The final correlation forms for each mixture are presented later in this chapter. At the end of this chapter the mixture correlations and the UIUC R12 correlation are compared.

5.1 R22/R123 Runs

Sixty-five experimental R22/R123 runs yielding 130 data points were made over a range of conditions listed in Table 5.1. Figure 5.1 shows the total energy balance error of the runs. Nearly all of the runs were within +5% to -8% error. The error was calculated similarly to the error for the R12/R22 runs, as presented in Chapter 4. The startup effects can be seen for the data taken over five separate days. The runs conditions were varied by adjusting the air-flow rate over each evaporator from approximately 0.6 m/s to 1.8 m/s in 0.2 m/s intervals (22.5 CFM to 67.5 CFM in 7.5 CFM intervals). The mass-flow rate and high-side pressure were adjusted to maintain reasonable values of subcooling. Superheat was no longer a requirement at the evaporator module exit because the temperature glide allowed state point location from the measured temperature and pressure data in the two-phase region. Table 5.1 lists other pertinent conditions maintained or measured during the course of the R22/R123 runs.

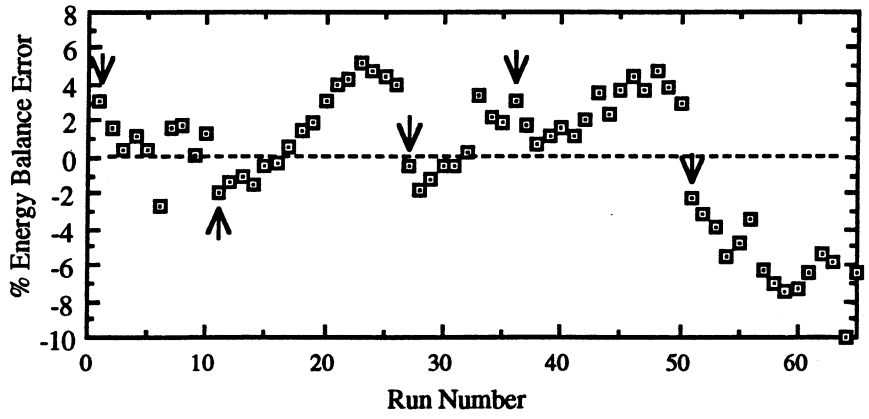

Figure 5.1: Total energy balance error for R22/R123 runs

Table 5.1: Statistics on R22/R123 runs

quantity	low	high	average
mass flux (kg/m^2-s)	25.5	84.9	40.0
heat flux, freezer evaporator (kW/m^2)	1.17	1.71	1.44
heat flux, fresh-food evaporator (kW/m^2)	1.73	2.84	2.27
evaporating pressure (kPa)	112.6	238.2	150.9
quality, freezer evaporator	0.06	0.52	0.29
quality, fresh-food evaporator	0.55	0.80	0.67
load, freezer evaporator (W)	123.7	180.8	152.9
load, fresh-food evaporator (W)	91.4	150.3	120.4
effectiveness, freezer evaporator	0.35	0.58	0.43
effectiveness, fresh-food evaporator	0.28	0.69	0.54
UA, freezer evaporator (W/K)	11.88	17.08	15.11
UA, fresh-food evaporator (W/K)	6.25	10.86	8.45
load, high-temp intercooler (W)	-	-	38.77
load, low-temp intercooler (W)	-	-	15.41
effectiveness, high-temp intercooler	-	-	0.88
effectiveness, low-temp intercooler	-	-	0.67
UA, high-temp intercooler (W/K)	-	-	4.95
UA, low-temp intercooler (W/K)	-	-	1.61
compartment temp., freezer section (°C)	-15.0	-3.2	-9.7
compartment temp., fresh-food section (°C)	2.2	9.2	5.2
module subcooling (°C)	1.7	44.7	13.5
module superheat (°C)	-26.1	1.3	-5.9
module pressure drop (kPa)	1.32	4.15	3.01
typical temperature glide at these operating conditions (°C)	NA	NA	30.4
air velocity, freezer evaporator (m/s)	0.64	2.02	1.30
air velocity, fresh-food evaporator (m/s)	0.67	1.83	1.31
refrigerant - side resistance, freezer evaporator (%)	32.1	54.2	44.5
refrigerant - side resistance, fresh-food evaporator (%)	16.4	47.6	29.3
refrigerant heat transfer coeff., freezer evaporator (W/m^2-K)	224.9	508.7	316.0
refrigerant heat transfer coeff., fresh-food evaporator (W/m^2-K)	181.3	715.3	365.4
air heat transfer coeff., freezer evaporator (W/m^2-K)	17.4	31.5	26.5
air heat transfer coeff., fresh-food evaporator (W/m^2-K)	21.4	36.4	31.1

Several significant points about the information in Table 5.1:

- For the R22/R123 runs, a series of high-mass flux experiments were performed. These were able to be accomplished because superheat was not required at the evaporator module exit; consequently, the load control system would have been unable to supply enough heat to keep the evaporator module's exit in the superheat region. These high-mass flux runs enhance the R22/R123 mixture correlation and permit comparison with R12 for high-mass flux flows later in this chapter.

- The average freezer and fresh-food evaporator effectivenesses for these runs were 43% and 54% respectively. The UA values for the evaporators varied as the air

velocity over them was varied. The average freezer and fresh-food evaporator UAs for these runs were 15.11 and 8.45 W/K respectively.

- The average high-temperature and low-temperature intercooler effectivenesses for these runs were 88% and 67% respectively. The average high-temperature and low-temperature intercooler UAs for these runs are 4.95 and 1.61 W/K respectively.

- As mentioned above, there was no requirement that the evaporator module's exit state be in the superheat region for the mixture runs. The table lists negative values of superheat, which means that some of the module's exit state points were in the two-phase region.

- The mixture's average pressure drop through the evaporator module was small at 3.01 kPa (0.44 psi). The R22/R123 had the *lowest* average pressure drop of any of the fluids tested.

- The minimum air velocities for these runs start at higher values than the pure-refrigerant runs, 0.65 m/s versus 0.4 m/s respectively.

- There is a large variation in the refrigerant-side resistance for these mixture runs. The refrigerant-side resistance variation is caused by a large variation in mass flux. The highest refrigerant-side resistance is very large, indicating low values of refrigerant heat transfer coefficients. Recall from Chapter 2 that mixture heat transfer coefficients are generally lower than the pure-refrigerant heat transfer coefficients for low heat and mass flux flow conditions. The fresh-food evaporator experiences a higher average refrigerant heat transfer coefficient; therefore, its average refrigerant-side resistance is lower. At higher qualities found in the fresh-food evaporator, the heat transfer coefficient is greater because the increase in convective boiling from the thinning liquid layer is greater than the decrease in nucleate boiling.

- The refrigerant heat transfer coefficients were obtained by performing an energy balance about each evaporator. The calculation method will be discussed later in this chapter. The values of the heat transfer coefficients are much lower than those for R12. Please refer to Chapter 2 and the end of this chapter for a detailed explanation.

- The air heat transfer coefficients were calculated from the air-side resistance model developed in Chapter 4.

5.2 R22/R141b Runs

A similar set of runs was made with the R22/R141b mixture. Sixty-two experimental runs yielding 124 data points were made over a range of conditions listed in Table 5.2. Figure 5.2 shows the total energy balance error for the runs. The start-up error is less apparent for these data than for previous data. The data was taken over six separate days. The runs conditions were varied by adjusting the air-flow rate over each evaporator from approximately 0.6 m/s to 1.8 m/s in 0.2 m/s intervals (22.5 CFM to 67.5 CFM in 7.5 CFM intervals). The mass-flow rate and high-side pressure were adjusted to maintain reasonable values of subcooling. As mentioned above, superheat was no longer a requirement at the evaporator module exit because the exit state point was able to be located in the two-phase region. Table 5.2 lists other pertinent conditions maintained or measured during the course of the R22/R141b runs.

Several significant points about the information in Table 5.2:

- The R22/R141b runs experienced higher average values of heat flux in the freezer and fresh-food evaporators. The average loads for the R22/R141b runs are higher than the R22/R123 runs.

- The average freezer and fresh-food evaporator effectivenesses for these runs were 38% and 54% respectively. The average freezer and fresh-food evaporator UAs for these runs were 13.96 and 8.56 W/K respectively.

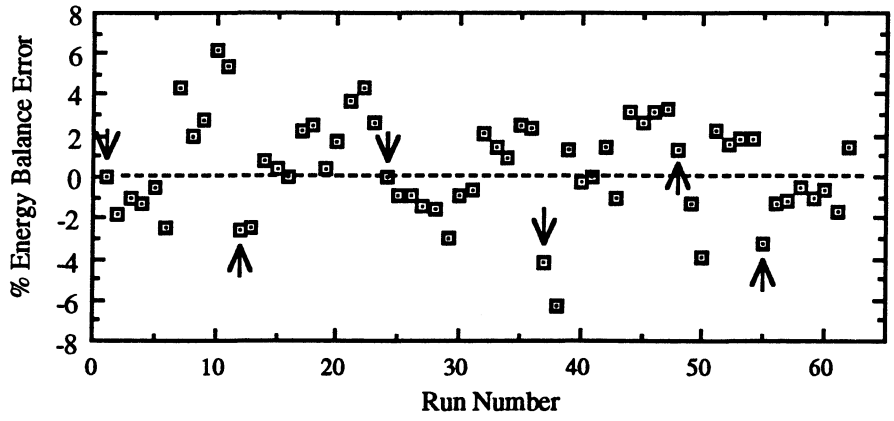

Figure 5.2: Total energy balance error for R22/R141b runs

Table 5.2: Statistics on R22/R141b runs

quantity	low	high	average
mass flux (kg/m^2-s)	26.9	41.6	35.2
heat flux, freezer evaporator (kW/m^2)	0.98	2.56	1.85
heat flux, fresh-food evaporator (kW/m^2)	1.76	4.16	2.66
evaporating pressure (kPa)	108.0	215.1	142.5
quality, freezer evaporator	0.00	0.54	0.27
quality, fresh-food evaporator	0.58	0.92	0.75
load, freezer evaporator (W)	104.3	271.0	195.5
load, fresh-food evaporator (W)	92.8	219.7	140.7
effectiveness, freezer evaporator	0.31	0.45	0.38
effectiveness, fresh-food evaporator	0.41	0.61	0.54
UA, freezer evaporator (W/K)	6.18	19.92	13.96
UA, fresh-food evaporator (W/K)	6.47	11.17	8.56
load, high-temp intercooler (W)	-	-	41.63
load, low-temp intercooler (W)	-	-	24.37
effectiveness, high-temp intercooler	-	-	0.76
effectiveness, low-temp intercooler	-	-	0.75
UA, high-temp intercooler (W/K)	-	-	4.52
UA, low-temp intercooler (W/K)	-	-	1.96
compartment temp., freezer section (°C)	-15.1	-4.8	-8.7
compartment temp., fresh-food section (°C)	4.1	6.7	4.7
module subcooling (°C)	2.0	18.8	9.8
module superheat (°C)	-10.0	11.7	4.6
module pressure drop (kPa)	2.19	5.27	3.94
typical temperature glide at these operating conditions (°C)	NA	NA	28.4
air velocity, freezer evaporator (m/s)	0.57	1.83	1.12
air velocity, fresh-food evaporator (m/s)	0.70	1.83	1.28
refrigerant - side resistance, freezer evaporator (%)	35.5	61.3	44.1
refrigerant - side resistance, fresh-food evaporator (%)	18.8	36.3	28.4
refrigerant heat transfer coeff., freezer evaporator (W/m^2-K)	96.8	457.1	307.4
refrigerant heat transfer coeff., fresh-food evaporator (W/m^2-K)	265.9	522.2	362.4
air heat transfer coeff., freezer evaporator (W/m^2-K)	15.9	31.5	24.2
air heat transfer coeff., fresh-food evaporator (W/m^2-K)	22.2	36.4	30.5

- The average high-temperature and low-temperature intercooler effectivenesses for these runs were 76% and 75% respectively. The average high-temperature and low-temperature intercooler UAs for these runs are 4.52 and 1.96 W/K respectively.

- The mixture's average pressure drop through the evaporator module was small at 3.94 kPa (0.57 psi).

- At typical operating conditions, the R22/R141b temperature glide is 2°C less (28.4°C) than the R22/R123 temperature glide.

- As mentioned above, the minimum air velocities for these runs start at higher values than the pure-refrigerant runs.
- There is a large variation in the refrigerant-side resistance for these mixture runs. The refrigerant-side resistance variation is caused by a large variation in heat flux. The refrigerant heat transfer coefficient is proportional to the applied heat flux as well as mass flux. As with the R22/R123 runs, the R22/R141b mixture is characterized by low heat transfer coefficients for low heat and mass flux flow conditions.
- The refrigerant heat transfer coefficients were obtained by performing an energy balance about each evaporator.
- The air heat transfer coefficients were calculated from the air-side resistance model developed in Chapter 4.

5.3 General Comments

The mixture runs can be put into perspective using the correlation map introduced in Figure 4.4 and repeated here in Figure 5.3. The R22/R123 runs were over a larger mass flux range and the R22/R141b runs were over a larger heat flux range. The resulting heat and mass flux ranges were dictated by the air velocity ranges over each evaporator and the constant

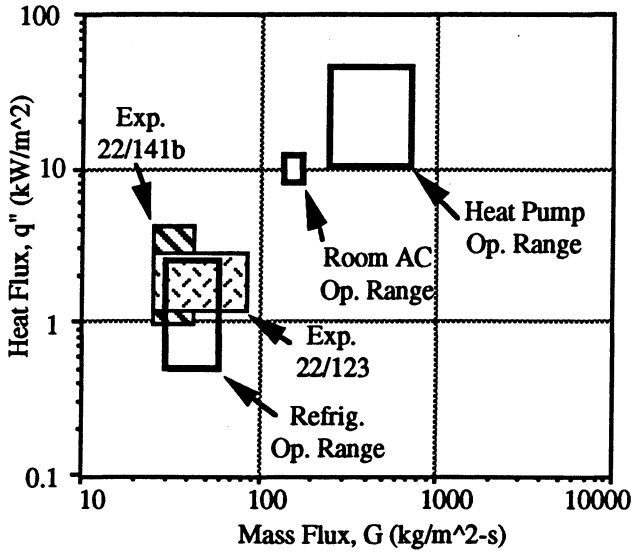

Figure 5.3: Map of heat flux versus mass flux showing the range of the mixture experimental data and the operation ranges of refrigerators, room air conditioners and heat pumps

compartment temperatures maintained during each run. The entering quality to the low-quality, eight-pass evaporator was changed by varying the amount of condenser subcooling. The exiting quality from the high-quality, four-pass evaporator was changed by varying the amount of system superheat. Both sets of runs were predominately within the refrigerator operating range shown in Figure 5.3. Figure 5.4 shows the actual data points plotted on the correlation map.

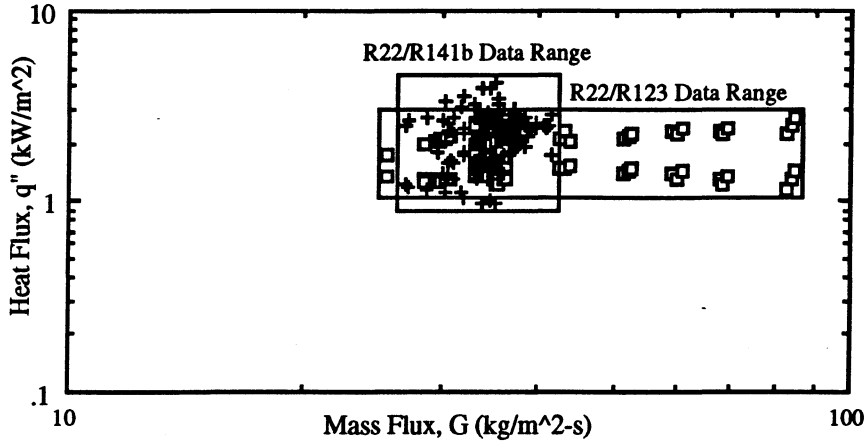

Figure 5.4: Map of heat flux versus mass flux showing the actual R22/R123 and R22/R141b data points

5.4 Calculation of Mixture Heat Transfer Coefficients

The loop was run at a variety of refrigerant conditions and air velocities. Before the data could be reduced, the proper interaction parameters for the mixtures needed to be selected. Appendix J describes the interaction parameter and the selected values. With knowledge of the air-side heat transfer coefficients from Chapter 4 and the heat exchanger's physical dimensions and load, it was possible to calculate the refrigerant heat transfer coefficients by breaking the evaporator into small, constant specific heat segments. The solution was iterative and is outlined below in Equations 5.1 to 5.4.

Refrigerant mixtures generally do not have constant specific heats over the entire saturation region. The R22/R123 and R22/R141b mixture specific heats vary from 31.3 to 5.67 kJ/kg-K and from 51.5 to 4.52 kJ/kg-K respectively between the bubble and due points. The R22/R141b mixture specific heat change in saturation is almost twice that of the R22/R123 mixture. This large variation occurs at low qualities for the R22/R141b mixture as can be seen in Figure 6.3.

Guess α_r (5.1)

$$UdA = \left[\frac{1}{\alpha_a(v)dA_a} + \frac{1}{\alpha_r dA_r} \right]^{-1} \tag{5.2}$$

i = 1, total # of segments

$$dq_i = UdA(T_{a_i} - T_{r_i}) \tag{5.3}$$

loop

$$\text{adjust } \alpha_r \text{ so that } \sum_i dq_i = q_{measured} \tag{5.4}$$

First a reasonable value for the refrigerant heat transfer coefficient was assumed. The UdA for each segment was calculated. The differential area, dA, was known from the tube geometry and length of the segment; the air-side heat transfer coefficient, α_a, was determined from the air-side resistance correlation; and the refrigerant heat transfer coefficient, α_r, was assumed. The heat transferred at each segment, dq_i, was calculated and totaled for the entire evaporator. The result was compared to the measured evaporator load, $q_{measured}$, and adjustments were made to the refrigerant heat transfer coefficient as required. This method worked well and converged in three to four iterations.

The outlet air temperature variation was checked after each evaporator pass (freezer and fresh-food) for several R22/R123 data reduction runs using the segmented evaporator model. The mixture glide will tend to cause a variation in the air temperature along the evaporator tube after each tube pass. The air is assumed to enter the evaporator at a uniform temperature because the air is well mixed at this point. It was further assumed that no mixing occurs between adjacent 'fin corridors' even though some does occur. (See E.6.2. The amount of air mixing would have to be determined by experiment and was beyond the scope of this study.) The freezer evaporator showed a *slight* drop in air temperature in the *refrigerant* flow direction. The odd passes were most effected because the variation tended to cancel after the even numbered rows when the refrigerant flow direction reversed. The fresh-food evaporator showed a larger air temperature variation (approximately 0.5 °C) after the odd rows and a reduced variation after the even rows. The variation was not able to canceled after the even rows. The temperature variation was larger because of the steeper mixture glide in the higher quality operational range of the fresh-food evaporator. For the experiments, the air velocities maintained over each evaporator were approximately constant. However in the optimization, the velocity over the fresh-food evaporator was usually less than the air velocity maintained over the freezer

evaporator. The low air velocity would lead to larger air temperature variations in the refrigerant flow direction for any given row.

The UA/LMTD method could not be applied to the entire heat exchanger operating with mixtures. Non-azeotropic refrigerant mixtures experience a temperature glide in saturation. The glide with respect to enthalpy is almost always nonlinear. This means that the specific heat is not constant and can vary greatly through the saturation dome. The LMTD/UA analysis breaks down because the mixture specific heats are non-constant. The LMTD/UA analysis assumes constant fluid specific heats. The geometry or cross-flow error is negligible for these evaporators and flow conditions; however, the variation in the specific heats of the mixtures cannot be ignored. A complete discussion on the application of the LMTD/UA method to mixtures can be found in Appendix E.

5.5 Correlation Development

This section will discuss the correlation development. Once again a flow map is used to predict the flow regime of the data. From the flow map information, a suitable correlation form was selected. Plots of the measured and correlated heat transfer coefficient are presented. The correlation forms are presented in Equations 5.5 to 5.7.

It is beneficial before developing a correlation to plot the data on a flow map. By doing this, the basic flow patterns and fundamental heat transfer modes can be incorporated into the correlation form. As with the R12 and R22 data, the R22/R123 and R22/R141b data were plotted on a Scott[1] flow map. All the data fall within the uncertainty band about the wavy flow regime, as shown in Figure 5.5, with the exception of the high-mass flux runs for R22/R123 in the freezer evaporator. The fresh-food data is to the left and the freezer data is to the right. The higher vapor velocity at higher qualities shift the fresh-food data to the left. The x and y coordinates for the Scott map are given in Equations 4.2 to 4.5.

An attempt was made to correlate the data using average and local correlations of various forms similar to those described in Equations 2.3 and 4.7. The local correlations produced the least error. These mixture combinations are characterized by a large temperature glide in the saturation region. Since many of the refrigerants' physical properties are strong functions of temperature, an average correlation cannot account for differences in property values at the same evaporating pressure. Because an energy balance was performed on both the freezer and fresh-food evaporators, two heat transfer coefficient values from different quality levels were obtained and used in the correlation.

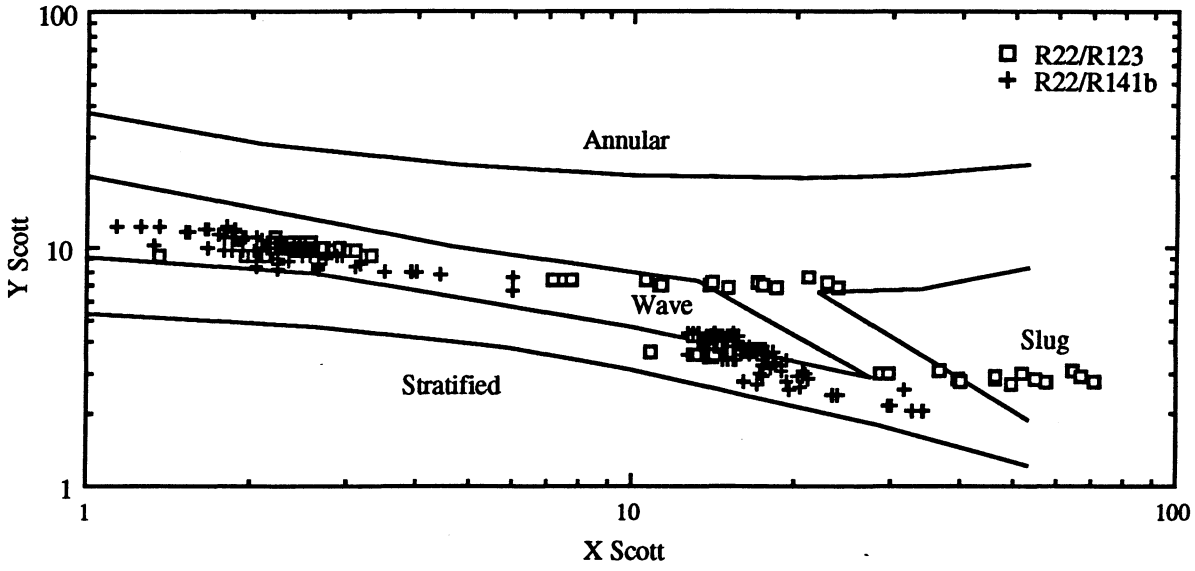

Figure 5.5: Scott flow map for predicting refrigerant-mixture flow regimes

Figures 5.6 and 5.7 show the plots of the correlated heat transfer coefficient against the measured heat transfer coefficient with +20%, 0% and -20% error lines. The uncertainty arises from the energy balance error and the uncertainty in the air-side resistance for each data point (see Appendix C for more information). Figure 5.6, the R22/R123 plot, shows good agreement between the proposed correlation and the measured data. For Figure 5.7, the R22/R141b plot,

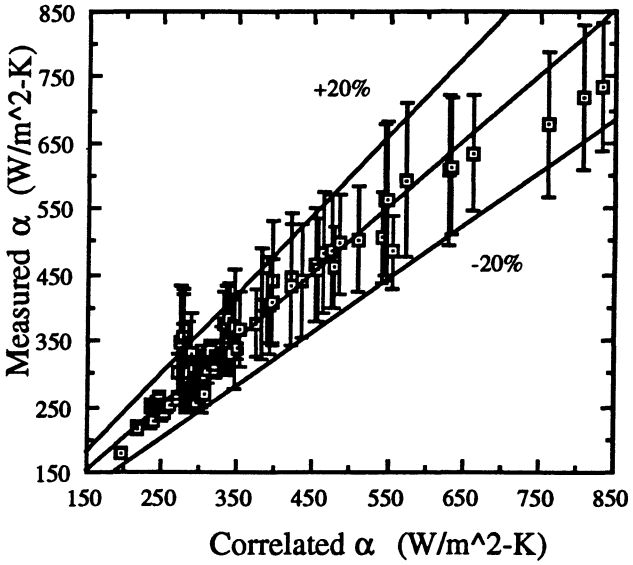

Figure 5.6: Local correlated heat transfer coefficient versus measured heat transfer coefficient G = 25-85 kg/m²-s; q" = 1.2-2.8 kW/m²; D = 7.9 mm; 65% R22/35% R123

the data points show a fair amount of scatter. The R22/R123 was run over a much wider range of mass fluxes, whereas the R22/R141b was run over a wider range of heat fluxes, as shown in Figure 5.4. The R22/R141b should be most affected by changes in heat flux because it is 80% R22, as compared to the R22/R123 mixture which is only 65% R22. The mixture which contains a higher percentage of the more volatile component will be most affected by heat flux. The scatter between the proposed correlation and the measured data for R22/R141b may be caused by the absence of a term in the correlation form related to the sensitivity of the mixture to heat flux such as mass diffusion.

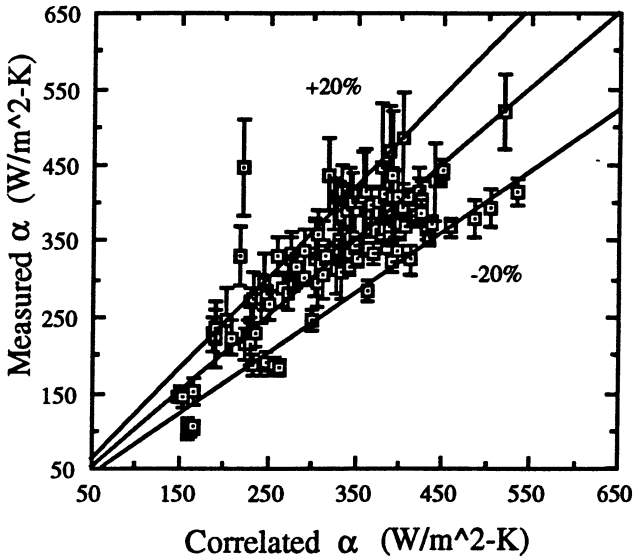

Figure 5.7: Local correlated heat transfer coefficient versus measured heat transfer coefficient G = 25-42 kg/m²-s; q" = 1.0-4.2 kW/m²; D = 7.9 mm; 80% R22/20% R141b

The local correlations for R22/R123 and R22/R141b are shown in Equations 5.5 and 5.6, respectively. Various forms were tried for each correlation; additive, as in Equation 5.5, and multiplicative, as in Equation 5.6. The method of non-linear least squares[2] was used to find the coefficients for Equation 5.5 and a linear least squares[3] method was used to calculate the coefficients for Equation 5.6. The correlation form that produced the least sum of the squared errors was chosen. The method used to calculate the uncertainty for the correlations is very stringent. The uncertainty is calculated based on a 95% confidence interval. If it is assumed that the distribution in the percent error is Gaussian, then there is a 95% probability that all error percentages fall within two standard deviations of the mean.

$$\frac{\alpha}{\alpha_l} = C_1 X_{vt}^{C_2} Fr_l^{C_3} + C_4 \left(Bo \times 10^4\right)^{C_5} \quad 2\sigma = \pm 15.26\% \tag{5.5}$$

where: $C_1 = 2.430$ $C_2 = -1.433$ $C_3 = 0.6850$ $C_4 = 2.580$ $C_5 = 0.3600$

$$\frac{\alpha}{\alpha_l} = C_1 X_{vt}^{C_2} Fr_l^{C_3} Bo^{C_4} \quad 2\sigma = \pm 37.89\% \tag{5.6}$$

where: $C_1 = \exp(8.815)$ $C_2 = -0.4386$ $C_3 = 0.5247$ $C_4 = 0.6756$

$$\alpha_l = 0.023 \frac{k_l}{D} Re_l^{0.8} Pr_l^{0.4} \tag{5.7}$$

The correlations contain three non-dimensional numbers. The Bo number is present to account for the change in the heat transfer coefficient with heat flux. The Martinelli parameter, X_{vt}, accounts for the relative pressure drop of the liquid and gas phases in saturation. The liquid phase is laminar and the gas phase is turbulent; therefore, the subscripts to X are vt. For annular flows with nucleate boiling suppressed, α/α_l could be exclusively correlated by the Martinelli parameter X_{tt}. For annular flows with nucleate boiling present, α/α_l is a function of X_{tt} and Bo. As the flow transitions from annular to wavy/stratified, the correlation must include the Froude number. The Froude number accounts for the relative change of the inertial forces to gravitational forces. It is generally believed that flows are annular for $Fr_{>=}0.04$.[4] As the mass flux decreases, gravitational forces cause the liquid to flow in the bottom of the tube and the upper tube wall becomes dry. This reduces the area available for convective boiling at the liquid-vapor interface. The Froude number also helps correct the overestimation of α_l, the Dittus-Boelter correlation, for test conditions with Reynolds numbers below 10,000.[5]

The R22/R123 correlation, Equation 5.5, has an additive form for including the effect of heat flux and is modeled after the pure-refrigerant Kandlikar[6] correlation described in Chapter 2. The R22/R141b correlation, Equation 5.6, has a multiplicative form. The additive form agrees with Chen's form of correlation based on the superposition of heat transfer coefficients due to nucleate and convective boiling effects.[7] The form of Equation 5.5 was tried on the R22/R141b data. The 95% confidence interval for the correlation was over 50%. When the form of Equation 5.6 was tried, the confidence interval dropped to 38%. Due to the limited range of mass flux over which the R22/R141b was run, the validity of not using Chen's form cannot be assessed.

5.5.1 Nucleate Boiling versus Convective Boiling for the R22/R123 Correlation

It is of interest to examine the breakdown between nucleate and convective boiling as predicted by the R22/R123 correlation shown in Table 5.3. The freezer evaporator is characterized by a large relative nucleate boiling component. In the freezer evaporator, the refrigerant mixture is at a low quality and the liquid flows in the bottom of the tube. There is a relatively large liquid heat transfer resistance between the vapor and wetted tube wall. This enhances nucleate boiling, increasing the chance of bubble formation at the bottom wall. The liquid resistance would tend to cause the liquid at the wetted tube wall to become superheated. The convective boiling component is small because the liquid is flowing in the bottom of the tube, reducing the amount of convective heat transfer area available to the liquid.

Table 5.3: Average percentage of nucleate and convective boiling for the R22/R123 correlation

evaporator	nucleate boiling	convective boiling
freezer	85.6%	14.4%
fresh-food	51.0%	49.0%

The fresh-food evaporator is characterized by a relatively large increase in the convective boiling component. As the mixture flows into the fresh-food evaporator, the vapor core velocity increases at the higher quality levels. The vapor core carries the remaining liquid up onto the tube wall, increasing the amount of convective heat transfer area; consequently, the convective boiling contribution increases. The nucleate boiling component drops 41% while the convective component rises 240%. The relatively small drop in the nucleate boiling component is caused by the increase in heat flux levels in the fresh-food evaporator. As the liquid is carried up on the tube wall it thins, and the heat transfer resistance between the vapor and the wetted tube wall decreases. This reduces the chance of nucleate boiling. The moderate drop is caused by the offsetting effects of the decreased liquid resistance and increased heat flux.

5.5.2 Boiling Number for Mixtures

When calculating the boiling number for mixtures, Equation 5.8, a question arises as to how to define h_{lg}. For pure refrigerants, h_{lg} is defined as the increase in enthalpy during vaporization or the saturated vapor enthalpy minus the saturated liquid enthalpy. It makes no difference whether h_{lg} is defined at constant pressure or constant temperature; the result is the same.

$$Bo = \frac{q''}{Gh_{lg}} \tag{5.8}$$

For mixtures, it makes a difference if h_{lg} is defined at a constant temperature or a constant pressure. Figure 5.8 shows the difference between the two definitions. The h_{lg} defined at constant pressure does not equal h_{lg} defined at constant temperature. Based on the physical system, it made more sense to define the mixture boiling number based on a constant-pressure h_{lg}. (For illustration purposes, the constant-temperature curve has been drawn as a straight line.) For R22/R123, the average constant-pressure boiling number from the experimental data is 6.7% less than the constant-temperature boiling number and 3.3% less for R22/R141b mixture data.

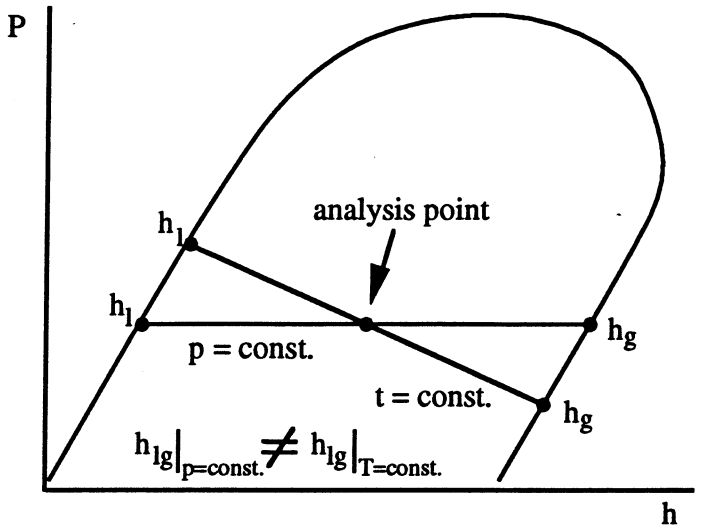

Figure 5.8: Plot showing the difference between h_{lg} at constant pressure versus h_{lg} at constant temperature

5.6 Comparison of Mixture Correlations to the UIUC R12 Correlation

Figure 5.9 shows a comparison between the local mixture correlations and the UIUC R12 average correlation. The local mixture correlations were integrated over the quality range of 10-90% to achieve the same evaporating temperature. The comparison was done over a heat and mass flux range that was common to all three fluids: G = 25-45 kg/m^2-s and q" = 2.0-2.8 kW/m^2 for an integrated evaporating temperature of -10°C and tube diameter of 7.9 mm.

Figure 5.10 shows a comparison between the R22/R123 mixture correlation and the UIUC R12 correlation at higher levels of mass flux. The comparison was done over a heat and mass flux range that was common to both fluids: G = 45-65 kg/m^2-s and q" = 2.0-2.8 kW/m^2 for an integrated evaporating temperature of -10°C and tube diameter of 7.9 mm. The uncertainty bars in both plots are the 95% confidence intervals determined for each mixture correlation.

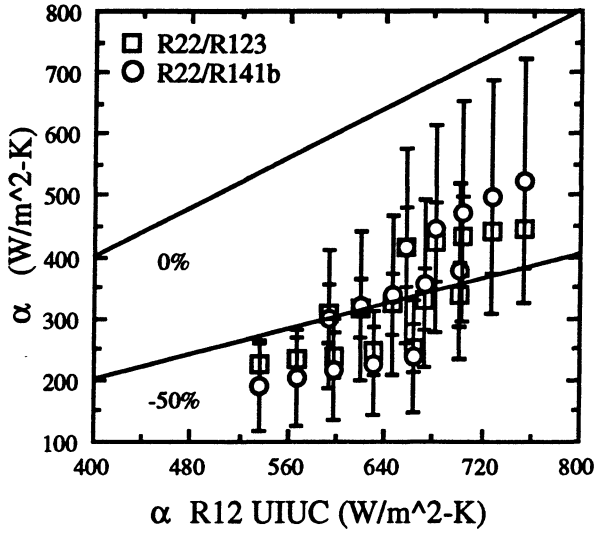

Figure 5.9: R22/R123 and R22/R141b mixture correlations versus UIUC R12 heat transfer coefficient correlation for G = 25-45 kg/m²-s by 10 kg/m²-s increments; q" = 2-2.8 kW/m² by 0.2 kW/m² increments; effective T_{sat} = -10°C; D = 7.9 mm

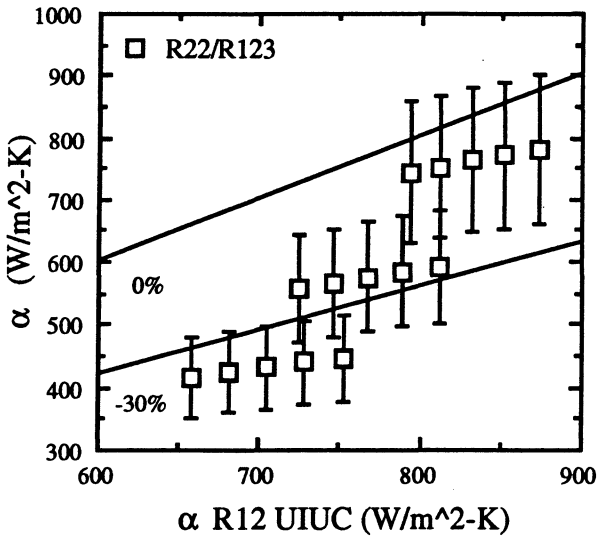

Figure 5.10: R22/R123 mixture correlation versus UIUC R12 heat transfer coefficient correlation for G = 45-65 kg/m²-s by 10 kg/m²-s increments; q" = 2-2.8 kW/m² by 0.2 kW/m² increments; effective T_{sat} = -10°C; D = 7.9 mm

Comparing the performance of both mixtures to R12 shows the mixtures severely under-perform R12 by 50% for the mass flux range of 25 - 45 kg/m²-s. At the higher mass fluxes, the heat transfer coefficient of the R22/R123 mixture rises more rapidly, approaching the R12 heat transfer coefficient values. At the low-mass fluxes, the relative contribution of convective boiling is less than at higher mass fluxes. For mixtures, it is believed that nucleate boiling is

suppressed due to the lowering of effective superheat at the wetted tube wall. Superheat is lowered because the more volatile component is driven away from the tube wall, enriching the remaining liquid with the less volatile component. At lower mass fluxes, nucleate boiling is the dominate heat transfer mechanism, but is severely reduced. As the mass flux increases, the convective boiling component quickly rises and increases the overall heat transfer coefficient. These results are consistent with those of Wattelet *et al.*[8]

The findings of Wattelet were similar to those presented in Figure 5.9 for low heat and mass flux flow conditions. Their results found that a mild zeotrope (~5°C glide) under-performed R12 by 20%. They concluded that the lower heat transfer coefficients were a result of decreased nucleate boiling and convective boiling. The decreased nucleate boiling was attributed to concentration gradients in the liquid. The decreased convective boiling was attributed to lower slip ratios and turbulence in the wavy-stratified flows, which may have decreased the mixing in the vapor stream, setting up concentration gradients in the vapor. For a more detailed explanation of heat transfer coefficient performance for pure refrigerants and mixtures for different flow regimes, see Chapter 2.

A comparison between the relative performance of the R22/R123 and R22/R141b mixtures indicates that the R22/R141b mixture under-performs the R22/R123 mixture at G = 25 kg/m^2-s. At higher levels of mass flux, the effect of heat flux increases for the R22/R141b and the mixture out-performs R22/R123. The increased effect of heat flux at higher mass fluxes may be caused by more tube wall contact with the refrigerant, increasing the number of possible nucleation sites. The more volatile R22/R141b mixture would be more prone to the onset of nucleate boiling at higher heat fluxes because it would take less effective superheat at the wall to begin bubble formation.

5.7 References

---

[1] Scott, D. S., "Properties of Co-Current Gas-Liquid Flow", *Advances in Chemical Engineering*, Vol. 4, pp. 199-277, Academic, New York, 1963.

[2] Pedersen, C. O., Non-Linear Least Squares True BASIC Program, July, 1992.

[3] Pedersen, C. O., Linear Least Squares True BASIC Program, July, 1992.

[4] Kandlikar, S.G., "A General Correlation for Saturated Two-Phase Boiling Heat Transfer Inside Horizontal and Vertical Tubes", *Journal of Heat Transfer*, Vol. 112, February, 1990, pp. 219-228.

---

[5] Wattelet, J. P., J. C. Chato, A. L. Souza and B. R. Christoffersen, "Evaporative Characteristics of R134a, MP39 and R12 at Low Mass Fluxes", ACRC TR-35, University of Illinois at Champaign Urbana, Air Conditioning and Refrigeration Center, May, 1993.

[6] Kandlikar, S.G., "A General Correlation for Saturated Two-Phase Boiling Heat Transfer Inside Horizontal and Vertical Tubes", *Journal of Heat Transfer*, Vol. 112, February, 1990, pp. 219-228.

[7] Chen, J. C., "Correlation for Boiling Heat Transfer to Saturated Fluids in Convective Flow", *Industrial Engineering Chemistry Process Design Development*, Vol. 5, No. 3, 1966, pp. 322-339.

[8] Wattelet, J. P., J. C. Chato, A. L. Souza and B. R. Christoffersen, "Evaporative Characteristics of R134a, MP39 and R12 at Low Mass Fluxes", ACRC TR-35, University of Illinois at Champaign Urbana, Air Conditioning and Refrigeration Center, May, 1993.

CHAPTER 6: OPTIMIZATION MODEL

The optimization problem was to minimize the life-cycle cost (LCC) of the modeled refrigerator for each pure refrigerant and refrigerant mixture (R12, R134a, 65% R22/35% R123 and 80% R22/20% R141b). The optimization program adjusted the evaporating pressure, the evaporator air-flow rates, the intercooler loads, and system superheat to achieve a minimum LCC. The results from Chapter 4, the evaporator air-side heat transfer coefficient curve fits, and Chapter 5, the mixture heat transfer coefficient correlations, were required to formulate the optimization problem and complete the refrigerator model. The air-side resistance equations had to be generalized as a function of both air velocity and the number of evaporator tube passes. The development of a fan power model, also a function of the required air velocity and the number of evaporator tube passes, was also required. Realistic relationships had to be obtained for the cost of incremental volume, heat exchangers, power and the evaporator fans.

6.1 Objective Function

The objective function is the LCC equation for the refrigerator. This function consists of three groups of terms: material cost, occupied volume cost and power costs. Retooling costs for the manufacturer were not considered in this analysis due to lack of information.

6.1.1 Material Cost

The first group of terms represents the material cost for the heat exchangers and the evaporator fans. There are four potential heat exchangers that can be used in the system: the freezer evaporator, the fresh-food evaporator, the high-temperature intercooler and the low-temperature intercooler. Some of the pure-refrigerant cases used a shared freezer and fresh-food evaporator which utilizes an air damper to control the air flow to each compartment (see Appendix D). This type of exchanger is identical to the exchanger currently found in domestic units.

Two types of evaporator fans were modeled for the optimization, a standard-efficiency fan and a high-efficiency fan. The cost of the high-efficiency fan was twice that of the standard fan and consumed only one-half the power. Specific cost information for the heat exchangers and fans will be presented later in this chapter.

Manufacturing costs were used to determine the costs of the exchangers and fans. The LCC analysis, however, was performed at the consumer level; therefore, an appropriate markup multiplier was necessary. The markup term did not affect the relative LCC of system A versus

system B, but it did present a more realistic distribution of material, occupied volume and operational costs. The markup term will be discussed in a later section.

6.1.2 Occupied Volume Cost

The second group of terms represents the heat exchanger occupied volume cost. As larger exchangers are used to meet various load configurations, two possible situations arise:

1. Additional internal volume of the refrigerator could be taken to accommodate the larger exchanger reducing the usable food storage space or
2. The overall internal volume of the unit could be increased to maintain the original food storage space.

For this analysis, it was assumed that the second situation would be possible and there were no external constraints on the overall volume of a domestic refrigerator. This assumption is not *entirely* realistic. Manufacturers must maintain certain refrigerator dimensions to enable the unit to fit in the existing space constraints of domestic kitchens. The first choice was ruled out, however, because it was *not known* how the customer would have perceived the loss of internal volume. The second choice also permitted consistent comparisons between units of the same usable internal volume.

A survey was conducted to determine the cost of additional volume to the consumer. Appendix F contains the results of this survey, which priced various sizes of refrigerator units with similar features and found that the average incremental volume cost was $\$44/ft^3$ ($\$1554/m^3$). This is comparable to the value used by the industry's research and design engineers.[1]

6.1.3 Power Costs

The third group of terms in the objective function is the cost of power consumed by the compressor and heat exchanger fans. The fan power model determined the power required to maintain air flow over an evaporator of a certain size. A fixed power consumption was assumed for the condenser fan. The compressor power was determined using a simple compressor model. The total power consumed by the fans and the compressor was multiplied by the total number of yearly operational hours, the unit cost of power and the present worth factor for the lifetime of the refrigerator. The number of operational hours was dependent upon the duty-cycle chosen. The duty-cycle will be discussed in a later section. It was assumed that the refrigerator model

contained no sweat heaters or defrost heaters. If all cases contained sweat and defrost heaters and were operated under the same conditions, the final comparative results would not change.

6.1.4 The Objective Function

Equation 6.1 is the objective function. Equations 6.2, 6.3 and 6.4 are the specific costs associated with each term.

$$LCC = \text{function(material cost, volume cost, operational cost)} \quad (6.1)$$

$$\text{material cost} = mu*(cof+coff+coli+cohi+cfanf+cfanff) \quad (6.2)$$

$$\text{volume cost} = uv*(ovf+ovff+ovli+ovhi) \quad (6.3)$$

$$\text{power cost} = dc*pa*up*hr*(pc+pf+pff+pcd)/1000.0 \quad (6.4)$$

The symbols in Equations 6.2 to 6.4 are as follows:

mu	- markup factor
cof	- cost to manufacture freezer evaporator ($)
coff	- cost to manufacture fresh-food evaporator ($)
coli	- cost to manufacture low-temp. intercooler ($)
cohi	- cost to manufacture high-temp. intercooler ($)
cfanf	- cost of the freezer evaporator fan ($)
cfanff	- cost of the fresh-food evaporator fan ($)
uv	- cost/volume ($/m^3)
ovf	- occupied volume of freezer evaporator (m^3)
ovff	- occupied volume of fresh-food evaporator (m^3)
ovli	- occupied volume of low-temp. intercooler (m^3)
ovhi	- occupied volume of high-temp. intercooler (m^3)
dc	- fraction, compressor run time (duty-cycle)
pa	- present worth factor
up	- power cost ($/kW-hr)
hr	- hours/year (hr/yr)
pc	- compressor power (W)
pf	- freezer fan power (W)
pff	- fresh-food fan power (W)
pcd	- power of condenser fan (W)

6.2 Independent Variables

There were six independent variables in the optimization. The impact of each variable is discussed in this section. The six independent variables are listed in Table 6.1.

Table 6.1: The six independent variables in the optimization

p	- low-side pressure for cycle (kPa)
velf	- velocity of air over freezer evaporator (m/s)
velff	- velocity of air over fresh-food evaporator (m/s)
lli	- load on the low-temperature intercooler (W)
lhi	- load on the high-temperature intercooler (W)
sh	- system superheat (°C)

The most important and influential independent variable is the *evaporating pressure*. As the evaporating pressure is varied, the operating cost changes significantly. If the evaporating pressure is increased, the system pressure ratio is reduced, thereby reducing the compressor work. The compressor therefore requires less energy and the operating cost decreases. An increase in evaporator pressure also reduces the temperature difference between the refrigerant and the air, requiring larger heat exchangers to meet the same load demand. As a result, the material and occupied volume costs increase.

The *air velocities* over the freezer and fresh-food evaporators affect the material, volume and operating costs. As the velocity over an evaporator is increased, the size of the exchanger can be reduced to meet the load demand, thereby reducing the material and occupied volume costs. At higher air velocities, the air-side heat transfer coefficient also increases. Since an evaporator is dominated by air-side resistance, increasing the air velocity is an effective means for reducing the evaporator size to meet a given load demand. However, as the velocity of the air is increased, the operating costs also increase due to the increased power consumption of the fan. The optimization program had to determine the air velocities that maximized the reduction of the material and occupied volume costs and minimized the increase in the operating costs.

The next two independent variables are the *high-* and *low-temperature intercooler loads*. The use of intercoolers can dramatically affect the performance of a mixture system and may improve the performance of a pure-refrigerant system, as discussed in Chapter 2. The addition of intercoolers has very little effect on material or occupied volume cost. The exchangers occupy little space and use a minimum amount of material, yet are able to dramatically affect the operating costs of a system.

The intercooler load (extent or degree of intercooling) was chosen as an independent variable for two reasons. First, as stated above, the use of intercoolers can dramatically affect the

performance of a mixture system. The independent variables should have a strong affect on the objective function. Second, knowing the intercooler load simplified the solution of the equations that described the thermodynamic cycle. The thermodynamic state points of the cycle are able to be calculated before the areas of the heat exchangers are determined.

The addition of *superheat* in some cases can lower the overall operating costs of a system by increasing system capacity. As discussed previously, this increase in capacity is offset by starting compression further out in the superheat region. The relative increase in system capacity weighted against the relative increase in compressor work dictates whether system superheat offers an advantage.

Each of the six independent variables had physical bounds that could not be exceeded. In most cases, the bounds are obvious. The evaporating pressure could vary from 0 kPa up to, but not including, the evaporating pressure that would cause a temperature pinch-point to occur in an evaporator or intercooler. An evaporator pinch-point occurs when the refrigerant temperature exceeds the air temperature at any point in the exchanger. The intercoolers, if used, must be checked for temperature pinch-points with the high-pressure liquid.

The air velocities for both evaporators were bounded between 0.4 m/s and 1.8 m/s. These were the limits of the experimental data that were taken (see Chapter 4). No information on the air-side heat transfer coefficient for the evaporators was available outside of these limits.

The load limits on the high- and low-temperature intercoolers could vary from 0 W up to, but not including, the intercooler load that would cause a pinch-point to occur with the high-pressure liquid for either intercooler.

Special consideration was given to the total intercooler load. The sum of both intercooler loads was constrained so that it would not exceed the usable amount of two-phase capacity. Equation 6.5 is the constraint on the sum of the intercooler loads.

$$lli + lhi \leq \dot{m}_r h_{lg} - (Load_f + Load_{ff}) \tag{6.5}$$

All six independent variables were chosen because of their physical significance. The equations were arranged to accommodate a sequential solving scheme (as opposed to matrix inversion), reducing the overall computation time for the optimization program.

6.3 Fixed Parameters

The fixed parameters are the numbers and values that the user of enters into the optimization program. These are constant for a series of optimization runs.

6.3.1 Compartment Temperatures

The freezer and fresh-food temperatures were chosen to conform to the American National Standard for household refrigerators.[2] There is really no lower limit on the freezer temperature. The lower the freezer temperature, the longer frozen foods can be safely stored. The only requirement is that the freezer temperature be less than or equal to -15°C, the suggested temperature based on the long term economical storage of most frozen foods.

The fresh-food temperature has defined upper and lower limits. The lower limit, 1.1°C, is as close to freezing, 0°C, as possible to still insure that no food in any section of the fresh-food compartment will freeze. The upper limit temperature, 5°C, is based on experience. Higher temperatures will shorten the safe storage periods of the food in this compartment.

The lower temperature limit in the freezer compartment must be chosen by considering the economic trade-off between longer food preservation and higher operating costs. The upper temperature limit in the fresh-food compartment must be chosen by considering the economic trade-off between lower operating costs and increased chance of food spoilage.

The freezer compartment temperature was chosen to be -17°C and the fresh-food compartment temperature was chosen to be 3°C. These temperature values were used as the air-inlet temperatures for the freezer and fresh-food evaporators. The exiting air temperature is always lower than the compartment temperature.

6.3.2 Module Inlet Temperature

The evaporator module inlet temperature is the high-pressure liquid refrigerant temperature that exits the condenser. In the experimental test setup, described in Chapter 3, the module inlet temperature was set with an immersed cable heater. This is the temperature at state point 1 shown in Figure 3.1. One logical restriction for this temperature is that it must be above ambient temperature. The condenser in a fully operational system would not be able to reduce the refrigerant temperature any lower than the air temperature with which it is exchanging heat.

The value of 44°C was chosen based on actual system data from a General Electric TBX18KMM top-mount refrigerant freezer taken by Staley.[3]

6.3.3 Compressor Isentropic Efficiency

An isentropic efficiency of 0.5 was chosen. This value is an average of the R12 and R134a compressor isentropic efficiencies feasible using current technology at a desired pressure ratio of 11. The isentropic efficiency versus pressure ratio relationships that were used were derived by Staley.[4] The compressor model will be discussed in another section.

6.3.4 Fan Efficiency

Two levels of fan efficiency were available: a 28.5% electrically-efficient low-efficiency fan and a 68.5% electrically-efficient high-efficiency fan. The data for each type were based on power consumption and pressure drop data given by a manufacturer.[5]

6.3.5 Condenser Fan

The condenser fan was assumed to have a steady-state power consumption of 10.5 W. This information was obtained from a manufacturer.[6] Since the condenser fan is common to all the different systems that were optimized and a fixed size condenser was assumed, the magnitude of the condenser fan power cannot change the relative ranking and performance of the optimized systems.

6.3.6 Cost of Energy

The cost of energy was chosen to be $0.075/kW-hr. This is slightly less than $0.079/kW-hr, the value currently used on "Energy Label" stickers found on all new appliances and used in a Department of Energy (DOE) impact study[7] for 1993 projected energy costs. The decision to use the 0.075 value was made before the 0.079 value had been found. Since the values were very close, the 0.075 value was used.

6.3.7 Refrigerator Duty-Cycle

The duty-cycle is the percentage of 'on' time for the refrigerator. For units with the same loading, the duty-cycle is directly related to the effectiveness of the cabinet insulation. A duty-cycle of 0.4 was chosen based on data in the DOE impact study.[8] The duty-cycle and the evaporator loads were required to simulate the heat leak into the cabinet over time. Since the objective of this study was steady-state modeling, the duty-cycle essentially allowed continuous operation at transient loading conditions.

6.3.8 Cost per Unit Volume

The incremental cost per unit volume was determined to be \$1554/m^3 (\$44/ft^3). This number was calculated from a survey of different sized refrigerators with similar features. Appendix F contains the results of the survey.

This figure was required to calculate the occupied volume cost for a heat exchanger in the refrigerator cabinet. As discussed earlier, the internal volume of the refrigerator was assumed to be a constant 0.51 m^3 (18.00 ft^3). The cost of adding additional volume to house a larger heat exchanger was taken into account using the cost per unit volume.

6.3.9 Markup

A markup factor was determine to maintain the proper relationship between the operational costs, calculated at the consumer level, and the material costs, calculated at the manufacturing level. The consumer must bear all the costs associated with owning and operating a refrigerator; therefore, the analysis included a retail markup from the manufacturer's equipment cost.

The markup was calculated to be 2.33, based on the consumer and manufacturer cost information in the previously mentioned DOE impact study.[9] The manufacturer cost for an 18 ft^3 top-mount auto-defrost refrigerator-freezer in 1987 dollars was given as \$220.00. The consumer price in 1987 dollars for the same unit was given as \$512.38. It was assumed that this ratio holds fairly constant over time; therefore, the 1993 markup factor was also assumed to be 2.33.

6.3.10 Discount Rate

The real discount rate was assumed to be zero. This assumption implies that the real rate of increase of energy prices equals the prevailing interest rate. The current Federal Funds Rate minus the twelve-month moving average change in the Consumer Price Index[10] is currently at zero percent. The historical average for the last twenty years has been approximately three percent. With the current value of the real interest rate around zero since mid-1992, the slow recovery coupled with the absence of any inflationary pressure ensures that the real interest rate will not be rising in the near future.

6.3.11 "Life Expectancy" of a Refrigerator

DOE considers the life expectancy of a refrigerator to be nineteen years.[11] Manufacturers assume a twenty-year life, while the customer expects a refrigerator to last 17 years.[12] An 18-year lifetime was chosen as the best compromise between the various expectations.

6.3.12 Freezer and Fresh-food Loads

The total evaporator load was chosen to be 200 W. Other studies done by Staley[13] and DOE[14] measured or used a load of approximately 170 W. Three different load combinations were considered for the distribution of the load between the freezer and fresh-food compartments: 50%/50% (100 W / 100 W), 60%/40% (120 W / 80 W), and 40%/60% (80 W / 120 W).

6.3.13 Fan Costs

Based on information from a manufacturer, the manufacturer's cost for a standard-efficiency evaporator fan (η_{OV} = 8%) was approximately $3.00. The cost of the high-efficiency model (η_{OV} = 16%) was $6.00.

6.4 Other Assumptions

Other assumptions that were part of the optimization model:

- Pressure drop was not included in the optimization model. For the R12, R22, R22/R123 and R22/R141b experimental runs (Chapters 4 and 5), the average measured pressure drop was 4.48 kPa (0.65 psi), 3.37 kPa (0.49 psi), 3.01 kPa (0.44 psi), and 3.94 kPa (0.57 psi) respectively. The total average pressure drop for all four fluids of 3.70 kPa (0.54 psi) was considered negligible.

- All components and connection lines were perfectly insulated and did not lose heat to the surroundings.

- The refrigerant at the entrance to the evaporator module (on the high-pressure side) was a saturated liquid. This fact, in conjunction with the specified 'condenser outlet' / evaporator module inlet temperature (section 6.3.2), fixed this state point.

- The compressor and condenser costs were fixed. It was assumed that combined costs of these components were approximately equal for all systems analyzed.

The author is fairly confident that a compressor could be built for a specific fluid that would provide the required cycle temperature lift at the same cost as another compressor for a different fluid. The assumption starts to break down for the condenser cost. There will be different sized condensers required for each optimized system. The mixture condensers will be larger and require more heat transfer area for cycle heat rejection due to the mixture glide.

- The optimization model was for steady-state operation. Transient operation was not considered for this study. Transient modeling and optimization would be a area for future study.
- Every system has a cabinet with 18 ft^3 of *usable* cabinet space (section 6.1.2).
- Industry retooling costs *were not considered* as part of this optimization model due to lack of information.
- Both the base case system and the optimized system configurations were simulated to be top-mount refrigerators with *no* sweat or defrost heaters.

6.5 Solution of Optimization Problem

Several methods were investigated to solve the optimization problem. The use of Lagrange multipliers was explored, but abandoned because of the complication in evaluating the partial derivatives involving the refrigerant properties. The refrigerant properties were in non-explicit form, calculated from a set of refrigerant property subroutines. Routines that employed numerical methods to evaluate the derivative were also unsuccessful because the solution surface around the optimum was very flat.

Other methods explored included EES (Engineering Equation Solver), IMSL routine BCONF (a gradient technique) and IMSL routine BCPOL (a direct search technique). EES was not used because of its inability to handle mixture properties. It was concluded that the best method to use would be one which would interface with the existing thermodynamic property subroutines; therefore, the IMSL subroutine libraries were explored for a suitable solution algorithm.

The first IMSL routine tried was NCONF, a general non-linear constrained minimization routine using a successive quadratic programming algorithm and a finite difference gradient. When applied to the optimization problem, this routine prematurely terminated at local optima.

The second IMSL routine, BCPOL, was used to solve the optimization problem. BCPOL uses a direct search complex method to find a minimum point of a function with simple bounds. The method is based on function comparison and no smoothness is assumed. This method worked best and consistently gave repeatable results.

6.6 Component Modeling

6.6.1 Evaporators

The model for the evaporator was originally planned to be the segmented evaporator model described in Chapter 5 and Appendix E. The optimization program, however, had six independent variables in the most computationally-intensive case. The use of the segmented model was not practical because of the numerous subroutine calls associated with its use. It was decided to assess the error of using the UA/LMTD method with the mixtures and carry the associated uncertainty of the error through to the LCC results. Great gains in computational time were made.

In Chapter 4, the pure-refrigerant heat transfer coefficient from an existing correlation and the evaporator UA value from the UA/LMTD method were used to calculate the heat transfer coefficient of the air as a function of velocity. In Chapter 5, the air-side heat transfer coefficient from Chapter 4 results and the system operating conditions measured by experiment were used to calculate the heat transfer coefficient of the refrigerant mixture. For the optimization, both the air-side and refrigerant-side heat transfer coefficient correlations were used to determine the size of the evaporator necessary to meet a required load.

The following equations illustrate the various versions of the evaporator model that were used and explain the solution procedure. As mentioned in Chapter 4, the air-side heat transfer coefficients were calculated using Equations 6.6 and 6.7.

$$\frac{1}{UA} = \frac{1}{\alpha_a A_a} + \frac{1}{\alpha_r A_r} \tag{6.6}$$

$$UA = \frac{q}{LMTD} \quad \text{where} \quad LMTD = \frac{\Delta T_2 - \Delta T_1}{\ln(\Delta T_2 / \Delta T_1)} \tag{6.7}$$

As discussed in Appendix E, the UA/LMTD analysis can be used without error on an exchanger operating with a pure refrigerant in the low heat and mass flux range. The heat transfer

coefficient of the air as a function of the velocity of air over the evaporator, α_a, was easily calculated using Equation 6.8.

$$\alpha_a(v) = \frac{\frac{1}{A_a}}{\frac{1}{UA} - \frac{1}{\alpha_r A_r}} \tag{6.8}$$

α_r was supplied from the UIUC R12 correlation at the measured flow conditions. UA was calculated using Equation 6.7 (q and Ts came from the experiment). The areas, A_r and A_a, are obtained from the physical dimensions of the exchanger.

The problem was slightly more complicated in Chapter 5 because, as discussed in Appendix E, the refrigerant-mixture specific heats were not constant. The evaporator had to be subdivided into small, constant-specific heat segments in order to apply Equation 6.6 on a localized basis. The heat transfer coefficient for the air as a function of the air velocity was determined in the previous pure-refrigerant runs. Using this information and the measured load information, the heat transfer coefficient of the refrigerant mixtures was determined. The iterative solution is outlined below:

Guess α_r (6.9)

$$UdA = \left[\frac{1}{\alpha_a(v)dA_a} + \frac{1}{\alpha_r dA_r}\right]^{-1} \tag{6.10}$$

i = 1, total # of segments

$$dq_i = UdA(T_{a_i} - T_{r_i}) \tag{6.11}$$

loop

$$\text{adjust } \alpha_r \text{ so that } \sum_i dq_i = q_{measured} \tag{6.12}$$

As mentioned above, the iterative procedure was abandoned to save computational time. In the optimization program, the sizes of the heat exchangers were no longer fixed. The air-side resistance model developed at the end of Chapter 4 had to be incorporated with Equation 6.6. The resulting model could calculate the number of heat exchanger passes given the air velocity,

the heat transfer coefficient of the refrigerant and the UA of the heat exchanger. The UA value was calculated using Equation 6.7. The length of each pass and the geometry of the tube and fins were fixed. The final form of the model is shown in Equation 6.13.

$$\text{pass\#}(v, UA, \alpha_r) = \frac{R_{a,1pass}(v) - m(v) + (\pi D \alpha_r)^{-1}\left[\frac{sfin}{2}\right]^{-1}}{\left[\left(\frac{UA}{len}\right)\left(\frac{sfin}{2}\right)\right]^{-1} - m(v)} \tag{6.13}$$

where:

$$m(v) = \frac{R_{a,8pass}(v) - R_{a,1pass}(v)}{7} \tag{6.14}$$

sfin is the fixed distance between each fin and len is the fixed pass length. The size of each evaporator was easily determined for a given air velocity, v, the UA value calculated from state point and system information, and refrigerant heat transfer coefficient calculated from the developed mixture correlations.

Calculation of Evaporator Mass and Volume

A subroutine was written to calculate the mass and occupied volume of the evaporator coil for a given number of tube passes. (Coil, or evaporator coil, is another way to refer to an evaporator.) The occupied volume ratio, the mass ratio and the cost to manufacture the coil were also calculated. The mass ratio and occupied volume ratio will be described in the next section.

Figure 6.1 shows the dimensions of the fin/tube section which was used to 'build' the optimized evaporators. Each pass length was 53.34 cm (21 in.) and the number of rows required to meet the given load was calculated from Equation 6.13. The total of the fin mass, tube mass

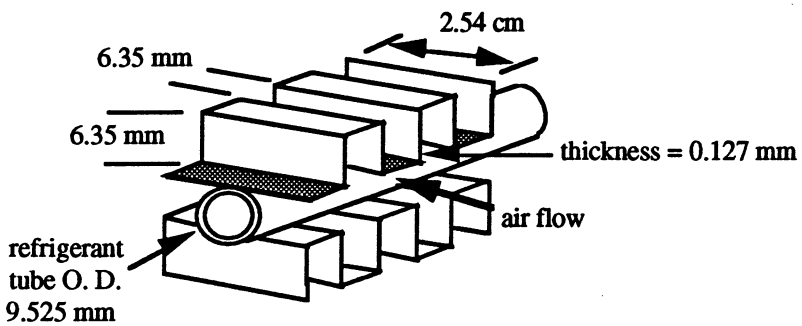

Figure 6.1: Fin dimensions of optimized evaporator fin/tube section

and return bend mass determined the total mass of the optimized evaporator. Care was taken to include the mass of the return bends of the evaporator. The return bends were assumed to have a radius of 1.27 cm (1/2 in.) and the total length of the bend extended 2.54 cm (1 in.) beyond the last applied fin.

For the occupied volume calculation, a 3.18 mm (1/8 in.) clearance in front and back and a 1.27 cm (1/2 in.) clearance on either side were added to allow for the passage of air over the evaporator. An air duct volume was also included in the occupied volume total (but not the occupied volume ratio as discussed in the next section). The duct volume was calculated to be 16.5 cm (6.5 in.) times the air duct face area at the evaporator. In the optimization cases where there was a single evaporator serving both the freezer and fresh-food compartments, the duct volume was doubled to account for the additional air passages.

Standard Evaporator Coil: Calculation of the Occupied Volume Ratio and Mass Ratio

The occupied volume ratio and the mass ratio were formed based on a 'standard' evaporator coil. The occupied volume ratio indicated how much more volume was displaced by the optimized coil (the air duct volume is *not* included). The mass ratio indicated how much more mass was required to build the optimized coil. The specifications of the standard evaporator and optimized evaporator fin/tube section are listed in Table 6.2. The standard evaporator is representative of those currently used in domestic refrigerators. A performance comparison between the standard coil and the optimized fin/tube section was done by Heun.[15]

Table 6.2: Comparison of standard evaporator coil versus optimized fin/tube section

	standard coil[16]	optimized fin/tube section (per pass)
mass	853.2 g	45.255 g/pass
occupied volume*	7.2267×10^{-3} m^3	4.056×10^{-4} m^3/pass
fin thickness	0.19 mm (0.0075 in.)	0.127 mm (0.005 in.)
# of passes	16	various
dimensions*	20.32 cm H x 62.23 cm W x 5.72 cm D (8 in. x 24.5 in. x 2.25 in.)	2.858 cm H x 55.88 cm W x 2.54 cm D (1.125 in. x 22 in. x 1 in.) per pass
area in air flow direct.*	355.64 cm^2	159.68 cm^2
outside evap. area	2.668 m^2	0.15 m^2/ pass
fins per inch	5	4
tube	9.53 mm (0.375 in.)	9.53 mm (0.375 in.)
tube wall	0.51 mm (0.020 in.)	0.51 mm (0.020 in.)
manufacture cost	\$5.20 = \$2.27 material + \$2.93 labor	\$ = 2.813*(mass in kg) + \$2.80

* includes 6.35 mm clearance on D, and 2.54 cm clearance on W

Construction Cost

The evaporator cost was estimated based on the evaporator mass. The manufacturing cost estimation was obtained from conversations with an evaporator manufacturer.[17] Two data points were obtained: the cost break-downs for a standard coil and a double-mass coil with standard coil fin geometry. A straight line was fit through the points to determine evaporator cost as a function of evaporator mass. Table 6.3 lists the two data points that were used. The manufacturing cost relation is shown in Equation 6.15 where m is the mass of the evaporator in kilograms. The cost relationship was assumed to hold for both the standard evaporator coil and the optimized evaporator coil.

Table 6.3: Manufacture cost data for evaporators

	standard coil	double mass coil
mass	853.2g	1706.4g
manufacture cost	\$5.20 = \$2.27 material + \$2.93 labor	\$6.70 = \$3.22 material + \$3.48 labor

$$\$ = 2.813\left(\frac{\$}{kg}\right)(m) + \$2.80 \tag{6.15}$$

6.6.2 Intercoolers

The intercoolers were modeled in a similar fashion as the evaporators. Equations 6.16 and 6.17 show the model used to calculate the size of the intercooler given a specific load and set of operating conditions. As explained in Chapter 3, the intercoolers were helically-wrapped and soldered copper tubes. The outside diameters for the low-pressure and high-pressure refrigerant tubes were 9.525 mm (3/8 in.) and 3.175 mm (1/8 in.) respectively. The thermal resistance of the tubes was negligible and the contact resistance between the two tubes was considered negligible because they were soldered together. Equation 6.17 is Equation 6.16, rewritten in terms of lengths. The term R_{sp} is introduced to account for the spiraling of the smaller high-pressure liquid tube around the larger low-pressure tube in order to define the intercooler in terms of one length.

$$UA = \frac{1}{\frac{1}{\alpha_{hp}A_{hp}} + \frac{1}{\alpha_{lp}A_{lp}}} \tag{6.16}$$

$$len_{lp} = \frac{UA}{\pi}\left[\frac{1}{\alpha_{hp}D_{hp}R_{sp}} + \frac{1}{\alpha_{lp}D_{lp}}\right] \tag{6.17}$$

where: hp - high-pressure side, lp - low-pressure side

$len_{hp} = len_{lp} R_{sp}$ and $R_{sp} = 1.176$

UA can be calculated from the UA/LMTD method shown in Equation 6.18.

$$UA = \frac{q}{LMTD} \quad \text{where} \quad LMTD = \frac{\Delta T_2 - \Delta T_1}{\ln(\Delta T_2 / \Delta T_1)} \tag{6.18}$$

No special provision needed to be made for the use of the UA/LMTD method with pure refrigerants or mixtures for the intercooler. The specific heats are constant for the pure refrigerant and can be assumed to be constant for the mixtures. The intercoolers exchange heat over a relatively small quality range and the specific heat of the mixture does not vary much, as shown in Figures 6.2 and 6.3, reproduced from Appendix E. The intercooler operation range is superimposed on the graphs. In addition to satisfying the assumption of constant-specific heats, the intercoolers were counter-flow; therefore, no additional modification or justification was needed in order to apply the UA/LMTD method. Please see Appendix E for further discussion. (In the uncertainty appendix, Appendix C, there is no mention of an uncertainty for using the UA/LMTD method for the mixture intercoolers for the reasons just stated.)

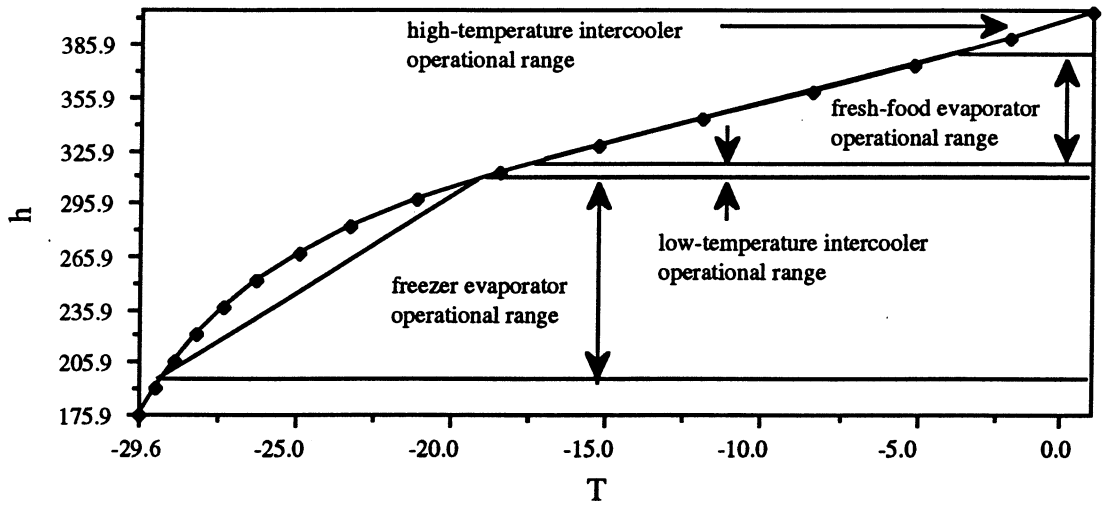

Figure 6.2: Enthalpy versus temperature for the 65% R22/35% R123 mixture at an evaporating pressure of 131 kPa (the evaporator and intercooler operational ranges are shown)

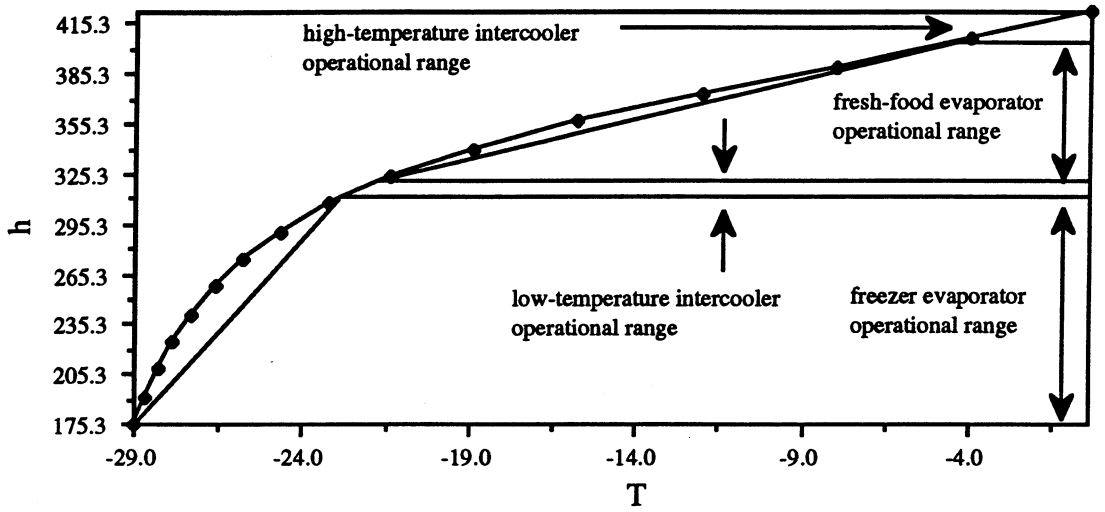

Figure 6.3: Enthalpy versus temperature for the 80% R22/20% R141b mixture at an evaporating pressure of 145 kPa (the evaporator and intercooler operational ranges are shown)

Calculation of Intercooler Mass and Volume

A subroutine was written to calculate the intercooler mass and occupied volume, given the intercooler length. R_{sp}, as defined above, was used to determine the length of the smaller diameter tubing.

Construction Cost

The construction cost of the intercooler was calculated based on information provided by a manufacturer.[18] The material cost was based on the $1.37/kg spot price of aluminum on April 18, 1992. A material markup factor was calculated based on the processed material cost (handling and extruding costs). The final cost of material was $2.61/kg. The labor cost was calculated to be 2.34 times the material cost. Equation 6.19 gives the construction cost as a function of the total intercooler mass, m (kg).

$$\$ = 2.61\left(\frac{\$}{kg}\right)(m)(1+2.34) \tag{6.19}$$

6.6.3 Fans

The optimization required the development of a fan model to determine the power consumption of the evaporator fan as a function of air velocity, pressure drop, geometry of the evaporator (which affects pressure drop), and fan efficiency. Air velocity is an independent

variable varied by the optimization program; pressure drop is a function of velocity and the geometry of the evaporator; and fan efficiency is selected to be either high or low, depending on the type of fan chosen for the system. This section will be divided into two parts. The first explains the development of the fan model as a function of air velocity and pressure drop. The second part explains the development of the fan model as a function of air velocity, pressure drop, and evaporator geometry.

Power as a Function of Air Velocity and Pressure Drop

Two fan types, standard-efficiency and high-efficiency, were modeled from typical evaporator fan operating conditions obtained from a manufacturer. A general system operating point for these two fans is presented in Table 6.4.[19]

Table 6.4: Operating conditions for standard and high-efficiency fans

fan	power	CFM	Δp_{tot} - system pressure drop	RPM	electrical efficiency
standard-efficiency	9.5 W	52.5 CFM	0.125 " H_2O	2850	28.5%
high-efficiency	4.75 W	52.5 CFM	0.125 " H_2O	2850	68.5%

For fans that produce a small change in pressure, air can be treated as incompressible and the ideal specific work is:

$$w = \int v dp = v\Delta p \tag{6.20}$$

The total ideal work can be written as:

$$W = \dot{m}v\Delta p = Q\Delta p = vA_{cros}\Delta p \quad \text{where} \quad Q = \dot{m}v = vA_{cros} \tag{6.21}$$

Pressure drop is a function of velocity. Rewriting Equation 6.21 to show the functional relationships gives:

$$W(v, \Delta p(v)) = vA_{cros}\Delta p(v) \tag{6.22}$$

The ideal fan work is a function of velocity, v, and the pressure rise across the fan, $\Delta p(v)$. The actual work can be calculated if the overall fan efficiency is known as shown in Equation 6.23.

$$W_{act}(v, \Delta p(v)) = \frac{W(v, \Delta p(v))}{\eta_{ov}} \tag{6.23}$$

The overall fan efficiency can be calculated from Equation 6.23 using the information in Table 6.4, the pressure drop, the volumetric flow rate of air, and the actual power consumed. η_{ov} = 8.12% for the standard-efficiency fan and 16.23% for the high-efficiency fan. Both operating points are at 52.5 CFM (0.02478 m^3/s) and 1/8 in. of H_20 (31.13 Pa); furthermore, η_{ov} is assumed constant over all operating conditions.

The only fan data available were the single operating points from Table 6.4. This is not enough information to simulate the fan at other operating conditions. As the velocity changes, the pressure drop through the fan duct will change. A relationship can be derived between pressure drop and velocity that will allow the calculation of consumed power at any pressure drop or air velocity.

An equivalent duct length, dz, can be calculated from the information in Table 6.4, using a pressure drop correlation. The pressure drop can be calculated as a function of air velocity using dz and the pressure drop correlation.

Defining the Reynolds number for the flow over the evaporator:

$$Re_D = \frac{vD_h}{\upsilon} \quad \text{where} \quad D_h = \frac{4A_{cros}}{P} \tag{6.24}$$

Pressure drop for a smooth surface with Reynolds number less than 20,000 can be defined:[20]

$$\Delta p(v) = 0.316 Re_D^{-1/4} \left(\frac{\rho v^2}{2D_h} \right) (dz) \tag{6.25}$$

Using the information from Table 6.2 to obtain A_{cros} and P for the standard evaporator and the information from Table 6.4 to obtain Δp and $v(Q, A_{cros})$ for the standard evaporator, dz can be calculated using Equation 6.25. Assuming that dz is constant, Equation 6.25 can be used to calculate the pressure drop at various velocities. By combining Equations 6.22 to 6.25, a plot of fan power consumption versus volumetric flow rate can be generated, as shown in Figure 6.4 for the standard 16-tube evaporator (Table 6.2).

Power as a Function of Air Velocity , Pressure Drop, and Evaporator Geometry

To further develop the fan power model, the relationship between pressure drop and evaporator size needed to be established. Pressure drop is a function of velocity, evaporator face area perpendicular to the air flow, and the evaporator length in the air-flow direction. This length

is a function of the number of tube passes only; therefore, the functional relationship for pressure drop can be written, $\Delta p = \Delta p(v, A_{cros}, pass\#)$.

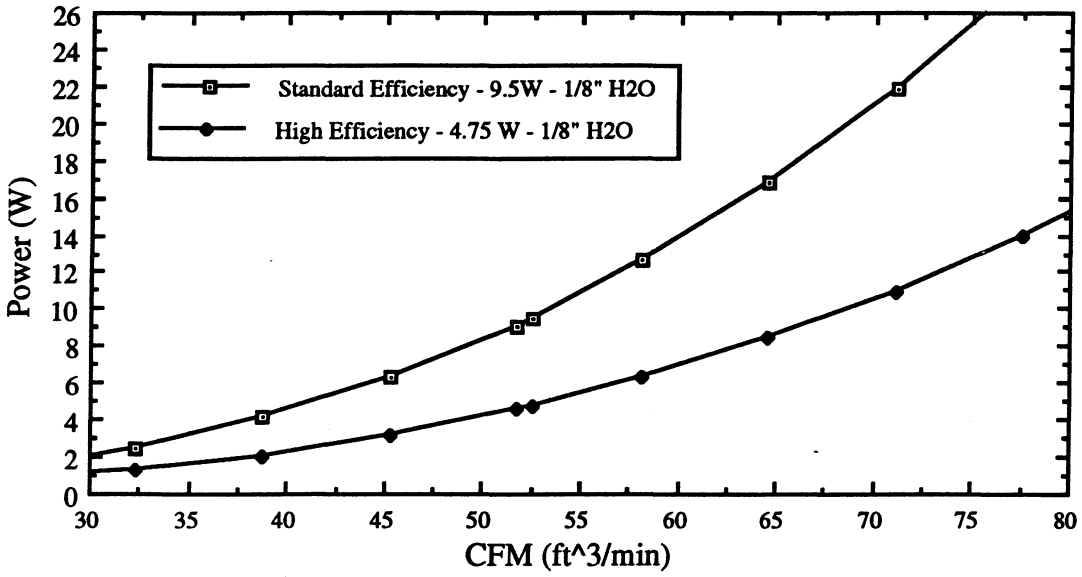

Figure 6.4: Fan model power versus CFM

To determine the relationship between pressure drop and evaporator geometry, the pressure drop attributable to air flow over the evaporator and the pressure drop attributable to the air flow through the delivery duct needed to be determined. Based on industry measurements[21], the pressure drop split between the evaporator and duct is approximately equal for a standard top-mount refrigerator as shown in Equation 6.26.

$$[\Delta p_{tot}(v)]_{std} = [0.5\Delta p_{tot}(v)]_{duct-std} + [0.5\Delta p_{tot}(v)]_{evap-std} \qquad (6.26)$$

It was assumed that the total pressure drop for the standard evaporator was the same as the total pressure drop for the optimized evaporator with 12 tube passes for all air velocities, as shown in Equation 6.27. In the experiment, the freezer evaporator was eight passes and the fresh-food evaporator was four passes. The experimental evaporators were designed for a total load of 200 W. Combining the two experimental evaporators into one equivalent evaporator results in a 12-pass evaporator. The optimized evaporator pressure drop was assumed to be 50% greater than the standard evaporator pressure drop, as shown in Equation 6.28. The cross-sectional area of the optimized evaporator is 55% less than the standard evaporator; therefore, the pressure drop across the optimized evaporator is greater. The velocity is higher for equivalent volumetric flow rates, and at higher velocities the pressure drop is greater. (See Equation 6.25)

$$[\Delta p_{tot}(v)]_{std} = [\Delta p_{tot}(v)]_{opt} \quad (6.27)$$

$$\Delta p_{tot}(v) = \Delta p_{duct_{opt}}(v) + \Delta p_{evap_{opt}}(v, A_{cros}, pass\#) = 0.25\Delta p_{tot}(v) + 0.75\Delta p_{tot}(v) \quad (6.28)$$

In Equation 6.25, pressure drop is linearly related to the change in equivalent duct length, dz. Equation 6.29 relates the optimized evaporator pressure drop to the number of tube passes for a fixed face area.

$$\Delta p(pass\#, v) = 0.25\Delta p_{tot}(v) + 0.75\left(\frac{pass\#}{12}\right)\Delta p_{tot}(v) \quad (6.29)$$

where

$$\Delta p_{tot}(v) = 0.316 Re_D^{-1/4}\left(\frac{\rho v^2}{2D_h}\right)(dz) \quad (6.30)$$

$$\Delta p_{tot}(v) = 6.5712v + 42.125v^2 - 3.9821v^3 \quad (6.31)$$

Equation 6.30 was curve fit as a function of velocity using the same equivalent duct length calculated in the previous section for the geometry of the standard evaporator, whose dimensions are given in Table 6.2. The resulting curve fit is given in Equation 6.31. As mentioned earlier, it was assumed that the total pressure drop for the standard evaporator was the same as the total pressure drop for the optimized evaporator for all air velocities (Equation 6.27).

The fan power as a function of pass number and velocity was calculated using Equation 6.32. $\Delta p(pass\#, v)$ was calculated using Equations 6.29 and 6.31. $\eta_{ov} = 8.12\%$ for the standard-efficiency fan and 16.23% for the high-efficiency fan.

$$Power(pass\#, v) = \left(\frac{\Delta p(pass\#, v) v A_{cros_{opt}}}{\eta_{ov}}\right) \quad (6.32)$$

6.6.4 Compressor

The compressor power consumption was modeled assuming an isentropic efficiency as shown in Equation 6.33.

$$\eta_s = \frac{w_s}{w_{act}} = \frac{h_{9s} - h_8}{h_9 - h_8} \tag{6.33}$$

As mentioned in an earlier section, the isentropic efficiency of 50% was chosen because it was an average of the R12 and R134a compressor efficiencies using current technology operating at reasonable pressure ratios. It was therefore assumed that a compressor could be built that would achieve a 50% isentropic efficiency for each specific mixture.

As illustrated in Figure 2.5, the compressor entering enthalpy was h_8 and the exit enthalpy was h_9. The isentropic work was calculated by finding the exit enthalpy, h_{9s}, of the compressor at the discharge pressure, which lies along the same isotrope as the compressor entering enthalpy, h_8. Solving Equation 6.33 for h_9, the 'actual' exit enthalpy of the compressor, and substituting into Equation 6.35 yields the actual work for the compression.

$$h_9 = h_8 + \frac{(h_{9s} - h_8)}{\eta_s} \tag{6.34}$$

$$W_{act} = \dot{m}(h_9 - h_8) \tag{6.35}$$

6.7 References

---

1 Private conversation with Jeff Anselmino, Whirlpool Corporation, Spring, 1993.

2 "American National Standard Household Refrigerators/Household Freezers", Association of Home Appliance Manufactures, ANSI/AHAM HRF-1-1988.

3 Staley, D. M, "Steady-State Performance of a Domestic Refrigerator/Freezer Using R12 and R134a", Master's Thesis, Department of Mechanical Engineering, University of Illinois at Urbana-Champaign, June, 1992, Appendix F, R12 Data, Date 6/19/91, p. 195.

4 Staley, D. M, "Steady-State Performance of a Domestic Refrigerator/Freezer Using R12 and R134a", Master's Thesis, Department of Mechanical Engineering, University of Illinois at Urbana-Champaign, June, 1992, Chapter 6, pp. 42, 44.

5 Proprietary Information.

6 Personal communication with Joe Ziegler at General Electric Appliance Division, Louisville, Kentucky.

---

[7] "Technical Support Document: Energy Conservation Standards for Consumer Products: Refrigerators and Furnaces", United States Department of Energy, DOE/CE-0277, November, 1989, p. 6-48.

[8] "Technical Support Document: Energy Conservation Standards for Consumer Products: Refrigerators and Furnaces", United States Department of Energy, DOE/CE-0277, November, 1989, p. 3-14.

[9] "Technical Support Document: Energy Conservation Standards for Consumer Products: Refrigerators and Furnaces", United States Department of Energy, DOE/CE-0277, November, 1989, pp. 3-47, 6-41.

[10] The Wall Street Journal, August 2, 1993, Section A, p. 1.

[11] "Technical Support Document: Energy Conservation Standards for Consumer Products: Refrigerators and Furnaces", United States Department of Energy, DOE/CE-0277, November, 1989, pp. B-22.

[12] Personal communication with Joe Ziegler at General Electric Appliance Division, Louisville, Kentucky.

[13] Staley, D. M, "Steady-State Performance of a Domestic Refrigerator/Freezer Using R12 and R134a", Master's Thesis, Department of Mechanical Engineering, University of Illinois at Urbana-Champaign, June, 1992, p. 113.

[14] "Technical Support Document: Energy Conservation Standards for Consumer Products: Refrigerators and Furnaces", United States Department of Energy, DOE/CE-0277, November, 1989, p. 3-14.

[15] Heun, M. K., "Thermal Performance Analysis of an Evaporator-Intercooler Module for a Lorenz Cycle", Master's Thesis, Department of Mechanical and Industrial Engineering, University of Illinois at Champaign-Urbana, 1991.

[16] Data on a 5 fin/inch 16 pass Peerless evaporator coil. Peerless of America, Inc., Chicago, IL. 60646.

[17] Mr. Peter Eckert, Peerless of America, Inc., Chicago, IL. 60646.

[18] Mr. Peter Eckert, Peerless of America, Inc., Chicago, IL. 60646.

[19] Proprietary Information.

[20] Incropera, F. P. and D. P. DeWitt, Fundamentals of Heat and Mass Transfer, 2nd ed., 1985, p. 372, Equation 8.20.

[21] Proprietary Information.

CHAPTER 7: OPTIMIZATION RESULTS

This chapter begins with an explanation of how the optimization results are presented. The remainder of the chapter is divided into five major sections. In the first section, the base-case R12 system is defined which serves as a bench mark to compare the other system configurations. The pure-refrigerant optimization results are presented in the second section. The mixture optimization results are presented in the third section. In the fourth section, a comparison is made between selected pure-refrigerant and refrigerant-mixture optimization results. The final section attempts to answer the question: How does the mixture system design optimum change if the mixture's interaction parameter, concentration, and heat transfer coefficient could be changed or improved?

As covered in Chapter 6, the optimization program attempts to minimize the life-cycle cost (LCC) of a selected refrigerant system by varying the independent variables. The LCC is the sum of the system and energy cost on the consumer level. The energy cost arises from the power required by the compressor, evaporator fan(s), and condenser fan. The manufacturing cost is the cost to the manufacturer to build the system. (These costs can also be referred to as first costs. However, it is important to remember that the manufacturers' retooling cost are not figured into these 'manufacturing' costs because this information was not available.) The manufacturing cost includes the heat exchanger costs (evaporator(s), suction-line heat exchanger or intercooler(s), condenser), occupied volume cost for the heat exchangers (essentially cabinet costs), fan costs, compressor costs, and other cabinet costs. Only the component and power costs which vary from system to system are modeled and are included in the LCC, energy cost, and manufacturing cost equations. Every system has a cabinet with 18 ft^3 of usable cabinet space, a compressor, a condenser, a condenser fan, etc.. The costs associated with these are figured into the base price of the unit.

The optimization results are presented on two types of graphs: LCC versus energy consumption cost (ene$), and manufacturing cost (man$) versus energy consumption cost. Energy consumption cost is the operation cost for the system over the lifetime of the unit. (Energy consumption cost is equivalent to energy consumption. The only difference between the two is the energy cost which is a constant.) These two graphs show the relative costs borne by the consumer and the manufacturer for a specific refrigerator system. The graphs illustrate how design improvements affect the consumer or the manufacturer and the relative trade-offs between the two. Every effort has been made to accurately determine the cost of building new

components and the impact these new components would have on manufacturing and consumer costs. See Chapter 6 for more information.

A base-case system was established and its results were used to modify the axes of the two types of result graphs. Each optimized system result is presented as a percent change relative to the base-case system. Figure 7.1 shows the two types of graphs. Improved systems would save energy and reduce the LCC. Beneficial systems for a consumer would plot down relative to the base-case system on the LCC plot. Almost inevitably, however, as LCC decreases, manufacturing costs rise. The additional equipment or modification required for a reduction in power consumption adds to the manufacturing cost. The corresponding trend on the manufacturing cost plot is upward and to the left for improved system designs.

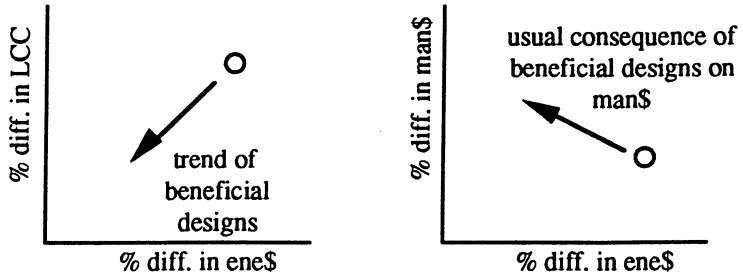

Figure 7.1: The two types of graphs on which the optimization results will be presented - percent difference in LCC versus percent difference in energy cost (left) and percent difference in manufacturing cost versus percent difference in energy cost (right)

It is possible to reduce LCC without a reduction in energy consumption. For example, manufacturing cost could be reduced by implementing a new, more efficient refrigerator assembly technique. The reduction in manufacturing cost would translate into a LCC reduction. The energy consumption of the unit would remain unchanged. This type of system improvement will not be considered in this study.

For a horizontal movement to the left on the LCC graph (LCC remains the same), the consumer could justify purchasing the system. Although the consumer gains no monetary benefit from the energy savings, the environment does realize a gain. The gain would be the reduction of emissions from the local power plant and conservation of natural resources. The current study does not take these into account. It might be of future interest to determine the costs associated with increased levels of carbon dioxide and the depletion of natural resources.

7.1 Base-Case System

The base-case system was defined to establish a reference point for evaluating other systems. The system is simulated to be a top-mount refrigerator with no sweat or defrost heaters. R12 is the working fluid for the system, and the refrigerant-side heat transfer coefficients are calculated from the UIUC R12 correlation presented in Chapter 4. The base system consisted of a single evaporator, cooling both the freezer and fresh-food compartments. Load balancing was performed by adjusting the mix of the freezer and fresh-food air at the evaporator inlet as explained in Appendix D. The evaporator was sized so that its mass equaled the mass of the standard evaporator in Table 6.2. The number of evaporator tube passes, built from the optimized fin/tube configuration from Table 6.2, was approximately 19 (18.853) passes. The total cooling load on the evaporator was 200 W with a 50%/50% load split between the freezer and fresh-food compartments. The fan velocity was set at 1.6 m/s which gave an equivalent volumetric flow rate of 52.5 CFM (0.02478 m^3/s). The fan power consumption was rather high at 18.8 W. A forced convection condenser was assumed and both the condenser and evaporator fans were standard-efficiency type fans. The suction-line heat exchanger was approximately 2.4 m in length, which is consistent with current designs. No optimization had to be performed on the base-case runs because all the independent variables were specified (no degrees of freedom existed).

To investigate the effect of varying load on the base-case R12 system, two *simulation* runs were performed for the load split configurations 40%/60% and 60%/40% between the freezer and fresh-food compartments, respectively. Figure 7.2 shows the results for the three load splits. As the evaporator load is shifted from the freezer compartment to the fresh-food compartment, energy consumption drops and the LCC is reduced. Since the two air streams are mixed in the single evaporator, a greater fresh-food load raises the mean temperature of the air entering the evaporator and the system can be operated at a higher evaporating pressure, reducing compressor work and saving energy. The manufacturing costs are flat because all the system components were specified (fixed). The 50%/50% R12 base-case system is at the origin of both plots because it is used as the basis of comparison for all other systems.

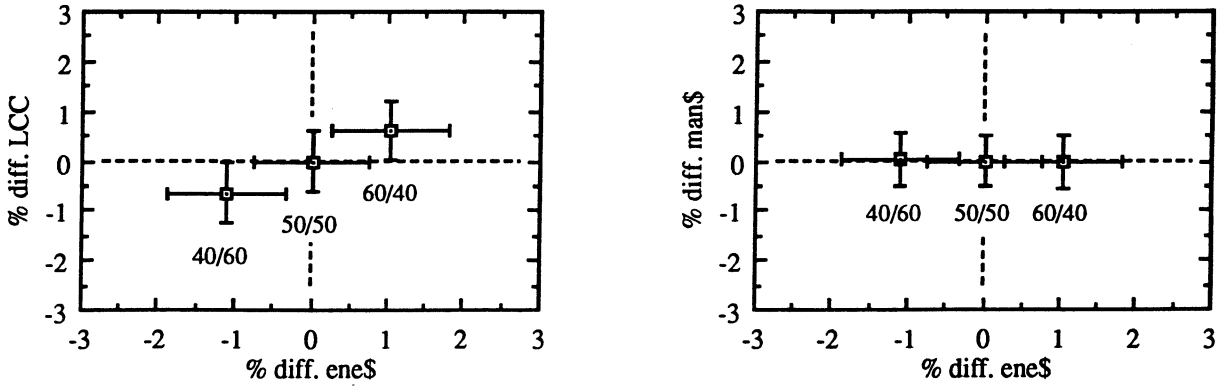

Figure 7.2: Simulation results - for the R12 base-case system - single-evaporator system with superheat, a suction-line heat exchanger (1E SLH/SH), and 60%/40%, 50%/50%, and 40%/60% load splits

In reality, the system simulation should have allowed for a variation in the duty-cycle to meet the load change. Since these were steady-state simulations (no transient information was available), the most logical way to meet the load shift was to adjust the low-side pressure holding the compartment temperatures and duty-cycle constant. The effect is the same. For greater fresh-food load splits, the compressor does not need to run as long to cool both compartments, reducing the system's energy consumption. The heat leak into the fresh-food compartment is not as great as the heat leak into the freezer compartment. The driving temperature difference between the fresh-food compartment and its surroundings is less than that of the freezer compartment and its surroundings.

The same base-case specifications were applied to an R134a system, with results similar to those in Figure 7.2. The R134a system used less energy and had a slightly lower LCC for the three different load cases. The manufacturing costs were essentially identical, and the R134a results were shifted slightly to the left.

Uncertainty bars in Figure 7.2 represent uncertainties associated with each run. The origin of the uncertainties are the air-side resistance correlation uncertainty and the UIUC R12 correlation mean deviation. See Appendix C for a discussion on uncertainties and uncertainty analysis. Both uncertainties contribute to sizing uncertainty for evaporators and intercoolers. This affects the cost of the exchangers, their occupied volume, the fan power required to circulate air over the evaporators, and the compressor power.

Statistics on the base-case system are presented in Table 7.1. The consumer cost of the refrigerator was adjusted to be $548.76 and the manufacturing cost of the unit was calculated to

be \$235.52 based on the markup factor. This adjustment accounted for other costs associated with the construction of the unit, including the costs of the condenser, condenser fan, compressor and cabinet construction. The refrigerator cost to the consumer was determined by a recent survey explained in Appendix F. The manufacturer's cost was determined based on a markup of 2.33 as described in section 6.3.9. The yearly power consumption cost for the base-case system is \$45.29. The estimated yearly power consumption cost of a real unit similar to the base-case system is \$54.00 (taken from the \$548.76 refrigerator's *Energy Guide* sticker as listed in Appendix F). The *Energy Guide* sticker assumes a power cost of 0.079 \$/kW-hr; whereas, the modeled base-case system uses 0.075 \$/kW-hr. The adjusted *Energy Guide* cost is \$51.26 based on 0.075 \$/kW-hr. The primary difference between the numbers is caused by the lack of a defrost heater in the modeled base-case system. Other discrepancies may be caused by the energy consumption measurement method used to obtain the *Energy Guide* value. The COP and the COP with the fan power included, $COP_{w\ fan}$, are listed. The definition of COP and $COP_{w\ fan}$ are given in Equations 7.1 and 7.2.

Table 7.1: Statistics for the R12 base-case single-evaporator system with superheat, a suction-line heat exchanger (1E SLH/SH), and a 50%/50% load split

quantity	BC (1E SLH/SH)
mass flux (kg/m^2-s)	30.5
heat flux (kW/m^2)	0.80
evaporating temperature (°C)	-23.6
evaporating pressure (kPa)	130.7
quality range	0.18 - 1.00
air velocity (m/s)	1.60
refrigerant-side resistance (%)	34.2
refrigerant heat transfer coeff. (W/m^2-K)	403.1
air heat transfer coeff. (W/m^2-K)	22.3
LCC (\$)	1364.02
unit cost to consumer (\$)	548.76
yearly power cost (\$)	45.29
yearly power consumption (kW-hr/yr)	603.9
unit cost to manufacturer (\$)	235.52
COP	1.40
$COP_{w\ fan}$	1.16
mass ratio	1.00
mass of evaporator (g)	853.2
occupied volume ratio	1.06
occupied volume (m^3)	7.647×10^{-3}
total outside evaporator area (m^2)	2.828
superheat (°C)	60.9
suction-line heat exchanger (m)	2.4

$$COP = \frac{\text{cooling load}}{\text{compressor power}} \tag{7.1}$$

$$COP_{w\,fan} = \frac{\text{cooling load}}{\text{compressor power} + \text{ fan power}} \tag{7.2}$$

The fan power includes the evaporator and condenser fan power. The system $COP_{w\,fan}$ is a more realistic definition of the performance of the system than the thermodynamic COP. The mass and occupied volume ratios are listed and were explained in section 6.6.1. The suction-line heat exchanger load and superheat level had to be specified so its calculated length would approximately equal a typical suction-line heat exchanger length of 2.4 m. The superheat level, 60.89 °C, appears out of line with typical systems. In a typical refrigerator system, the superheat level is approximately 45 °C. Even at these higher levels of superheat, the exit temperature of the suction-line heat exchanger, 37.23 °C, was comfortably less than the entering high-pressure liquid temperature of 44 °C.

7.2 Pure-Refrigerant Results

In order to evaluate the impact of additional system components on LCC, a number of R12 and R134a system configurations were optimized. All system configurations were compared to the R12 base-case (BC) system discussed in section 7.1, which is a single-evaporator system with superheat, a suction-line heat exchanger, and a 50%/50% load split. The optimized system configurations for R12 and R134a that were examined were:

1) single evaporator, no suction-line heat exchanger, no superheat allowed to exist at the exit of the evaporator and a 50%/50% load split - (1E)

2) single evaporator, no suction-line heat exchanger, superheat allowed to exist at the exit of the evaporator and a 50%/50% load split - (1E SH)

3) single evaporator, suction-line heat exchanger, superheat allowed to exist at the exit of the suction-line heat exchanger and 40%/60%, 50%/50%, 60%/40% load splits - (1E SLH/SH)

4) single evaporator, suction-line heat exchanger, superheat allowed to exist at the exit of the suction-line heat exchanger, a 50%/50% load split and a high-efficiency fan - (1E SLH/SH HEF)

5) dual evaporator (one in the freezer compartment, one in the fresh-food compartment), no suction-line heat exchanger, no superheat allowed to exist at the exit of the evaporator and a 50%/50% load split - (2E)

6) dual evaporator, no suction-line heat exchanger, superheat allowed to exist at the exit of the evaporator and a 50%/50% load split - (2E SH)

7) dual evaporator, suction-line heat exchanger, superheat allowed to exist at the exit of the suction-line heat exchanger and a 50%/50% load split - (2E SLH/SH)

8) dual evaporator, suction-line heat exchanger, superheat allowed to exist at the exit of the suction-line heat exchanger, a 50%/50% load split and high-efficiency evaporator fans - (2E SLH/SH HEF)

There are no pure-refrigerant systems where the effect of adding a suction-line heat exchanger is examined *by itself.* A suction-line heat exchanger *with no superheat* would do nothing *thermodynamically* for the pure-refrigerant cycle. If a suction-line heat exchanger were to be added to the system, heat would be merely exchanged between the high-pressure liquid and low-pressure two-phase fluid. The optimization would drive the size of the suction-line heat exchanger to zero and give the same results as a system where superheat was not allowed.

The pure-refrigerant systems are summarized in Table 7.2. They are presented in pairs in the following sections: 1E & 2E Systems, 1E SH & 2E SH Systems, 1E SLH/SH & 2E SLH/SH Systems, and 1E SLH/SH HEF & 2E SLH/SH HEF Systems. Summary plots of all the pure-refrigerant system results are presented in Figures 7.7 and 7.8. It is recommended to turn to these summary plots often in order to gain perspective when making a comparison to a previous system. The pure-refrigerant optimization results are presented in tables immediately following

Table 7.2: Pure-refrigerant system configuration abbreviations for R12 and R134a (base-case system is for R12 only)

abbreviation	description
BC (1E SLH/SH)*	base-case R12 single-evaporator system with a suction-line heat exchanger and superheat
1E	single-evaporator system with no suction-line heat exchanger and no superheat
2E	dual-evaporator system with no suction-line heat exchanger and no superheat
1E SH	dual-evaporator system with superheat and no suction-line heat exchanger
2E SH	dual-evaporator system with superheat and no suction-line heat exchanger
1E SLH/SH	single-evaporator system with a suction-line heat exchanger and superheat
2E SLH/SH	dual-evaporator system with a suction-line heat exchanger and superheat
1E SLH/SH HEF	single-evaporator system with a suction-line heat exchanger, superheat, and a high-efficiency evaporator fan
2E SLH/SH HEF	dual-evaporator system with a suction-line heat exchanger, superheat, and high-efficiency evaporator fans

* The base-case system is a special case of the R12 1E SLH/SH system. As a reminder of this fact, the summary tables in each section will include the (1E SLH/SH) designation.

the LCC and man$ comparison graphs in each section. These tables list only pertinent information. More detailed information can be found in Appendix L for these systems.

The UIUC R12 correlation is used to calculate the optimization program's refrigerant heat transfer coefficients for the pure-refrigerant systems. The typical freezer evaporator heat flux for these systems, 0.5 kW/m^2, is below the correlation's lower heat flux limit of 2.0 kW/m^2. This unfortunate situation was unavoidable. There were no correlations found that could approach the heat flux level at which the freezer evaporators operated. After discussions with Wattelet,[1] it was concluded that the UIUC R12 correlation could over predict the heat transfer coefficient by as much as 33% for heat flux levels below 2.0 kW/m^2.

7.2.1 1E and 2E Systems

These optimized systems have one (1E) and two (2E) evaporators, respectively, with no superheat, no suction-line heat exchanger, and a 50%/50% load split between the freezer and fresh-food compartments. Figure 7.3 and Table 7.3 report the optimization results. The 2E systems use less energy and have a lower LCC than the 1E systems; however, the 2E systems are more expensive to build. The increased manufacturing cost of the 2E systems is more than offset by the decreased power consumption resulting in a lower LCC than the 1E systems. The 1E systems cost the same to manufacture as the base-case (BC) system, yet they use more energy; therefore, the LCCs of the 1E systems are greater than the BC system LCC.

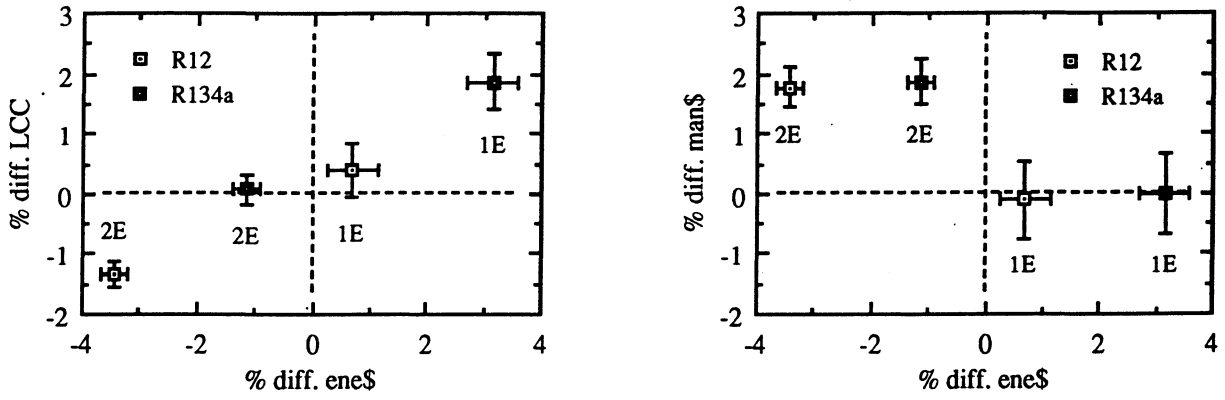

Figure 7.3: Optimization results - 1E and 2E systems for R12 and R134a relative to the BC system - 50%/50% load splits

The extra manufacturing cost for the 2E systems is due to the additional evaporator fan and evaporator. As shown in Table 7.3, the total occupied volume ratio (evaporator area) is actually less for the 2E system than for the 1E system. (Comparing occupied volume ratios is equivalent to comparing evaporator areas because the exchangers are built out of the same

fin/tube configuration.) However, the minimum cost for producing an additional exchanger causes the heat exchanger cost for the 2E system to exceed that of the 1E system.

Table 7.3: Optimization statistics for R12 and R134a 1E and 2E systems - 50%/50% load splits

quantity	BC (1E SLH/SH)	R12 1E	R12 2E	R134a 1E	R134a 2E
mass flux (kg/m^2-s)	30.5	41.9	41.6	33.1	32.8
heat flux (kW/m^2)	0.80	0.67	0.45 / 2.95	0.65	0.44 / 2.97
evaporating temperature (°C)	-23.6	-24.6	-32.1	-24.5	-23.0
evaporating pressure (kPa)	130.7	125.8	133.4	109.2	116.5
quality range	0.18 - 1.00	0.40 - 1.00	0.40 - 0.70 0.70 - 1.00	0.43 - 1.00	0.42 - 0.71 0.71 - 1.00
air velocity (m/s)	1.60	1.08	1.06 / 0.47	1.09	1.07 / 0.48
refrigerant-side resistance (%)	34.2	24.0	27.4 / 20.1	23.8	27.0 / 20.3
refrigerant heat transfer coeff. (W/m^2-K)	403.1	482.0	465.6 / 719.9	483.7	468.7 / 713.1
air heat transfer coeff. (W/m^2-K)	22.3	16.2	18.7 / 19.2	16.1	18.5 / 19.4
LCC ($)	1364.02	1369.15	1345.71	1389.50	1364.84
unit cost to consumer ($)	548.76	548.20	558.52	548.63	558.95
yearly power cost ($)	45.29	45.61	43.73	46.72	44.77
yearly power consumption (kW-hr/yr)	603.9	608.1	583.1	622.9	597.0
unit cost to manufacturer ($)	235.52	235.28	239.71	235.46	239.89
COP	1.40	1.29	1.33	1.25	1.30
$COP_{w\ fan}$	1.16	1.15	1.20	1.13	1.17
mass ratio of evaporator	1.00	1.20	0.89 / 0.14 1.03	1.23	0.91 / 0.14 1.05
occupied volume ratio	1.06	1.27	0.94 / 0.14 1.08	1.30	0.96 / 0.14 1.10
superheat (°C)	60.9	NA	NA	NA	NA
suction-line heat exchanger (m)	2.4	NA	NA	NA	NA

The 2E systems use less energy than the 1E systems. Higher evaporating pressures in the 2E system reduce compressor power consumption. Less temperature difference is required between the refrigerant and the freezer compartment air to meet the reduced load, which is shared with the fresh-food evaporator. In addition, the fan power required by the 2E system is less than that of the 1E system. Only a very small amount of air-flow rate is required to meet the load demand on the fresh-food evaporator because of the large temperature difference between the refrigerant and the fresh-food compartment air. Furthermore, the reduced fan and compressor power lowers the energy consumption of the 2E systems below that of the BC system.

The manufacturing costs are essentially the same for the BC system and the 1E systems. Since both systems have only one evaporator, each system has a single-evaporator fan. The 1E systems have larger evaporators; however, the heat exchanger costs are less due to the absence of

a suction-line heat exchanger. The increased occupied volume cost effectively cancels the decreased heat exchanger cost leaving the manufacturing costs of the 1E system approximately equal to the BC system.

The 1E systems consume more energy than the BC system. The BC system has a lower energy consumption because of the suction-line heat exchanger operating with superheat. This will be explained in section 7.2.2. Less fan power is required for the 1E system, but not enough to counter its increased compressor power. Recall the BC system had an unusually large fan power consumption to achieve a volumetric flow rate of 52.5 CFM.

The R134a 1E and 2E systems use approximately 2% more energy than the R12 systems. As shown in the next two sections, 7.2.2 and 7.2.3, as superheat and a suction-line heat exchanger are added to the systems, the gap will narrow and the R134a systems will begin to use less energy than the equivalent R12 systems.

7.2.2 1E SH and 2E SH Systems

These optimized systems have one and two evaporators respectively, with superheat allowed to exist at the exit of the last evaporator, and no suction-line heat exchanger (1E SH and 2E SH). A 50%/50% load split between the freezer and fresh-food compartments was specified. Figure 7.4 and Table 7.4 report the optimization results. Similar to the previous 2E systems, these 2E SH systems use less energy and have a lower LCC than the 1E and 1E SH systems. However, the 2E SH systems are still more expensive to build. Once again, the 1E SH systems cost the same to manufacture as the base-case (BC) system, yet use more energy; therefore, the LCC of these systems cannot be less than the BC LCC.

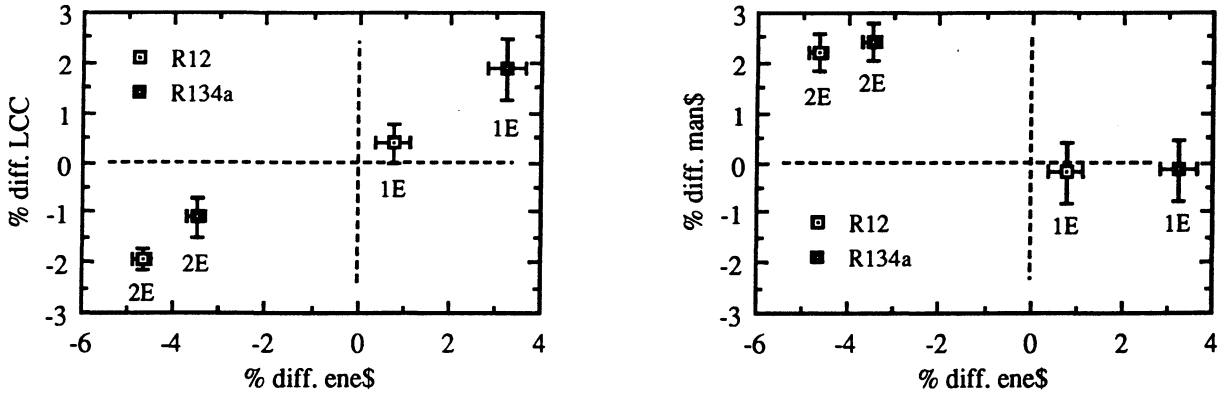

Figure 7.4: Optimization results - 1E SH and 2E SH systems for R12 and R134a relative to the BC system - 50%/50% load splits (on these individual plots the SH and SLH designations will not be included unless they are required for clarity)

For the R12 and R134a 1E SH systems, the presence of superheat is not optimal, because the rapid rise in the refrigerant temperature in the superheat region at the end of the evaporator would create a heat exchanger pinch-point, which would require more evaporator area to meet the load demand. The pinch-point could occur even with little superheat because of the relatively small temperature difference between the refrigerant and the air, which is very close to the freezer compartment temperature. The cost of larger exchanger area significantly influences the optimization and any potential benefit from the superheat would never be realized. Consequently, the optimization drives the superheat to zero. As shown in Figures 7.4 and 7.3, the 1E SH and 1E system results are identical.

Table 7.4: Optimization statistics for R12 and R134a 1E SH and 2E SH systems - 50%/50% load splits

quantity	BC (1E SLH/SH)	R12 1E SH	R12 2E SH	R134a 1E SH	R134a 2E SH
mass flux (kg/m^2-s)	30.5	41.9	37.1	33.1	28.7
heat flux (kW/m^2)	0.80	0.68	0.45 / 1.51	0.67	0.46 / 1.14
evaporating temperature (°C)	-23.6	-24.6	-23.4	-24.6	-23.4
evaporating pressure (kPa)	130.7	125.1	132.0	108.6	114.8
quality range	0.18 - 1.00	0.41 - 1.00	0.40 - 0.74 0.74 - 1.07	0.43 - 1.00	0.42 - 0.75 0.75 - 1.08
air velocity (m/s)	1.60	1.07	1.02 / 0.63	1.08	1.03 / 0.62
refrigerant-side resistance (%)	34.2	24.1	28.6 / 25.3	24.0	28.9 / 25.0
refrigerant heat transfer coeff. (W/m^2-K)	403.1	483.3	428.7 / 545.8	485.2	425.6 / 506.3
air heat transfer coeff. (W/m^2-K)	22.3	16.3	18.3 / 19.7	16.3	18.4 / 18.0
LCC ($)	1364.02	1369.18	1337.84	1389.50	1348.87
unit cost to consumer ($)	548.76	547.72	560.76	547.94	562.11
yearly power cost ($)	45.29	45.64	43.17	46.75	43.71
yearly power consumption (kW-hr/yr)	603.9	608.5	575.6	623.4	582.8
unit cost to manufacturer ($)	235.52	235.07	240.67	235.17	241.25
COP	1.40	1.28	1.35	1.25	1.33
$COP_{w\ fan}$	1.16	1.15	1.22	1.12	1.20
mass ratio of evaporator	1.00	1.18	0.88 / 0.27 1.15	1.19	0.88 / 0.35 1.23
occupied volume ratio	1.06	1.24	0.93 / 0.28 1.22	1.26	0.93 / 0.37 1.30
superheat (°C)	60.9	0.0	20.7	0.0	22.8
suction-line heat exchanger (m)	2.4	NA	NA	NA	NA

Thermodynamically, superheat will improve cycle performance for R12 and R134a cycles. The superheat at the exit of the evaporator gives the cycle more refrigerating effect. The initial benefit of additional refrigerating effect exceeds the penalty of increased specific work caused by starting compression further out in the superheat region. The change of the slope of the constant entropy lines as the compressor inlet point is moved further out into the superheat region is not enough to offset the gain in refrigerating effect. Constant entropy lines flatten out

further away from the saturation dome in the superheated vapor region. This is a fluid-specific characteristic and does not hold for all fluids. For R22, the increase in compressor work cancels the increased refrigerating effect obtained with superheat at typical refrigerator operating conditions.

For the R12 and R134a 2E SH systems, optimal superheat is greater than zero. Superheat can exist in these systems because of the larger temperature difference between the refrigerant and the air, which is at the fresh-food compartment temperature. The benefit of having superheat is realized before fresh-food evaporator area costs begin to influence the LCC.

The 2E SH systems use less energy than the 2E systems. Furthermore, the difference in energy savings between the R134a 2E SH and 2E systems is greater than the savings between the R12 2E SH and 2E systems. The rate at which the constant entropy lines flatten while moving away from the saturation dome at constant pressure is greater for R12 than R134a; therefore, more benefit is gained for the R134a system as superheat is added. This can be seen by comparing the energy savings of the two refrigerant systems in Figures 7.3 and 7.4.

The manufacturing cost comparison details are similar for the 1E SH/2E SH and 1E/2E systems with one exception. The heat exchanger costs of the 2E SH systems have increased because of the larger fresh-food evaporator. This can be clearly seen by comparing the occupied volume and mass ratios in Tables 7.3 and 7.4. The freezer evaporator area remains approximately the same, but fresh-food evaporator area approximately doubles. The larger fresh-food evaporators are necessary because of the presence of superheat at its exit. The superheat rapidly causes an increase in the evaporator area as the temperature difference between the fluids decreases.

7.2.3 1E SLH/SH and 2E SLH/SH Systems

These optimized systems have one and two evaporators respectively, a suction-line heat exchanger, *and* superheat is allowed to exist (1E SLH/SH and 2E SLH//SH). A 50%/50% load split between the freezer and fresh-food compartments was specified. In addition, 60%/40% and 40%/60% load splits were specified for the 1E SLH/SH systems. The 2E SLH/SH systems were optimized for a 50%/50% load split only to minimize the number of optimization runs. Figure 7.5 and Table 7.5 report the optimization results. Similar to the previous 2E and 2E SH systems, these 2E SLH/SH systems use less energy and have a lower LCC than the 1E SLH/SH systems. However, the 2E SLH/SH systems are still more expensive to build. The 1E SLH/SH systems cost slightly more to manufacture than the base-case (BC) system, use less energy, and have a

lower LCC than the BC system. The 40%/60%, 50%/50%, and 60%/40% 1E SLH/SH optimized systems behave predictably. When the load is shifted away from the colder freezer compartment, energy is saved and LCC decreases.

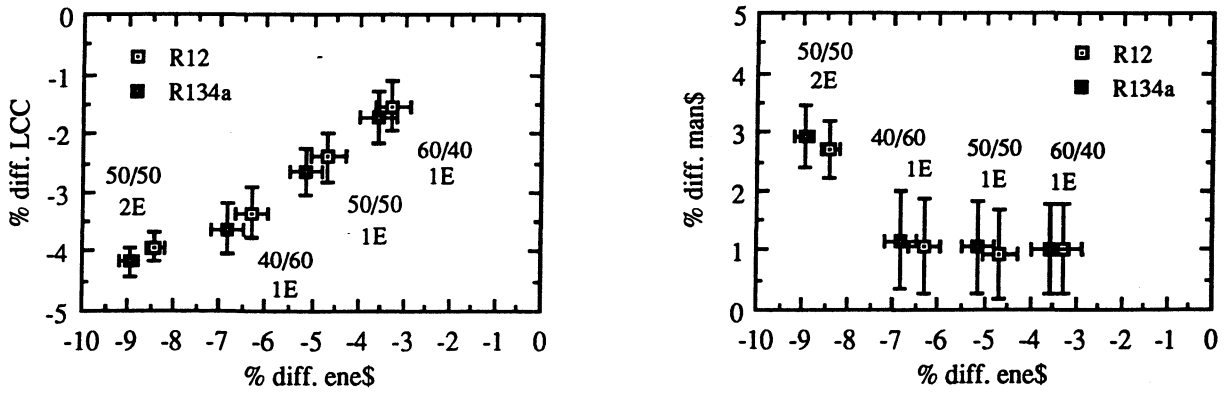

Figure 7.5: Optimization results - 1E SLH/SH and 2E SLH/SH systems for R12 and R134a relative to the BC system - 50%/50% load splits (60%/40% and 40%/60% load splits for 1E SLH/SH systems only) (on these individual plots the SH and SLH designations will not be included unless they are required for clarity)

For the R12 and R134a 1E SLH/SH and 2E SLH/SH systems, there were large amounts of superheat that existed entirely in the suction-line heat exchanger. The optimization drives the inlet quality of the suction-line heat exchanger to one. The least expensive way to have superheat in a system is in the suction-line heat exchanger. As seen in the 1E SH and 2E SH systems, the presence of superheat in an evaporator can add significant heat exchanger area and *cost* to that system.

With the addition of superheat and a suction-line heat exchanger, the R134a systems behave nearly identically to the R12 systems. The large energy use gap that existed in the previous systems all but disappeared in these systems. In fact, the R134a systems use less energy than their R12 counterpart systems. The full benefit of superheat for the R134a and R12 systems is realized with the addition of a suction-line heat exchanger. For the 1E SLH/SH and 2E SLH/SH systems, the superheat is entirely in the suction-line heat exchanger, not in the end of the freezer or fresh-food evaporator. When superheat was present in the 1E SH and 2E SH systems, the growing evaporator size cut short the superheating benefit. As discussed earlier, R134a gains more benefit from superheating than the equivalent R12 system.

These 1E SLH/SH systems have the same components as the BC system. The difference between the two is that these systems are *optimized*. The BC system was *simulated* for a particular set of conditions and specifically sized heat exchangers. As mentioned, the 1E

SLH/SH systems cost approximately 1% more than the BC system, yet their LCCs are approximately 2.5% lower (for the 50%50% load split system) than the BC system. For the 1E SLH/SH systems, the evaporators are approximately 18% larger, and the suction-line heat exchangers are approximately 56% longer than the BC system. The superheat levels were similar for both, yet the optimization sized the components and set the operating conditions to minimize LCC. The major source of energy cost savings between the BC and 1E SLH/SH systems is the reduction in the air velocity over the evaporator. Recall that the BC system's air velocity was high to maintain a volumetric flow rate of 52.5 CFM.

Table 7.5: Optimization statistics for R12 and R134a 1E SLH/SH and 2E SLH/SH systems - 50%/50% load splits only

quantity	BC (1E SLH/SH)	R12 1E SLH/SH	R12 2E SLH/SH	R134a 1E SLH/SH	R134a 2E SLH/SH
mass flux (kg/m^2-s)	30.5	29.9	30.1	22.9	23.0
heat flux (kW/m^2)	0.80	0.68	0.46 / 3.14	0.68	0.45 / 3.05
evaporating temperature (°C)	-23.6	-25.2	-23.5	-25.2	-23.6
evaporating pressure (kPa)	130.7	122.7	131.2	105.6	113.8
quality range	0.18 - 1.00	0.17 - 1.00	0.17 - 0.59 0.59 - 1.00	0.18 - 1.00	0.18 - 0.59 0.59 - 1.00
air velocity (m/s)	1.60	1.04	1.02 / 0.51	1.03	1.01 / 0.49
refrigerant-side resistance (%)	34.2	28.1	31.9 / 21.6	28.4	32.0 / 21.8
refrigerant heat transfer coeff. (W/m^2-K)	403.1	386.2	369.1 / 689.6	378.5	362.1 / 661.3
air heat transfer coeff. (W/m^2-K)	22.3	16.1	18.4 / 20.2	16.0	18.2 / 19.6
LCC ($)	1364.02	1331.23	1310.39	1327.68	1307.02
unit cost to consumer ($)	548.76	553.9	563.65	554.51	564.82
yearly power cost ($)	45.29	43.19	41.49	42.95	41.23
yearly power consumption (kW-hr/yr)	603.9	575.8	553.2	572.7	549.8
unit cost to manufacturer ($)	235.52	237.72	241.91	237.98	242.41
COP	1.40	1.36	1.41	1.36	1.41
$COP_{w\ fan}$	1.16	1.22	1.27	1.22	1.28
mass ratio of evaporator	1.00	1.18	0.88 / 0.13 1.01	1.19	0.89 / 0.13 1.02
occupied volume ratio	1.06	1.24	0.93 / 0.14 1.07	1.26	0.94 / 0.14 1.08
superheat (°C)	60.9	66.2	63.7	67.0	65.0
suction-line heat exchanger (m)	2.4	3.6	3.2	3.9	3.7

The manufacturing cost is slightly more for the 1E SLH/SH system than for the BC system. The heat exchanger costs and occupied volume costs are more because of the larger evaporator and the addition of the larger suction-line heat exchanger. The manufacturing costs are more for the 1E SLH/SH systems than for the previous 1E and 1E SH systems. The only difference is that the addition of the suction-line heat exchanger increases the total exchanger costs. It is interesting to note that the evaporator size remains unchanged for the respective 1E SLH/SH and 1E SH systems.

The 1E SLH/SH systems now use less energy than the BC system. The energy consumption is drastically reduced, especially for the R134a 1E SLH/SH system. The R12 system reduces its energy consumption by 5% and the R134a system reduces its energy consumption 8% relative to the 1E SH systems! The full benefit of superheat is now realized for the 1E SLH/SH systems.

7.2.4 1E SLH/SH HEF and 2E SLH/SH HEF Systems

These optimized systems have one and two evaporators respectively, a suction-line heat exchanger, high-efficiency evaporator fans, and superheat is allowed to exist (1E SLH/SH HEF and 2E SLH//SH HEF). A 50%/50% load split between the freezer and fresh-food compartments was specified. Figure 7.6 and Table 7.6 report the optimization results. For comparison, the 1E SLH/SH (50%/50%) and 2E SLH/SH systems are also presented in Figure 7.6. The only difference between the 1E & 2E SLH/SH systems and the 1E & 2E SLH/SH HEF systems is the addition of the high-efficiency fans. The high-efficiency fan systems use less energy than the equivalent standard-efficiency fan systems, but are more expensive to build.

The addition of a high-efficiency fan increases manufacturing costs for both the 1E SLH/SH HEF and 2E SLH/SH HEF systems. For the 1E SLH/SH HEF systems, the energy savings from using a high-efficiency fan outweigh the additional cost, and LCC decreases. For the 2E SLH/SH HEF systems, the energy savings is not enough to offset the increased equipment costs, and the LCC stays the same.

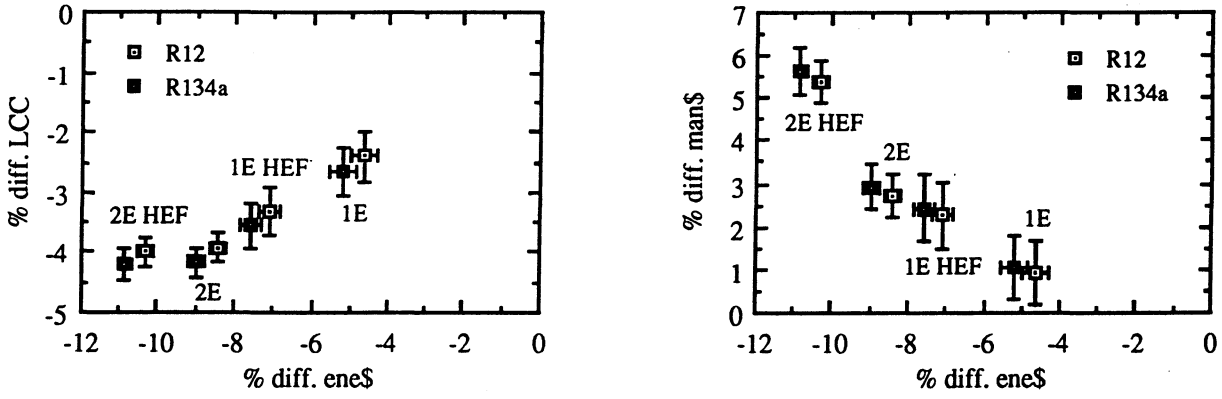

Figure 7.6: Optimization results - 1E SLH/SH HEF and 2E SLH/SH HEF systems for R12 and R134a relative to the BC system - 50%/50% load splits (on these individual plots the SH and SLH designations will not be included unless they are required for clarity)

Table 7.6: Optimization statistics for R12 and R134a 1E SLH/SH HEF and 2E SLH/SH HEF systems - 50%/50% load splits

quantity	BC (1E SLH/SH)	R12 1E SLH/SH HEF	R12 2E SLH/SH HEF	R134a 1E SLH/SH HEF	R134a 2E SLH/SH HEF
mass flux (kg/m^2-s)	30.5	30.0	30.0	22.9	22.9
heat flux (kW/m^2)	0.80	0.65	0.43 / 3.58	0.65	0.42 / 3.82
evaporating temperature (°C)	-23.6	-24.2	-22.7	-24.4	-22.7
evaporating pressure (kPa)	130.7	127.9	135.7	109.9	118.2
quality range	0.18 - 1.00	0.17 - 1.00	0.17 - 0.58 0.58 - 1.00	0.18 - 1.00	0.17 - 0.59 0.59 - 1.00
air velocity (m/s)	1.60	1.23	1.24 / 0.63	1.19	1.21 / 0.68
refrigerant-side resistance (%)	34.2	29.4	33.5 / 22.1	29.4	33.2 / 22.6
refrigerant heat transfer coeff. (W/m^2-K)	403.1	385.4	368.0 / 754.4	377.9	360.6 / 771.2
air heat transfer coeff. (W/m^2-K)	22.3	17.1	19.8 / 22.8	16.8	19.1 / 24.0
LCC ($)	1364.02	1318.76	1309.49	1315.56	1306.40
unit cost to consumer ($)	548.76	561.29	578.24	562.16	579.67
yearly power cost ($)	45.29	42.08	40.62	41.86	40.37
yearly power consumption (kW-hr/yr)	603.9	561.1	541.7	558.1	538.3
unit cost to manufacturer ($)	235.52	240.90	248.17	241.27	248.79
COP	1.40	1.39	1.43	1.39	1.44
$COP_{w\ fan}$	1.16	1.25	1.29	1.26	1.30
mass ratio of evaporator	1.00	1.23	0.92 / 0.11 1.03	1.23	0.96 / 0.11 1.07
occupied volume ratio	1.06	1.30	0.98 / 0.12 1.1	1.3	1.02 / 0.11 1.13
superheat (°C)	60.9	64.5	63.0	66.0	64.3
suction-line heat exchanger (m)	2.4	3.3	3.2	3.8	3.7

7.2.5 Summary

Figures 7.7 and 7.8 summarize all results for the pure-refrigerant systems except the 1E SH systems. For the 1E SH systems, the optimization drives the superheat level to zero and the results are the same as for the 1E systems; therefore, there are no 1E SH system results shown in the figures. Also, there were no pure-refrigerant systems where the effect of adding a suction-line heat exchanger was examined *by itself.* A suction-line heat exchanger *with no superheat* would do nothing *thermodynamically* for the pure-refrigerant cycle. The optimization would drive the size of the suction-line heat exchanger to zero and give the same results as the 1E or 2E systems.

Superheat present in the exit of the 1E SH systems is not economically justified. For the 1E SH systems (not shown), the refrigerant at the exit of the evaporator is exchanging heat with the evaporator inlet air, which is essentially at the temperature of the freezer compartment. This small temperature difference does not allow much superheat to exist in the exit of the evaporator

before a pinch-point situation occurs. At this point, the cost of evaporator area gets prohibitively expensive. The relative rise in evaporator area cost exceeds the energy savings from increasing the refrigerating effect using superheat. For this system, the minimum LCC is achieved with no superheat. As this relative rise in evaporator area cost is decreased, the feasibility of having superheat increases as will be discussed in the next paragraph.

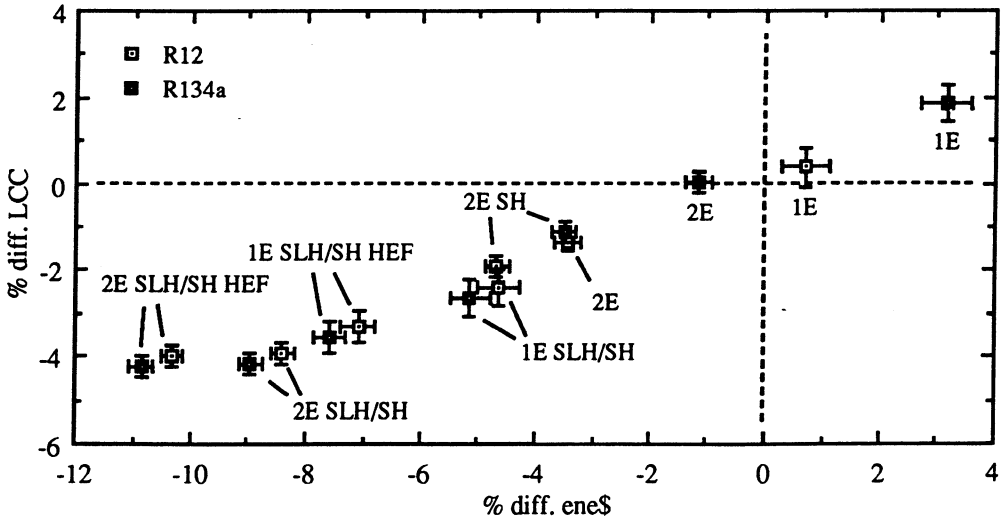

Figure 7.7: Optimization results - for all R12 and R134a systems relative to the BC system

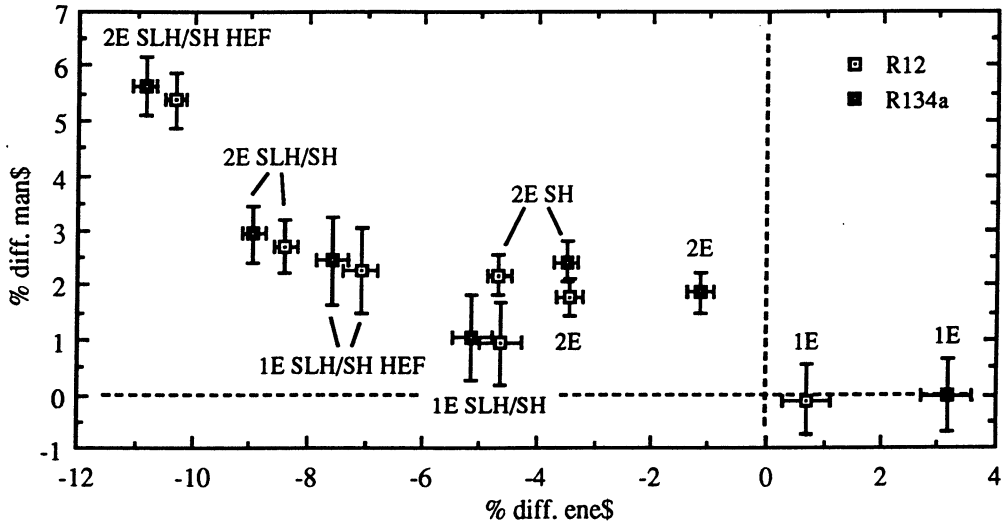

Figure 7.8: Optimization results - for all R12 and R134a systems relative to the BC system

All the 2E systems use less energy than equivalent 1E systems. Higher evaporating pressures in the 2E system reduce compressor power consumption. Less temperature difference is required between the refrigerant and the freezer compartment air to meet the reduced load, which is shared with the fresh-food evaporator. In addition, the fan power required by the 2E system is less than that of the 1E system. Only a very small amount of air-flow rate is required to meet the load demand on the fresh-food evaporator because of the large temperature difference between the refrigerant and the fresh-food compartment air.

Superheat present in the exit of the 2E SH systems is economically justified. Energy consumption is reduced and LCC drops despite a slightly higher manufacturing cost for this system. In this system, the refrigerant at the exit of the fresh-food evaporator is exchanging heat with the fresh-food evaporator inlet air, which is essentially at the temperature of the fresh-food compartment. This larger temperature difference allows some superheat to exist in the exit of the evaporator before a pinch-point situation occurs. Initially, the relative rise in fresh-food evaporator area cost does not exceed the energy savings from increasing the refrigerating effect using superheat. For this system, the minimum LCC is achieved with some amount of superheat. For the 2E SH systems, less additional evaporator area is required to achieve a beneficial level of superheat than the 1E SH systems due to the greater mean-temperature difference between the refrigerant and the air.

The presence of superheat and a suction-line heat exchanger is *always* economically justified for the R12 and R134a 1E SLH/SH and 2E SLH/SH systems. In these systems, the refrigerant in the low-pressure side of the suction-line heat exchanger is exchanging heat with the refrigerant in the high-pressure side, which is near the condenser exit temperature. This increased temperature difference allows large amounts of superheat to exist in the suction-line heat exchanger. In every SLH/SH system, the optimization places the superheat entirely in the suction-line heat exchanger. The low-side pressure inlet quality to the suction line heat exchanger is driven to one. The relative rise in suction-line heat exchanger area cost does not exceed the energy savings from increasing the refrigerating effect using superheat.

For the 1E and 2E systems, the R134a systems consume *more* energy relative to the R12 systems. For the 1E SLH/SH and 2E SLH/SH systems, the R134a systems consume *less* energy. The rate at which the constant entropy lines flatten while moving away from the saturation dome at constant pressure is greater for R12 than R134a; therefore, more benefit is gained for the R134a systems as superheat is allowed to be used to its maximum advantage with a suction-line heat exchanger.

The addition of high-efficiency fans provides some benefit for single-evaporator systems, however, the addition of the high-efficiency fans to the dual-evaporator systems fails to lower the LCC. The increase in manufacturing cost offsets the additional energy savings and the LCC remains the same.

7.2.6 Best Pure Refrigerant System

The best optimized pure-refrigerant system configuration from the perspective of the consumer was chosen to be the R134a 2E SLH/SH (see Table 7.7). The perspective assumes that the consumer has *available* cash to purchase the refrigerator unit. Recall that a zero discount rate was assumed. Under current economic conditions this implies that the inflation rate equals the interest rate on the available cash used to purchase the refrigerator. This assumption breaks down if the consumer chooses to purchase the refrigerator using an available line of credit at a relatively high interest rate (approximately 12%) under current economic conditions. For this system, the manufacturing cost is predicted to be around 3% greater and the LCC is 4% less than that of the BC system. When high-efficiency fans are added to the 2E SLH/SH system, the manufacturing cost rise nearly doubles to 5.5%, yet the LCC remains unchanged at 4% below that of the BC system. The total evaporator area of the 2E SLH/SH system is only 1.9% greater than that of the BC system. The 2E SLH/SH HEF system *seems* to be the best choice from an environmental standpoint because of the additional energy savings. However, the objective function did not include the savings associated with natural resource conservation and reduction of emissions from the local power plant; therefore, no decision can be made as to which system configuration would be the best from an environmental standpoint. A new objective function would need to be formulated and each system configuration would have to be re-optimized to make this determination.

Although no economic decision can be made from the manufacturer's viewpoint, the relative ranking of initial costs from this optimization and the complexity of the system configuration might have some bearing on their decision to investigate a particular system configuration on the basis of *their* economic criteria. The objective function for this study did not include the manufacturers' retooling costs and other considerations which the manufacturers must take into account. Furthermore, the discount rate would need to be much larger, between 20 and 30%.

Table 7.7: Specifications for best optimized pure-refrigerant system configuration for consumer

quantity	R134a 2E SLH/SH
mass flux (kg/m^2-s)	23.0
heat flux (kW/m^2)	0.45 / 3.05
evaporating temperature (°C)	-23.6
evaporating pressure (kPa)	113.8
quality range	0.18 - 0.59 0.59 - 1.00
air velocity (m/s)	1.01 / 0.49
refrigerant-side resistance (%)	32.0 / 21.8
refrigerant heat transfer coeff. (W/m^2-K)	362.1 / 661.3
air heat transfer coeff. (W/m^2-K)	18.2 / 19.6
LCC ($)	1307.02
unit cost to consumer ($)	564.82
yearly power cost ($)	41.23
yearly power consumption (kW-hr/yr)	549.8
unit cost to manufacturer ($)	242.41
COP	1.41
$COP_{w\ fan}$	1.28
mass ratio	0.89 / 0.13 1.02
tot. mass of evaporators (g)	870.3
occupied volume ratio	0.94 / 0.14 1.08
tot. occupied volume of evaporators (m^3)	7.791×10^{-3}
total outside evaporator area (m^2)	2.881
superheat (°C)	65.0
suction-line heat exchanger (m)	3.7

One system configuration which the manufacturers *may* want to investigate further would be the R134a 1E SLH/SH system. This component configuration is the same one currently used by manufacturers in production. The manufacturing costs are only 1% greater, and the LCC 2.5% less, than for the BC system. The evaporator area of this system is 18.8% larger than that of the BC system. The manufacturers would avoid systems with added components, manufacturing complexity and cost, such as the 2E SLH/SH and 2E SLH/SH HEF systems. Manufacturers would dislike having to raise the initial cost of their unit out of line with the market. Keeping the initial cost low is very important for the manufacturers. Higher unit prices would erode their market share.

The R134a 1E SLH/SH optimized system and the BC system results are different. One would expect that the current system in use today, as approximated by the BC system, would be optimally designed, and that the optimization results for the R134a 1E SLH/SH and BC system would be approximately equal. Both systems have one evaporator, a suction-line heat exchanger,

and superheat. This is the same component configuration for current domestic refrigerator systems, despite the fact that one is an R12 system and the other is an R134a system. The R12 and R134a 1E SLH/SH system results are approximately equal. The results for the BC and R134a 1E SLH/SH are different because the air-flow rate over the BC evaporator is not optimal. For the BC system, typical operating conditions were specified to be used with an evaporator constructed from the UIUC optimized fin/tube section from Table 6.2, not the standard evaporator coil. The cross-sectional area of the standard evaporator coil is over twice that of the optimized fin/tube section used to construct the BC evaporator. For a specified volumetric flow rate of 52.5 CFM, the BC evaporator fan must maintain a higher air velocity; consequently, the fan power consumption is high relative to the typical 10 W in current systems. A better (and more realistic) basis of comparison for the pure-refrigerant and refrigerant mixture systems might be the optimized R12 or R134a 1E SLH/SH system. This system contains the same components as current systems with superheat. This change does not affect any of the presented results; it only shifts the relative comparison point.

7.3 Refrigerant-Mixture Results

To assess the impact of additional system components on LCC, a number of mixture system configurations were optimized. All system configurations were compared to the R12 base-case (BC) system discussed in section 7.1.

The 65% R22/35% R123 and 80% R22/20% R141b refrigerant-mixture systems are listed below:

1) dual evaporator; no intercoolers; and a 50%/50% load split - (No IC)

2) dual evaporator; low-temperature intercooler; and a 50%/50% load split - (LI)

3) dual evaporator; high-temperature intercooler; and a 50%/50% load split - (HI)

4) dual evaporator; low and high-temperature intercoolers; and 40%/60%, 50%/50% and 60%/40% load splits - (HI/LI)

5) dual evaporator; low and high-temperature intercoolers; a 50%/50% load split; and high-efficiency evaporator fans - (HI/LI HEF)

The use of a mixture to achieve two-temperature level cooling was a primary goal of this study. A single evaporator system with a high-glide refrigerant mixture would be very inefficient; therefore, for this study, *all* mixture systems have two evaporators: one in the low-temperature freezer compartment and one in the higher temperature fresh-food compartment.

Thermodynamic gains for mixture systems are realized in two ways (see Chapter 2 for a full discussion). First, the mixture glide reduces the heat transfer irreversibility in the evaporators by better matching the air and refrigerant-temperature profiles. Second, lower refrigerant temperatures can be achieved through the use of intercooling with no decrease in the evaporating pressure. The addition of an intercooler, with the outlet of the evaporator module fixed at the saturated vapor line, decreases the quality of the mixture entering the module. The temperature of a mixture decreases at low qualities for a constant pressure. The lower refrigerant temperature can be exploited in two ways: by decreasing the exchanger size, because the mean-temperature difference between the refrigerant and air has increased, or by raising the low-side pressure. Usually, the most cost effective course of action is to raise the low-side pressure.

The first thermodynamic gain, irreversibility reduction, increases evaporator area, assuming constant evaporator load. The optimization had to determine the trade-off between energy savings and additional heat exchanger cost in the LCC minimization. The second thermodynamic gain, intercooling, could decrease evaporator area or reduce compressor power. The optimization needed to determine the most cost effective amount of intercooling to minimize LCC.

Mixture systems with both high and low-temperature intercoolers and superheat were considered. It was found that the mixture optimization drives any superheat in the system to zero; consequently, the optimized results are identical to the two intercooler-only systems. The gain in refrigeration effect from superheat is offset by the increased compression power and larger heat exchanger areas. The compression power increases because the compression is started further out in the superheat region. The beneficial effect of intercooling, moving the evaporator heat transfer processes back further in the saturation dome towards the saturated liquid line, is reduced by superheat. A more detailed discussion on the benefits of intercooling can be found in Chapter 2 and in subsequent sections. The presence of superheat moves the evaporator heat transfer process back towards the saturated vapor line. This forces the evaporator areas to increase because the mean-temperature difference between the air and refrigerant is reduced.

As before, the optimization results are presented on LCC and manufacturing cost (man$) versus energy consumption cost (ene$) graphs. The axes of the two plots are modified to present the results as a percent change relative to the BC system. The origin of the uncertainties on these plots are from the air-side resistance correlation uncertainty and the corresponding mixture correlation uncertainty.

The refrigerant-mixture systems are summarized in Table 7.8. They are presented one at a time in the following sections: No IC Systems, LI Systems, HI Systems, HI/LI Systems, and HI/LI HEF Systems. Summary plots of all the refrigerant-mixture system results are presented in Figures 7.15 and 7.16. It is recommended to turn to these summary plots often in order to gain perspective when making a comparison to a previous system. The refrigerant-mixture optimization results are presented in tables immediately following the LCC and man$ comparison graphs in each section. These tables list only pertinent information. More detailed information can be found in Appendix L for these systems.

Table 7.8: Refrigerant-mixture system configuration abbreviations for R22/R123 and R22/R141b (base-case system is a R12 system)

abbreviation	description
BC (1E SLH/SH)*	base-case R12 single-evaporator system with a suction-line heat exchanger and superheat
No IC	dual-evaporator system with no intercoolers
LI	dual-evaporator system with a low-temperature intercooler
HI	dual-evaporator system with a high-temperature intercooler
HI/LI	dual-evaporator system with high and low-temperature intercoolers
HI/LI HEF	dual-evaporator system with high and low-temperature intercoolers and high-efficiency evaporator fans

* The base-case system is a special case of the R12 1E SLH/SH system. As a reminder of this fact, the summary tables in each section will include the (1E SLH/SH) designation.

The mixture correlations formulated in Chapter 5 are used to calculate the refrigerant heat transfer coefficients for the refrigerant-mixture systems. The typical freezer evaporator heat flux for these systems, 0.35 kW/m^2, is below the correlation's lower heat flux limit of 1.0 kW/m^2. This unfortunate situation was unavoidable. There is no available mixture information at these heat flux levels. The author is reasonably confident that the extrapolation to the lower heat flux level will not significantly alter the mixture optimization results.

7.3.1 No IC Systems

These optimized systems have two evaporators and no intercoolers (No IC). The optimization runs were performed for a 50%/50% load split between the freezer and fresh-food evaporators. Figure 7.9 and Table 7.9 report the optimization results. The No IC mixture systems use 5 to 7% more energy, and have LCCs 4.5 to 6% greater and manufacturing costs 4 to 5% greater than the BC system.

The No IC manufacturing costs are greater than the BC system cost due to additional evaporator area. The mixture glide enables better matching between the temperature profiles of the refrigerant and the air. This provides thermodynamic benefits by reducing the evaporators'

heat transfer irreversibility, but at the price of increased evaporator area. The R22/R123 evaporator area is 80% greater, and the R22/R141b evaporator area 93% greater, than the BC system. Additional manufacturing costs are incurred as well because of the additional evaporator and evaporator fan.

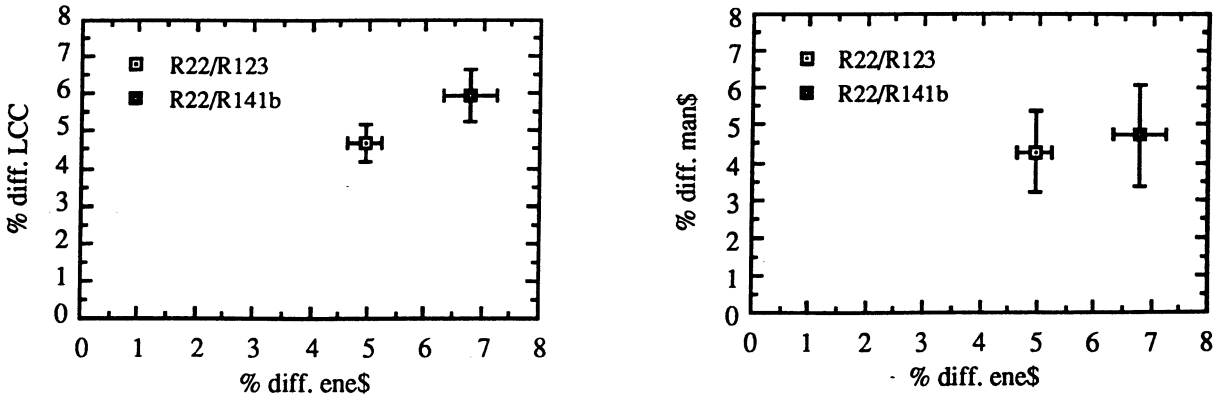

Figure 7.9: Optimization results - No IC systems for R22/R123 and R22/R141b relative to the BC system - 50%/50% load splits

The percentages in the above paragraph were calculated using the occupied volume ratio of the BC system. The BC system was designed to have a mass ratio of one. As shown in Table 7.9, the occupied volume ratio settled at 1.06. The additional occupied volume of the R22/R123 No IC system, 80%, is calculated using its total occupied volume ratio of 1.91 and the BC system's ratio of 1.06. Since the evaporators being compared were constructed out of the same fin/tube arrangement, these numbers are equivalent to heat exchanger area.

There is an approximate 2% difference in the energy consumption between the R22/R123 and R22/R141b No IC systems. The R22/R141b system must maintain a lower relative evaporating pressure to offset lower refrigerant heat transfer coefficients for these flow conditions. The heat flux for the these optimization runs was very small - less than 1 kW/m^2. The low heat fluxes are consequences of the larger evaporators required for mixtures, especially for the freezer. Greater surface area reduces the heat flux and, as a result, the heat transfer coefficients for the freezer evaporator are very low. The approximate R22/R141b refrigerant-side resistance is 68% of the total heat transfer resistance for the freezer evaporator, corresponding to a refrigerant heat transfer coefficient of 60 W/m^2-K. For the R22/R123 mixture, the refrigerant-side resistance is much lower for the freezer evaporator (44%), indicating a higher refrigerant heat transfer coefficient of 154 W/m^2-K. The extremely low refrigerant heat transfer coefficients are one of the problems associated with mixtures in the low heat and mass flux range, as discussed in Chapter 2. The BC system has a 34% refrigerant-side resistance.

This is slightly higher than the 17.2% to 26% refrigerant-side resistance calculated by Admiraal and Bullard.[2]

Table 7.9: Optimization statistics for R22/R123 and R22/R141b No IC systems - 50%/50% load splits

quantity	BC (1E SLH/SH)	R22/R123 No IC	R22/R141b No IC
mass flux (kg/m^2-s)	30.5	27.9	25.4
heat flux (kW/m^2)	0.80	0.29 / 0.92	0.29 / 0.72
evaporating temperature (°C)	-23.6	NA	NA
evaporating pressure (kPa)	130.7	105.8	120.2
quality range	0.18 - 1.00	0.42 - 0.74 0.74 - 1.00	0.40 - 0.73 0.73 - 1.00
air velocity (m/s)	1.60	0.82 / 0.62	0.62 / 0.72
refrigerant-side resistance (%)	34.2	44.1 / 42.2	67.6 / 65.2
refrigerant heat transfer coeff. (W/m^2-K)	403.1	153.8 / 216.2	59.8 / 87.7
air heat transfer coeff. (W/m^2-K)	22.3	12.9 / 16.8	13.3 / 17.5
LCC ($)	1364.02	1427.87	1445.13
unit cost to consumer ($)	548.76	572.27	574.58
yearly power cost ($)	45.29	47.53	48.36
yearly power consumption (kW-hr/yr)	603.9	633.8	644.9
unit cost to manufacturer ($)	235.52	245.61	246.60
COP	1.40	1.21	1.19
$COP_{w\ fan}$	1.16	1.11	1.09
mass ratio of evaporator	1.00	1.37 / 0.44 1.81	1.38 / 0.56 1.94
occupied volume ratio	1.06	1.45 / 0.46 1.91	1.46 / 0.59 2.05
superheat (°C)	60.9	NA	NA
suction-line heat exchanger or low/high temperature intercooler (m)	2.4	NA	NA

One reason why the refrigerant-side resistance of the BC system is larger than Admiraal's results is that the air-velocity over the BC evaporator is unusually high at 1.6 m/s. The higher air velocity decreases the air-side resistance and raises the refrigerant-side resistance percentage. In Table 7.5 the refrigerant-side resistance of 28% for the optimized 1E SLH/SH system is more in-line with Admiraal's results. A closer look at the two evaporators reveals that the optimized evaporator has more fin area than the evaporator in the Admiraal study. This would account for the slightly lower air-side resistance (higher refrigerant-side resistance) of the optimized evaporator.

There are larger manufacturing cost uncertainties associated with the mixture systems than for the pure-refrigerant systems. This is caused by the large uncertainty in the refrigerant-mixture correlations, which translates into heat exchanger size uncertainty, which in turn affects

manufacturing costs. In the next section, the addition of intercoolers will begin to make the mixture systems more attractive as an alternative to pure-refrigerant systems.

7.3.2 LI Systems

These optimized systems have two evaporators and a low-temperature intercooler (LI). The low-temperature intercooler is placed between the freezer and fresh-food evaporators, as shown in Figure 2.4. The optimization runs were performed for a 50%/50% load split between the freezer and fresh-food evaporators. Figure 7.10 and Table 7.10 report the optimization results. The LI systems experience a tremendous drop in energy use as compared to the No IC systems. The R22/R123 LI system reduces its energy consumption by 10.5%, and the R22/R141b LI system by 5.5%, compared to the No IC counterparts. More benefit was gained with the insertion of a intercooler in the R22/R123 system than in the R22/R141b system. The manufacturing costs remain about the same, approximately 4 to 5% greater than the BC system.

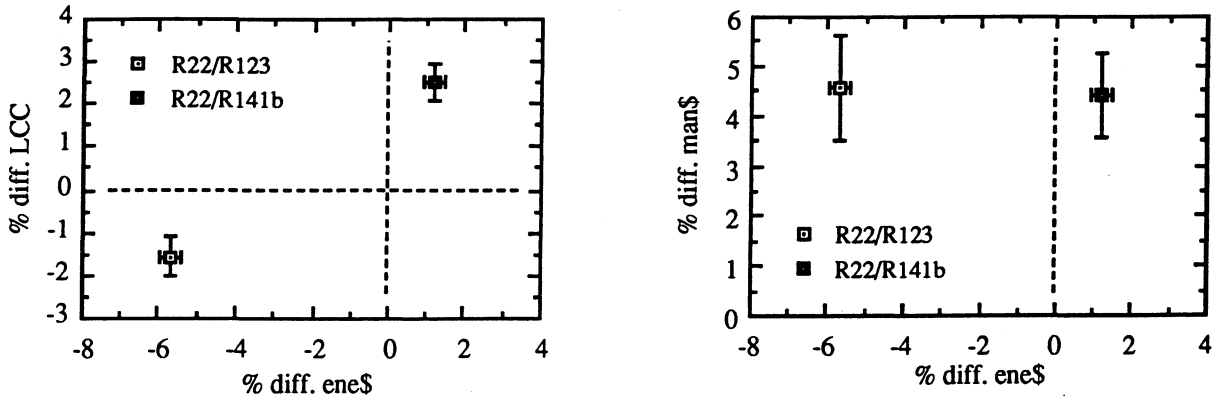

Figure 7.10: Optimization results - LI systems for R22/R123 and R22/R141b relative to the BC system - 50%/50% load splits

The large drop in energy consumption for the R22/R123 LI system is due to the unique curvature of the temperature glide in saturation. The curve is shaped so that the insertion of the low-temperature intercooler is able to relieve a pinch-point at the entrance to the freezer evaporator. This can be seen by examining the change in occupied volume ratios for the freezer evaporator from Table 7.9 to Table 7.10. This argument can also be applied to the R22/R141b LI system. The pinch-point for both fluids is shifted from the freezer evaporator to the fresh-food evaporator. The R22/R123 LI system freezer evaporator area is reduced by 50% while the fresh-food evaporator area increases 150% as compared to the R22/R123 No IC system. The change is not as dramatic for the R22/R141b LI system. The freezer evaporator area is reduced by 40%, while the fresh-food evaporator area increases only 70%.

Table 7.10: Optimization statistics for R22/R123 and R22/R141b LI systems - 50%/50% load splits

quantity	BC (1E SLH/SH)	R22/R123 LI	R22/R141b LI
mass flux (kg/m^2-s)	30.5	27.4	25.2
heat flux (kW/m^2)	0.80	0.58 / 0.37	0.47 / 0.42
evaporating temperature (°C)	-23.6	NA	NA
evaporating pressure (kPa)	130.7	132.6	135.1
quality range	0.18 - 1.00	0.05 - 0.41 0.73 - 1.00	0.07 - 0.43 0.73 - 1.00
air velocity (m/s)	1.60	0.74 / 0.78	0.87 / 0.81
refrigerant-side resistance (%)	34.2	45.3 / 43.3	68.4 / 70.6
refrigerant heat transfer coeff. (W/m^2-K)	403.1	188.0 / 173.2	74.1 / 60.2
air heat transfer coeff. (W/m^2-K)	22.3	16.6 / 14.1	17.1 / 15.4
LCC ($)	1364.02	1342.87	1397.97
unit cost to consumer ($)	548.76	573.80	572.98
yearly power cost ($)	45.29	42.73	45.83
yearly power consumption (kW-hr/yr)	603.9	569.7	611.1
unit cost to manufacturer ($)	235.52	246.27	245.91
COP	1.40	1.35	1.26
$COP_{w\ fan}$	1.16	1.23	1.15
mass ratio of evaporator	1.00	0.69 / 1.09 1.78	0.85 / 0.95 1.80
occupied volume ratio	1.06	0.73 / 1.15 1.88	0.89 / 1.00 1.89
superheat (°C)	60.9	NA	NA
suction-line heat exchanger or low/high temperature intercooler (m)	2.4	1.2	0.6

One subtle effect of adding intercooling to the mixture system is an indirect increase (or decrease) to the mixture heat transfer coefficient. As mentioned above, the heat transfer area decreases for the freezer evaporator and increases for the fresh-food evaporator with the addition of the low-temperature intercooler. For the same loading conditions, the heat flux increases in the freezer evaporator and decreases in the fresh-food evaporator. A comparison of the conditions in Tables 7.9 and 7.10 reveals that the mass flux is essentially unchanged; therefore, the refrigerant heat transfer coefficient change is driven primarily by the change in the heat flux. The heat transfer coefficient increases in the freezer evaporator and decreases in the fresh-food evaporator. A compounding effect takes place; as the intercooler addition provides a larger temperature difference between the refrigerant and the air, the optimization sizes a smaller evaporator. The smaller evaporator increases heat flux which in turn raises the refrigerant heat transfer coefficient and allows the optimization to select a smaller evaporator area to accomplish the same heat transfer. However, there is a competing effect which may work against the rising heat transfer coefficient. The average quality in the freezer evaporator is lowered with the insertion of a low-temperature intercooler. If the heat transfer coefficient is dominated by

convective boiling, the average heat transfer coefficient will tend to be lower at the lower qualities. Section 3.2.1 contains a complete discussion of this effect.

The manufacturing cost for the LI systems is virtually the same as for the No IC systems. The addition of the low-temperature intercooler causes a slight decrease in the required heat exchanger area which offsets its cost. The R22/R123 LI total evaporator area dropped 3% (from the R22/R123 No IC system) to be 77% greater than the BC system. The R22/R141b LI total evaporator area dropped 15% (from the R22/R141b No IC system) to be 78% greater than the BC system.

The dramatic gains in energy savings shift the LCC of the R22/R123 LI system below the LCC of the BC system. The energy savings for the R22/R141b LI system are not enough to move its LCC below the BC LCC. The R22/R123 LI system is an excellent example of the energy savings potential of a mixture system despite the very low refrigerant heat transfer coefficients that characterize low heat and mass flux flow conditions. The R22/R123 LI system energy consumption decreases 10.5% as compared to the R22/R123 No IC system with virtually no increase in manufacturing costs! The intercooling allowed the LI system to take advantage of the mixture temperature glide.

7.3.3 HI Systems

These optimized systems have two evaporators and a high-temperature intercooler (HI). The high-temperature intercooler is placed after the fresh-food evaporator as shown in Figure 2.4. The optimization runs were performed for a 50%/50% load split between the freezer and fresh-food evaporators. Figure 7.11 and Table 7.11 report the optimization results. The HI systems experience a greater drop in energy consumption cost than the LI systems relative to the No IC systems. The R22/R123 HI system reduces its energy consumption by 14% relative to the R22/R123 No IC system, and the R22/R141b HI system reduces its energy consumption by 9% relative to the R22/R141b No IC system. (The energy savings for the R22/R123 and R22/R141b LI systems were 10.5% and 5.5%, respectively, as compared to the No IC systems.) The R22/R123 system received more benefit from the addition of a high-temperature intercooler than the R22/R141b system. The manufacturing costs for the HI systems drop slightly relative to the No IC systems.

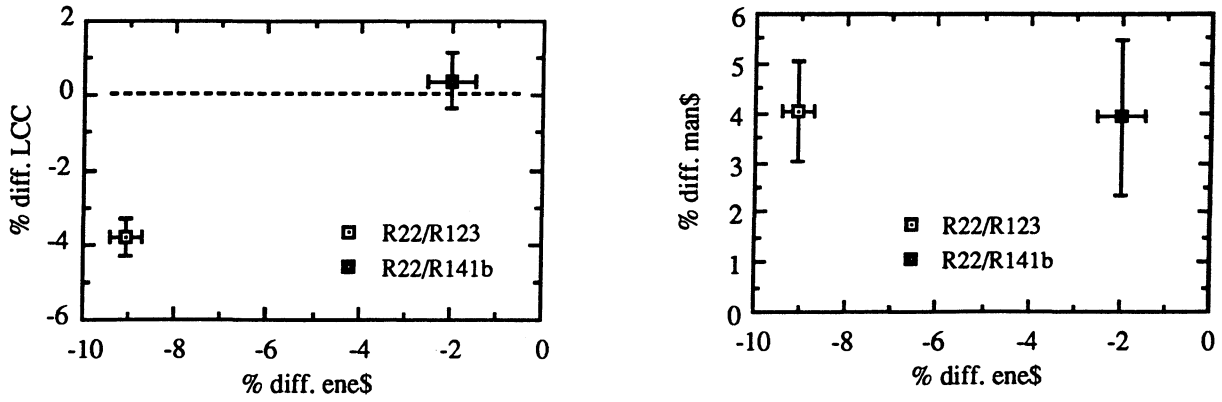

Figure 7.11: Optimization results - HI systems for R22/R123 and R22/R141b relative to the BC system - 50%/50% load splits

Table 7.11: Optimization statistics for R22/R123 and R22/R141b HI systems - 50%/50% load splits

quantity	BC (1E SLH/SH)	R22/R123 HI	R22/R141b HI
mass flux (kg/m^2-s)	30.5	27.2	25.1
heat flux (kW/m^2)	0.80	0.34 / 1.20	0.31 / 1.79
evaporating temperature (°C)	-23.6	NA	NA
evaporating pressure (kPa)	130.7	143.5	142.8
quality range	0.18 - 1.00	0.11 - 0.47 0.47 - 0.79	0.09 - 0.45 0.45 - 0.79
air velocity (m/s)	1.60	0.90 / 0.56	0.88 / 0.54
refrigerant-side resistance (%)	34.2	47.8 / 44.5	70.2 / 46.9
refrigerant heat transfer coeff. (W/m^2-K)	403.1	154.4 / 199.1	56.2 / 196.4
air heat transfer coeff. (W/m^2-K)	22.3	15.1 / 17.0	14.1 / 18.5
LCC ($)	1364.02	1312.40	1369.25
unit cost to consumer ($)	548.76	571.00	570.23
yearly power cost ($)	45.29	41.19	44.39
yearly power consumption (kW-hr/yr)	603.9	549.2	591.9
unit cost to manufacturer ($)	235.52	245.06	244.73
COP	1.40	1.41	1.30
$COP_{w\ fan}$	1.16	1.28	1.18
mass ratio of evaporator	1.00	1.16 / 0.33 1.49	1.30 / 0.22 1.52
occupied volume ratio	1.06	1.23 / 0.35 1.58	1.37 / 0.24 1.61
superheat (°C)	60.9	NA	NA
suction-line heat exchanger or low/high temperature intercooler (m)	2.4	2.4	1.8

The addition of a high-temperature intercooler alone reduces energy consumption of the system more than the addition of a low-temperature intercooler alone for these mixtures. This occurs because the glide of both mixtures is steepest at the higher qualities where the high-temperature intercooler is inserted. The addition of the intercooler moves the evaporator heat

transfer further back into the saturation dome where the curvature of the temperature-glide curve is not as great, increasing the temperature difference between the refrigerant and the air. As a result, the evaporating pressure is raised because potential heat exchanger pinch-points have been relieved.

The total evaporator area for the R22/R123 HI system is 49% greater than the BC system area, down from 80% for the No IC system. The R22/R141b HI system total evaporator area is 52% greater, down from 93% for the No IC system. The greatest reduction in area occurs for the fresh-food evaporators. Since the refrigerant glides are steepest at the higher qualities, the insertion of the high-temperature intercooler shifts the fresh-food evaporator heat transfer process away from a potential pinch-point. When this happens, the temperature difference between the air and the refrigerant increases and the fresh-food evaporator area can decrease. Manufacturing costs, therefore, actually decrease for these mixture systems.

The R22/R123 HI system experiences an 8.5% drop in its LCC from the No IC system, lowering it almost 4% below the LCC of the BC system. The R22/R141b LCC drops, but not enough to compete with the BC system.

7.3.4 HI/LI Systems

These optimized systems have two evaporators, a high-temperature intercooler *and* a low-temperature intercooler (HI/LI). The high- and low-temperature intercoolers are placed as shown in Figure 2.4. The optimization runs were performed for 60%/40%, 50%/50% and 40%/60% load splits between the freezer and fresh-food evaporators. Figure 7.12 and Table 7.12 report the optimization results. As with the pure-refrigerant systems, when the load was shifted to the warmer fresh-food compartment, the system energy consumption is reduced and the LCC decreases. The manufacturing costs for the three load variations for each HI/LI system are essentially constant.

Comparing the 50%/50% results for these systems to the HI systems shows that returning the low-temperature intercooler to the system has little or no effect. For the R22/R141b HI/LI system, the LCC drops from 0.38 to 0.37%. The addition of the low-temperature intercooler essentially does not change the optimization results. As shown in Table 7.12, the optimization did not drive the low-temperature intercooler length to zero. There was some other combination of intercooler lengths that gave a slightly lower LCC result. From the manufacturer's point of view, the less complex system with only the high-temperature intercooler would be one system configuration which might warrant further investigation.

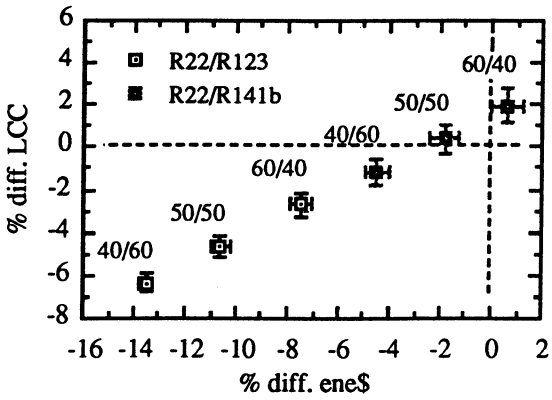

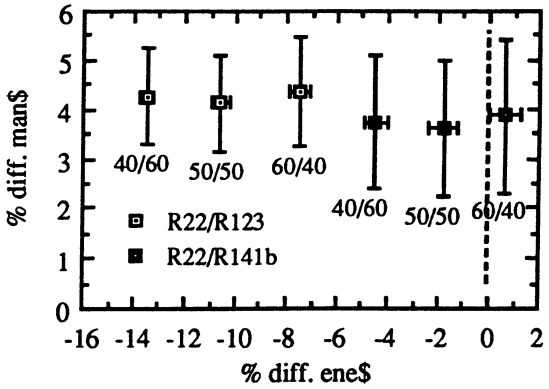

Figure 7.12: Optimization results - HI/LI systems for R22/R123 and R22/R141b relative to the BC system - 40%/60%, 50%/50%, and 60%/40% load splits

Table 7.12: Optimization statistics for R22/R123 and R22/R141b HI/LI systems - 50%/50% load splits only

quantity	BC (1E SLH/SH)	R22/R123 HI/LI	R22/R141b HI/LI
mass flux (kg/m^2-s)	30.5	27.1	25.1
heat flux (kW/m^2)	0.80	0.37 / 1.05	0.34 / 1.37
evaporating temperature (°C)	-23.6	NA	NA
evaporating pressure (kPa)	130.7	148.6	143.1
quality range	0.18 - 1.00	0.03 - 0.40 0.50 - 0.81	0.05 - 0.42 0.55 - 0.86
air velocity (m/s)	1.60	0.91 / 0.60	0.93 / 0.60
refrigerant-side resistance (%)	34.2	47.7 / 46.0	71.2 / 52.4
refrigerant heat transfer coeff. (W/m^2-K)	403.1	161.5 / 190.2	57.3 / 158.2
air heat transfer coeff. (W/m^2-K)	22.3	15.7 / 17.2	15.1 / 18.5
LCC ($)	1364.02	1300.36	1369.05
unit cost to consumer ($)	548.76	571.35	568.58
yearly power cost ($)	45.29	40.50	44.47
yearly power consumption (kW-hr/yr)	603.9	540.0	592.9
unit cost to manufacturer ($)	235.52	245.21	244.02
COP	1.40	1.44	1.30
$COP_{w\ fan}$	1.16	1.30	1.18
mass ratio of evaporator	1.00	1.09 / 0.38 1.47	1.20 / 0.29 1.49
occupied volume ratio	1.06	1.15 / 0.40 1.55	1.26 / 0.31 1.57
superheat (°C)	60.9	NA	NA
suction-line heat exchanger or low/high temperature intercooler (m)	2.4	1.5 / 1.4	0.6 / 0.5

The R22/R123 HI/LI system does benefit from returning the low-temperature intercooler to the system, although the gains are small. As with the R22/R141b systems, the majority of the energy savings comes from the addition of the high-temperature intercooler only. With the addition of the low-temperature intercooler, the R22/R123 HI/LI system's LCC decreases from

-3.8 to -4.7%. Energy consumption of the same system falls to 10.5% below the BC system, an additional 1.5% below the R22/R123 HI system's energy consumption.

For the R22/R123 HI/LI system, the addition of the low-temperature intercooler enables the optimization to find a more favorable location along the mixture glide curve for the freezer and fresh-food evaporator heat transfer that further minimizes LCC. The R22/R123 HI/LI system still has temperature glide to exploit at the middle qualities where the low-temperature intercooler is inserted.

The manufacturing costs are lower for HI/LI systems than for the No IC systems. The R22/R123 HI/LI manufacturing costs are 4.1% as compared to the No IC system's 4.3%. The R22/R123 HI/LI system's energy consumption cost is approximately -11% compared to the No IC system's +5% - a difference of 16%! This is a case where the addition of components does not increase the total manufacturing costs. The additional cost of the intercooler is offset by a decrease in the evaporator areas. The total evaporator area for the R22/R123 HI/LI system is 46% greater than the BC system, down from 49% for the HI system. The R22/R141b HI/LI system total evaporator area is 48% greater than the BC system, down from 52%.

7.3.5 HI/LI HEF Systems

These optimized systems have two evaporators, a high-temperature intercooler and a low-temperature intercooler, and high-efficiency evaporator fans (HI/LI HEF). The optimization runs were performed for a 50%/50% load split between the freezer and fresh-food evaporators. Figure 7.13 and Table 7.13 report the optimization results. For a comparison, the HI/LI (50%/50%) systems are also presented in Figure 7.13. The only difference between the HI/LI

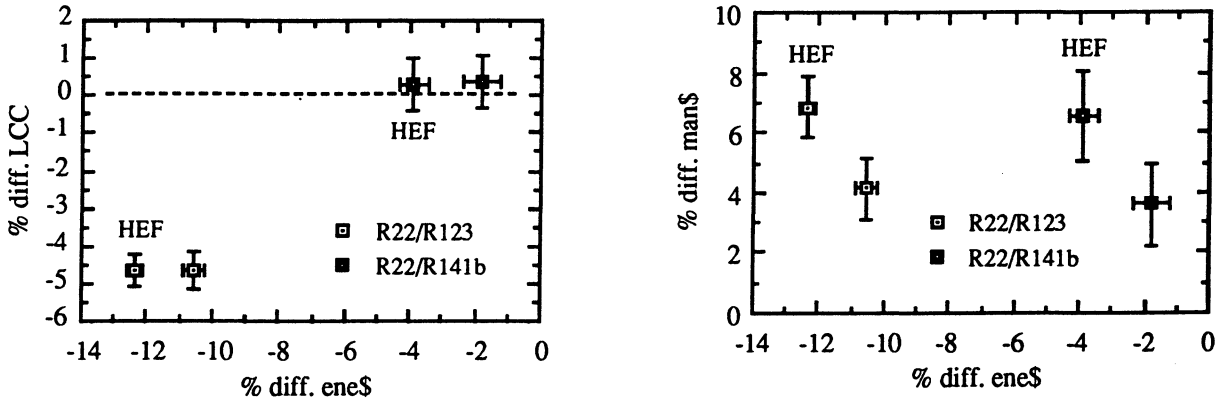

Figure 7.13: Optimization results - HI/LI HEF systems for R22/R123 and R22/R141b relative to the BC system - 50%/50% load splits

and HI/LI HEF systems is the addition of the high-efficiency fans. The HI/LI HEF systems use less energy than the equivalent standard-efficiency fan, HI/LI, systems and are more expensive to build.

Table 7.13: Optimization statistics for R22/R123 and R22/R141b HI/LI HEF systems - 50%/50% load splits

quantity	BC (1E SLH/SH)	R22/R123 HI/LI HEF	R22/R141b HI/LI HEF
mass flux (kg/m^2-s)	30.5	27.1	25.0
heat flux (kW/m^2)	0.80	0.34 / 1.14	0.3 / 1.54
evaporating temperature (°C)	-23.6	NA	NA
evaporating pressure (kPa)	130.7	151.8	147.6
quality range	0.18 - 1.00	0.03 - 0.41 0.50 - 0.81	0.05 - 0.42 0.53 - 0.85
air velocity (m/s)	1.60	1.01 / 0.72	1.06 / 0.68
refrigerant-side resistance (%)	34.2	48.7 / 49.4	73.2 / 53.1
refrigerant heat transfer coeff. (W/m^2-K)	403.1	157.0 / 193.0	52.5 / 172.7
air heat transfer coeff. (W/m^2-K)	22.3	15.9 / 20.1	15.2 / 20.9
LCC ($)	1364.02	1300.72	1368.22
unit cost to consumer ($)	548.76	586.31	584.68
yearly power cost ($)	45.29	39.69	43.53
yearly power consumption (kW-hr/yr)	603.9	529.2	580.4
unit cost to manufacturer ($)	235.52	251.63	250.93
COP	1.40	1.46	1.33
$COP_{w\ fan}$	1.16	1.32	1.21
mass ratio of evaporator	1.00	1.18 / 0.35 1.53	1.33 / 0.26 1.59
occupied volume ratio	1.06	1.25 / 0.37 1.62	1.41 / 0.28 1.69
superheat (°C)	60.9	NA	NA
suction-line heat exchanger or low/high temperature intercooler (m)	2.4	1.4 / 1.5	0.6 / 0.7

The addition of a high-efficiency fan increases manufacturing costs. The HI/LI HEF systems do save approximately 2% in power consumption; however, the energy savings is not enough to offset the increased equipment costs, and the LCC stays the same. The manufacturing costs for the HI/LI HEF systems are approximately 3% greater than the HI/LI systems.

7.3.6 Mixture Temperature Glides

This section will briefly present the two mixture glides graphically and summarize the benefits of the mixture glide for intercooling. Recall the explanation for Figure 2.10 given in Chapter 2. Intercooling can help achieve lower evaporating temperatures with no decrease in evaporating pressure. It is desirable to use intercooling in the quality range where the refrigerant temperature glide is the steepest to maximize this advantage. Figure 7.14 shows the temperature glide for both mixtures. The evaporating pressures are approximately 140 kPa which is an

average of the HI, LI and HI/LI evaporating pressure optimization results for each mixture. The average temperature glide of the R22/R141b mixture is approximately 4°C lower than the R22./R123 mixture. Recall that the R22/R141b mixture had a much lower refrigerant heat transfer coefficient and the optimization was driven to a lower evaporating pressure to achieve the desired heat transfer. Comparing the two temperature glides, the R22/R123 mixture has a steeper glide in the lower quality range where the freezer and low-temperature intercooler would operate. The glide is only marginally steeper than the R22/R141b glide in the upper fresh-food evaporator quality range. However, the R22/R141b glide exceeds the R22/R123 glide in the quality range where the high-temperature intercooler would operate.

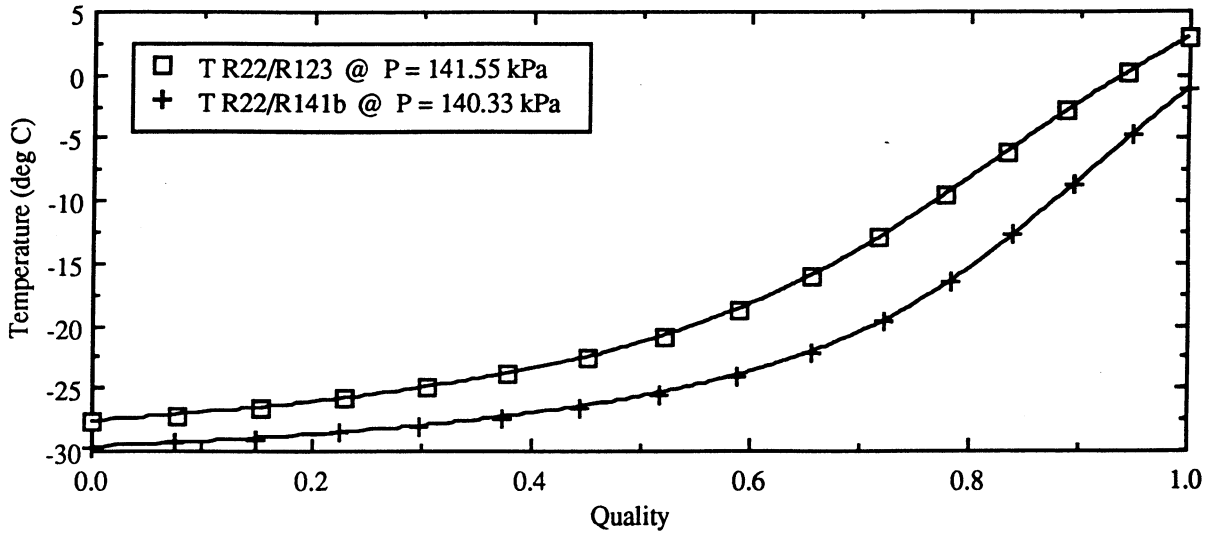

Figure 7.14: Temperature glides for 65% R22/35% R123 and 80% R22/20% R141b.

7.3.6 Summary

Figure 7.15 and 7.16 summarize the refrigerant-mixture results for all the systems. There were no mixture systems optimization configurations with superheat. Superheat was found to be counterproductive for these mixture systems. The mixture optimization drives any superheat in the system to zero. The gain in refrigeration effect from having superheat is offset by the increased compression power and larger heat exchanger areas. The beneficial effect of intercooling, moving the evaporator heat transfer processes back further in the saturation dome *away* from the saturated vapor line, is countered by superheat. The superheat serves to move the evaporator heat transfer process back *towards* the saturated vapor line. By moving the heat transfer process back toward the saturated vapor line, the evaporator areas increase because the mean-temperature difference between the air and refrigerant is reduced.

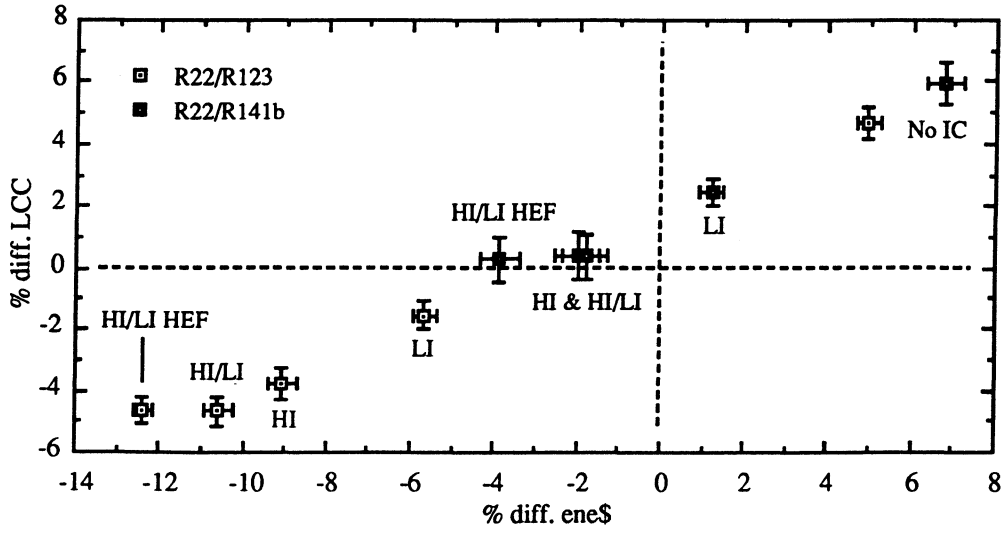

Figure 7.15: Optimization results - for all R22/R123 and R22/R141b systems relative to the BC system

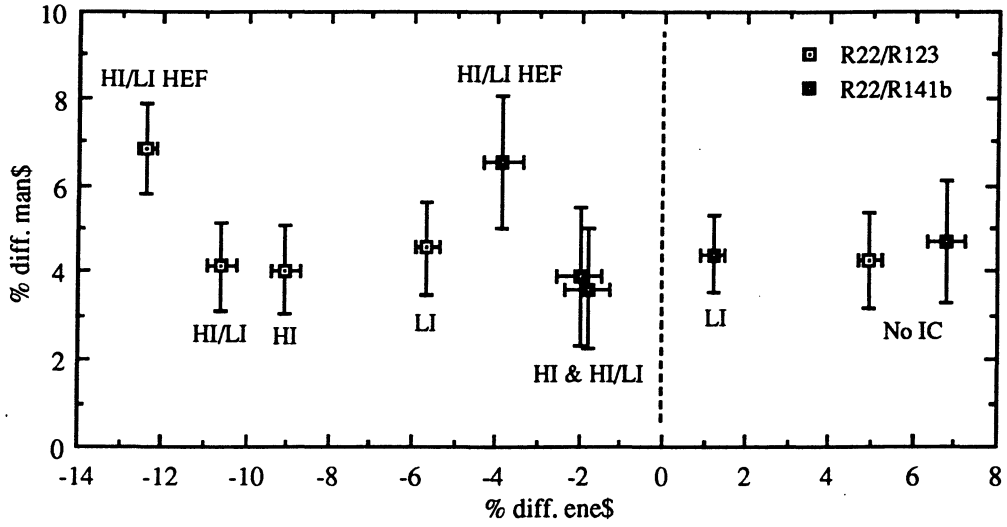

Figure 7.16: Optimization results - for all R22/R123 and R22/R141b systems relative to the BC system

The No IC systems are expensive to build and operate. The total evaporator area is approximately 1.86 times the area of the BC system. The R22/R141b system uses more energy than the R22/R123 system because of its low heat transfer coefficients in the low heat and mass flux range.

With the addition of a low-temperature intercooler between the freezer and fresh-food evaporators, the energy consumption of the LI systems drops tremendously. The R22/R123 LI

system benefited most from the addition of the low-temperature intercooler. Manufacturing costs remain essentially the same. The total evaporator area dropped to approximately 1.77 times the BC system. The large drop in energy consumption for the systems is due to the unique curvature of the temperature glide in saturation. The curve is shaped so that the insertion of the low-temperature intercooler is able to relieve a system pinch-point. These systems are excellent examples of the energy savings potential of mixture systems despite the very low refrigerant heat transfer coefficients that characterize low heat and mass flux flows. A large energy savings was realized for these systems with virtually no increase in manufacturing costs.

The mixture HI systems experience a greater drop in energy use than the LI systems. The manufacturing costs for the HI systems drop slightly from the manufacturing cost level of the No IC systems. The total evaporator area dropped further to approximately 1.5 times the area of the BC system. The addition of a high-temperature intercooler alone is able to reduce energy consumption of the system more than the addition of a low-temperature intercooler alone for these mixtures. This occurs because the glide of both mixtures is steepest at the higher qualities where the high-temperature intercooler is inserted. The addition of the intercooler moves the evaporator heat transfer further back into the saturation dome where the curvature of the temperature-glide curve is not as great, increasing the temperature difference between the refrigerant and the air. As a result, the evaporating pressure is able to be raised because potential heat exchanger pinch-points have been relieved.

The HI/LI systems experience little or no energy savings as compared to the HI systems. The addition of the low-temperature intercooler essentially does not change the optimization results for the R22/R141b HI/LI system as compared to the HI system. The less complex R22/R141b system with only the high-temperature intercooler would be a system which the manufacturers may want to investigate further. The R22/R123 HI/LI system does benefit from the addition of the low-temperature intercooler back to the system, but the gains are small as compared to the HI system. The majority of the energy savings comes from the addition of the high-temperature intercooler only. The addition of the low-temperature intercooler enables the optimization to find a more favorable location along the mixture glide curve for the freezer and fresh-food evaporator heat transfer that further minimizes LCC. The manufacturing costs decrease for the HI/LI systems as compared to the No IC systems! This is a case where the addition of a component does not increase the total manufacturing cost. The intercooler addition is offset by a decrease in the evaporator areas. The total evaporator area drops further to approximately 1.47 times the area of the BC system.

The addition of a high-efficiency fan increases manufacturing costs. The HI/LI HEF systems do save energy; however, the energy savings is not enough to offset the increased equipment costs, and the LCC stays the same.

The ratio of air temperature difference to the refrigerant temperature difference was calculated for each mixture system configuration evaporator. This was done to determine how well the air temperature glides were matched by the optimization to the refrigerant temperature glides. The freezer and fresh-food evaporator ratios for R22/R123 and R22/R141b were 1.25/0.58 and 1.84/0.61 respectively for the system configurations with the lowest LCC. A number greater that one indicates that the air temperature difference exceeds the refrigerant temperature difference. No definite conclusions were drawn from this exercise. It was hoped that the ratio would tend to 1.0 for the minimum LCC system configurations.

7.3.7 Best Mixture System

From the perspective of the customer, the best optimized refrigerant-mixture system configuration is the R22/R123 HI/LI system (see Table 7.14). (Once again this assumes that the consumer has the available cash to purchase the unit.) The manufacturing cost is predicted to be approximately 4% greater, the LCC is 4.5% less, and the system uses 10.5% less energy than the BC system. As with the pure-refrigerant systems, when high-efficiency fans are added to the R22/R123 HI/LI system, the manufacturing cost nearly doubles to 7%, yet the LCC remains unchanged at 4.5% below the BC system. The R22/R123 HI/LI HEF system *seems* to be the best choice from an environmental standpoint because of the additional energy savings. However, as explained previously, the objective function would need to be rewritten.

Table 7.14 lists the specifications for the optimized R22/R123 HI/LI system. The evaporators take 46% more area than the BC evaporator. The air velocities are reasonable at 0.91 and 0.60 m/s which corresponds to 33 and 22.5 CFM for the freezer and fresh-food evaporators respectively. The low-temperature and high-temperature intercooler lengths are nearly identical at approximately 1.5m.

One system configuration which the manufacturers *may* want to investigate further would be the R22/R123 HI system. The LCC savings is nearly the same for the R22/R123 HI/LI system, at 3.75% below the BC system. The manufacturing costs are slightly lower than the R22/R123 HI/LI system. The total evaporator area is 49% greater than the BC system. Even though the first costs are nearly identical, the manufacturers would tend to favor a less complex

system. The R22/R123 HI system has one less heat exchanger, which reduces the number of required system tube joints.

Table 7.14: Specifications for best optimized mixture system configuration for consumer

quantity	R22/R123 HI/LI
mass flux (kg/m^2-s)	27.1
heat flux (kW/m^2)	0.37 / 1.05
evaporating temperature (°C)	NA
evaporating pressure (kPa)	148.6
quality range	0.03 - 0.40 0.50 - 0.81
air velocity (m/s)	0.91 / 0.60
refrigerant-side resistance (%)	47.7 / 46.0
refrigerant heat transfer coeff. (W/m^2-K)	161.5 / 190.2
air heat transfer coeff. (W/m^2-K)	15.7 / 17.2
LCC ($)	1300.36
unit cost to consumer ($)	571.35
yearly power cost ($)	40.50
yearly power consumption (kW-hr/yr)	540.0
unit cost to manufacturer ($)	245.21
COP	1.44
$COP_{w\ fan}$	1.30
mass ratio	1.09 / 0.38 1.47
tot. mass of evaporators (g)	1254.2
occupied volume ratio	1.15 / 0.40 1.55
tot. occupied volume of evaporators (m^3)	1.118×10^{-2}
total outside evaporator area (m^2)	4.135
superheat (°C)	NA
suction-line heat exchanger or low/high temperature intercooler (m)	1.5 / 1.4

7.3.8 Other Considerations

As seen several times during the optimization of the mixture systems, large performance improvements were gained with the insertion of an intercooler. In many of these cases, the manufacturing costs actually *decreased*! The cost of adding an intercooler was more than offset by the reduction in evaporator area. At first glance, this might be misleading to the reader. As stated, the manufacturers' retooling costs were not considered in this study. One way to lower retooling costs is to produce an *innovative design* which will reduce the complexity of the refrigerant tube routing and minimize the number of solder joints. Reducing the number of solder joints increases reliability by decreasing the likelihood of refrigerant leaks.

Figures 7.17 and 7.18 show one potential design for the evaporator module which incorporates both high- and low-temperature intercoolers. The tubing is continuous, eliminating solder joints, and the evaporators are folded over a separation plate. The fold-over design could potentially fit into the same evaporator location in current refrigerator models.

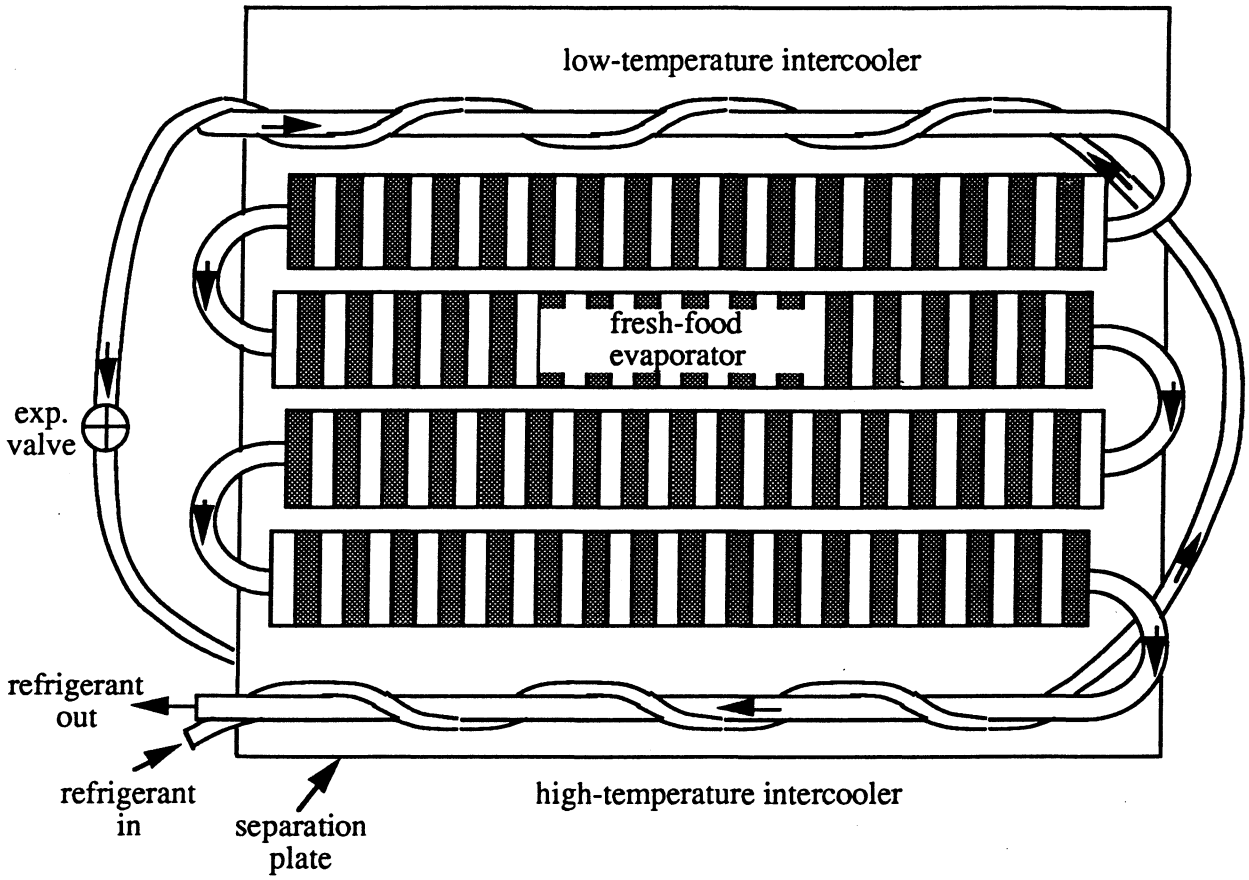

Figure 7.17: Potential heat exchanger component configuration for a HI/LI evaporator module - front view[3]

Another way to reduce complexity and increase reliability would be to use only one fan motor to move the air over both evaporators. An extended, double-shaft fan motor could be mounted through the separation plate. Fan blades could be mounted on both ends of the shaft. Each fan blade would be designed to move the proper amount of air over each evaporator. Other design and manufacturing innovations will be required before manufacturers might consider a two evaporator, one or two intercooler production system.

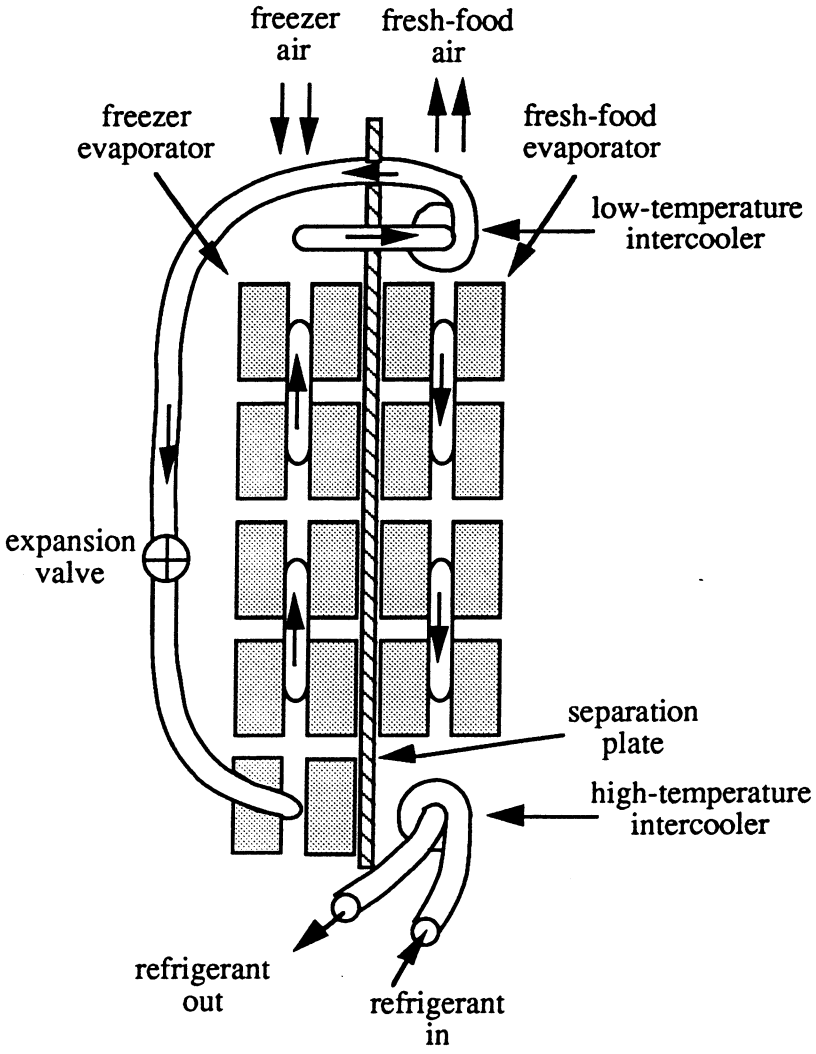

Figure 7.18: Potential heat exchanger component configuration for a HI/LI evaporator module - side view[4]

7.4 Comparisons between Pure-Refrigerant and Mixture Results

Figures 7.19 and 7.20 illustrate the comparison between selected optimized pure-refrigerant and refrigerant-mixture systems. The plot abbreviations are listed in Table 7.15. Only the R22/123 mixture systems and the R134a pure-refrigerant systems are shown. They were the best performing systems. The R22/R123 systems are HI, HI/LI and HI/LI HEF. The R134a systems are 1E SLH/SH, 1E SLH/SH HEF, 2E SLH/SH, and 2E HI/LI HEF.

The best overall system with the lowest LCC is the R22/R123 HI/LI system; however, the uncertainty bars of the R22/R123 HI/LI system overlap with the R134a 2E SLH/SH and 2E SLH/SH HEF systems. Therefore, the *only conclusions* that can be drawn are that the R22/R123

HI/LI system performs as well as the R134a 2E SLH/SH and 2E SLH/SH HEF systems. There are relative trade-offs between first costs and operating costs. The importance of each will need to be judged by the manufacturer and the consumer. However, recall that the pure refrigerant correlation was suspected to over predict the heat transfer coefficients for the R134a systems. This may slightly raise the LCC of these systems. As will be seen in the next section, even large variations in refrigerant heat transfer coefficients do not impact the LCC appreciably.

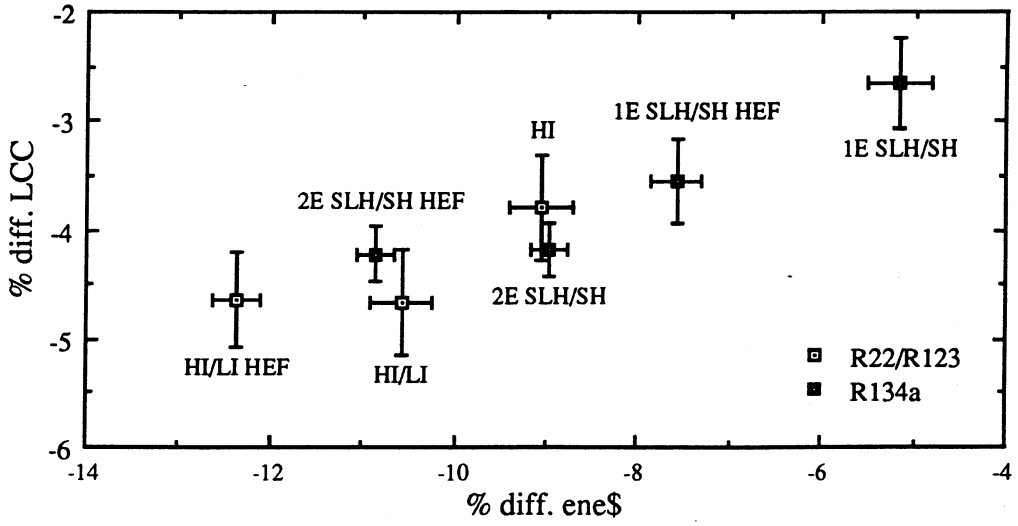

Figure 7.19: Optimization results - for select 50%/50% load split R134a and R22/R123 systems relative to the BC system - LCC versus ene$

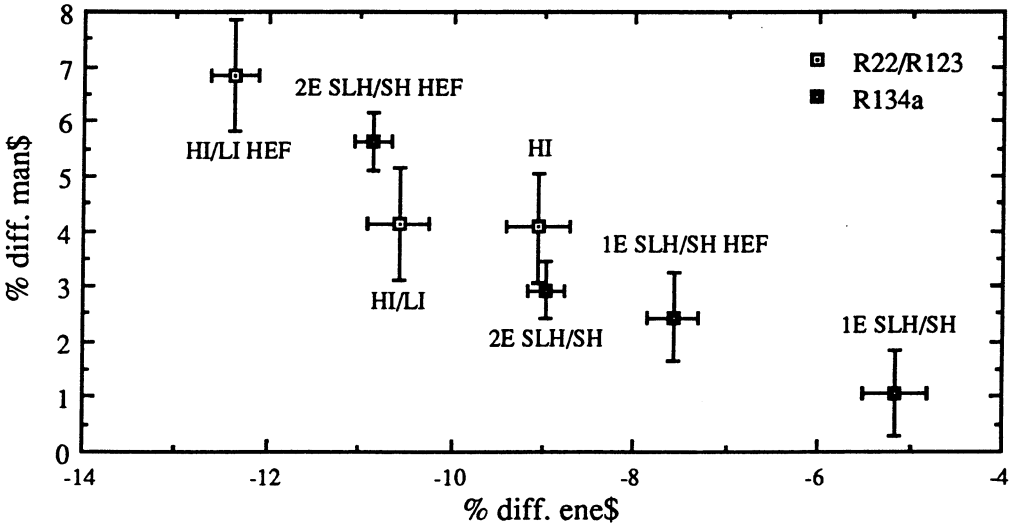

Figure 7.20: Optimization results - for select 50%/50% load split R134a and R22/R123 systems relative to the BC system - man$ versus ene$

Table 7.15: Plot abbreviations for Figures 7.19 and 7.20

abbreviation	description
1E SLH/SH	R134a single-evaporator system with a suction-line heat exchanger and superheat
1E SLH/SH HEF	R134a single-evaporator system with a suction-line heat exchanger, superheat, and a high-efficiency evaporator fan
2E SLH/SH	R134a dual-evaporator system with a suction-line heat exchanger and superheat
2E SLH/SH HEF	R134a dual-evaporator system with a suction-line heat exchanger, superheat, and high-efficiency evaporator fans
HI	R22/R123 dual-evaporator system with a high -temperature intercooler
HI/LI	R22/R123 dual-evaporator system with high and low-temperature intercoolers
HI/LI HEF	R22/R123 dual-evaporator system with high and low-temperature intercoolers and high-efficiency evaporator fans

A better basis of comparison for the best systems might be the optimized 1E SLH/SH R134a system. As discussed previously, the BC system had a large fan power consumption because the volumetric flow rate for a typical standard evaporator system was specified for the BC system. The BC system's evaporator was constructed out of the optimized fin/tube arrangement (Table 6.2). The comparisons between the best mixture and pure systems relative to the BC system *and* the R134a 1E SLH/SH system are summarized in Tables 7.16 and 7.17. In addition, a comparison of the R22/R123 HI/LI system is made with the R134a 2E SLH/SH system in Table 7.16.

Table 7.16: Comparison of best pure-refrigerant and refrigerant-mixture optimized system configurations

system	COP_w fan	% energy savings	% cost increase	% LCC decrease	% COP_w fan increase	% area increase	tot. outside evap. area (m^2)	relative to
R134a 2E SLH/SH	1.28	9.0	2.9	4.2	10.3	1.9	2.881	BC
R22/R123 HI/LI	1.30	10.6	4.1	4.7	12.1	46.2	4.135	BC
R134a 2E SLH/SH	1.28	4.0	1.9	1.6	4.9	-14.3	2.881	R134a 1E SLH/SH
R22/R123 HI/LI	1.30	5.7	3.0	2.1	6.6	23.0	4.135	R134a 1E SLH/SH
R22/R123 HI/LI	1.30	1.8	1.2	0.5	1.6	43.5	4.135	R134a 2E SLH/SH

Table 7.17: Specifications for best pure-refrigerant and refrigerant-mixture optimized system configurations and base-case systems

quantity	BC (1E SLH/SH)	R134a 1E SLH/SH	R134a 2E SLH/SH	R22/R123 HI/LI
mass flux (kg/m^2-s)	30.5	22.9	23.0	27.1
heat flux (kW/m^2)	0.80	0.68	0.45 / 3.05	0.37 / 1.05
evaporating temperature (°C)	-23.6	-25.2	-23.6	NA
evaporating pressure (kPa)	130.7	105.6	113.8	148.6
quality range	0.18 - 1.00	0.18 - 1.00	0.18 - 0.59 0.59 - 1.00	0.03 - 0.40 0.50 - 0.81
air velocity (m/s)	1.60	1.03	1.01 / 0.49	0.91 / 0.60
refrigerant-side resistance (%)	34.2	28.4	32.0 / 21.8	47.7 / 46.0
refrigerant heat transfer coeff. (W/m^2-K)	403.1	378.5	362.1 / 661.3	161.5 / 190.2
air heat transfer coeff. (W/m^2-K)	22.3	16.0	18.2 / 19.6	15.7 / 17.2
LCC ($)	1364.02	1327.68	1307.02	1300.36
unit cost to consumer ($)	548.76	554.51	564.82	571.35
yearly power cost ($)	45.29	42.95	41.23	40.50
yearly power consumption (kW-hr/yr)	603.9	572.7	549.8	540.0
unit cost to manufacturer ($)	235.52	237.98	242.41	245.21
COP	1.40	1.36	1.41	1.44
$COP_{w\ fan}$	1.16	1.22	1.28	1.30
mass ratio	1.00	1.19	0.89 / 0.13 1.02	1.09 / 0.38 1.47
tot. mass of evaporators (g)	853.2	1015.3	870.3	1254.2
occupied volume ratio	1.06	1.26	0.94 / 0.14 1.08	1.15 / 0.40 1.55
tot. occupied volume of evaporators (m^3)	7.647×10^{-3}	9.090×10^{-3}	7.791×10^{-3}	1.118×10^{-2}
total outside evaporator area (m^2)	2.828	3.362	2.881	4.135
superheat (°C)	60.9	67.0	65.0	NA
suction-line heat exchanger or low/high temperature intercooler (m)	2.4	3.9	3.7	1.5 / 1.4

The breakdown in the costs for all system configurations was fairly consistent. Table 7.18 shows the cost breakdown for the pure-refrigerant and mixture system configurations.

Table 7.18: Average cost breakdown for all mixture and pure refrigerant system configurations

	% of LCC			% of LCC
unit cost	40%	evap. fans and evap. module hxer costs	10%	4%
		cond. fan, cond., comp., cabinet costs etc.	90%	36%
power cost	60%	evap. and cond. fan power costs	10%	6%
		comp. power cost	90%	54%

7.5 Variation of Selected Mixture Properties

The question addressed in this section is: "How will the design of the R22/R123 HI/LI optimum system change if the mixture concentration were different, if the interaction parameter were different, or if the mixture heat transfer coefficients were different?" The results are presented in Figure 7.21 and Table 7.19.

The R22 concentration was changed from 65% to 61.5% to examine the effect on the optimized system design. The composition shift had negligible effect on the overall optimization results. The system used less energy and the LCC was slightly less than the base-case R22/R123 HI/LI system. (Note: the results in this section are compared to the R22/R123 HI/LI system from Table 7.12 *not* the R12 base-case (BC) system as the previous results - hence the *base-case* R22/R123 HI/LI system description) As shown in Table 7.19, the mass and occupied volume ratios (evaporator areas) did not vary significantly; however, there was a shifting in the allocation of intercooler lengths from the low-temperature intercooler to the high-temperature intercooler. The change in the intercooler lengths was caused by the concentration difference which altered the temperature-glide of the mixture.

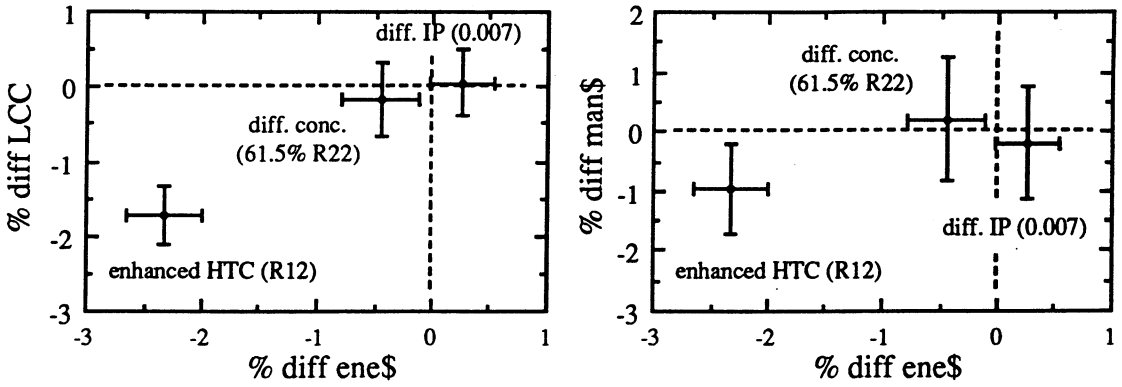

Figure 7.21: Results for 50%/50% load split R22/R123 HI/LI special case systems relative to the 50%/50% R22/R123 HI/LI system - LCC versus ene$ (left) - man$ versus ene$ (right)

These results are questionable because the R22/R123 heat transfer coefficient correlation was *only* valid for a mixture of 65% R22 and 35% R123; however, the trend in the results is believed to be correct. Examining the ideal simulation results for R22/R123 in Figure 2.8, the maximum COP for a typical mixture air-glide of 10°C is close to a mixture concentration of 60% R22, not 65%.

The R22/R123 interaction parameter was changed from 0.003 to 0.007 to examine the effect on the optimized system design. A higher interaction parameter lowers the attractive

forces between the species of the mixture, R22 and R123. This will raise the pressure of the mixture and increase the entropy of the superheated vapor. The interaction parameter must be experimentally measured or estimated. The value of 0.003 was estimated by Bare[5] and the 0.007 value was estimated by Morrison.[6] The change in the interaction parameter had negligible effect on the overall optimization results. The origin was within the uncertainty bars for both LCC and manufacturing costs. The system used more energy and the LCC was slightly more than the base-case R22/R123 HI/LI system. As shown in Table 7.19, the mass and occupied volume ratios did not vary significantly. Similarly to the concentration change case, there is a shift in the allocation of intercooler lengths from the low-temperature intercooler to the high-temperature intercooler. The new interaction parameter causes the temperature-glide profile to change so that there is a better intercooler length combination.

Table 7.19: Special case optimization statistics for R22/R123 (50%/50% load splits)

quantity	R22/R123 base-case HI/LI	R22/R123 HTC of R12 HI/LI	R22/R123 conc = 61.5% HI/LI	R22/R123 IP = 0.007 HI/LI
mass flux (kg/m^2-s)	27.1	27.0	27.2	27.2
heat flux (kW/m^2)	0.37 / 1.05	0.43 / 1.39	0.36 / 0.95	0.38 / 1.12
evaporating temperature (°C)	NA	NA	NA	NA
evaporating pressure (kPa)	148.6	155.2	140.4	148.0
quality range	0.03 - 0.40 0.50 - 0.81	0.03 - 0.40 0.49 - 0.81	0.04 - 0.41 0.50 - 0.81	0.03 - 0.41 0.49 - 0.80
air velocity (m/s)	0.91 / 0.60	0.95 / 0.58	0.89 / 0.62	0.87 / 0.58
refrigerant-side resistance (%)	47.7 / 46.0	30.3 / 25.1	47.8 / 46.3	47.0 / 45.1
refrigerant heat transfer coeff. (W/m^2-K)	161.5 / 190.2	375.0 / 510.5	156.5 / 185.3	162.8 / 194.5
air heat transfer coeff. (W/m^2-K)	15.7 / 17.2	17.3 / 18.2	15.3 / 17.0	15.4 / 17.0
LCC ($)	1300.36	1277.84	1298.24	1301.04
unit cost to consumer ($)	571.35	565.77	572.48	570.19
yearly power cost ($)	40.50	39.56	40.32	40.60
yearly power consumption (kW-hr/yr)	540.0	527.46	537.60	541.37
unit cost to manufacturer ($)	245.21	242.82	245.70	244.72
COP	1.44	1.48	1.45	1.43
$COP_{w\ fan}$	1.30	1.33	1.30	1.29
mass ratio of evaporator	1.09 / 0.38 1.47	0.92 / 0.29 1.21	1.11 / 0.42 1.53	1.06 / 0.36 1.42
occupied volume ratio	1.15 / 0.40 1.55	0.98 / 0.31 1.29	1.18 / 0.45 1.63	1.13 / 0.38 1.51
superheat (°C)	NA	NA	NA	NA
suction-line heat exchanger or low/high temperature intercooler (m)	1.5 / 1.4	1.5 / 0.8	1.1 / 1.8	1.1 / 1.7

These results are also questionable for the similar reasons as the previous case. The R22/R123 heat transfer coefficient correlation was *only* valid for the mixture 65% R22/35% R123 where the properties are evaluated with a interaction parameter of 0.003; however, the

trend in the results *may* be correct. For a higher interaction parameter, the system pressure would tend to be higher and the work of compression would be higher for identical conditions. No clear trend can be obtained from the comparison of R22/R123 HI/LI base-case and HI/LI IP=0.007 systems shown in Table 7.19 since the optimization has the low-side pressure as an independent variable. The HI/LI IP=0.007 system has an increased work of compression, however, the system pressure is slightly lower and the compression work is expected to increase.

The most interesting case examined was the substitution of the UIUC R12 correlation into the mixture optimization program. The effect of the reduced mixture heat transfer coefficient was assessed by comparing the two optimized systems. Recall that the mixture heat transfer coefficients under-performed the pure refrigerant heat transfer coefficients by approximately 50% under low heat and mass-flux flow conditions (See Figure 5.9). As shown in Figure 7.21, the LCC of the modified system improves by approximately 1.75%. The system uses approximately 2.5% less energy than the base-case R22/R123 HI/LI system. The higher heat transfer coefficient does have a significant effect on the LCC as compared to the other two cases examined; however, the manufacturing costs only fall 1% as compared to the base case. As shown in Table 7.19, there is a 17% reduction in the total evaporator area for the higher heat transfer coefficient system. In addition, the low-side pressure of the system can be raised because of the reduced heat transfer resistance. This reduces the compressor power consumption. Once again, there is a shift in the allocation of intercooler lengths; however, the low-temperature intercooler length remains unchanged and the high-temperature intercooler is shortened.

Relative to the other two cases, the change in LCC for the modified heat transfer coefficient system was significant; however, this 1.75% reduction in LCC must be put into perspective with the results in Figure 7.15. The LCC was influenced more by fundamental changes in system components, such as the insertion of an intercooler. The LCC drops approximately 9% from the R22/R123 No IC system to the HI/LI system. More than doubling the refrigerant heat transfer coefficient only reduces the LCC 1.75%. Clearly the greater gains are to be had in modifying the thermodynamics of the refrigerant cycle.

The energy savings of 2.5% for the R22/R123 HI/LI modified with the R12 heat transfer coefficient is approximately the same as reported by Stoecker and Boggs[7] (section 2.3.4). Stoecker and Boggs performed system simulations on a R12/R114 system and on a modified R12/R114 system using an R12 correlation to quantify the importance of the low mixture heat transfer coefficients on performance. The R12/R114 modified heat transfer coefficient system

realized a 1.5% energy savings over the R12/R114 system. There are greater energy savings for the R22/R123 modified heat transfer coefficient system than the R12/R114 modified heat transfer coefficient system. A possible explanation for the difference in the results is that the R22/R123 modified heat transfer coefficient system was *optimized* to be used with the R12 coefficients, whereas the R12/R114 modified heat transfer coefficient system was *simulated* at the same conditions as the R12/R114 system.

7.6 Variation of Discount Rate and Markup Factor

It was of interest to examine the optimization results for another value of material markup (see 6.3.9) and discount rate (see 6.3.10). The markup factor was reduced from 2.33 to 1.0. This can be justified for small changes in overall size and weight of the unit and for modified internal components. The unit's shipping and handling costs should be the same, therefore the markup should be equal to one. Table 7.20 shows the results of changing the markup value for two different discount rates, zero and four percent. The higher discount rate of four percent was examined because it is more realistic and is consistent with the historical average of the Federal Funds Rate minus the twelve-month moving average change in the Consumer Price Index for the last twenty years (see 6.3.10).

Examining Table 7.20 for a markup of one, the LCC decreases because the cost of the unit decreases as compared to the same system optimized for an identical discount rate and a markup of 2.33. The energy consumption cost remains essentially unchanged. The results are similar for both sets of discount rates. The relative ranking of the various optimization runs remains unchanged with the mixture system always having the lowest LCC for the configurations with the same discount rate and markup factor. However at the higher discount rate the difference between the LCC of the mixture and pure-refrigerant system narrows. At the higher rate, the system which is less equipment intensive, the pure-refrigerant system (much smaller evaporators - see Table 7.16), benefits the most from the lower cost of energy. For optimization runs with high discount rates, the lower cost, less energy efficient systems will tend to have the lower LCCs.

Table 7.20: Comparison of best refrigerant-mixture and pure-refrigerant optimized system configurations as the discount rate and markup factor are varied

system	energy cost	energy kWhr/yr	unit cost	LCC	discount rate	markup
R134a 2E SLH/SH	742.20	549.77	564.82	1307.02	0.0	2.33
R134a 2E SLH/SH	739.61	547.86	544.87	1284.48	0.0	1.0
R134a 2E SLH/SH	524.40	552.32	562.13	1086.52	4.0	2.33
R134a 2E SLH/SH	521.87	549.66	542.77	1064.64	4.0	1.0
R22/R123 HI/LI	729.01	540.00	571.35	1300.36	0.0	2.33
R22/R123 HI/LI	726.47	538.12	550.96	1277.42	0.0	1.0
R22/R123 HI/LI	516.46	543.96	567.17	1083.21	4.0	2.33
R22/R123 HI/LI	513.73	541.08	547.49	1061.21	4.0	1.0

7.7 Two-Capillary Tube R134a Single-Evaporator System Configuration

It was of interest to examine a two-capillary tube single-evaporator pure-refrigerant system configuration. It was assumed that this system had a valving setup that could switch a different capillary tube in-line for handling either the freezer or fresh-food cooling duty. The duty cycle was assumed to be 0.4 for both the freezer and fresh-food cooling cycles. The cooling load was equally distributed, 50%/50%, with a 100 W loading for each compartment. To keep costs low, a single evaporator was used to serve both compartments. A damper system was assumed to switch the air-flow from one compartment to another at the same time the capillary tubes are switched.

The optimization was run twice, one for each compartment. The larger evaporator and suction-line heat exchanger were chosen for the design. As shown in Table 7.21, the optimization settled at an equivalent LCC which was 4.8% less than that of the best optimized system configuration for the R22/R123 mixture determined previously. In addition, the two-capillary tube system used 4.9% less energy and was 4.6% less expensive to build than the R22/R123 HI/LI optimized system configuration. The optimization settled at values which were very similar for both compartment duty cycles as shown in Table 7.22. The optimization results for both duty cycles are given in the table.

Manufacturers might want to investigate this system in more detail. The optimization was unable to take into account the cost of the capillary tube switching system. This could add

significantly to the initial cost of the system and raise its LCC above the other system configurations.

Table 7.21: Comparison of best pure-refrigerant and refrigerant-mixture optimized system configurations with a two-capillary tube single-evaporator pure-refrigerant system

system	energy cost	energy kWhr/yr	unit cost	LCC
R134a 2E SLH/SH	742.20	549.77	564.82	1307.02
R22/R123 HI/LI	729.01	540.00	571.35	1300.36
R134a 1E SLH/SH two cap tube	692.94 (4.9 % less than 22/123)	513.29 (4.9 % less than 22/123	545.33 (4.6 % less than 22/123	1238.27 (4.8 % less than 22/123

Table 7.22: Specifications for the best pure-refrigerant and refrigerant-mixture optimized system configurations and a two-capillary tube single evaporator pure refrigerant system

quantity	R134a 2E SLH/SH	R22/R123 HI/LI	R134a 1E SLH/SH 2 cap tube
mass flux (kg/m^2-s)	23.0	27.1	11.6 / 11.9
heat flux (kW/m^2)	0.45 / 3.05	0.37 / 1.05	0.51 / 0.62
evaporating temperature (°C)	-23.6	NA	-25.2 / -5.9
evaporating pressure (kPa)	113.8	148.6	105.9 / 234.7
quality range	0.18 - 0.59 0.59 - 1.00	0.03 - 0.40 0.50 - 0.81	0.19 - 1.00 0.16 - 1.00
air velocity (m/s)	1.01 / 0.49	0.91 / 0.60	0.89 / 0.88
refrigerant-side resistance (%)	32.0 / 21.8	47.7 / 46.0	41.2 / 39.5
refrigerant heat transfer coeff. (W/m^2-K)	362.1 / 661.3	161.5 / 190.2	237.8 / 275.5
air heat transfer coeff. (W/m^2-K)	18.2 / 19.6	15.7 / 17.2	17.8 / 19.1
LCC ($)	1307.02	1300.36	1238.27
unit cost to consumer ($)	564.82	571.35	545.33
yearly power cost ($)	41.23	40.50	38.50
yearly power consumption (kW-hr/yr)	549.8	540.0	513.29
unit cost to manufacturer ($)	242.41	245.21	234.05
COP	1.41	1.44	1.36 / 2.15
$COP_{w\ fan}$	1.28	1.30	1.15 / 1.68
mass ratio*	0.89 / 0.13 1.02	1.09 / 0.38 1.47	0.79
tot. mass of evaporators (g)*	870.3	1254.2	674.03
occupied volume ratio*	0.94 / 0.14 1.08	1.15 / 0.40 1.55	0.84
tot. occupied volume of evaporators (m^3)*	7.791×10^{-3}	1.118×10^{-2}	6.070×10^{-3}
total outside evaporator area (m^2)*	2.881	4.135	2.241
superheat (°C)	65.0	NA	64.8 / 42.9
suction-line heat exchanger or low/high temperature intercooler (m)*	3.7	1.5 / 1.4	2.55

* for largest heat exchanger for the two-capillary tube system

7.8 References

---

[1] Personal communication with Jon P. Wattelet, University of Illinois, Air-Conditioning and Refrigeration Center, September, 1993.

[2] Admiraal, D. M. and C. W. Bullard, "Heat Transfer in Refrigerators Condensers and Evaporators", ACRC TR-48, University of Illinois at Champaign Urbana, Air Conditioning and Refrigeration Center, August, 1993, p. 35.

[3] Heun, M. K., "Thermal Performance Analysis of an Evaporator-Intercooler Module for a Lorenz Cycle", Master's Thesis, Department of Mechanical and Industrial Engineering, University of Illinois at Champaign-Urbana, 1991, part of Figure 7.7.

[4] Heun, M. K., "Thermal Performance Analysis of an Evaporator-Intercooler Module for a Lorenz Cycle", Master's Thesis, Department of Mechanical and Industrial Engineering, University of Illinois at Champaign-Urbana, 1991, part of Figure 7.7.

[5] Personal communication with Jane Bare, United States Environmental Protection Agency, Research Triangle Park, North Carolina, July, 1991.

[6] Personal communication with Graham Morrison at the National Bureau of Standards and Technology, Gaithersburg, Maryland, July, 1991.

[7] Stoecker, W. F. and D. Boggs, "Performance and Simulation of Once-Through and Separating Cycles Using Non-azeotropic Refrigerant Mixtures", ORNL - Sub - 81-7762/5 & 01, June, 1986.

CHAPTER 8: CONCLUSIONS AND RECOMMENDATIONS

This chapter will summarize the significant results of this project. The first section reviews the project motivation and the basic thermodynamic advantages of NARMs. Next, the component models which were required for the steady-state optimization model are reviewed. The third section summarizes the experimental work for this project. The next four sections cover the significant results from the optimization study: the optimization results for pure-refrigerant system configurations, the optimization results for mixture system configurations, the best optimal system configuration, and the effects of variations in concentration, interaction parameter, and heat transfer coefficients on the optimization results. The chapter concludes with suggestions for future work.

8.1 Motivation and Scope of this Study

Some Non-Azeotropic Refrigerant Mixtures (NARMs) have been identified as potential replacements for R12 because of their low ozone depletion potential, low global warming potential and promising thermodynamic characteristics which could improve cycle efficiency. A NARM experiences a variable temperature glide during a constant-pressure phase change process, making it a logical candidate for the two-temperature level cooling found in refrigerators.

There are two main thermodynamic advantages to using a NARM over a pure refrigerant. The *first* advantage of NARMs is that the refrigerant and air-temperature glides can be better matched to improve the performance of the system over that of a pure-refrigerant system. This matching thermodynamically reduces the irreversibility of the heat exchange process, thereby increasing performance. The *second* advantage to using NARMs is that lower refrigerant temperatures can be achieved through the use of intercooling with no decrease in the evaporating pressure. When an intercooler is inserted in the system, the evaporator heat transfer process is shifted further back into the saturation dome. The addition of the intercooler, with the outlet of the evaporator module fixed at the saturated vapor line, decreases the quality of the mixture entering the module. The temperature of a mixture decreases at low qualities for a constant pressure. Intercooling may be justified in some cases but not in others, depending on the NARM glide and the load distribution between the freezer and the fresh-food compartments.

The major objective of this research was to investigate optimal pure refrigerant and NARM refrigerator system configurations that minimized life-cycle cost. A steady-state optimization model was used to minimize the life-cycle cost of each system configuration

studied. The system configurations were composed of various combinations of four different heat exchangers, two fan types, two pure refrigerants, R12 and R134a, and two NARMs, 65% R22 / 35% R123 and 80% R22 / 20% R141b.

8.2 Formulation of Optimization Models

To formulate the steady state optimization model, a number of component models and heat transfer correlations had to be developed or found in the literature. The components that were modeled were the evaporator, intercooler (suction-line heat exchanger), evaporator fan, and compressor. Both heat transfer and cost models were needed for the evaporator and intercooler. Heat transfer correlations had to be developed for both the R22/R123 and R22/R141b mixtures. A heat transfer correlation valid for R12, R22, and R134a was selected from the literature.

To develop the evaporator heat transfer model, a flow loop was constructed that contained two evaporators and two intercoolers. The flow loop was charged with the pure refrigerants, R12 and R22. Heat transfer and flow measurements were taken under a variety of conditions for each pure refrigerant. Energy balances were performed on the evaporators. From these energy balances, an air-side heat transfer model for the evaporators was developed. The intercooler heat transfer model was developed from existing single- and two-phase heat transfer correlations and the UA/LMTD heat exchanger analysis method. Cost models for the evaporators and intercoolers were developed from information obtained from a manufacturer.

An isentropic compressor power model was developed. The model assumed a constant isentropic efficiency to make the optimization system comparisons fair. A basic assumption was made that an equally efficient compressor could be manufactured for each fluid system and range of operating conditions. The fan power model was developed using two experimental data points fit to an 'equivalent duct length' correlation.

The R22/R123 and R22/R141b heat transfer correlations were developed from flow data and the evaporator air-side heat-transfer model. A finite-difference energy balance method on the two flow loop evaporators was performed to obtain the mixture heat transfer coefficients in the low and high quality two-phase regions. The finite-difference analysis was necessary because mixtures generally do not have constant specific heats in the two-phase region. The heat transfer coefficient data was fit to an appropriate correlation form.

With the appropriate component models and heat transfer correlations in place, the system optimization model was assembled. The optimization's life-cycle cost objective function

was comprised of three costs: component costs, operating costs, and occupied volume costs. The independent variables were: evaporating pressure, evaporator air velocities, intercooler loads (suction-line heat exchanger load), and superheat level. The most useful outputs of the optimization program were: life-cycle cost, manufacturing and consumer cost, total energy consumption, and heat exchanger sizes.

8.3 Summary of Experimental Work

A refrigerant test loop was constructed that delivered refrigerant to a test cabinet at a desired pressure and temperature. The cabinet contained two evaporators and two intercoolers. The low-temperature (freezer) evaporator transferred heat in the quality range of approximately 0-50%, and the high-temperature (fresh-food) evaporator transferred heat in the quality range of approximately 50-100%. The use of separate heat exchangers for each compartment enabled the effect of quality change and heat flux to be studied independently.

The evaporators used in this experiment were built in-house by bonding the fin stock to the tube with an adhesive. The construction technique allowed for separate, staggered fin rows; more metal to metal contact between the fin and tube; and reduced fin stock thickness. In addition to enhancing heat transfer and saving material, the new technique could be used to simplify the manufacture of evaporators. At the end of the experiments, the integrity of the adhesive's fin/tube bond was examined for separation possibly caused by the numerous thermal cyclings. Only an insignificant number of separations had occurred.

The test loop was designed to operate without a condenser and without a compressor, *eliminating* the need for *oil* in the system. A chiller, a gear pump, and a heater replaced the compressor and condenser. After the initial runs of the test loop, it was determined that a diaphragm compressor was needed to help the system reach the desired evaporating pressures and prevent gear pump cavitation. To further prevent gear pump cavitation, a subcooler was added to the system.

The research mixtures were chosen by the project monitor, the United States Environmental Protection Agency. The first pair, 65% R22 / 35% R123, was the best-performing pair based on previous testing in actual refrigerators. The second pair, 80% R22 / 20% R141b, was the best-performing pair according to an Environmental Protection Agency refrigerator model. Both of these NARMs have a temperature glide of approximately 30°C at typical refrigerator operating conditions in keeping with the recommendations of Lorenz and Meutzner[1] for refrigerator applications.

The two test mixtures were found to be incompatible with charging hose material and Viton. After several uses, the charging hoses became permeable to the refrigerant mixtures. The mixtures also attacked the Viton o-rings that were in the test setup. The best material for the o-ring was determined to be Neoprene; however, Neoprene was observed to harden and crack when exposed to the mixtures over an extended period of time.

Highlights of the R12 experimental runs:

- Fifty-six experimental runs were made yielding 112 data points.
- All runs had an energy balance error within +2% to -7%.
- The average refrigerant-side resistance for the two evaporators was approximately 23%.
- The measured pressure drop through the low pressure side of the evaporator module was 4.48 kPa (0.65 psi).

Highlights of the R22 experimental runs:

- Thirty-nine experimental runs were made yielding 78 data points.
- All runs had an energy balance error within +/- 4%.
- The average refrigerant-side resistance for the two evaporators was approximately 20%.
- The measured pressure drop through the low pressure side of the evaporator module was 3.37 kPa (0.49 psi).

Highlights of the R22/R123 experimental runs:

- Sixty-five experimental runs were made yielding 130 data points.
- All runs had an energy balance error within +5% to -8%.
- The average refrigerant-side resistance for the freezer and fresh-food evaporators was 44.5% and 29.3% respectively.
- The measured pressure drop through the low pressure side of the evaporator module was 3.01 kPa (0.44 psi).

Highlights of the R22/R141b experimental runs:

- Sixty-two experimental runs were made yielding 124 data points.
- All runs had an energy balance error within +/- 7%.
- The average refrigerant-side resistance for the freezer and fresh-food evaporators was 44.1% and 28.4% respectively.

- The measured pressure drop through the low pressure side of the evaporator module was 3.94 kPa (0.57 psi).

The energy balance error was calculated by comparing the heat-leak from the surroundings into the refrigerator cabinet plus the load supplied to each compartment with the calculated energy absorbed by the refrigerant. A majority the experimental data points were found to be in the wavy regime as plotted on a Scott flow map. The R22/R123 had the lowest average measured pressure drop of the four fluids tested.

From the experimental data, the mixture heat transfer coefficients were determined. The heat transfer coefficient data were fit to an appropriate correlation. The heat transfer coefficients of the mixtures *were 50% less than those of R12* in the mass flux range of 25 - 45 kg/m^2-s. For mass fluxes above 45 kg/m^2-s, the heat transfer coefficients of the mixtures rose rapidly, and approached the R12 values.

8.4 Optimization Results for R12 and R134a Systems

This is a summary of the significant findings for the pure refrigerant system configuration optimization study. Eight evaporator module configurations for two pure refrigerants, R12 and R134a, were optimized. The evaporator module configurations were: evaporator only, evaporator operating with superheat, evaporator with superheat and a suction-line heat exchanger, and evaporator with superheat, a suction-line heat exchanger and high-efficiency evaporator fans. Both single and dual evaporator configurations were examined. The significant findings for the R12 and R134a systems were:

- A system with a suction-line heat exchanger operating with *no* superheat has *no thermodynamic advantage* over a system with *no* suction-line heat exchanger *and* no system superheat.
- Dual-evaporator systems use less energy and have lower life-cycle cost than equivalent single-evaporator systems.
- Superheat present in the exit of a *single*-evaporator system *without* a suction-line heat exchanger *does not* lower life-cycle cost.
- Superheat present in the exit of *dual*-evaporator system *without* a suction-line heat exchanger *can* lower life-cycle cost.

- The presence of superheat *and* a suction-line heat exchanger *always* lowers life-cycle cost.
- Optimized R134a systems with a suction-line heat exchanger *and* superheat have lower life-cycle costs than equivalent optimized R12 systems.
- The addition of high-efficiency evaporator fans *lowers* the life-cycle cost for single-evaporator systems; however, the addition of the high-efficiency fans to dual-evaporator systems *does not* lower life-cycle cost.
- The average refrigerant-side resistance for the pure refrigerant optimized system configurations was 26.5%. For the dual evaporator systems, the average freezer and fresh-food evaporator refrigerant-side resistance was 29.3% and 22.4% respectively. There was little difference between the refrigerant heat transfer coefficients for R12 and R134a.
- The best *optimized* pure-refrigerant system configuration from the perspective of the *consumer* is the R134a *dual*-evaporator system with a suction-line heat exchanger and system superheat. The life-cycle cost is 4% less, the manufacturing cost is 3% greater, and the energy consumption is 9% less than that of a *modeled* base-case R12 system. The *total* evaporator area of the R134a system is *only* 1.9% greater than the area of the base-case system.
- The optimization indicated that the system which would be most advantageous for the *manufacturer* to build would be the R134a *single*-evaporator system with a suction-line heat exchanger and system superheat. Consequently this is the same system configuration and refrigerant used in current systems. The manufacturers would avoid systems with added components, manufacturing complexity and cost, such as the dual-evaporator or high-efficiency evaporator fan systems. For this system, the life-cycle cost is 2.5% less, the manufacturing cost is 1% greater, and the energy consumption is 5% less than that of the *modeled* base-case R12 system. The evaporator area of this system is 18.8% larger than that of the base-case system.

8.5 Optimization Results for R22/R123 and R22/R141b Systems

This is a summary of the significant findings for the mixture system configuration optimization study. Five evaporator module configurations for two mixtures, R22/R123 and

R22/R141b, were optimized. The evaporator module configurations were: evaporators only, evaporators with a low-temperature intercooler only, evaporators with a high-temperature intercooler only, evaporators with both high and low-temperature intercoolers, and evaporators with high and low-temperature intercoolers and high-efficiency evaporator fans. Only dual-evaporator system configurations were considered. The significant findings for the 65% R22 / 35% R123 and 80% R22 / 20% R141b systems were:

- System superheat *does not* lower life-cycle cost.
- Intercooling *always* lowers life-cycle cost.
- Maximum intercooling benefit (achieving a lower evaporating temperature with no decrease in evaporating pressure) is achieved when intercooling is implemented at the steepest segments of the mixture temperature glide.
- An optimized system with a high-temperature intercooler has a *lower* life-cycle cost and performs *better* than an optimized system with a low-temperature intercooler (for the same mixture).
- The addition of high-efficiency evaporator fans *does not* lower life-cycle cost.
- Optimized R22/R123 systems have lower life-cycle costs and perform better than equivalent R22/R141b systems.
- An optimized R22/R123 system with high and low-temperature intercoolers has a slightly lower life-cycle cost and performs marginally better than an optimized R22/R123 system with a high-temperature intercooler.
- An optimized R22/R141b system with high and low-temperature intercoolers has the same life-cycle cost and performs no better than an optimized R22/R141b system with a high-temperature intercooler.
- The average refrigerant-side resistance for the optimized R22/R123 and R22/R141b system configurations were 45.9% and 63.9% respectively. The average freezer and fresh-food evaporator refrigerant-side resistance for the R22/R123 and R22/R141b systems were 46.7%/45.1% and 70.1%/57.6% respectively. There was a significant difference between the refrigerant heat transfer coefficients for the R22/R123 and R22/R141b mixtures. The R22/R123

heat transfer coefficients were greater than the R22/R141b coefficients for similar operating conditions.

- The best optimized mixture system configuration from the perspective of the *consumer* is the R22/R123 system with both high and low-temperature intercoolers. The life-cycle cost is 4.5% less, the manufacturing cost is 4% greater, and the energy consumption is 10.5% less than that of the *modeled* base-case R12 system. The total evaporator area of the R22/R123 system is 46% greater than the area of the base-case system.

- The *manufacturer* may want to investigate the R22/R123 system with a high-temperature intercooler only. The life-cycle cost is 3.75% less, the manufacturing cost is 4% greater, and the energy consumption is 9% less than that of the *modeled* base-case R12 system. The total evaporator area of this system is 49% larger than that of the base-case system. The manufacturers would favor this system because it performs well with only one intercooler in the system.

8.6 Optimal System

This section compares the best optimal mixture and pure-refrigerant system configurations which were studied. These results are only valid for the pure refrigerants, R12 and R134a, and the mixtures, 65% R22 / 35% R123 and 80% R22 / 20% R141b, subject to the fixed variable selection and the assumptions of the optimization model.

The optimized *mixture* system configuration with the lowest life-cycle cost is the R22/R123 (dual-evaporator) system with high and low-temperature intercoolers. The optimized *pure* refrigerant system configuration with the lowest life-cycle cost is the R134a dual-evaporator system with a suction-line heat exchanger and system superheat. The R22/R123 system's life-cycle cost is 0.5% less, the manufacturing cost is 0.7% greater, and the energy consumption is 1.8% less than that of the R134a system. However, the total evaporator area of the R22/R123 system is 43.5% larger than that of the R134a system.

A better comparison for the R22/R123 system would be the optimized R134a single-evaporator system with a suction-line heat exchanger and superheat, the same component configuration as the current manufactured systems. The R22/R123 system's life-cycle cost is 2.1% less, the manufacturing cost is 3.0% greater, and the energy consumption is 5.7% less than that of this R134a system. The total evaporator area of the R22/R123 system is 23% larger than that of the R134a system.

For all mixture and pure-refrigerant system configurations, the cost breakdown was fairly consistent. Forty percent of the life-cycle cost was determined to be the refrigerator cost and the other 60% was the power cost.

8.7 Variation of Selected Mixture Properties

This section summarizes the affects on the optimal R22/R123 system (section 8.6) design by changing one important mixture variable, concentration, and by changing two important mixture properties, the interaction parameter and heat transfer coefficient. The changes in the concentration and the interaction parameter were small. The heat transfer coefficient was changed drastically by substituting an R12 correlation into the mixture's optimization model.

- The R22 concentration was changed from 65% to 61.5%. The small composition change had negligible effect on the system's life-cycle cost.
- The interaction parameter was changed from 0.003 to 0.007. The small change in the interaction parameter had negligible effect on the system's life-cycle cost.
- The R22/R123 heat transfer coefficient correlation was substituted with an R12 correlation. The life-cycle cost is 1.75% less, the manufacturing cost is 1% less, and the energy consumption is 2.5% less than that of the unmodified system. There is a 17% reduction in the total evaporator area for the modified system. The refrigerant-side resistance fell approximately 19% to 27.5% for the modified mixture system.

8.8 Future Work

In this last section, suggestions for future work are made. Hopefully the results presented in this study will help answer many of the questions concerning the application of refrigerant mixtures to domestic refrigerators and help guide future work done in this area.

- Valid mixture heat transfer data taken in this experiment. When horizontal-tube heat transfer coefficient data becomes available for mixtures, a comparison between the horizontal-tube data and the evaporator energy balance data from this experiment can be performed to assess the effect of evaporator tube bends and non-uniform air-side heat flux.
- Build the optimum mixture system as determined from this study and test in the laboratory.

- Perform a *full* cycle steady-state mixture optimization that includes an improved compressor model and the condenser.
- Investigate a mixture or pure-refrigerant system configuration that would use a natural convection fresh-food evaporator.
- Investigate a two-capillary tube pure-refrigerant system configuration that would use a single evaporator to serve both compartments on an alternating duty cycle with each capillary tube. Further research would need to be done on the capillary tube switching system. Preliminary results from this study indicated that these systems may perform better than the best mixture system configuration.
- Investigate the area of controls for mixture systems. Methods for accurately sensing superheat must be developed. The temperature glide of the mixture makes the traditional method of sensing superheat by temperature less reliable because the temperature glide masks the onset of superheat. Variable speed fans and compressors could be utilized to enhance system performance. In addition, adaptive defrost heater scheduling could further reduce energy consumption. These types of adaptive control routines could be easily controlled using microprocessor technology. For mixtures, the most important system control would need to handle load variations in both compartments as ambient conditions and door opening schedules change.
- Include industry retooling costs in the life-cycle cost equation for the optimization.
- Determine the effect of oil on the thermodynamic properties for mixtures and include in the optimization.
- Expand optimization to include concentration and refrigerant components as independent variables. The scope of this optimization would be limited to the available interaction parameter and heat transfer coefficient experimental data for each component pair and concentration.
- Develop a *transient* mixture optimization model which would include the effect of frost formation and the use of defrost heaters. Kruse[2] reported a 10% energy savings in pull-down tests for mixture of R22/R142b relative to R12.

8.9 References

---

[1] Lorenz, A. and K. Meutzner, "On Application of Non-Azeotropic Two-Component Refrigerants in Domestic Refrigerators and Home Freezers", XIV International Congress of Refrigeration, Paper B2.42, 1975 Moscow.

[2] Kruse, H., "Non-Azeotropic Refrigerant Mixture R22/R142b for a Two Temperature Refrigerator as Replacement for R12", presentation at USEPA Contractors Meeting, Washington, October, 1989.

APPENDIX A: AIR AND REFRIGERANT PHYSICAL PROPERTIES

This appendix covers all the curve fits and correlations used to obtain the physical properties of air and the refrigerants. The refrigerant properties were obtained for R12, R22, R134a, and the mixtures 65% R22/35% R123 and 80% R22/20% R141b. The air and pure refrigerants correlations are listed first followed by the mixture property correlations. The accuracy of the curve fits and correlations are discussed in the last section. Following the last section, there are sample physical property subroutines. The physical properties were required to calculate the non-dimensional numbers used to describe the flow and form the basis of the heat transfer coefficient correlations developed in Chapters 4 and 5.

A.1 Air

Density and specific heat were fit from air table[1] data over the temperature range of 250K to 300K.

$$\rho = -4.666T + 2561.188 \tag{A.1}$$

$$c_p = (0.001/50.0)T + 1.001 \tag{A.2}$$

A.2 R12, R22 and R134a

All R12 and R22 properties, except surface tension, were curve fit to ASHRAE Handbook[2] data over the temperature range of 240K to 310K. The surface tension relations and all the R134a properties were taken from a paper by Jung and Radermacher.[3] The thermal conductivity equations are presented first, followed by the viscosity and surface tension equations.

R12:

$$k_l = 0.001(177.38 - 0.36226T) \tag{A.3}$$

$$k_v = 0.001\left(-1.2518 + 1.9030e^{-2}T + 5.8929e^{-5}T^2\right) \tag{A.4}$$

$$\mu_l = 0.001\left(5523.6 - 47.010T + 0.14180T^2 - 1.4697e^{-4}T^3\right) \tag{A.5}$$

$$\mu_v = 0.001\left(7.3042 - 1.6369e^{-2}T + 1.1786e^{-4}T^2\right) \tag{A.6}$$

$$\sigma = 56.52(1 - T_r)^{1.27} \tag{A.7}$$

R22:

$$k_l = 0.001(236.38 - 0.49857T) \tag{A.8}$$

$$k_v = 0.001(-7.1417 + 6.0833e^{-2}T) \tag{A.9}$$

$$\mu_l = 0.001(3461.6 - 28.514T + 8.5226e^{-2}T^2 - 8.8131e^{-5}T^3) \tag{A.10}$$

$$\mu_v = 0.001(11.554 - 4.9214e^{-2}T + 1.8571e^{-4}T^2) \tag{A.11}$$

$$\sigma = 61.23(1 - T_r)^{1.23} \tag{A.12}$$

R134a:

$$k_l = 0.258258 - 0.73235e^{-3}T + 0.46428e^{-6}T^2 \tag{A.13}$$

k_v = see Equations A.20 to A.27

$$\mu_l = 10\text{^}(-5.82061 + 738.6060 / T + 0.138540e^{-1}T - 0.164426e^{-4}T^2) \tag{A.14}$$

μ_v = see Equations A.31 to A.33

$$\sigma = 60.80(1 - T_r)^{1.26} \tag{A.15}$$

A.3 R123, R141b, R22/R123 and R22/R141b

The mixture properties were calculated using relations found in the Jung and Radermacher[4] paper with the exception of the liquid viscosities of R123 and R141b which were curve fit from data found in a paper by Shankland.[5]

R123:

k_l = see Equation A.18

$$\mu_l = 4.4872 - 2.2778e^{-2}T + 3.0696e^{-5}T^2 \quad \text{(A.16)}$$

R141b:

k_l = see Equation A.18

$$\mu_l = 5.1815 - 2.6093e^{-2}T + 3.4663e^{-5}T^2 \quad \text{(A.17)}$$

R22/R123:

k_l = see Equation A.19

k_v = see Equations A.20 to A.27

μ_l = see Equations A.28 to A.30

μ_v = see Equations A.31 to A.33

σ = see Equations A.34 and A.35

R22/R141b:

k_l = see Equation A.19

k_v =see Equations A.20 to A.27

μ_l = see Equations A.28 to A.30

μ_v = see Equations A.31 to A.33

σ = see Equations A.34 and A.35

A.4 Liquid Thermal Conductivity Model

Pure:

The liquid thermal conductivity is the most important transport property for two-phase heat transfer work. Intermolecular forces are important because the thermal conductivity of the liquid depends on the frequency of the molecular collisions. Jung and Radermacher modified a correlation by Yata *et al.*[6] based on Gray's[7] relaxation transport theory.

$$k_l = \frac{\left[0.620967 - 1.03607\left(\frac{T}{T_{nbp}}\right) + 0.65212\left(\frac{T}{T_{nbp}}\right)^2 - 0.15226\left(\frac{T}{T_{nbp}}\right)^3\right]}{\left[v_l^{2/3}\left(\frac{MW}{T}\right)^{0.5}\left(\frac{1}{v_{l_r}}\right)^2\right]} \qquad \text{(A.18)}$$

Mixtures:

The mixture correlation was developed by Filippov.[8] The components should be chosen such that the value of k_{l1} is less than k_{l2}.

$$k_l = w_1 k_{l1} + w_2 k_{l2} - 0.72 w_1 w_2 (k_{l2} - k_{l1}) \qquad \text{(A.19)}$$

A.5 Vapor Thermal Conductivity Model for Pure Refrigerants /Mixtures

Vapor thermal conductivity was determined from the method of Stiel and Thodos[9] which is based on Eucken and modified Eucken methods.[10]

$$k_v = \frac{\left[k_v^* \lambda z_c^{\,5} + 14.0e^{-8}\left(e^{-0.535\rho_r} - 1.0\right)\right]}{\left[\lambda z_c^{\,5}\right]} \quad \text{for } \rho_r < 0.5 \qquad \text{(A.20)}$$

$$k_v = \frac{\left[k_v^* \lambda z_c^{\,5} + 13.1e^{-8}\left(e^{0.67\rho_r} - 1.069\right)\right]}{\left[\lambda z_c^{\,5}\right]} \quad \text{for } 0.5 < \rho_r \le 2.0 \qquad \text{(A.21)}$$

$$k_v = \frac{\left[k_v^* \lambda z_c^{\,5} + 2.976e^{-8}\left(e^{1.155\rho_r} + 1.069\right)\right]}{\left[\lambda z_c^{\,5}\right]} \quad \text{for } 2.0 < \rho_r \le 2.8 \qquad \text{(A.22)}$$

where:

$$k_v^* = \left(\frac{\mu_v^*}{1000}\right)\left(1.235c_v + \frac{1.9R}{MW}\right) \tag{A.23}$$

$$\lambda = T_c^{1/6} MW^{1/2} \left(\frac{p_c}{101.325}\right)^{-2/3} \tag{A.24}$$

$$z_c = \frac{1000 MW p_c}{\rho_c R T_c} \tag{A.25}$$

$$\mu_v^* = \frac{\left[(0.5124T_r - 0.0517)^{0.82} z_c^{0.81}\right]}{\xi} \tag{A.26}$$

$$\xi = T_c^{1/6} MW^{-1/2} \left(\frac{p_c}{1000}\right)^{-2/3} \tag{A.27}$$

A.6 Liquid Viscosity Mixture Model

The Grunberg and Nissan[11] liquid viscosity mixture correlation was used.

$$\mu_l = \exp(XM \ln \mu_1 + (1 - XM) \ln \mu_2 + \delta\mu) \tag{A.28}$$

where:

$$\delta\mu = 0.85 D_{exc} - 0.085 \tag{A.29}$$

$$D_{exc} = \rho_{12}\left(\frac{XM}{\rho_1} + \frac{(1 - XM)}{\rho_2}\right) - 1.0 \tag{A.30}$$

A.7 Vapor Viscosity Model for Pure Refrigerants and Mixtures

The law of corresponding states is utilized to predict the viscosity of a vapor. Stiel and Thodos[12] developed a correlation based on an extensive dimensional analysis.

$$\mu_v = \frac{\left[\mu_v^* \xi + 0.761931 \rho_r^{1.111}\right]}{\xi} \quad \text{for } \rho_r < 0.1 \tag{A.31}$$

$$\mu_v = \frac{\left[\mu_v^* \xi + 2.79283(9.045\rho_r + 0.63)^{1.739}\right]}{\xi} \quad \text{for } 0.1 < \rho_r \leq 0.9 \qquad \text{(A.32)}$$

$$\mu_v = \frac{\left[\mu_v^* \xi + 4.6*10\text{^}\left(3.0 - 10^{(0.6439 - 0.1005\rho_r)}\right)\right]}{\xi} \quad \text{for } 0.9 < \rho_r \leq 2.6 \qquad \text{(A.33)}$$

where:

μ_v^* = see Equation A.26

ξ = see Equation A.27

z_c = see Equation A.25

A.8 Surface Tension Model for Mixtures

Surface tension is very important for heat transfer processes which may have nucleate boiling present. Most estimation methods for surface tension are empirical and based on the law of corresponding states. Brock and Bird's predictive method was used.[13]

$$\sigma = \left(\frac{p_c}{100}\right)^{2/3} T_c^{1/3} \psi (1.0 - T_r)^{11/9} \qquad \text{(A.34)}$$

where:

$$\psi = 0.1196\left[1.0 + \frac{T_{nbp_r} \ln\left(\frac{p_c}{101.325}\right)}{\left(1.0 - T_{nbp_r}\right)}\right] - 0.279 \qquad \text{(A.35)}$$

A.9 Accuracy of Property Correlations

Of the physical properties, the two most important for heat transfer work are the liquid thermal conductivity and surface tension. Of the deviation information available for the correlations, the deviations are largest for these two physical properties.

A.9.1 Liquid Thermal Conductivity

k_l : pure: mean deviation ± 3.7%, maximum deviation ± 10.3%[14]

k_l : mixtures: mean deviation for fluid mixtures other than refrigerant mixtures ± 5%[15]

A.9.2 Vapor Thermal Conductivity

k_v^* : pure: mean deviation ± 2.66%, maximum deviation ± 8.74%[16]

k_v : pure: "good agreement"[17]

k_v : mixtures: no measured data available[18]

A.9.3 Liquid Viscosity

μ_l : mixtures: mean deviation ± 2%[19]

A.9.4 Vapor Viscosity

μ_v^*: pure: mean deviation ± 1.62%, maximum deviation ± 4.97%[20]

μ_v^*: mixtures: mean deviation ± 1.62%, maximum deviation ± 4.97%[21]

μ_v^*: pure: mean deviation ± 0.3%, maximum deviation ± 1.4%[22]

A.9.5 Surface Tension

σ : pure: mean deviation ± 2.23%, maximum deviation ± 6.94%[23]

σ : mixtures: mean deviation ± 15%[24]

A.10 Subroutine Listings

Listed below are two sample property subroutines. The first is for pure R12, and the second is for the mixture 65% R22/35% R123. It is relatively simple to change the internal calls to switch the property calculations to different pure refrigerants or refrigerant mixtures. Following the two subroutine listings are the relevant property functions.

A.10.1 R12 Property Subroutine

```
      subroutine props(xq,t,mwab,pc)
c
      real coeff(9,22),crit(5,22),a(3,2),b(3,2)
```

```
      common /esdata/ coeff,crit
      common /rdata1/ a,b,ffo,ff1
c
      common/props/cplmix,cpvmix,klmix,kvmix,pholmix,phovmix,
     1          vislmix,visvmix,xa,stmix
      real klmix,kvmix
c
      real kl12,kv12,kl22,kv22,kl,klc,kv
      real mwa,mwb,mwab
      real kl1,kl2,k1,k2
c for r12
      ir1 = 2
      ir2 = ir1
      f = 0.0
      xma = 1.0
      call bconst (ir1,ir2,f,0.0)
      mwa=crit(1,ir1)
      mwb=crit(1,ir2)
      xa=1.0
      mwab=mwa
      tc = 385.0
      call critx(xa,tc,pc,vc)

      cplmix = cpl12(t)
      klmix = kl12(t)
      pholmix = phol12(t)
      vislmix = vl12(t)
      stmix = st12(t,tc)
      cpvmix = cpv12(t)
      kvmix = kv12(t)
      phovmix = phov12(t)
      visvmix = visv12(t)
      return
      end
```

A.10.2 65% R22/35% R123 Property Subroutine

```
      subroutine props(xq,t,mwab)
c
      real coeff(9,22),crit(5,22),a(3,2),b(3,2)
      common /esdata/ coeff,crit
      common /rdata1/ a,b,ffo,ff1
c
      common/props/cplmix,cpvmix,klmix,kvmix,pholmix,phovmix,
     1          vislmix,visvmix,xa,stmix
      real klmix,kvmix
c
      real kl12,kv12,kl22,kv22,kl,klc,kv
      real mwa,mwb,mwab
      real kl1,kl2,k1,k2

c  data for r22
      kl1 = kl22(t)
      phol1 = phol22(t)
      visl1 = visl22(t)
```

```
c  data for r123
        ir1 = 13
        ir2 = ir1
        f = 0.0
        xma = 1.0
        call bconst (ir1,ir2,f,0.0)
        mwa=crit(1,ir1)
        mwb=crit(1,ir2)
        xa=1.0
        mwab=mwa
        call bublp(101.325,xa,xv,tnbp,vl,vv,.true.,lcrit)
        call tqin(t,xq,xa,p,h,s,xl,xv,vl,vv)
        h = h/mwab
        tc = 456.9
        call critx(xa,tc,pc,vc)
        kl2 = klc(vl,mwab,t,vc,tnbp)
        phol2 = phol(h,p,xa,mwab)
        visl2 = visl123(t)

c  data for r22/r123 mixture
        ir1 = 6
        ir2 = 13
        f=0.003
        xma = .65
        call bconst (ir1,ir2,f,0.0)
        mwa=crit(1,ir1)
        mwb=crit(1,ir2)
        xa=xma/mwa/(xma/mwa+(1.0-xma)/mwb)
        mwab=xa*mwa+(1.0-xa)*mwb
        call bublp(101.325,xa,xv,tnbp,vl,vv,.true.,lcrit)
        call tqin(t,xq,xa,p,h,s,xl,xv,vl,vv)
        h = h/mwab
        tc = 399.96
        call critx(xa,tc,pc,vc)
        cplmix = cpl(t,vl,xa,mwab)
        cpvmix = cpv(t,vv,xa,mwab)
c  cal liquid thermal conductivity of mixture
        if (kl1.gt.kl2) then
                k1 = kl1
                k2 = kl2
                w1 = xma
                w2 = 1.0-xma
        else
                k1 = kl2
                k2 = kl1
                w1 = 1-xma
                w2 = xma
        endif
        klmix = w1*k1 + w2*k2 - 0.72*w1*w2*(k1-k2)
        kvmix = kv(cvv(t,vv,xa,mwab),t,tc,pc,1.0/vc,1.0/vv,mwab)
        pholmix = phol(h,p,xa,mwab)
        phovmix = phov(h,p,xa,mwab)
        stmix = surten(tnbp,t,tc,pc)
c  cal liquid viscosity of mixture
        d = pholmix*(xa/phol1 + (1.0-xa)/phol2) - 1.0
        delmu = 0.85*d - 0.085
```

```
      vislmix = exp(xa*log(visl1) + (1.0-xa)*log(visl2) + delmu)
      visvmix = visv(t,tc,pc,1.0/vc,1.0/vv,mwab)
      return
      end
```

A.10.3 Property Functions

```
c ****************************************************************
      function phoair(t)
c
c  Input:        t - temperature in K
c  Output:       phoair - density of air in g/m^3
c
c  from incropera air tables p767 for 250 to 300k in g/m3
c
      phoair = -4.666*t+2561.188
      return
      end
c ****************************************************************
      function cpair(t)
c
c  Input:        t - temperature in K
c  Output:       cpair - air specfic heat in j/g-k
c
c  from incropera air table p767 for 250 to 300k in j/gk
      cpair = (.001/50)*t+1.001
      return
      end
c ****************************************************************
      function cpl12(t)
c  liquid !!
c  from ashrae hb p17.5 for r12 240 to 310k in j/(g k)
      cpl12 = 1.2564-3.8893e-3*t+9.8810e-6*t**2
      return
      end
c ****************************************************************
      function cpl22(t)
c  liquid !!
c  from ashrae hb p17.15 for r22 240 to 310k in j/(g k)
      cpl22 = 2.6033-1.3220e-2*t+2.9167e-5*t**2
      return
      end
c ****************************************************************
      function cpl(t,vl,xa,mwab)
c  liquid !!
c  input:
c       t temperature in K
c       vl liquid molar volume m^3/kmol
c       xa mole fraction of 1st comp
c       mwab molecular weight of mix in g/mol
c  output:
c       cpl liquid specific heat of mix in j/(g-k)
c
      real coeff(9,22),crit(5,22),a(3,2),b(3,2)
      common /esdata/ coeff,crit
```

```
      common /rdata1/ a,b,ffo,ff1
c
      real mwab
c
      call hcvcps(5,t,vl,xa,h,cvl,cpl,vs)
      cpl = cpl/mwab
      return
      end
c ****************************************************************
      real function kl12(t)
c  liquid !!

c  from ashrae hb p17.5 for r12 240 to 310k in mw/(m k)
      temp = 177.38-.36226*t
c  convert to w/(m k)
      kl12 = temp/1000.0
      return
      end
c ****************************************************************
      real function kl22(t)
c  liquid !!
c  from ashrae hb p17.55 for r22 240 to 310k in mw/(m k)
      temp = 236.38-.49857*t
c  convert to w/(m k)
      kl22 = temp/1000.0
      return
      end
c ****************************************************************
      real function kl(a,b,c,t)
c
c  Input:
c      a-d      coefficients for different refrigerants
c      t - temperature in K
c  Output:
c      kl - liquid thermal conductivity in W/m-K
c
      kl = a + b*t + c*t**2
      return
      end
c ****************************************************************
      real function klc(v,mwab,t,vc,tb)
c
c  Input:
c      v - liquid molar volume in m^3/kmol
c      mwab - molecular weight in kg/kmol
c      t - temperature in K
c      vc - molar volume at crtical point in m^3/kmol
c      tb - NBP in K
c  Output:
c      klc - liquid thermal conductivity in W/m-K
c
      real mwab
      klc = (0.620967-1.03607*(t/tb)+0.65212*(t/tb)**2-
     1    0.15226*(t/tb)**3)/(v**0.6667*(mwab/t)**0.5*(vc/v)**2)
      return
      end
c ****************************************************************
```

```
      function phol12(t)
c  liquid !!
c  from ashrae hb p17.5 for r12 238 to 307k in g/m^3
      phol12 = 1.788e6+367.6*t-6.6043*t**2
      return
      end
c ***************************************************************
      function phol22(t)
c  liquid !!
c  from ashrae hb p17.15 for r22 239 to 307k in g/m^3
      phol22 = 1.58e6+1249.9*t-8.5761*t**2
      return
      end
c ***************************************************************
      function phol(h,p,xa,mwab)
c  liquid !!
c  input:
c      h enthaply in j/g
c      p pressure in kpa
c      xa mole fraction of 1st comp
c      mwab molecular weight of mix in g/mol
c  output:
c      phol liquid density in g/m^3
c
      real coeff(9,22),crit(5,22),a(3,2),b(3,2)
      common /esdata/ coeff,crit
      common /rdata1/ a,b,ffo,ff1
c
      real mwab
c
      call hpin(h*mwab,p,xa,t,xq,xl,xv,vl,vv,hl,hv)
      phol = 1000.0*mwab/vl
      return
      end
c ***************************************************************
      function vl12(t)
c  liquid !!
c  from ashrae hb p17.5 for r12 240 to 310k in upa s
      temp = 5523.6-47.010*t+.14180*t**2-1.4697e-4*t**3
c  convert to g/(m-s)
      vl12 = temp/1e3
      return
      end
c ***************************************************************
      function visl22(t)
c  liquid !!
c  from ashrae hb p17.55 for r22 240 to 310k in upa s
      temp = 3461.6-28.514*t+8.5226e-2*t**2-8.8131e-5*t**3
c  convert to g/(m-s)
      visl22 = temp/1e3
      return
      end
c ***************************************************************
      function visl141b(t)
c  liquid !!
c  from shankland 1990 IJR paper fig 3 in g/(m-s)
      visl141b = 5.1815 - 2.6093e-2*t + 3.4663e-5*t**2
```

```
      return
      end
c ***************************************************************
      function visl123(t)
c  liquid !!
c  from shankland 1990 IJR paper fig 3 in g/(m-s)
      visl123 = 4.4872 - 2.2778e-2*t + 3.0696e-5*t**2
      return
      end
c ***************************************************************
      function visl(a,b,c,d,t)
c
c  Input:
c       a-d     coefficients for different refrigerants
c       t       temperature in K
c  Output:
c       visl    liquid viscosity in g/(m-s)
c
      if (d.eq.0.0) then
            visl = exp(a + b/t + c*t)
      else
            visl = 10**(a + b/t + c*t + d*t**2)
      endif
      return
      end
c ***************************************************************
      function vislc(t,tf,tb,n)
c
c  Input:
c       t       temperature in K
c       tf      freezing point in K
c       tb      NBP in K
c       n       # of carbon atoms
c  Output:
c       vislc   liquid viscosity in g/(m-s)
c
      real n
      a = 1.0/(32.0-4.0*tf*(1.0-(tf/tb)**0.5))
      b = 0.01*(8.7-0.038*(tb-tf))
      vislc = 1.05*exp(a*(t-tf)*n**0.5) +
     1        0.01*exp(b*(tb+20.0-t)*n**0.5)
      return
      end
c ***************************************************************
      function surten(tnbp,t,tc,pc)
c
c  Input:
c       tnbp    normal boiling point in K
c       t       temperature in K
c       tc      critical temperature in K
c       pc      critical pressure in kPa
c  Output:
c       surten  surface tension in mN/m or dynes/cm
c
      tr = t/tc
      trnbp = tnbp/tc
      pcbar = pc/100.0
```

```
      q = 0.1196*(1.0+trnbp*log(pcbar/1.01325)/(1.0-trnbp))-0.279
      surten = pcbar**(2.0/3.0)*tc**(1.0/3.0)*q*(1.0-tr)**(11.0/9.0)
      return
      end
c ***************************************************************
      function st12(t,tc)
c  Input:
c       t       temperature in K
c       tc      critical temperature in K
c  Output:
c       st12    surface tension in mN/m or dynes/cm
c
      st12 = 56.52*(1-t/tc)**1.27
      return
      end
c ***************************************************************
      function st22(t,tc)
c  Input:
c       t       temperature in K
c       tc      critical temperature in K
c  Output:
c       st22    surface tension in mN/m or dynes/cm
c
      st22 = 61.23*(1-t/tc)**1.23
      return
      end
c ***************************************************************
      function st123(t,tc)
c  Input:
c       t       temperature in K
c       tc      critical temperature in K
c  Output:
c       st123   surface tension in mN/m or dynes/cm
c
      st123 = 57.5*(1-t/tc)**1.26
      return
      end
c ***************************************************************
      function cpv12(t)
c  vapor !!
c  from ashrae hb p17.5 for r12 240 to 310k in j/(g k)
      cpv12 = -5.6531+6.8821e-2*t-2.5929e-4*t**2+3.3586e-7*t**3
      return
      end
c ***************************************************************
      function cpv22(t)
c  vapor !!
c  from ashrae hb p17.15 for r22 240 to 310k in j/(g k)
      cpv22 = -7.2483+9.4280e-2*t-3.8333e-4*t**2+5.3030e-7*t**3
      return
      end
c ***************************************************************
      function cpv(t,vv,xa,mwab)
c  vapor !!
c  input:
c       t temperature in K
c       vv molar volume in m^3/kmol
```

```
c       xa mole fraction of 1st comp
c       mwab molecular weight of mix in g/mol
c  output:
c       cpv vapor specific heat of mix in j/g-k
c
        real coeff(9,22),crit(5,22),a(3,2),b(3,2)
        common /esdata/ coeff,crit
        common /rdata1/ a,b,ffo,ff1
c
        real mwab
c
        call hcvcps(5,t,vv,xa,h,cvv,cpv,vs)
        cpv = cpv/mwab
        return
        end
c ***************************************************************
        function cvv(t,vv,xa,mwab)
c  vapor !!
c  input:
c       t temperature in K
c       vv vapor molar volume in m^3/kmol
c       xa mole fraction of 1st comp
c       mwab molecular weight of mix in g/mol
c  output:
c       cvv vapor specific heat (at constant vol) in j/g-k
c
        real coeff(9,22),crit(5,22),a(3,2),b(3,2)
        common /esdata/ coeff,crit
        common /rdata1/ a,b,ffo,ff1
c
        real mwab
c
        call hcvcps(5,t,vv,xa,h,cvv,cpv,vs)
        cvv = cvv/mwab
        return
        end
c ***************************************************************
        real function kv12(t)
c  vapor !!

c  from ashrae hb p17.5 for r12 240 to 310k in mw/(m k)
        temp = -1.2518+1.9030e-2*t+5.8929e-5*t**2
c  convert to w/(m k)
        kv12 = temp/1000.0
        return
        end
c ***************************************************************
        real function kv22(t)
c  vapor !!

c  from ashrae hb p17.55 for r22 240 to 310k in mw/(m k)
        temp = -7.1417+6.0833e-2*t
c  convert to w/(m k)
        kv22 = temp/1000.0
        return
        end
c ***************************************************************
```

```
      real function kv141b(t)
c  vapor !!

c  from shankland 1990 IJR paper fig 1 in w/(m k)
      kv141b = 74.644e-6*t - 12.20313e-3
      return
      end
c ****************************************************************
      real function kv123(t)
c  vapor !!

c  from shankland 1990 IJR paper fig 1 in w/(m k)
      kv123 = 89.928e-6*t - 15.47822e-3
      return
      end
c ****************************************************************
      real function kv(cvv,t,tc,pc,phoc,pho,mwab)
c  vapor !!
c
c  Input:
c      cvv      specific heat (const vol) in j/g-K
c      t        temperature in K
c      tc       critical temperature in K
c      pc       critical pressure in kPa
c      phoc     critical density in kmol/m^3
c      pho      vapor density in kmol/m^3
c      mwab     molecular weight in kg/kmol
c  Output:
c      kv       vapor thermal conductivity in w/(m-k)
c
      real kvs,lamda,mwab
      r = 8.314
      xi = tc**(1.0/6.0)*mwab**(-1.0/2.0)*(pc/1000.0)**(-2.0/3.0)
      zc = pc/(phoc*r*tc)
      tr = t/tc
      viss = ((0.5124*tr - 0.0517)**(0.82)*zc**(-0.81))/xi
      c1 = 1.235
      c2 = 1.9
      kvs = (1000.0*viss/1e6)*(c1*cvv+c2*r/mwab)
      phor = pho/phoc
      lamda = tc**(1.0/6.0)*mwab**(1.0/2.0)*(pc/101.325)**(-2.0/3.0)
      if (phor.le.0.5) then
            kv = (kvs*lamda*zc**5+14.0e-8*(exp(-0.535*phor)-
     1            1.0))/(lamda*zc**5)
      else if ((phor.gt.0.5).and.(phor.le.2.0)) then
            kv = (kvs*lamda*zc**5+13.1e-8*(exp(0.67*phor)-
     1            1.069))/(lamda*zc**5)
      else if ((phor.gt.2.0).and.(phor.le.2.8)) then
            kv = (kvs*lamda*zc**5+2.976e-8*(exp(1.155*phor)+
     1            1.069))/(lamda*zc**5)
      else
            write(*,*) 'phor > 2.8 - kv cal not valid'
      endif
      return
      end
c ****************************************************************
      function phov12(t)
```

```
c  vapor !!
c  from ashrae hb p17.5 for r12 238 to 307k in g/m^3
          phov12 = -4.7967e5+6261.2*t-27.888*t**2+4.2595e-2*t**3
          return
          end
c ****************************************************************
          function phov22(t)
c  vapor !!
c  from ashrae hb p17.15 for r22 239 to 307k in g/m^3
          phov22 = -7.4327e5+9467.0*t-41.030*t**2+6.0837e-2*t**3
          return
          end
c ****************************************************************
          function phov(h,p,xa,mwab)
c  vapor !!
c  input:
c         h enthaply in j/g
c         p pressure in kpa
c         xa mole fraction of 1st comp
c         mwab molecular weight of mix in g/mol
c  output:
c         phov liquid density in g/m^3
c
          real coeff(9,22),crit(5,22),a(3,2),b(3,2)
          common /esdata/ coeff,crit
          common /rdata1/ a,b,ffo,ff1
c
          real mwab
c
          call hpin(h*mwab,p,xa,t,xq,xl,xv,vl,vv,hl,hv)
          phov = 1000.0*mwab/vv
          return
          end
c ****************************************************************
          function visv12(t)
c  vapor !!
c  from ashrae hb p17.5 for r12 240 to 310k in upa s
          temp = 7.3042-1.6369e-2*t+1.1786e-4*t**2
c  convert to g/(m-s)
          visv12 = temp/1e3
          return
          end
c ****************************************************************
          function visv22(t)
c  vapor !!
c  from ashrae hb p17.55 for r22 240 to 310k in upa s
          temp = 11.554-4.9214e-2*t+1.8571e-4*t**2
c  convert to g/(m-s)
          visv22 = temp/1e3
          return
          end
c ****************************************************************
          function visv(t,tc,pc,phoc,pho,mwab)
c
c  Input:
c         t         temperature in K
c         tc        critical temperature in K
```

```
c       pc      critical pressure in kPa
c       phoc    critical density in kmol/m^3
c       pho     vapor density in kmol/m^3
c       mwab    molecular weight in kg/kmol
c  Output:
c       visv    vapor viscosity in g/(m-s)
c
        real mwab
        r = 8.314
        xi = tc**(1.0/6.0)*mwab**(-1.0/2.0)*(pc/1000.0)**(-2.0/3.0)
        zc = pc/(phoc*r*tc)
        tr = t/tc
        viss = ((0.5124*tr - 0.0517)**(0.82)*zc**(-0.81))/xi
        phor = pho/phoc
        if (phor.le.0.1) then
                visv = (viss*xi + 0.761931*phor**1.111)/xi
        else if ((phor.gt.0.1).and.(phor.le.0.9)) then
                visv = (viss*xi + 2.79283*(9.045*phor +
    1                   0.63)**1.739)/xi
        else if ((phor.gt.0.9).and.(phor.le.2.6)) then
                c1 = 3.0 - 10**(0.6439-0.1005*phor)
                visv = (viss*xi + 4.6*10**c1)/xi
        else
                write(*,*) 'caution phor > 2.6 and there is no
    1                   visv soln'
        endif
        visv = visv/1e3
        return
        end
c ***************************************************************
```

A.11 References

---

1 Incropera, F. P. and D. P. DeWitt, Fundamentals of Heat and Mass Transfer, 2nd ed., 1985, p. 767.

2 1989 ASHRAE Handbook , Fundamentals, SI ed., 1989, pp. 17.5, 17.15.

3 Jung, D. and R. Radermacher, "Transport Properties and Surface Tension of Pure and Mixed Refrigerants", *ASHRAE Transactions*, V. 97, Pt. 1, 1991.

4 Jung, D. and R. Radermacher, "Transport Properties and Surface Tension of Pure and Mixed Refrigerants", *ASHRAE Transactions*, V. 97, Pt. 1, 1991.

5 Shankland, I. R., "CFC Alternatives for Thermal Insulation Foams", *International Journal of Refrigeration*, Vol. 13, March, 1990, pp. 113-121.

6 Yata, J., Minamiyama, T. and S. Tanaka, "Measurement of thermal conductivity of liquid fluorocarbons", *International Journal of Thermophysics*, Vol. 5, No. 2, 1984, pp. 209-218.

[7] Gray, P., " A configuration relaxation model for transport processes in a monatomic liquid", *Molecular Physics*, Vol. 7, No. 3, 1964, pp. 235-253.

[8] Filippov, L. P., Vest. Moak. Univ., *Ser. Fiz. Mat. Estestv. Nauk.*, Vol. 8, 1955, pp. 67-69.

[9] Stiel, L. I., and G. Thodos, "The thermal conductivity of non polar substances in the dense gaseous and liquid regions", *AIChE Journal*, Vol. 10, 1964, pp. .26-30.

[10] Eucken, A. "Uber das warmeleitvermogen, die spezifische warme und die innerer reibung der gase", *Phys. Z.*, Vol. 14, 1913, pp. 324-336.

[11] Grunberg, L., and A. H. Nissan, "Mixture law for viscosity", *Nature*, Vol. 164, 1949, pp. 799-800.

[12] Stiel, L. I., and G. Thodos, "The viscosity of polar substances in the dense gaseous and liquid regions", *AIChE Journal*, Vol. 10, 1964, pp. .275-277.

[13] Brock, J. R., and R. B. Bird, *AIChE Journal*, Vol. 1, 1955, p. 174.

[14] Jung, D. and R. Radermacher, "Transport Properties and Surface Tension of Pure and Mixed Refrigerants", *ASHRAE Transactions*, V. 97, Pt. 1, 1991.

[15] Reid, R. C., J. M. Prausnitz, and B. E. Poling, The Properties of Gases and Liquids, 4th ed., New York: McGraw-Hill, 1987.

[16] Jung, D. and R. Radermacher, "Transport Properties and Surface Tension of Pure and Mixed Refrigerants", *ASHRAE Transactions*, V. 97, Pt. 1, 1991.

[17] Jung, D. and R. Radermacher, "Transport Properties and Surface Tension of Pure and Mixed Refrigerants", *ASHRAE Transactions*, V. 97, Pt. 1, 1991.

[18] Jung, D. and R. Radermacher, "Transport Properties and Surface Tension of Pure and Mixed Refrigerants", *ASHRAE Transactions*, V. 97, Pt. 1, 1991.

[19] Grunberg, L., and A. H. Nissan, "Mixture law for viscosity", *Nature*, Vol. 164, 1949, pp. 799-800.

[20] Nagaoka, K., Y Tanaka, H Kubota, and T. Makita, "A new correlation for the viscosity of gaseous fluorocarbon refrigerants", *International Journal of Thermophysics*, Vol. 7, No. 5, 1986, pp. 1023-1031.

[21] Nagaoka, K., Y Tanaka, H Kubota, and T. Makita, "A new correlation for the viscosity of gaseous fluorocarbon refrigerants", *International Journal of Thermophysics*, Vol. 7, No. 5, 1986, pp. 1023-1031.

[22] Jung, D. and R. Radermacher, "Transport Properties and Surface Tension of Pure and Mixed Refrigerants", *ASHRAE Transactions*, V. 97, Pt. 1, 1991.

---

[23] Jung, D. and R. Radermacher, "Transport Properties and Surface Tension of Pure and Mixed Refrigerants", *ASHRAE Transactions*, V. 97, Pt. 1, 1991.

[24] Jung, D. and R. Radermacher, "Transport Properties and Surface Tension of Pure and Mixed Refrigerants", *ASHRAE Transactions*, V. 97, Pt. 1, 1991.

APPENDIX B: MIXTURE CHARGING PROCEDURE AND ERROR

This appendix explains the charging procedure and the error associated with charging mixtures. Two methods were considered for charging the mixtures. The first method involved loading the mixture components directly into the refrigerant loop. The drawback of this method is that the total charge amount could not be well regulated. This method was also complicated when additional refrigerant had to be added to the system. The second method, which was chosen, involves loading the mixture components into an intermediate mixing tank. The system then would be charged from the mixing tank. This method proved to be superior for charging exact amounts and for adding additional refrigerant to the system. Unfortunately, there is a charging error associated with the second method. It was decided that the charging error was small compared to the inexact charge delivery and other difficulties sited above associated with the first method.

B.1 Charging Vessels

The charging vessels for the pure refrigerants, R12 and R22, were the original cans from the manufacturer. For the refrigerant mixtures, the components were mixed into a secondary charging vessel.

To prepare the refrigerants for mixing, the higher boiling point components, R123 and R141b, were placed in sealed containers with a desiccant and placed under a slight vacuum to remove any air above the refrigerant. These two refrigerants have a saturation pressure at room temperature which is slightly higher than atmospheric pressure, and water absorption is common. The desiccant is used to remove moisture which may have gotten into the refrigerants.

For each mixture, 65% R22/35% R123 and 80% R22/20% R141b, a virgin charging vessel was evacuated and weighed. The vessel was hooked up to the container of the higher boiling point component, the R123 or R141b, and the refrigerant was transferred as a vapor. The container had been placed on a mass balance; and when the approximate amount of charge had been delivered, the process was stopped. A heat gun was used on the container to drive the vapor into the charging vessel. The hoses were removed, and the charging vessel was weighed to determine exactly how much refrigerant had been transferred.

Next, the R22 can was placed on the mass balance and hooked up to the charging vessel. The R22 was charged as a liquid. Again, the heat gun was used to drive the R22 into the charging vessel. When the approximate amount of R22 had been delivered to the charging

vessel, the process was stopped; and the charging vessel was weighed to determine the exact amount of R22 that had been added. The mass composition of each mixture was determined.

B.2 Procedure

The proper amount of refrigerant charge in the test loop was determined to be approximately 2.26 kg or about 5 lbs.. The internal volume of the loop was estimated to be 2.5 L. In preparation for charging, the loop was evacuated for approximately one hour. The system was typically left under a vacuum until the next morning to allow diffusion of the previous charge from valve stems and the filter dryer to occur. Leaks were easily identified if a substantial rise in pressure had occurred. The vacuum pump was allowed to run about 15 minutes in preparation for loading the charge.

The charging vessel was hooked up to the manifold gauge set and was placed on a mass balance upside down to allow only liquid to enter the loop. The mass balance was zeroed. The vacuum pump was valved off, and the line from the charging vessel to the loop was opened. The refrigerant loop was started to allow complete charging of the system without having to heat the charging vessel.

B.3 Accuracy of Charging a Mixture

Error was minimized by charging the mixtures as a liquid. The accuracy of mixing the components was negligible. The mass balance has a resolution of ± 0.05 g and the total charge was 2.26 kg. This is a percent error of $2.21e^{-3}$. The inaccuracy results from charging a mixture of a known total composition, liquid and gas, as a liquid only. The composition of the liquid is not the same as the bulk composition. The vapor in the charging vessel is rich in the more volatile component, R22.

Figure B.1 shows the charging error for both refrigerant mixtures. The percent charge error from the total mass composition is plotted against the percent vapor volume in the charging vessel. The error remains small, staying below two percent for vapor volumes of less than 60%. At vapor volumes from 90% to 99% the charging error ranges from 10% to 50% for R22/R123 and for R22/R141b the range is 6% to 40%.

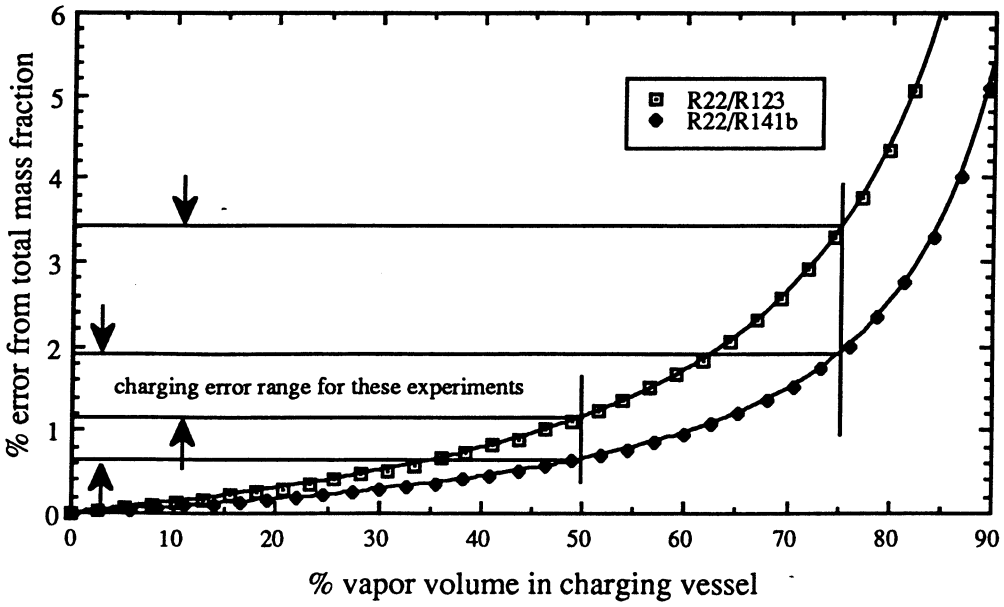

Figure B.1: Charging error versus the percent vapor volume in the charging vessel

The lines on the plot show the range of charging error that occurred for the experiment. The error ranged from 1.15% to 3.35% for R22/R123 and 0.7% to 1.9% for R22/R141b. To obtain the total charging error, each error curve has to be integrated from 50% to 75% vapor volume. The error points were fit with a 4th order polynomial, %Dev, valid for 20% to 80% vapor volume, VV.

$$\%Dev = 0.46866 - 5.9414e^{-2}VV + 3.6132e^{-3}VV^2 - 6.7911e^{-5}VV^3 + 4.9686^{e-7}VV^4$$

for R22/R123 (B.1)

$$\%Dev = 0.28239 - 3.4876e^{-2}VV + 2.0667e^{-3}VV^2 - 3.8575e^{-5}VV^3 + 2.8152^{e-7}VV^4$$

for R22/R141b (B.2)

where:

$$ChargingError = \frac{1}{25}\int_{50}^{75} \%Dev \cdot dVV \quad (B.3)$$

The integrated charging error for R22/R123 was 2.005% and 1.154% for R22/R141b. This translates into an actual charging mass fraction of 0.637 instead of 0.65 for R22/R123 and 0.791 instead of 0.80 for R22/R141b.

B.4 Origin of Charging Error

The bulk composition for a two-phase mixture is not the same as the composition of the liquid phase or the vapor phase. Because most of the mass of a two-phase sample is liquid, even up to high percentages of vapor volume, the composition of the liquid phase is very near to the bulk composition. Figure B.2 shows a pressure-composition diagram for a typical refrigerant mixture. As more and more of the liquid is removed, the quality of the mixture increases. Since temperature is held constant, the pressure in the charging vessel drops and the remaining liquid becomes enriched in the less volatile component, B.

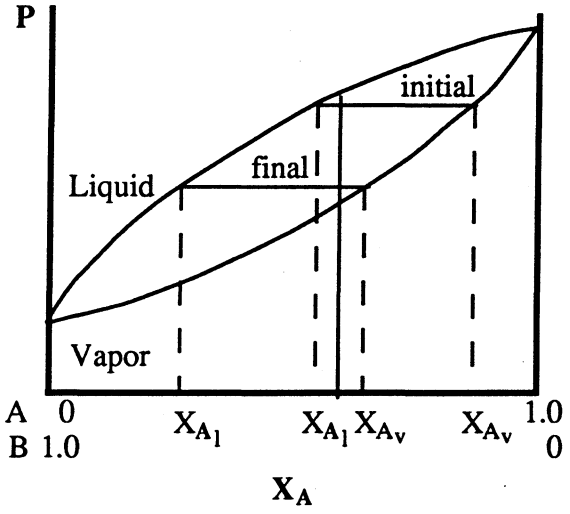

Figure B.2: Pressure versus concentration plot at constant temperature

Figure B.3 shows the change in quality and pressure as the vapor volume in the charging vessel increases for a 80% R22/20% R141b mixture. At 80% vapor volume, the quality of the mixture is only 2.5%, and the pressure in the vessel has dropped about 11%. In Figure B.2, at low vapor volumes up to relatively high vapor volumes, the charging process would remain close to the "initial" line. At very high vapor volumes, the process would rapidly move to the "final" line.

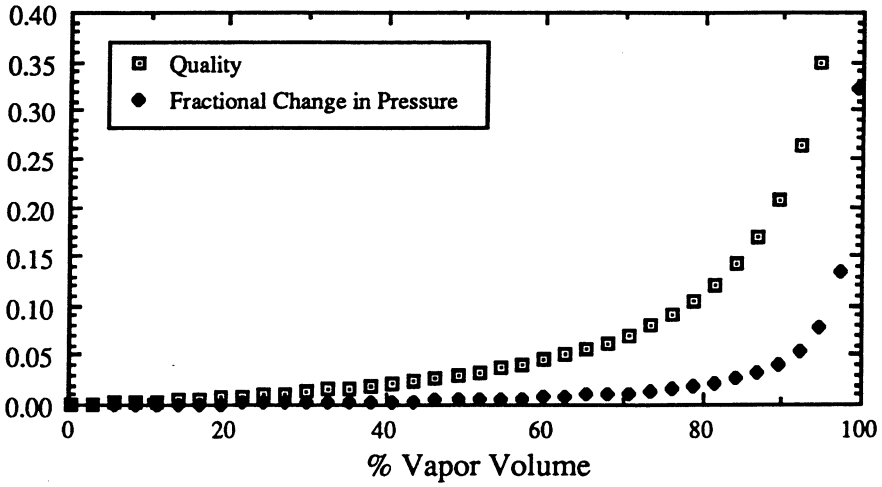

Figure B.3: Change of quality and pressure as a function of change in vapor volume for a R22/R141b charging vessel

B.5 Other Considerations

The two mixtures were found not to be compatible with the charging hose material. After several uses, the charging hoses became permeable to the refrigerant mixtures. Submersing a pressurized hose into a bucket of water revealed massive leakage along the length of the hose. Care was taken after the discovery of the leakage to *never* leave a charging hose attached to the refrigerant loop after the initial charging was complete. No problem with the manifold gauge set valves was observed.

APPENDIX C: UNCERTAINTY ANALYSIS

This appendix describes the method used to determine the uncertainty in the calculated values of air-side resistance and the refrigerant heat transfer coefficients. The fundamental basis for the uncertainty for the experimental data is the energy balance error. This was assumed to include the transducer and measurement uncertainty for the thermocouples, pressure transducers, and mass-flow meter. The measured power consumption plus heat leak into each cabinet was assumed to be correct. The load control systems were calibrated with a commercially available energy analyzer. The relevant uncertainties for the experiment and the mean deviations are listed here. This analysis was necessary to understand how much confidence to place in the final optimization results presented in Chapter 7.

The uncertainty analysis for this project was handled using the successive perturbation technique as described by Moffat.[1] Also, there is an excellent discussion in Staley's thesis on experimental uncertainty analysis in section 5.3 and practical examples given in Appendix D.[2] The relevant uncertainties and mean deviations for this experiment are given in Table C.1. The uncertainties for the power measurement, mass-flow rate, high and low-pressure enthalpy are typical of the equipment used in this experiment.[3]

Table C.1: List of uncertainties and mean deviations for this experiment

description	uncertainty/mean deviation
use of UA method for 65% R22/35% R123	+/- 7.1%
use of UA method for 80% R22/20% R123	+/- 4.07%
air-side resistance for 8 finned tube passes	+/- 3.3%
air-side resistance for single finned tube	+/- 5.0%[4]
R12/R22 refrigerant correlation	+/- 10.0%
65% R22/35% R123 refrigerant correlation	+/- 15.26%
80% R22/20% R141b refrigerant correlation	+/- 37.89%
power measurement	+/- 1.05 W
mass-flow rate	+/- 0.1%
high-pressure enthalpy	+/- 0.63 J/g
low-pressure enthalpy	+/- 0.326 J/g

C.1 Pure-Refrigerant Data Reduction

For the pure-refrigerant runs the uncertainty analysis included two components. The first component was the energy balance error, the error between the energy input to the compartments and the energy absorbed by the refrigerant as it passed through the evaporator module. The second component was the mean deviation for the pure-refrigerant correlation that was used. For each run, the sequential perturbation method (SPM) was used to find the uncertainty of the calculated air-side resistance value.

The energy balance error was calculated from Equation C.1. The power values were measured at steady state from watt meters. At steady state, the total energy consumption of the electrical devices in the compartments was ultimately converted into heat loading on the evaporators in both compartments. The enthalpy values were measured at the inlet and outlet of the refrigerant connections to the insulated box. Any undesired heat leak from the intercoolers into the fresh-food compartment or inaccurate measurement of fluid temperatures between internal components was avoided.

There was uncertainty in the fluid property measurement values and power measurement values that are required in Equation C.1. The accuracy of the thermocouples, pressure transducers and mass-flow meter must be considered. For the power measurements the accuracy of the watt transducer must be taken into account. Using the SPM, an uncertainty for Equation C.1 was calculated to be 0.68%.

$$\text{Error} = \frac{\dot{m}_r(h_8 - h_1) - (\text{Load}_f + \text{Load}_{ff})}{(\text{Load}_f + \text{Load}_{ff})} \pm 0.68\% \qquad \text{(C.1)}$$

For each run at various evaporator air velocities, an air-side resistance uncertainty was calculated. The air-side resistance uncertainties (in K/W) were curve fit as a function of evaporator air velocity as shown in Figures C.1 and C.2.

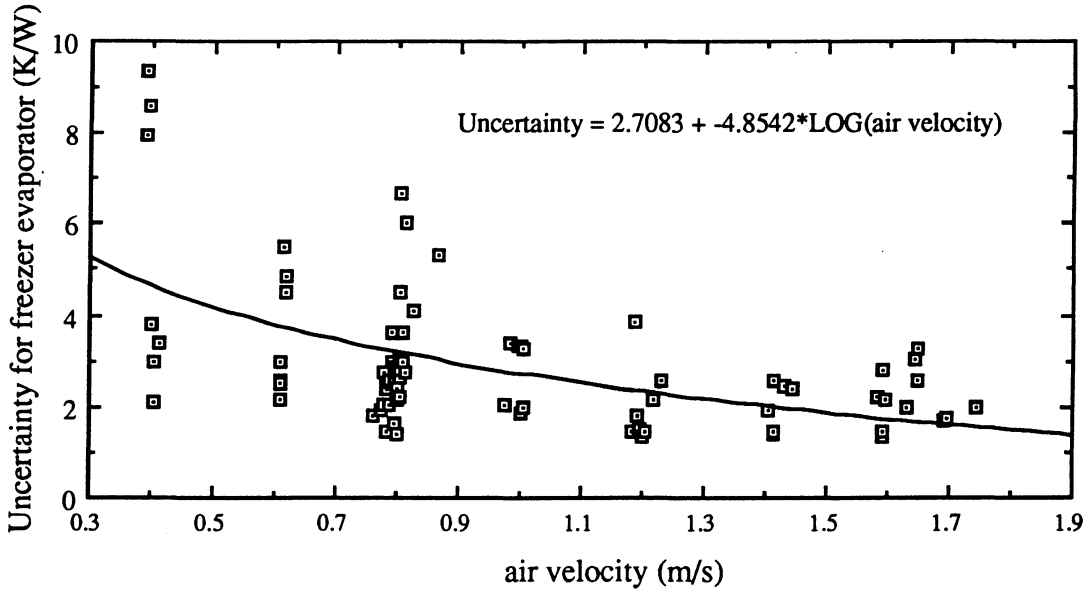

Figure C.1: Uncertainty in the air-side resistance values for the freezer evaporator

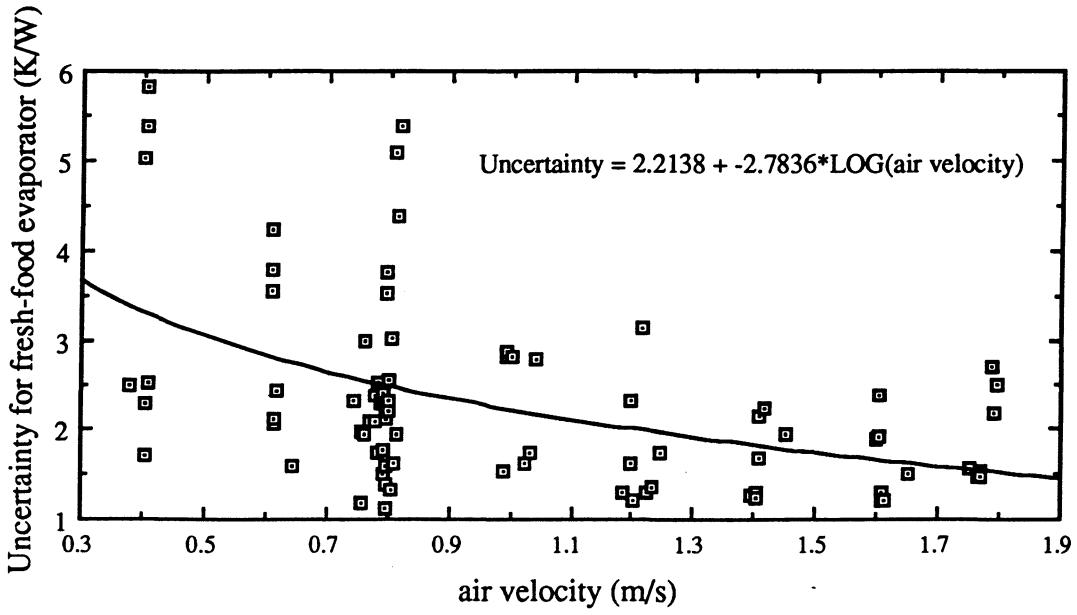

Figure C.2: Uncertainty in the air-side resistance values for the fresh-food evaporator

Notice that the uncertainty is greater at the lower air velocities. At the lower air velocities the air-side resistance is much greater; consequently, the uncertainty as a percentage of the air-resistance value is approximately constant over the air velocity range.

C.2 Mixture Data Reduction

For the refrigerant-mixture runs the uncertainty analysis also included two components. As before, the first component was the energy balance error. The second component was the air-side resistance uncertainty for the evaporators from the pure-refrigerant runs. The SPM was used to find the uncertainty of the calculated mixture heat transfer coefficient value from each run.

When all the runs were completed, the heat transfer coefficient values were fit to an appropriate correlation. The 95% confidence interval of the correlated values from the experimental values were calculated.

C.3 Life-Cycle Cost Optimization

The uncertainty in the life-cycle cost was determined by calculating the uncertainty of the heat exchanger sizes. An evaporator sizing model was developed that used the air-side resistance values from a single-pass and an eight-pass evaporator. For a specific air velocity, UA and refrigerant heat transfer coefficient, the number of passes could be determined. For the

intercoolers, the size could be calculated by using the UA value and the refrigerant heat transfer coefficient value.

The evaporator pass number uncertainty for the pure optimization runs was determined from the SPM and required the uncertainties of the single and eight-pass air-side resistances and the mean deviation of the refrigerant heat transfer coefficient correlation.

The evaporator pass number uncertainty for the mixture optimization runs was also determined from the SPM and required the uncertainties of the single and eight-pass air-side resistances, the mean deviation of the refrigerant heat transfer coefficient correlation and the error associated with using the UA/LMTD method with mixtures. Refer to Appendix E, section E.7, for further explanation on how the UA/LMTD error was calculated.

For the pure-refrigerant runs, the intercooler size uncertainty was calculated using the pure-refrigerant correlation mean deviation. For the mixture runs, the intercooler size uncertainty was calculated using the uncertainty of the UA value for use with mixtures and the mixture correlation mean deviation. Again, the SPM was used for both the pure-refrigerant and mixture runs.

The uncertainty in the heat exchanger sizes translates into uncertainty in the heat exchanger cost, occupied volume cost, and uncertainty in the evaporator fan power consumption. These three uncertainties are the basis for the overall uncertainty in the life-cycle cost of an optimized system.

C.4 Sequential Perturbation Method Example

To illustrate the Sequential Perturbation Method, a simple example will be presented. The uncertainty in the load, q, from Equation C.2 will be determined.

$$q = \dot{m}_r(h_{out} - h_{in}) \tag{C.2}$$

Nominal values for the mass-flow rate and enthalpy must be known.

$$h_{out} = 180\frac{kJ}{kg} \tag{C.3}$$

$$h_{in} = 50\frac{kJ}{kg} \tag{C.4}$$

$$\dot{m}_r = 1.5\frac{g}{s} \tag{C.5}$$

The first step is to calculate the nominal or base value of q. Plugging Equations C.3 to C.5 into Equation C.2, the base value of q equals 195 W as shown in Equation C.6. The next step involves calculating a new value of q for perturbed versions of Equation C.2. q should be recalculated, perturbing each variable in Equation C.2 with which there is an associated uncertainty in Table C.1. In this case, Equation C.2 would be recalculated a total of three times. Finally, each result is subtracted by the base case, the results are squared and the square root is taken on the sum of the squares.

$$195\text{W} = \left(1.5\frac{g}{s}\right)\left(180\frac{kJ}{kg} - 50\frac{kJ}{kg}\right) \text{ base case} \tag{C.6}$$

$$195.2\text{W} = \left(1.5\frac{g}{s}[1+0.001]\right)\left(180\frac{kJ}{kg} - 50\frac{kJ}{kg}\right) \text{ perturbed mass-flow rate} \tag{C.7}$$

$$195.49\text{W} = \left(1.5\frac{g}{s}\right)\left((180+0.326)\frac{kJ}{kg} - 50\frac{kJ}{kg}\right) \text{ perturbed outlet enthalpy} \tag{C.8}$$

$$194.06\text{W} = \left(1.5\frac{g}{s}\right)\left(180\frac{kJ}{kg} - (50+0.63)\frac{kJ}{kg}\right) \text{ perturbed inlet enthalpy} \tag{C.9}$$

$$1.06 = \sqrt{(0.2)^2 + (0.49)^2 + (-0.94)^2} \tag{C.10}$$

Equation C.10 gives the uncertainty for the use of Equation C.2 in the range of the nominal values. The proper statement of Equation C.2 is shown below in Equation C.11.

$$q = \dot{m}_r(h_{out} - h_{in}) \pm 1.06\text{W} \tag{C.11}$$

C.5 References

---

[1] Moffat, Robert J., "Describing the Uncertainty in Experimental Results", *Experimental Thermal and Fluid Science*, Vol. 1, 1988, pp. 3-17.

---

[2] Staley, D. M, "Steady-State Performance of a Domestic Refrigerator/Freezer Using R12 and R134a", Master's Thesis, Department of Mechanical Engineering, University of Illinois at Urbana-Champaign, June, 1992.

[3] Staley, D. M, "Steady-State Performance of a Domestic Refrigerator/Freezer Using R12 and R134a", Master's Thesis, Department of Mechanical Engineering, University of Illinois at Urbana-Champaign, June, 1992.

[4] Heun, M. K., "Thermal Performance of an Evaporator-Intercooler Module for a Lorenz Cycle", Master's Thesis, Department of Mechanical Engineering, University of Illinois at Urbana-Champaign, 1991, p. 54.

APPENDIX D: LOAD VARIATION MODEL FOR A SINGLE EVAPORATOR

This appendix explains the development of a load model for a single evaporator that has to cool two compartments. When two compartments are cooled using a single evaporator, the load split between the compartments affects the entering air temperature to the evaporator. Refrigerators in production today utilize a damper to control the mixing of the air streams from the freezer and fresh-food compartments to provide load control between the compartments. To model the load variation between the freezer and fresh-food compartments, an expression must be derived to give the evaporator air-inlet temperature as a function of the compartment temperatures, T_f and T_{ff}, the mass-flow rate of air over the evaporator, $\dot{m}_a$, and the load in each compartment, q_f and q_{ff}, as shown in Figure D.1. This analysis was necessary to be able to determine the inlet air temperature in the single-evaporator optimization cases explored in Chapter 7.

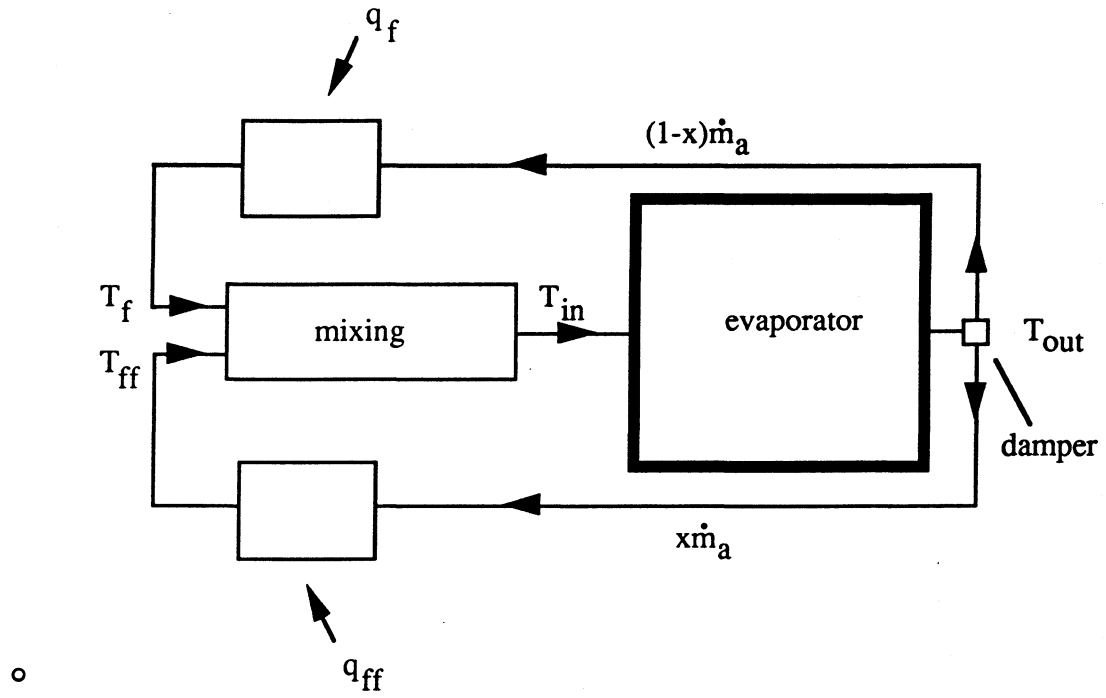

Figure D.1: Schematic of air-flow path in a refrigerator

Three energy balance equations describe the air loop in the refrigerator. The first equation is an energy balance about the air inlet to the evaporator where the mixing of the freezer and fresh-food air takes place. This mixing is assumed to take place adiabatically. The other two equations are balances about the individual compartments.

Energy balance about the adiabatic mixing section:

$$(T_f - T_{in})\bar{c}_p(1-x)\dot{m}_a + (T_{ff} - T_{in})\bar{c}_p x\,\dot{m}_a = 0.0 \qquad \text{(D.1)}$$

where:

$$\bar{c}_p = \frac{c_p(T_f) + c_p(T_{ff})}{2.0} \qquad \text{(D.2)}$$

Equation D.1 reduces to:

$$T_{in} = T_f(1-x) + T_{ff}x \qquad \text{(D.3)}$$

Energy balance about the freezer compartment:

$$(T_f - T_{out})\bar{c}_p(1-x)\dot{m}_a = q_f \qquad \text{(D.4)}$$

Energy balance about the fresh-food compartment:

$$(T_{ff} - T_{out})\bar{c}_p x\,\dot{m}_a = q_{ff} \qquad \text{(D.5)}$$

Solving Equation D.4 for T_{out} and substituting the result into Equation D.5 and after *some* manipulation:

$$x^2\bar{c}_p\dot{m}_a(T_f - T_{ff}) + x\left[(q_f + q_{ff}) - \bar{c}_p\dot{m}_a(T_f - T_{ff})\right] - q_{ff} = 0.0 \qquad \text{(D.6)}$$

Equation D.6 is quadratic in x, the fraction of the total mass-flow rate of air to the fresh-food compartment. Equation D.6 is solved using the quadratic formula, Equation D.7. Only the positive root is meaningful.

$$x = \frac{-b \pm \sqrt{b^2 - 4ac}}{2a} \quad \text{where} \quad 0 \le x \le 1 \qquad \text{(D.7)}$$

where:

$$a = \bar{c}_p\dot{m}_a(T_f - T_{ff}) \qquad \text{(D.8)}$$

$$b = (q_f + q_{ff}) - \bar{c}_p \dot{m}_a (T_f - T_{ff}) \tag{D.9}$$

$$c = -q_{ff} \tag{D.10}$$

Taking the positive root of Equation D.7 and plugging the result into Equation D.3 gives the desired result, the air-inlet temperature of the evaporator.

APPENDIX E: UA/LMTD AND ε/NTU METHODS

This appendix explains under what conditions it is valid to use the UA/LMTD or ε/NTU methods to analyze heat exchangers. The assumptions and the derivation of both methods are presented first. Two assumptions, the assumption of the fluids having constant-specific heats and the assumption of constant overall heat transfer coefficient between the fluids, are looked at in detail. This appendix attempts to answer two questions. How does geometry affect the UA/LMTD analysis that is derived for a fully counter-flow or parallel-flow exchanger? How should an exchanger be analyzed when neither of the above mentioned assumptions apply? A generalized method for analyzing heat exchangers is presented. The last section attempts to quantify the error using the UA/LMTD method for two specific refrigerant mixtures. The analysis in this appendix was required to be able to determine what method needed to be used for the heat exchangers in the experiment when the system was charged with mixtures.

E.1 Assumptions

The UA/LMTD and the ε/NTU methods are based on five assumptions:[1]

1) The heat exchanger is insulated from its surroundings, therefore the only heat exchange is between the hot and cold fluids
2) Axial conduction along the tubes is negligible.
3) Potential and kinetic energy changes are negligible.
4) The specific heats of the fluids are constant.
5) The overall heat transfer coefficient is constant.

The first three conditions will be assumed to be valid. This discussion will focus on the validity of assumptions four and five for pure refrigerants and refrigerant mixtures.

E.2 Method Derivation

Both the UA/LMTD methods derivations are based on the same fundamental equations. Applying an energy balance to the hot and cold sides of the exchanger yields

$$q = \dot{m}_h\left(h_{h,i} - h_{h,o}\right) \tag{E.1}$$

$$q = \dot{m}_c\left(h_{c,o} - h_{c,i}\right) \tag{E.2}$$

Applying assumption four to Equations E.1 and E.2, these expressions reduce to

$$q = \dot{m}_h c_{p,h}\left(T_{h,i} - T_{h,o}\right) \tag{E.3}$$

$$q = \dot{m}_c c_{p,c}\left(T_{c,o} - T_{c,i}\right) \tag{E.4}$$

Equations E.3 and E.4 are independent of flow arrangement and heat exchanger type. The heat transfer in a heat exchanger can be expressed in terms of Equation E.5

$$q = UA\Delta T_m \tag{E.5}$$

where U is the overall heat transfer coefficient and ΔT_m is an appropriate mean value of temperature difference.

Applying an energy balance to a differential element of a parallel-flow heat exchanger yields

$$dq = -\dot{m}_h c_{p,h} dT_h \equiv -C_h dT_h \tag{E.6}$$

$$dq = \dot{m}_c c_{p,c} dT_c \equiv C_c dT_c \tag{E.7}$$

where C_h and C_C are the heat capacity rates of the hot and cold fluids. Applying Equation E.5 to the differential element yields

$$dq = U\Delta T dA \tag{E.8}$$

This equation is true provided that the segment area, dA, is 'sufficiently small' to substantiate assumptions 4 and 5 for the specific exchanger analysis. ΔT is the local temperature difference between the fluids:

$$\Delta T = T_h - T_c \tag{E.9}$$

In differential form Equation E.9 yields

$$d(\Delta T) = dT_h - dT_c \tag{E.10}$$

Substituting Equations E.6 and E.7 into Equation E.10 gives

$$d(\Delta T) = -dq\left(\frac{1}{C_h} + \frac{1}{C_c}\right) \tag{E.11}$$

Substituting Equation E.8 into Equation E.11 and integrating across the heat exchanger applying assumption 5 yields:

$$\int_1^2 \frac{d(\Delta T)}{\Delta T} = -U\left(\frac{1}{C_h} + \frac{1}{C_c}\right)\int_1^2 dA \tag{E.12}$$

$$\ln\left(\frac{\Delta T_2}{\Delta T_1}\right) = -UA\left(\frac{1}{C_h} + \frac{1}{C_c}\right) \tag{E.13}$$

From Equation E.13, both the UA/LMTD and the ε/NTU forms are derived. Substituting Equations E.3 and E.4 into Equation E.13 with some manipulation will give the UA/LMTD heat exchanger equation

$$q = UA\left(\frac{\Delta T_2 - \Delta T_1}{\ln(\Delta T_2/\Delta T_1)}\right) \tag{E.14}$$

where ΔT_1 and ΔT_2, the endpoint temperature differences, are defined by the inlet, point 1, and the outlet, point 2, of the hot fluid. For a parallel-flow heat exchanger

$$\begin{aligned} \Delta T_1 &= T_{h,i} - T_{c,i} \\ \Delta T_2 &= T_{h,o} - T_{c,o} \end{aligned} \tag{E.15}$$

For a counter-flow heat exchanger ΔT_1 and ΔT_2 are defined

$$\begin{aligned} \Delta T_1 &= T_{h,i} - T_{c,o} \\ \Delta T_2 &= T_{h,o} - T_{c,i} \end{aligned} \tag{E.16}$$

The number of transfer units (NTU) can be defined as

$$NTU = \frac{UA}{C_{min}} \tag{E.17}$$

where C_{min} is the smaller of C_h or C_c. Heat exchanger effectiveness (ε) can be defined as

$$\varepsilon = \frac{q}{q_{max}} = \frac{C_h(T_{h,i} - T_{h,o})}{C_{min}(T_{h,i} - T_{c,i})} \text{ or } \frac{C_c(T_{c,o} - T_{c,i})}{C_{min}(T_{h,i} - T_{c,i})} \quad \text{(E.18)}$$

Substituting Equations E.17 and E.18 into Equation E.13 and rearranging the resulting expression depending on the geometry dependent temperature definitions, the following expressions for counter-flow and parallel-flow heat exchangers can be derived:

$$\varepsilon = \frac{1 - \exp\left[-NTU\left((1 + C_{min}/C_{max})\right)\right]}{1 + (C_{min}/C_{max})} \text{ parallel-flow} \quad \text{(E.19)}$$

$$\varepsilon = \frac{1 - \exp\left[-NTU\left((1 - C_{min}/C_{max})\right)\right]}{1 - (C_{min}/C_{max})\exp\left[-NTU\left((1 - C_{min}/C_{max})\right)\right]} \text{ counter-flow} \quad \text{(E.20)}$$

E.3 Assumption Four

For a refrigerator evaporator, the two fluids that exchange heat are air and refrigerant. The air will be assumed to have a constant-specific heat over the operating temperature range of the evaporator. For a pure refrigerant or azeotrope in phase change, the specific heat is constant (although its value is infinite). For refrigerant mixtures, the specific heat is most likely non-constant. A non-constant-specific heat in phase change implies that the plot of saturation temperature versus enthalpy is non-linear. (There may be some combinations of refrigerants that would give a linear saturation temperature versus enthalpy plot.)

E.4 Assumption Five

The fifth assumption of constant overall heat transfer coefficient depends on the local heat transfer of the air and the refrigerant and how each changes as they flow through the exchanger. For pure refrigerants under the conditions of low heat and mass flux, the refrigerant heat transfer coefficient should remain approximately constant with quality. If the change in the air-side heat transfer coefficient is minimal as the air flows over the evaporator, assumption five is satisfied. For refrigerant mixtures, the validity of assumption five is questionable. The refrigerant-mixture heat transfer coefficient in the low heat and mass flux range is a weak function of quality. Fortunately, in many cases for mixtures, the variation of the heat transfer coefficient with quality is small and assumption five is valid.

E.5 When to Apply Each Method

The UA/LMTD derivation assumes either true parallel-flow or true counter-flow geometry. If the five assumptions listed in the first section are met and the heat exchanger is either fully parallel-flow or fully counter-flow, the UA/LMTD analysis can always be used to evaluate the heat exchanger's performance. The ε/NTU method can also be applied in all cases if the five assumptions are met and the correct equation form (for the specific exchanger geometry) is used.

Most evaporators are not true parallel-flow or true counter-flow, they are usually a combination of cross-flow and counter-flow geometries. How does geometry affect the UA/LMTD analysis that is derived for a fully counter-flow or parallel-flow exchanger? How should an exchanger be analyzed when neither assumption four nor five applies?

When does Geometry Matter for the UA/LMTD Method?

Assume that all five assumptions listed in the first section are valid. For a pure-refrigerant case with $C_{min}/C_{max} = 0.0$, the UA/LMTD analysis can be applied without error for any heat exchanger geometry with no difference between small or large effectivenesses. For a fluid with a constant-specific heat and a temperature glide through the exchanger ($C_{min}/C_{max} > 0.0$), the UA/LMTD method can no longer be applied without a correction unless the exchanger geometry is true parallel or counter-flow. The error is reduced for non-parallel and non-counter-flow exchangers with small effectivenesses but can be great for exchangers with large effectivenesses. The worst case results when the air-temperature glide exactly matches the refrigerant-temperature glide ($C_{min}/C_{max} = 1.0$) and the effectiveness is large. Table E.1 shows the various cases for which geometry matters when applying the UA/LMTD method.

Table E.1: The influence of geometry on the results of the UA/LMTD method - assumptions 1-5 hold

	$\frac{C_{min}}{C_{max}} = 0$	$\frac{C_{min}}{C_{max}} > 0$
ε small	no influence	small influence
ε large	no influence	large influence
	UA method applies without correction to all exchanger geometries	UA method has to be applied with correction unless geometry is parallel or counter-flow

Kays and London addressed the question of cross-counter-flow geometry problem with unmixed flow within the passes as shown in Figure E.1. The counter-flow curve where n, the number of passes, equals infinity is the UA/LMTD analysis result. The five assumptions hold and C_{min}/C_{max} = 1.0 which gives the largest variation in results due to geometry. Notice at the smaller effectivenesses that geometry plays almost no role in the sizing of the exchanger. As effectiveness increases, the effect of geometry increases dramatically.

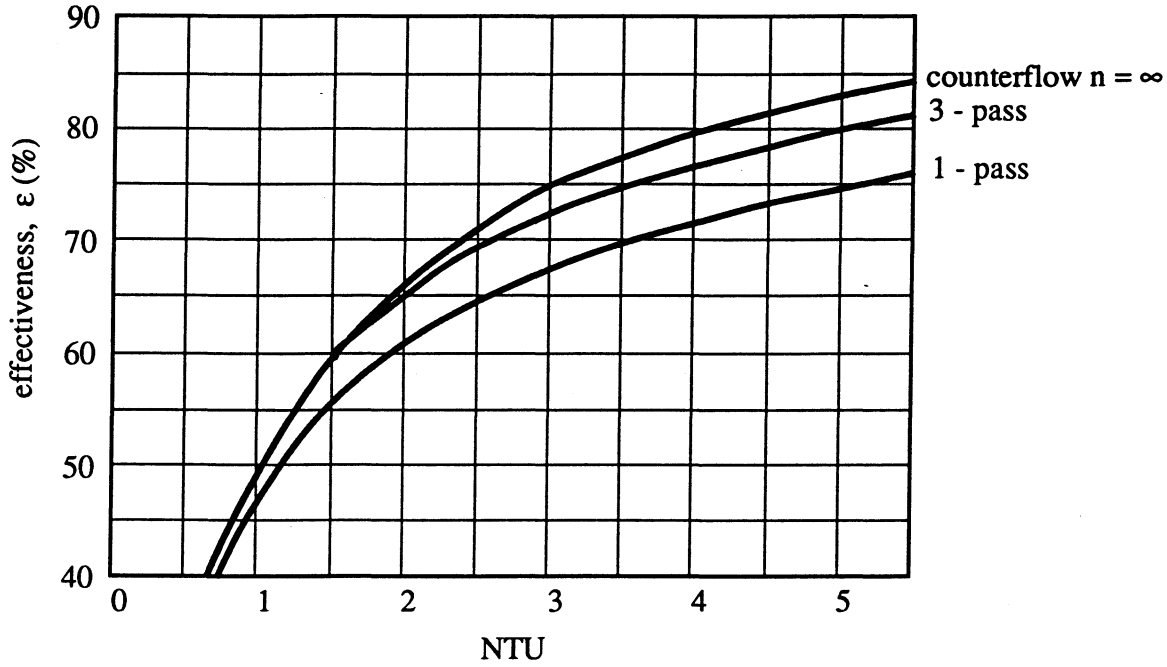

Figure E.1: Heat transfer effectiveness as a function of NTUs and number of passes for a multi-pass cross-counter-flow exchanger - C_{min}/C_{max} = 1; unmixed flow within passes, one fluid unmixed between passes - taken from Kays and London[2]

What is the error of using the UA/LMTD method without correction for a cross-counter-flow exchanger at the worst case of C_{min}/C_{max} = 1.0? Most cross-counter-flow evaporators are approximately 50% effective and greater than three passes; so in examining Table E.2, the error is negligible. In the literature, a correction method has been set up for the UA/LMTD method called the F correction factor.[3]

Table E.2: Error between using the UA/LMTD without correction for a one-pass and a three-pass cross-counter-flow exchanger as presented in Figure E.1

effectiveness	error for one-pass	error for three passes
40%	12.5%	~0.0%
50%	15.8%	~0.0%
60%	25.0%	3.6%
70%	48.8%	9.3%

E.6 When Neither Assumption Four nor Five Applies

E.6.1 Solution by Others: Literature Review

There are three papers, Conklin and Granryd[4], Granryd and Conklin[5], and Conklin and Vineyard[6], that address the calculation of heat exchanger performance when assumption four or five is not met. The Conklin and Granryd paper describes a general approach for analyzing the thermal performance of heat exchangers in which the overall heat transfer coefficient varies as a function of enthalpy (or quality). For this analysis, assumption five is not met but the other four assumptions are satisfied. In this paper, the formulation of the ε/NTU method was modified as a function of non-dimensional enthalpy and was shown to be unchanged with a variable overall heat transfer coefficient. To use this new formulation, a true, area-weighted mean value of the overall heat transfer coefficient must be used. A general method for evaluating a true mean overall heat transfer coefficient given a variable local overall heat transfer coefficient was presented.

The next paper by Granryd and Conklin explores modifying the ε/NTU method to work with a varying specific heat fluid. For this analysis, assumption four is not met but the other four assumptions are satisfied. This paper derives ε/NTU relationships for fluids having a linear and quadratic dependence of specific heat with respect to quality. A criterion is developed that helps identify potential occurrence or absence of heat exchanger pinch-points in heat exchangers operation with refrigerant mixtures.

The last paper by Conklin and Vineyard present experimental verification of the ε/NTU relationships derived in the previous paper by Granryd and Conklin. This paper compares the measured thermal performance and calculated thermal performance from the unmodified constant-specific heat ε/NTU relationships and the modified non-constant ε/NTU relationships. The measured and modified ε/NTU thermal performance showed good agreement when the pressure drop through the heat exchanger was small. There were two experimental runs performed, 71% R22/29% R114 and 75% R143a/25% R124. The average error between the

measured NTU and the calculated NTU by the modified and unmodified ε/NTU equations for the tested evaporator are listed in Table E.3. The advantage of using the non-constant-specific heat ε/NTU equations does not enhance the accuracy of the calculation appreciably.

Table E.3: Error between the measured NTU and calculated NTU for the constant and non-constant-specific heat methods

mixture	average error modified ε/NTU	average error unmodified ε/NTU
71% R22/29% R114	7.77%	13.18%
75% R143a/25% R124	17.46%	20.46%

The methods presented by Granryd, Conklin, and Vineyard require additional analysis and seem more difficult to implement than a general method of breaking the heat exchanger into small segments as presented in the next section.

E.6.2 Solution by Breaking Exchanger into Segments

When neither assumption four, constant fluid specific heats, nor assumption five, constant overall heat transfer coefficient applies, the exchanger must be broken up into small constant-specific heat/constant heat transfer coefficient segments. The length of each segment will be dictated by the relative change in the specific heat and the heat transfer coefficient through the evaporator. Figure E.2 shows an evaporator broken up into uniform segments. An energy balance is performed about each element. A set of simultaneous equations can be written from the segment energy balances. If the proper information is known, the equations can be solved by marching through the evaporator starting at the outlet. For example, if the air-inlet temperature (refrigerator compartment temperature), air mass-flow rate and refrigerant outlet conditions are known, the last segment's refrigerant inlet conditions and air-outlet conditions can be readily determined. The calculation proceeds from right to left across the bottom row of the exchanger. The second row calculations are determined in the same way because the air-outlet temperature for the first row becomes the air-inlet temperature for the second row. There may be some mixing between adjacent tube rows which would have to be determined by experiment. For more information see Equations 5.1 to 5.4.

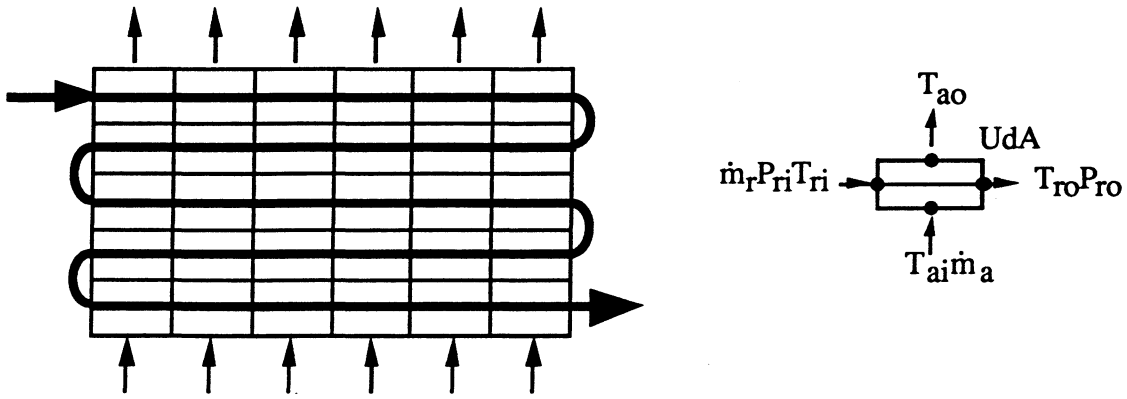

Figure E.2: A segmented evaporator that would be used to evaluate the performance of an evaporator for which neither assumption four nor five applied

E.7 Actual Error for Using the UA/LMTD Method with Mixtures

In this section, the actual error associated with using the UA/LMTD method to analyze the eight-pass freezer and four-pass fresh-food evaporators with the mixtures 65% R22/35% R123 and 80% R22/R141b will be discussed. In many situations it is not convenient to break the evaporator up into small segments to analyze the heat exchanger. For this project, the evaporators needed to be sized with every call of the optimization program as discussed in Chapter 6. The combination of many calls to the evaporator sizing routine with the associated large number of calls to the thermodynamic property routines for every segment took tremendous amounts of computation time on the main frame computer. Therefore, it was decided to use the UA/LMTD method (knowing that there would be an error in the results) for sizing the evaporators. The nature of the error for using UA/LMTD method was able to be narrowed down to violation of assumption four on the refrigerant-side. The potential geometry problem proved negligible.

Recall that the UA/LMTD method is derived from an exchanger whose geometry is fully counter-flow or parallel-flow. The evaporators used in the experiment are a cross-counter-flow design with eight and four tubes passes for the freezer and fresh-food evaporators respectively. One would expect that the UA/LMTD method would give erroneous results for a constant-specific heat fluid with $C_{min}/C_{max} > 0.0$ as described previously. As shown in Table E.2, if effectiveness of these evaporators is 60% or less, the geometry error for exchangers with three or more passes is negligible. (The average effectiveness of the freezer and fresh-food evaporator was calculated to be 41% and 54% respectively.) Again it must be pointed out that Figure E.1 is the worst case with a $C_{min}/C_{max} = 1.0$. Even with non-constant-specific heat mixtures, the local value of C_{min}/C_{max} is limited to a maximum value of 1.0.

For the mixture analysis, the only source of error to consider is the non-constant-specific heats of the mixtures. For the mixture data reduction, the evaporators were analyzed two ways. The UA value was calculated with the UA/LMTD method, and another UA value, UA_{sum}, was calculated by breaking the evaporator into small segments. The evaporator analysis subroutine breaks up the actual heat exchanger geometry into ten segments per pass making a total of 80 segments for the freezer evaporator and 40 segments for the fresh-food evaporator.

In the evaporator analysis subroutine there are several assumptions that were made. The air-side heat transfer coefficient was assumed constant over the entire evaporator. The air was assumed to have a constant-specific heat over the temperature range which the evaporator operated. The refrigerant-mixture's heat transfer coefficient was assumed to be independent of quality over the operating range of each evaporator. This is a valid assumption because the refrigerant-side heat transfer coefficient is a weak function of quality in the low heat and mass flux range over which the evaporators were operating.

The subroutine starts by first guessing a refrigerant heat transfer coefficient from which a UA value for each segment, UdA, is calculated. Equation E.21 shows how UdA is calculated from the segment size, dA_a and dA_r, and the heat transfer coefficients for the air and the refrigerant, α_a and α_r.

$$\frac{1}{UdA} = \frac{1}{\alpha_a dA_a} + \frac{1}{\alpha_r dA_r} \tag{E.21}$$

An energy balance is performed about each segment. For each segment, the UdA is used to calculate a heat transfer amount for the segment, dq. The dq is calculated by multiplying the local temperature difference between the air and the refrigerant by the local UdA as shown in Equation E.22. All of these dqs are summed up and compared to the measured evaporator load. If the two do not equal, the refrigerant heat transfer coefficient is adjusted and the entire evaporator is recalculated. This process is repeated until the summed dq is equal to the total measured q.

$$dq = UdA(T_{a_i} - T_{r_i}) \tag{E.22}$$

A maximum error of approximately 10% was found comparing UA to UA_{sum} for the mixtures. Figures E.3 and E.4 show the errors between the two methods for the mixtures R22/R123 and R22/R141b. Examining Figure E.3 for the R22/R123 runs, nearly all the error is distributed over the freezer evaporator operating range. The freezer evaporator, as mentioned

above, has eight passes; and its UA value is approximately twice that of the four-pass fresh-food evaporator. Little or no error is distributed over the fresh-food operating range. The mean deviation for the R22/R123 runs was 7.1% with a mean deviation of 5.24% for the freezer evaporator calculations and 1.13% for the fresh-food evaporator calculations. Looking at Figure E.4 for the R22/R141b runs, the error is distributed over the operating ranges of the freezer and fresh-food evaporators. The mean deviation for these runs was 4.07% with a mean deviation of 4.06% for the freezer evaporator calculations and 4.10% for the fresh-food evaporator calculations.

Figures E.5 and E.6 explain the two different error distributions between the freezer and fresh-food evaporators for both mixtures. Figure E.5 is a plot of enthalpy versus temperature for the average evaporating pressure of 131 kPa for R22/R123. Figure E.6 is the same plot for the R22/R141b mixture for the average evaporating pressure of 145 kPa. The operational range for each evaporator is marked on the plots.

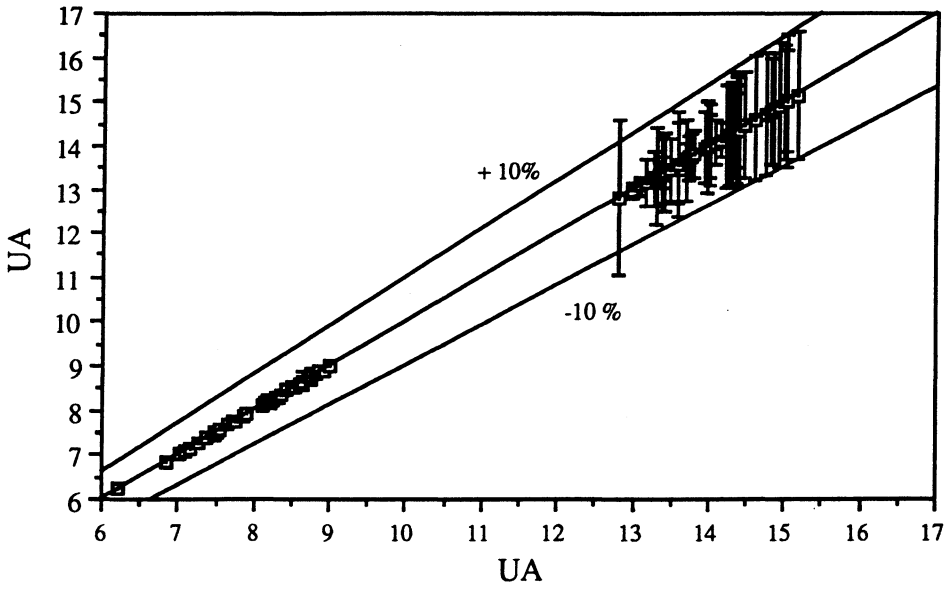

Figure E.3: Error between UA calculated from the UA/LMTD method and the segmented evaporator UA_{sum} - the mean deviations for the 65% R22/35% R123 mixture were 7.1% for both evaporators, 5.24% for the freezer evaporator, and 1.13% for the fresh-food evaporator

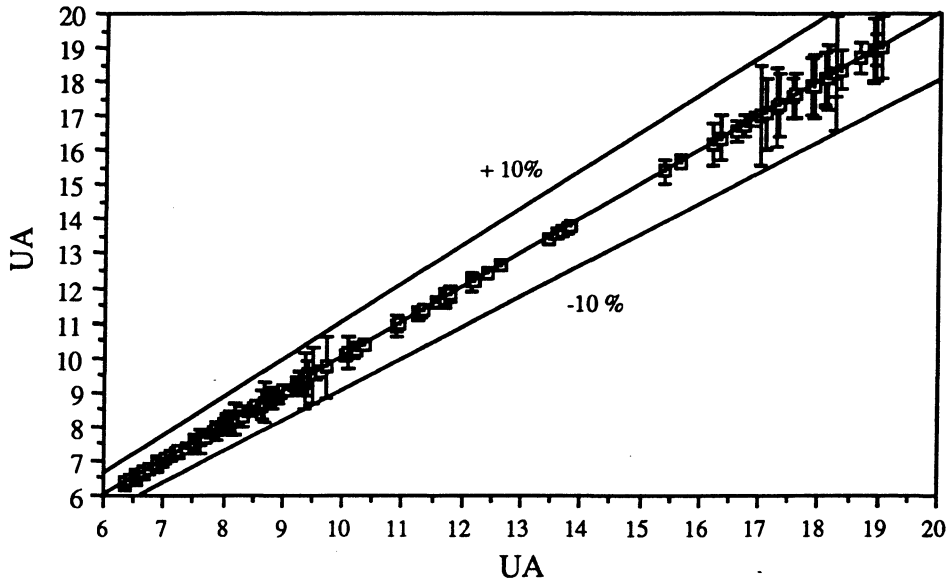

Figure E.4: Error between UA calculated from the UA/LMTD method and the segmented evaporator UA_{sum} - the mean deviations for the 80% R22/20% R141b mixture were 4.07% for both evaporators, 4.06% for the freezer evaporator, and 4.10% for the fresh-food evaporator

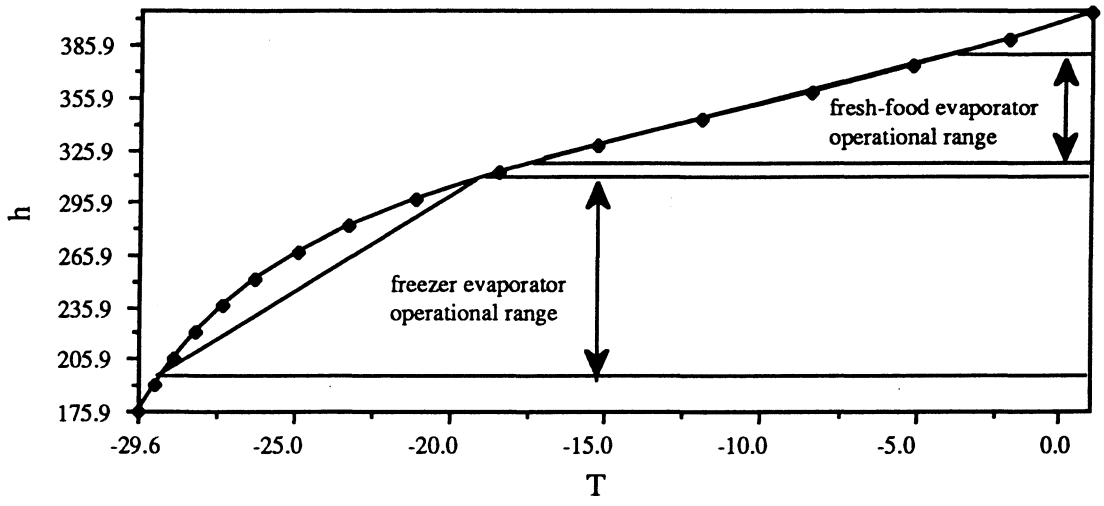

Figure E.5: Enthalpy versus temperature for the 65% R22/35% R123 mixture at an evaporating pressure of 131 kPa (the evaporator operating ranges are shown)

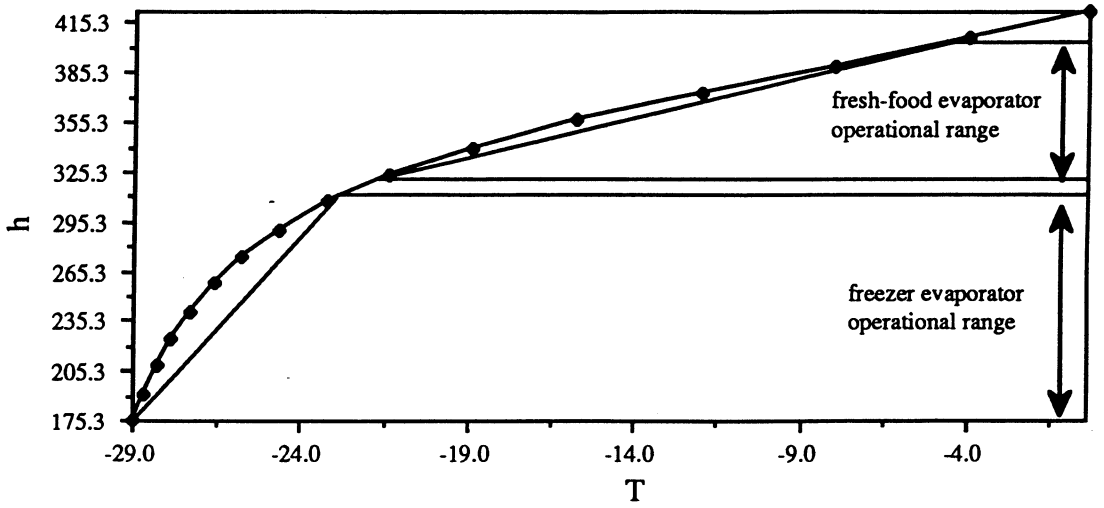

Figure E.6: Enthalpy versus temperature for the 80% R22/20% R141b mixture at an evaporating pressure of 145 kPa (the evaporator operating ranges are shown)

If the enthalpy versus temperature plots as a straight line, the specific heat of the mixture is constant. If there is curvature in the enthalpy versus temperature line, then the specific heat is varying. Notice in Figure E.5 the specific heat varies through the operation range of the freezer evaporator but is essentially constant through the fresh-food operation range. (A straight line can be superimposed on the enthalpy versus temperature line over the fresh-food operating range.) Looking back at Figure E.3, the UA/LMTD method is valid for the fresh-food evaporator because the specific heat is constant. The UA/LMTD is not valid for the freezer evaporator analysis and is in error by approximately 10% because the specific heat is not constant as shown in Figure E.5.

Because there is little or no error between the UA/LMTD method and the segmented UA_{sum} results for the fresh-food evaporator operating with R22/R123 is proof that geometry effects are negligible (as assumed in the beginning of this analysis). The specific heat of the refrigerant is constant in the fresh-food operating range as shown in Figure E.5. Since all five assumptions are valid and the UA/LMTD method is accurate, geometry effects are negligible.

The same argument applies for the R22/R141b figures, Figures E.4 and E.6. In these cases the specific heat of the mixture is varying through both the freezer and fresh-food evaporators. This is reflected in the even error distribution over the freezer and fresh-food operating ranges as shown in Figure E.4. Again, the maximum error over both ranges is limited to approximately 10%.

To be able to use the UA/LMTD method with the optimization program, a 7.1% uncertainty in the UA calculation was used for the R22/R123 mixture; and a 4.07% uncertainty was used for the R22/R141b mixture. This would account for the inaccuracies in using the UA/LMTD method with mixtures. In the final analysis with the life-cycle cost results, the consequence of using the UA/LMTD method for the heat exchanger analysis did not significantly add to the overall life-cycle cost uncertainty.

E.8 Summary

To summarize this section, the ε/NTU method can be used if the five assumptions hold and the geometry can be matched to an existing solution for that geometry. The UA/LMTD method can be used if the five assumptions hold *and* **1)** the geometry is either true parallel-flow or true counter-flow *or* **2)** $C_{min}/C_{max} \sim 0.0$ (correct solution is independent of geometry) *or* **3)** for $C_{min}/C_{max} > 0.0$, effectivenesses are 50% or less and the exchanger has three or more passes.

If neither assumption four, constant-specific heats, nor assumption five, constant overall UA, applies, then the exchanger must be broken up into small segments. The segments must be sized such that the specific heat of the fluids and their heat transfer coefficients do not change significantly over the length of the segment.

For the UA/LMTD R22/R123 and R22/R141b evaporator analysis, geometry effects were negligible and assumptions 1, 2, 3, and 5 were proved correct for this range of experiments. Assumption 4, the constant-specific heat assumption (for the refrigerant), was the source of the UA/LMTD analysis error.

E.9 References

---

[1] Incropera, F. P. and D. P. DeWitt, Fundamentals of Heat and Mass Transfer, 2nd ed., 1985, pp. 508-509.

[2] Kays, W. M. and A. L. London, Compact Heat Exchangers, 3rd ed., 1984, Fig. 2-20, p. 66.

[3] Incropera, F. P. and D. P. DeWitt, Fundamentals of Heat and Mass Transfer, 2nd ed., 1985, p. 512-515.

[4] Conklin, J. C. and E. Granryd, "Thermal Performance Analysis for Heat Exchangers Having a Variable Overall Heat Transfer Coefficient", presented at the Winter Annual Meeting of the American Society of Mechanical Engineers, December 1-6, 1991, paper 91-WA-NE-7.

---

[5] Granryd, E. and J. C. Conklin, "Thermal Performance Analysis for Heat Exchangers using Non-azeotropic Refrigerant Mixtures", presented at the Winter Annual Meeting of the American Society of Mechanical Engineers, November 25-30, 1990, paper HTD-Vol. 151, AES-Vol. 18.

[6] Conklin, J. C. and E. A. Vineyard, "Heat Exchanger Thermal Performance for Two Non-azeotropic Refrigerant Mixtures", XVIII International Congress of Refrigeration, August 10 - 17, 1991, paper # 237.

APPENDIX F: REFRIGERATOR VOLUME COST / ENERGY USE SURVEY

This appendix covers the calculation of the unit volume cost for domestic refrigerators. A survey was taken; and based on that data, a unit volume cost was determined by comparing the cost of different sized units with similar features. The power consumption per year was also calculated as a function of the unit's internal volume. General Electric and Whirlpool models were surveyed as well as Kenmore models made by General Electric and Whirlpool. The unit volume cost was required in able to determine the incremental cost of having a larger cabinet (maintaining the same internal volume) when a larger heat exchanger was required by the optimization program as described in Chapter 6.

On March 4, 1993, a survey was conducted at two local retailers to determine the cost of incremental volume for refrigerators with similar features. The two stores were Best Buy in Champaign, Illinois, and Sears, also in Champaign. Whirlpool and General Electric models were surveyed at Sears under their own names and under the Kenmore brand name. Only Whirlpool models were surveyed at the Best Buy store.

The styles consisted of all top-mount refrigerators with various options. The options broke down into four categories: with/without ice maker, with wire shelves, with glass shelves or with split-glass shelves. Comparing the prices of models with identical features, a cost per unit volume was established as well as the cost of the ice maker and shelf options.

The incremental energy consumption per unit volume was also calculated from the survey data. Based on the Energy Guide sticker on the unit, which represents the average cost of operating the unit at 0.079 $/kW-hr for one year, the average energy consumption per year was calculated.

Table F.1 lists the model number, size, energy cost and features of the units surveyed. Three units from Sears do not have any shelf information. Also, some of the models found at Sears had a combination of split-glass shelves and glass shelves.

Figures F.1, F.2 and F.3 are based on the information in Table F.1. Figure F.1 shows the cost versus volume and power consumption versus volume plots on a double y axis graph for the Whirlpool models from Best Buy with split-glass shelves. Notice that the relationship between cost and volume is approximately linear. The slope of the line is 41.66 indicating that the incremental volume cost is $\$41.66/ft^3$. The relationship between power consumption and volume is not as linear as the cost/volume relationship. The slope of the best fit line for this data is 17.625 indicating that 17.625 kW-hr/yr are required for each ft^3 of additional volume.

Table F.1: Comparison of various Whirlpool and General Electric top-mount refrigerators with various features

man.	model #	store	cost	size	Energy Guide	ice maker	wire shelves	glass shelves	split glass shelves
WP	ET18NKXA	Best B	548.76	18.1	54		X		
WP	ET18NKXA	Best B	597.91	18.1	54	X	X		
WP	ET18NKXA	Best B	628.82	18.1	54			X	
WP	ET18NKXA	Best B	627.96	19.9	56		X		
WP	ET18NKXA	Best B	727.83	19.9	56			X	
WP	ET18NKXA	Best B	727.83	18.1	49				X
WP	ET18NKXA	Best B	798.75	19.9	51				X
WP	ET18NKXA	Best B	877.82	21.7	54				X
GE	61961-8	Sears	749.99	19.1	71				X
WP	63031-8	Sears	679.99	19.9	56		X		
GE	63141-8	Sears	729.99	20.62	59		X		
GE#	63151-8	Sears	729.99	20.62	59			X	X
GE	63171-2-8	Sears	779.99	20.62	59				X
WP	63261-8	Sears	779.99	21.7	54	X			X
WP*#	80272-8	Sears	929.99	21.7	54				
GE#	63851-8	Sears	629.99	18.19	55			X	X
WP#	63061-8	Sears	699.99	19.9	56				X
GE#	63471-2-8	Sears	899.99	23.61	57				X
GE	63571-2-5-8	Sears	1049.99	24.73	58	X			
WP#	63861-8	Sears	669.99	18.1	58				X
GE#	63871-8	Sears	659.99	18.19	55				X
WP*#	80842-8	Sears	629.99	18.1	54		X		
WP*#	80862-8	Sears	699.99	18.1	54			X	X
WP#	63821-8	Sears	549.99	18.1	54		X		
GE	63651-8	Sears	599.99	15.62	50				X
GE	63421-8	Sears	529.99	14.26	48		X		
WP	69221-8	Sears	489.99	11.56	62				
GE*	84191-8	Sears	729.99	20.7	74				X
GE*	84471-8	Sears	849.93	23.6	71			X	X
GE*	82832-8	Sears	629.99	18.2	55		X		
GE*	84871-8	Sears	629.99	18.2	68				X

- 1993 Energy Saving Standards in Effect * - under own name not Kenmore

Figure F.2 shows the cost versus volume plot for all Whirlpool models from Best Buy after the cost of the units was adjusted to compensate for the various options. It was determined that the incremental cost for an ice maker is $50.15, for glass shelves, $81.06, and for split-glass shelves, $180.07. The incremental volume cost is $43.02/ft^3.

Figure F.3 shows the cost versus volume plot for all Whirlpool and GE models with split-glass shelves from Best Buy and Sears. The best fit line yields an incremental volume cost of $46.94/ft^3. The value chosen for the economic simulation is an average of the results from Figures F.1, F.2 and F.3. The average incremental volume cost is $44/ft^3.

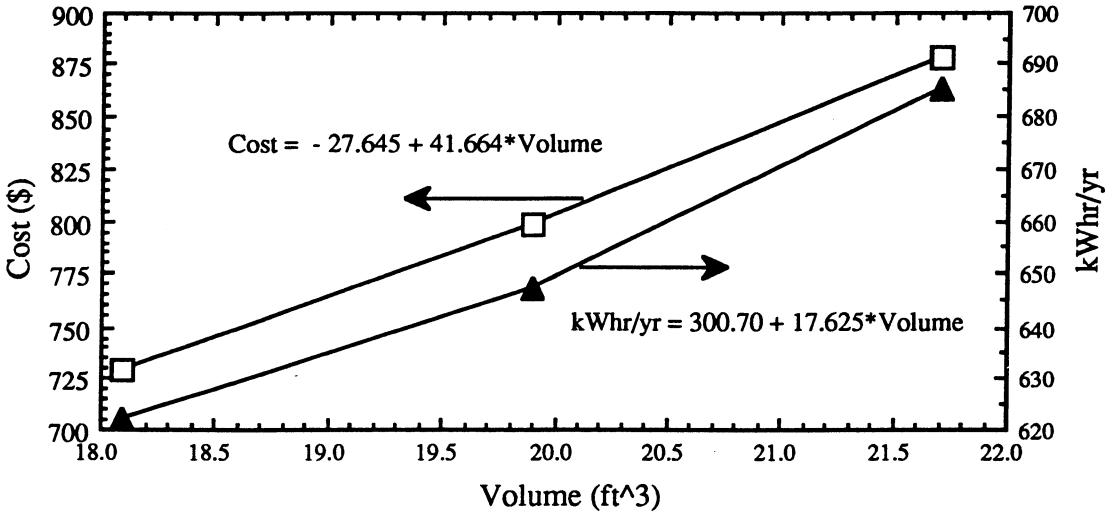

Figure F.1: Whirlpool models from Best Buy with split-glass shelves

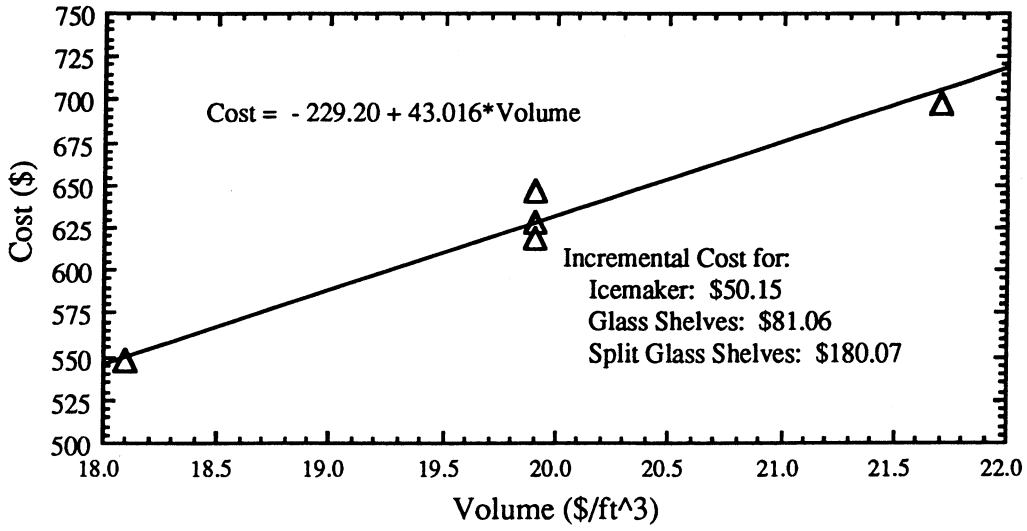

Figure F.2: All whirlpool models from Best Buy - adjusted cost comparison

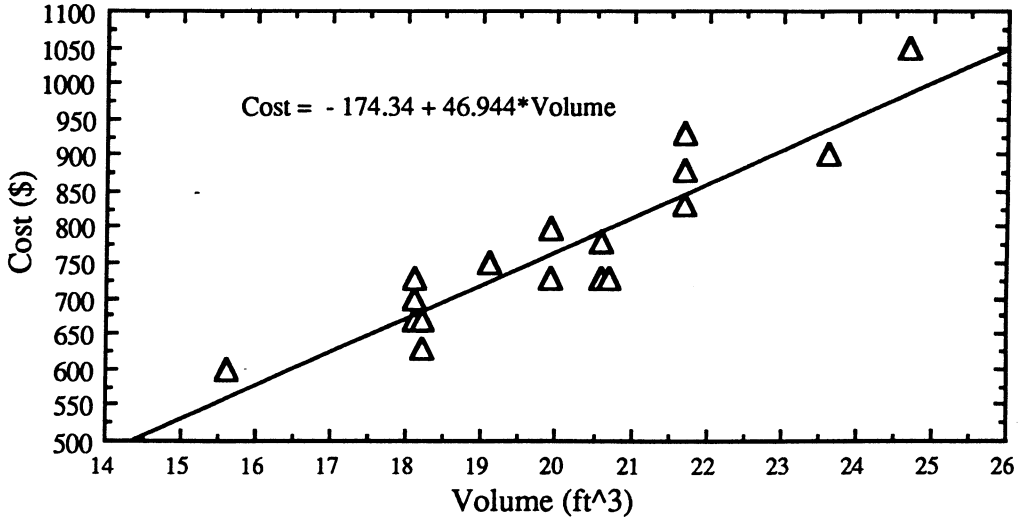

Figure F.3: Whirlpool and General Electric Models with split-glass shelves from Best Buy and Sears

APPENDIX G: CABINET CONSTRUCTION / REVERSE HEAT-LEAK TESTS

This appendix describes the construction and reverse heat-leak testing of an insulated box used in this experiment as a refrigerator cabinet mockup. The box was constructed out of commercially available foam board. The reverse heat-leak tests were performed in an environmental test chamber. The UA value of the cabinet was required to determine the total evaporator load, which included heat-leak from the environment, for each compartment.

It was necessary for the experiment to build a well-insulated box that would have the same internal dimensions as a typical domestic refrigerator cabinet. The box would contain the required heat exchangers, two evaporators and two intercoolers. One evaporator was placed in the top (freezer) compartment, and the other evaporator was placed in the bottom (fresh-food) compartment. The intercoolers were placed vertically in the fresh-food compartment due to space constraints in the freezer compartment.

In order to be able to determine the total load on each evaporator, the energy transferred through the box wall (cabinet load) was required. The load on each evaporator was the sum of the auxiliary heater power in that compartment plus the heat leak through the cabinet walls at steady state as shown in Equation G.1 for the freezer compartment.

$$q_f = UA_{f(w/o-mul)}(T_{amb} - T_f) + UA_{mul}(T_{ff} - T_f) + Power_f \qquad (G.1)$$

Notice that the heat leak from the fresh-food compartment must also be taken into account. The wall that separates the freezer and fresh-food compartments is called the mullion, and the driving temperature difference is T_{ff} - T_f. The UA values for the freezer and fresh-food compartments (less mullion) and the mullion UA value had to be determined through a series of reverse heat-leak tests.

G.1 Construction

Figure G.1 shows the plans for the insulated box. The box was constructed of 2.54 cm (1 in) Cellotex foam boards. The internal dimensions duplicate those of a General Electric 18 ft^3 refrigerator. The walls are a total of 10.16 cm (4 in) thick with an R-value of 7 per inch giving the walls a nominal R-value of 28. The mullion is 6.36 cm (2.5 in) thick and is removable. The boards were assembled with aluminum tape and clear silicon caulk. All corners were staggered and a thermal break was cut along the door lip to prevent conductive edge losses along the foam board foil covering. Foam tape was applied to ensure an air tight seal around the door edges.

The doors were held on with ten rubber straps connected to thick dowels which ensured that the door seal was tight away from the strap-applied pressure points.

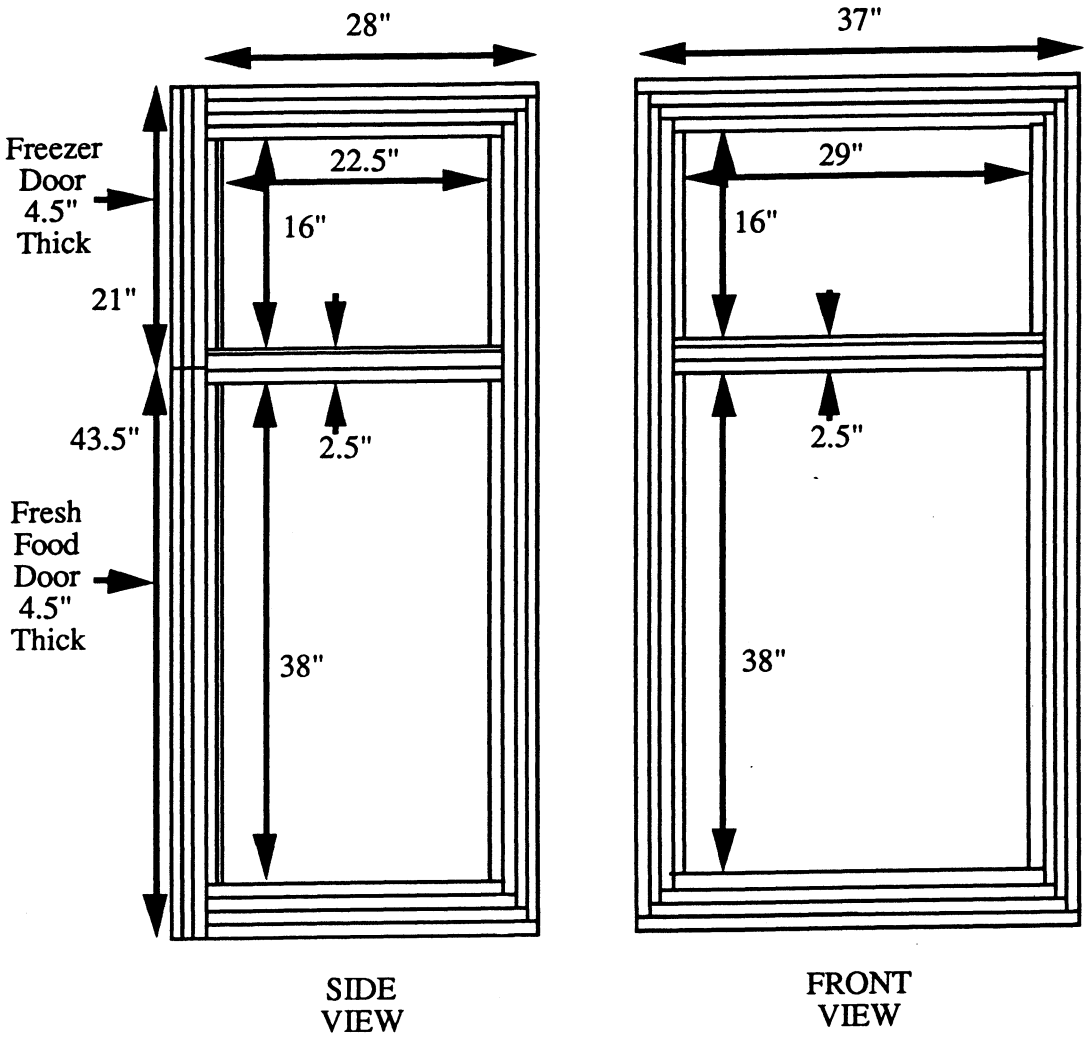

Figure G.1: Layout and dimensions of the insulated box used for the experiment (all dimensions in inches)

Damage to the foam boards could easily be repaired using a commercially available insulating foam. After the damaged areas were filled, they were covered with aluminum tape. Tears that developed in the foil surface were also fixed with aluminum tape. The box took approximately 14-1 inch and 1-0.5 inch 4 foot by 8 foot Cellotex sheets at a cost of $15 per sheet. With the aluminum tape, caulk, dowels and straps, the total material cost of the unit was approximately $300.

G.2 Reverse Heat-Leak Tests

The insulated box built for the experiment had to be tested to determine the UA values for each compartment and the mullion. Reverse heat-leak tests were conducted in the Air Conditioning and Refrigeration Center's environmental test chamber. The reverse heat-leak tests were carried out by maintaining the temperature inside the insulated box higher than the ambient (test chamber) temperature. At steady state, the power required to maintain constant temperature inside the box with an auxiliary heater with the ambient and box temperatures were used to calculate the compartment's UA value.

Four runs were conducted, and two types of tests were required for each run. The first test required that both compartment doors be closed and the auxiliary heaters were set to maintain identical temperatures in both compartments approximately 28°C (50°F) higher than the test chamber temperature. Equations G.2 and G.3 were used to calculate the UA values for each compartment less the mullion UA. Referring to Equation G.1, because $T_f = T_{ff}$ there was no contribution to the load from the mullion; furthermore, q_f was zero because the evaporators were not in the compartment and functioning for the tests.

$$UA_{f(w/o-mul)} = \frac{Power_f}{(T_f - T_{amb})} \tag{G.2}$$

$$UA_{ff(w/o-mul)} = \frac{Power_{ff}}{(T_{ff} - T_{amb})} \tag{G.3}$$

The second test required that only the fresh-food compartment door be closed. This test gave the UA of the fresh-food compartment with the mullion UA included, $UA_{ff(w-mul)}$. The mullion UA is calculated in Equation G.4.

$$UA_{mul} = UA_{ff(w-mul)} - UA_{ff(w/o-mul)} \tag{G.4}$$

The results from the four runs were averaged to give the final values of $UA_{f(w/o-mul)}$, $UA_{ff(w/o-mul)}$ and UA_{mul}. Constant temperature was maintained in each compartment with the auxiliary heaters (modified hair dryers). These hair dryers were placed to provided a circulating air pattern within each compartment to minimize stagnate air pockets. The hair dryer's wiring was connected to the test chamber controllers. The step down transformers for the hair dryer blower motors were in each respective compartment. The total power consumed by the hair dryer blower motor, heating element and step down transformer was measured by watt

transducers which were an integral part of the test chamber. The auxiliary heating control system is explained in detail in Appendix H.

The tests ranged in time from 135 minutes to 550 minutes. The data were taken after the cabinet came to steady state. Typically the heaters (hair dryers) were allowed to run overnight to ensure that the cabinet was at steady state before the tests were started. As expected, the data were flat over the test interval. Table G.1 gives the ambient temperature, freezer temperature, fresh-food temperature and heater powers for the four test runs. Table G.2 gives the results for the mullion tests where the freezer door was left open. The UA value of the mullion is calculated from Equation G.4.

Table G.1: Summary of $UA_{f(w/o\text{-}mul)}$ and $UA_{ff(w/o\text{-}mul)}$ tests

test	time at steady state (min)	ambient temp. (°C)	freezer temp. (°C)	fresh-food temp. (°C)	freezer heater power (W)	fresh-food heater power (W)	$UA_{f(w/o\text{-}mul)}$ (W/K)	$UA_{ff(w/o\text{-}mul)}$ (W/K)
1	400	11.67	36.98	36.98	14.18	22.78	0.560	0.900
2	135	11.63	37.02	37.02	14.45	23.54	0.569	0.927
3	250	10.27	36.77	36.77	15.61	23.39	0.589	0.883
4	250	9.56	36.72	36.85	13.17	26.95	0.485	0.988
Ave.							0.551	0.925

Table G.2: Summary of $UA_{ff(w\text{-}mul)}$ tests

test	time at steady state (min)	ambient temp. (°C)	fresh-food temp. (°C)	fresh-food heater power (W)	$UA_{ff(w\text{-}mul)}$ (W/K)
1	550	10.08	36.72	36.30	1.363
2	400	9.59	36.63	35.48	1.312
Ave.					1.338

As a check, the UA values of the box were calculated using the known R-value of the foam board and the outside dimensions of the box. Table G.3 summarizes the findings for the UA values showing the comparison to the calculated UA values. The calculated method under-predicts the experimental values. Notice the measured UA values of the two compartments are within 20% of the calculated values. Only the UA of the mullion shows a large error. This error is due to finning effects caused by the foam board foil covering. The finning effectively increases the exposed area of the mullion and causes the experimental results to exceed the calculated values.

Table G.3: Comparison of experimental and calculated UA values for insulated box

configuration	UA experimental (W/K)	UA calculated (W/K)	percent difference
$UA_{F(w/o\text{-}mul)}$	0.551	0.497	-9.8
$UA_{FF(w/o\text{-}mul)}$	0.925	0.877	-5.2
$UA_{FF(w\text{-}mul)}$	1.338	1.110	-17.0
UA_{mul}	0.413	0.232	-43.8

APPENDIX H: REFRIGERATOR MOCKUP LOAD CONTROL SYSTEM

This appendix describes the load control system used to load the evaporators during the experimental runs. In order to load the evaporators in the freezer and fresh-food compartments, a load control system had to be built and tested. The design followed that of Staley.[1] The total load on each evaporator was determined by summing the load from the load control system and the heat-leak load through the cabinet from the surroundings as explained in the beginning of Appendix G. The design and operation of the system will be covered.

H.1 Design

A modified, commercially-available hair dryer was used as the load device. The hair dryer was rewired so the internal fan would run continuously and so the heating elements were in series, reducing the heating output. The continuously running fan served to prevent stratification of the air in the compartment ensuring uniform temperature distribution at the inlet of the evaporator.

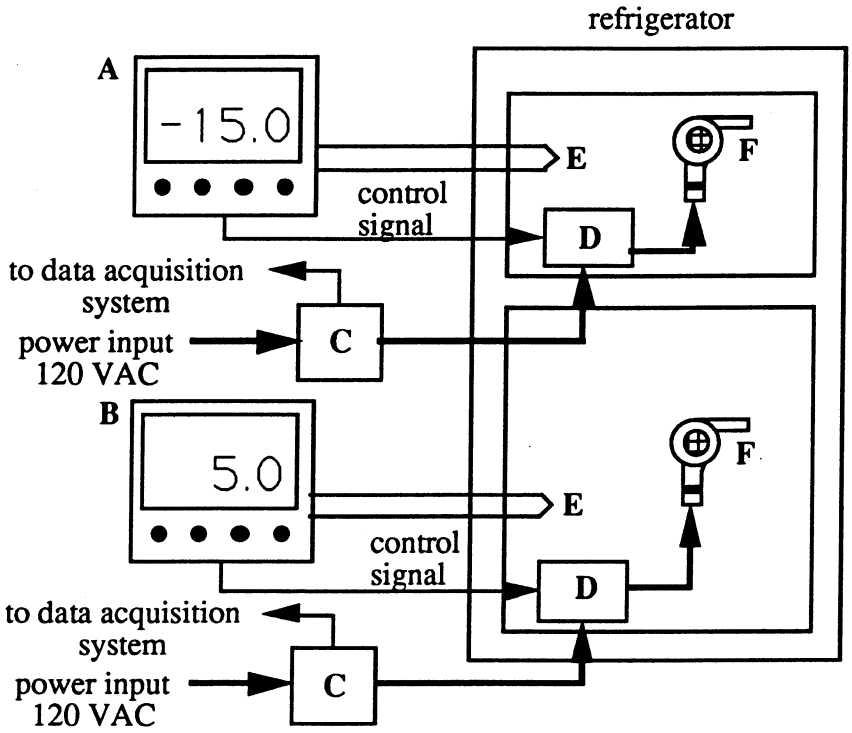

Figure H.1: Load control system: A - freezer temperature controller, B - fresh-food temperature controller, C - watt transducer & signal conditioner, D - control box, E - thermocouple, and F - hair dryer assembly[2]

The system consisted of a PID (proportional, integral, derivative) temperature controller, a hair dryer, a control box for the hair dryer containing a step-down transformer and a solid-state relay, and a watt meter. Two identical systems were built, one for the freezer compartment and one for the fresh-food compartment. Figure H.1 shows the load control systems. Since the transformer and solid-state relay dissipate heat during operation, an energy balance error would have occurred if the control box were not placed in the compartment with the hair dryer.

H.2 Operation

The user inputs a set-point temperature to the PID controller. The controller sends a pulse width modulated control signal to the solid-state relay which in turn switches the heater in the hair dryer on or off depending on the temperature level inside the compartment. The watt meter measures the power consumed by the heater, the hair dryer fan, the step-down transformer and the solid-state relay. This power measurement is read by the data acquisition system.

The output of the watt meter to the data acquisition sensor had to be smoothed. The pulse width modulated control signal produced a square wave power output curve. The average power drawn by the heater system, not the instantaneous power, was the quantity of interest. An averaging circuit was added to the output circuitry of the watt meter to obtain an average power output reading.

The averaging circuit is an RC circuit, a low pass filter, consisting of only a single resistor and capacitor. Research done by Staley[3] showed that the optimum time constant to properly smooth the output was 24 seconds. To achieve this time constant a 470 micro farad capacitor and a 51 kilo Ohm resistor were chosen.

To ensure accurate measurement of the averaged power reading, the output to the data acquisition system was buffered with a simple op amp circuit. This prevented voltage signal attenuation which would occur because the filtering circuit raised the output impedance of the system to the same order of magnitude as the input impedance of the data acquisition system. Verification studies on an identical load control system have been done by Staley.[4] Figure H.2 shows the complete load system schematic.

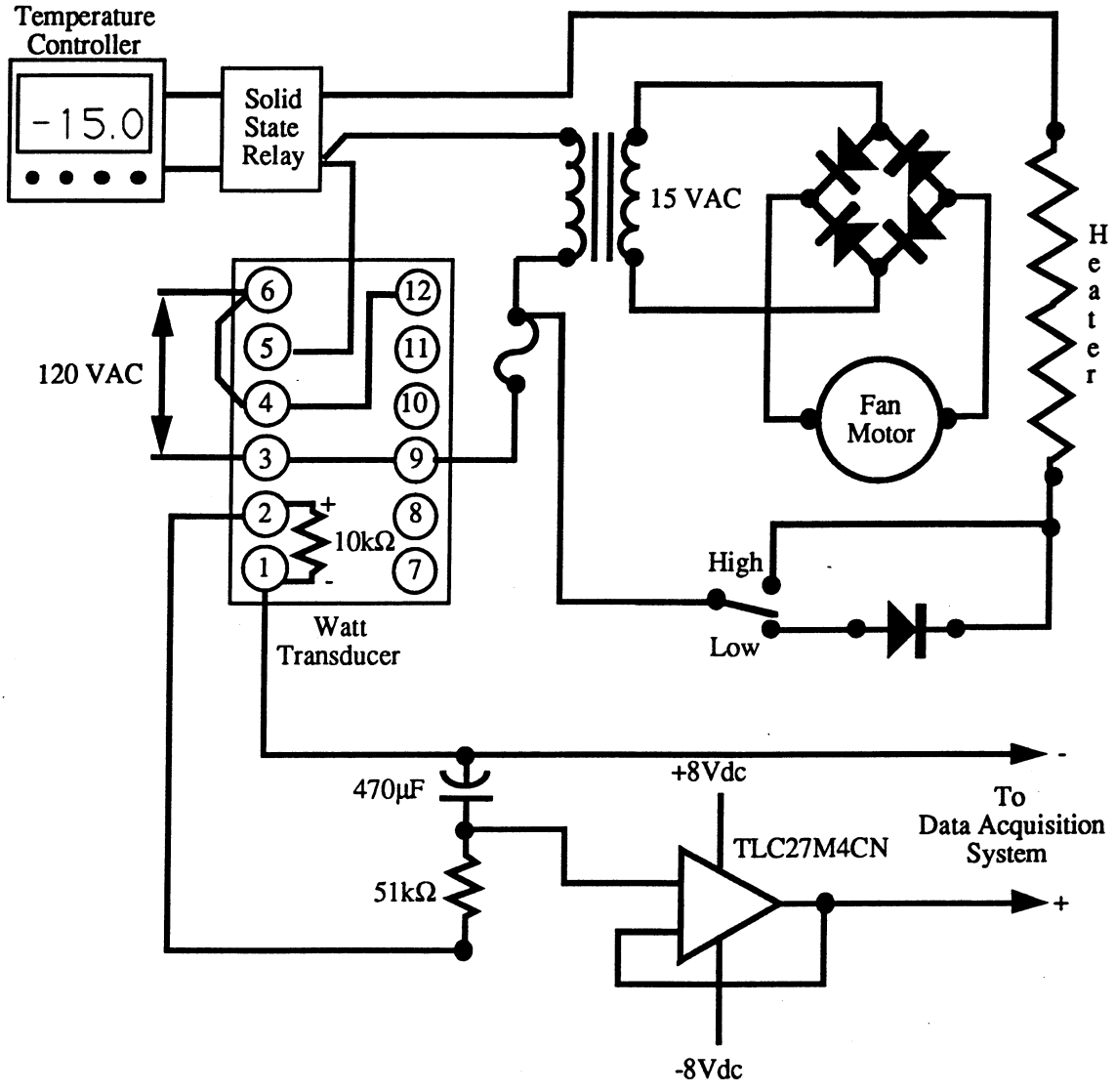

Figure H.2: Load control system schematic[5]

H.3 References

---

[1] Staley, D. M, "Steady-State Performance of a Domestic Refrigerator/Freezer Using R12 and R134a", Master's Thesis, Department of Mechanical Engineering, University of Illinois at Urbana-Champaign, June, 1992, pp. 15-22.

[2] Staley, D. M, "Steady-State Performance of a Domestic Refrigerator/Freezer Using R12 and R134a", Master's Thesis, Department of Mechanical Engineering, University of Illinois at Urbana-Champaign, June, 1992, modified Fig. 3-4, p. 16.

---

[3] Staley, D. M, "Steady-State Performance of a Domestic Refrigerator/Freezer Using R12 and R134a", Master's Thesis, Department of Mechanical Engineering, University of Illinois at Urbana-Champaign, June, 1992, pp. 17-18.

[4] Staley, D. M, "Steady-State Performance of a Domestic Refrigerator/Freezer Using R12 and R134a", Master's Thesis, Department of Mechanical Engineering, University of Illinois at Urbana-Champaign, June, 1992, pp. 19-22.

[5] Staley, D. M, "Steady-State Performance of a Domestic Refrigerator/Freezer Using R12 and R134a", Master's Thesis, Department of Mechanical Engineering, University of Illinois at Urbana-Champaign, June, 1992, modified Fig. 3-5, p. 17.

APPENDIX I: DATA ACQUISITION PROGRAM

This appendix contains a brief description of the data acquisition program used in this experiment with a sample output screen followed by a complete listing of the program. The program was run on a Macintosh SE microcomputer which was gathering data from a Fluke 2240A Datalogger as described in Chapter 3. The program was written in True BASIC and utilized a commercially available subroutine library to enable communication with the Macintosh serial port.

I.1 Program Description

The program was written to incorporate on screen graphics to display major operating variables over the test run period. At a glance, the user could tell if the system was operating at or near steady state. In each plot window, the current value, low, high and average value of the variable were displayed. There were eight plot windows with three windows tracking two variables each. Figure I.1 shows a sample screen output from the program. The upper left window shows the amount of subcooling, SC, entering the evaporator module at point 1. (The system state points are defined in Chapter 3.) The upper right window shows the air velocity over the freezer and fresh-food evaporators, VelF-b and VelFF, calculated from an energy balance on the air. (The freezer air velocity is the solid black line denoted by the -b extension on VelF.) The second line of plot windows display the compartment temperature and the evaporator air-inlet temperature (TF-b, TFin and TFF-b, TFFin). The freezer temperatures are on the left, and the fresh-food temperatures are on the right. (The compartment temperatures are the solid black lines denoted by the -b extension.) The third line of windows display the evaporator loads, LF and LFF. The freezer load is on the left, and the fresh-food load is on the right. The bottom left window displays the amount of superheat, SH8, leaving the evaporator module at point 8. The bottom right window shows the refrigerant mass-flow rate, mdot, over the test run period.

At the top of the output screen, the program displays the total run time for the current test. To the right, the program gives the user the option of stopping the program by typing 'Q' or changing the graph x or y ranges while the program continues to run by hitting the space bar. The left column of numbers displays the current temperatures at all eight of the evaporator module state points with the low, high and average values to the right. At the bottom of the left column, the time base for the graphs, the total evaporator load, and the load split ratio are displayed. The second line from the top of the right column displays the temperature and pressure immediately following the gear pump. The next four lines display the pressure at stations 1, 3, 4 and 8. Next, the temperature and pressure immediately following the chiller are

displayed. The third to the last line displays the temperature difference between the evaporator inlet air minus the evaporator outlet air. The freezer value is on the left, and the fresh-food value is on the right. The next line is the respective air-flow rates over the evaporators in cubic feet per minute. Lastly, the amount of superheat (if any) is displayed for station 7.

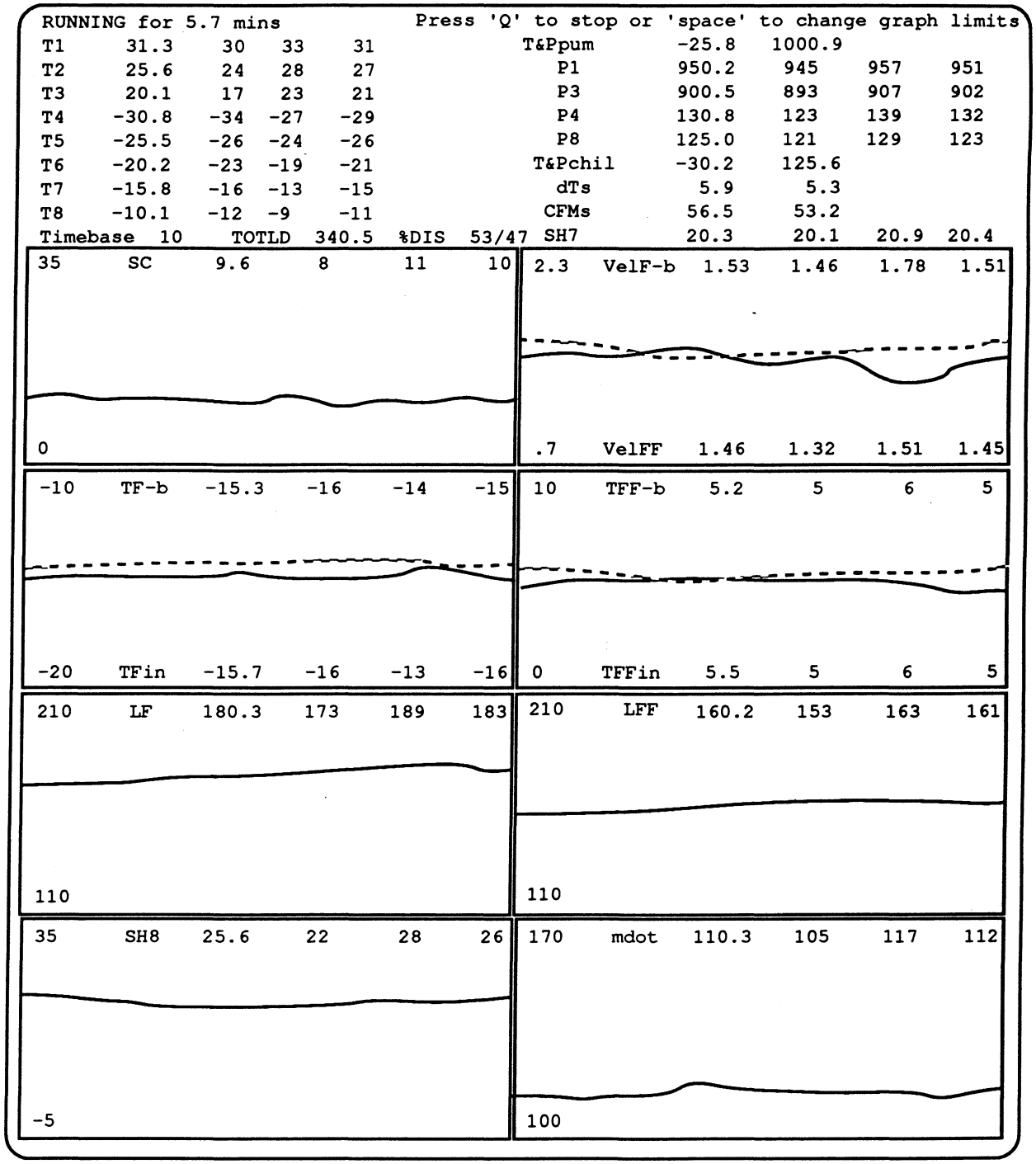

Figure I.1: Sample data acquisition screen

The scan time was once every six seconds or ten times a minute. When a run was started, the program would track all the variables storing their low, high, average and standard deviation values in an output file. Each run was a minimum of ten minutes in length. Ten minutes was chosen to ensure that any short term fluctuations in the data was sufficiently smoothed by averaging the data. During a particular run, if the standard deviation value for any variable was unusually 'large', then the run was thrown out.

I.2 Program Listing

```
LIBRARY "Comlib*"
DIM Data(0 To 60)
DIM T(0 To 10)
DIM P(0 To 10)
DIM Pmin(0 To 10)
DIM Pmax(0 To 10)
DIM Psum(0 To 10)
DIM Psumsq(0 To 10)
DIM Pstdev(0 To 10)
DIM Tmin(0 To 10)
DIM Tmax(0 To 10)
DIM Tsum(0 To 10)
DIM Tsumsq(0 To 10)
DIM Tstdev(0 To 10)

CALL InitializeDA

DO
  CALL Receive (S$)          ! Get Any Input From Network
  IF S$ <> "" Then CALL Process(S$)  ! Routine To Store Data
LOOP

SUB Calcs
   DECLARE DEF Cpair,Phoair,SuperH,SubC
   !First, Reassign The Temperatures And Pressures To Make The
   !Code Readable.

   LET Count = Count + 1
   LET runtime = (time-tymestart)/60

   LET T(1) = Data(31)
   LET T(2) = Data(32)
   LET T(3) = Data(33)
   LET T(4) = Data(34)
   LET T(5) = Data(35)
   LET T(6) = Data(36)
   LET T(7) = Data(37)
   LET T(8) = Data(38)

   LET Tamb = Data(30)
   CALL Minmaxstat(Tamb,Tambmin,Tambmax,Tambsum,Tambsumsq,Tambstdev)
   LET Tchil = Data(46)
   CALL Minmaxstat(Tchil,Tchilmin,Tchilmax,Tchilsum,Tchilsumsq,Tchilstdev)
```

```
LET Tpum = Data(47)
CALL Minmaxstat(Tpum,Tpummin,Tpummax,Tpumsum,Tpumsumsq,Tpumstdev)

LET TFin = Data(40)
CALL Minmaxstat(TFin,TFinmin,TFinmax,TFinsum,TFinsumsq,TFinstdev)
LET DTF = Data(41)
CALL Minmaxstat(DTF,DTFmin,DTFmax,DTFsum,DTFsumsq,DTFstdev)
LET TF = Data(42)
CALL Minmaxstat(TF,TFmin,TFmax,TFsum,TFsumsq,TFstdev)

LET TFFin = Data(43)
CALL Minmaxstat(TFFin,TFFinmin,TFFinmax,TFFinsum,TFFinsumsq,TFFinstdev)
LET DTFF = Data(44)
CALL Minmaxstat(DTFF,DTFFmin,DTFFmax,DTFFsum,DTFFsumsq,DTFFstdev)
LET TFF = Data(45)
CALL Minmaxstat(TFF,TFFmin,TFFmax,TFFsum,TFFsumsq,TFFstdev)

LET PowF = Data(53)
LET PowFF = Data(54)

LET Ppum = Data(55)
CALL Minmaxstat(Ppum,Ppummin,Ppummax,Ppumsum,Ppumsumsq,Ppumstdev)
LET Mdot = Data(59)
CALL Minmaxstat(Mdot,Mdotmin,Mdotmax,Mdotsum,Mdotsumsq,Mdotstdev)

LET P(1) = Data(56)
LET P(3) = Data(51)
LET P(4) = Data(57)
LET P(8) = Data(58)
LET P(2) = P(1)-0.66667*(P(1)-P(3))
LET P(5) = P(4)-.66667*(P(4)-P(8))
LET P(6) = P(5)
LET P(7) = P(8)+.3334*(P(4)-P(8))

FOR kk = 1 to 8
  CALL Minmaxstat(T(kk),Tmin(kk),Tmax(kk),Tsum(kk),Tsumsq(kk),Tstdev(kk))
  CALL Minmaxstat(P(kk),Pmin(kk),Pmax(kk),Psum(kk),Psumsq(kk),Pstdev(kk))
NEXT kk

!Calculate The Heat Input To Each Compartment
!This Is The Sum Of The Heat Leak Into Each Cabinet And The Power
!Dissipated By The Variac And Hair Dryer In Each Cabinet.

LET UAcabF = .5508          !W/K
LET UAcabFF = .9245         !W/K
LET UAcabint = 1.3375 - .9245     !W/K
LET FLeak = UAcabF*(Tamb-TF) + UAcabint*(TFF-TF)  !Answer In Watts
LET FFLeak = UAcabFF*(Tamb-TFF) - UAcabint*(TFF-TF)   !Answer In Watts
LET FLoad = PowF + FLeak     !Watts
CALL Minmaxstat(FLoad,FLoadmin,FLoadmax,FLoadsum,FLoadsumsq,FLoadstdev)
LET FFLoad = PowFF + FFLeak   !Watts
CALL Minmaxstat(FFLoad,FFLoadmin,FFLoadmax,FFLoadsum,FFLoadsumsq,FFLoadstdev)

!Calculate The Air Velocities In Each Evaporator.  They Must Be Between
!.3 - .8 M/S To Be In The Same Range As Matt'S Experimental Data.

LET Area = 24*1.125*2.54^2*(1/100)^2
```

```
    IF DTFF > .01 THEN
      LET VelFF = FFLoad/(Phoair(TFFin-DTFF/2)*Cpair(TFFin-DTFF/2)*DTFF*Area)
      LET MdotFF = FFLoad/(Cpair(TFFin-DTFF/2)*DTFF)
    ELSE
      LET VelFF = 5
      LET MdotFF = 5
    END IF
    CALL Minmaxstat(VelFF,VelFFmin,VelFFmax,VelFFsum,VelFFsumsq,VelFFstdev)
    CALL Minmaxstat(MdotFF,MdotFFmin,MdotFFmax,MdotFFsum,MdotFFsumsq,MdotFFstdev)

    IF DTF > .01 THEN
      LET VelF = FLoad/(Phoair(TFin-DTF/2)*Cpair(TFin-DTF/2)*DTF*Area)
      LET MdotF = FLoad/(Cpair(TFin-DFF/2)*DTF)
    ELSE
      LET VelF = 5
      LET MdotF = 5
    END IF
    CALL Minmaxstat(VelF,VelFmin,VelFmax,VelFsum,VelFsumsq,VelFstdev)
    CALL Minmaxstat(MdotF,MdotFmin,MdotFmax,MdotFsum,MdotFsumsq,MdotFstdev)

    LET CFMFF = (60*VelFF*Area/.3048^3)
    CALL Minmaxstat(CFMFF,CFMFFmin,CFMFFmax,CFMFFsum,CFMFFsumsq,CFMFFstdev)

    LET CFMF = (60*VelF*Area/.3048^3)
    CALL Minmaxstat(CFMF,CFMFmin,CFMFmax,CFMFsum,CFMFsumsq,CFMFstdev)

    !Get Sat Temps Based On Pressure

    LET SH = T(8)-SuperH(P(8))
    CALL Minmaxstat(SH,SHmin,SHmax,SHsum,SHsumsq,SHstdev)
    LET SH7 = T(7)-SuperH(P(7))
    CALL Minmaxstat(SH7,SH7min,SH7max,SH7sum,SH7sumsq,SH7stdev)

    LET SC1 = SubC(P(1))-T(1)
    CALL Minmaxstat(SC1,SC1min,SC1max,SC1sum,SC1sumsq,SC1stdev)

    CALL ScreenOutput
END SUB

SUB ScreenOutput
    !Print The Results To The Screen
    WINDOW #12
    SET CURSOR 1,1
    IF end = 1 then
      PRINT "HALTED:                Press 'S' to start or 'space' to change graph limits"
    ELSE
      PRINT USING Format$: runtime
    END IF
    PRINT USING Format2$: "T1",T(1),Tsum(1)/Count,Tmin(1),Tmax(1),"T&Ppum",Tpum,Ppum
    PRINT USING Format1$:
"T2",T(2),Tsum(2)/Count,Tmin(2),Tmax(2),"P1",P(1),Psum(1)/Count,Pmin(1),Pmax(1)
    PRINT USING Format1$:
"T3",T(3),Tsum(3)/Count,Tmin(3),Tmax(3),"P3",P(3),Psum(3)/Count,Pmin(3),Pmax(3)
    PRINT USING Format1$:
"T4",T(4),Tsum(4)/Count,Tmin(4),Tmax(5),"P4",P(4),Psum(4)/Count,Pmin(4),Pmax(4)
```

```
    PRINT USING Format1$:
 "T5",T(5),Tsum(5)/Count,Tmin(5),Tmax(5),"P8",P(8),Psum(8)/Count,Pmin(8),Pmax(8)
    PRINT USING Format2$: "T6",T(6),Tsum(6)/Count,Tmin(6),Tmax(6),"T&Pchil",Tchil, P(8)
    PRINT USING Format2$: "T7",T(7),Tsum(7)/Count,Tmin(7),Tmax(7),"dTs",DTF,DTFF
    PRINT USING Format2$: "T8",T(8),Tsum(8)/Count,Tmin(8),Tmax(8),"CFMs",CFMF,CFMFF
    LET Totld = FLoad+FFload
    IF Totld=0 THEN LET totld=1
    LET DIS = 100*FLOAD/Totld
    PRINT USING Format3$: "Timebase",Plen/10,"TOTLD",Totld,"%DIS",DIS,100-
  DIS,"SH7",SH7,SH7sum/Count,SH7min,SH7max

    !Plot Graphs
    CALL PLOTTING(22,Mdot,Mdotsum/count,Mdotmax,Mdotmin,Lbmdot,Ubmdot,"mdot",0)
    CALL PLOTTING(32,FFLoad,FFLoadsum/count,FFLoadmax,FFLoadmin,Lbload1,Ubload1,"LFF",0)
    CALL PLOTTING(42,FLoad,FLoadsum/count,FLoadmax,FLoadmin,Lbload2,Ubload2,"LF",0)
    CALL PLOTTING(52,SH,SHsum/count,SHmax,SHmin,Lbsh,Ubsh,"SH8",0)
    CALL PLOTTING(53,SC1,SC1sum/count,SC1max,SC1min,Lbsc,Ubsc,"SC",0)
    CALL PLOTTING(62,TF,TFsum/count,TFmax,TFmin,LbTF,UbTF,"TF-b",0)
    CALL OVERLAY(63,TFin,TFinsum/count,TFinmax,TFinmin,LbTF,UbTF,"TFin",0)
    CALL PLOTTING(72,TFF,TFFsum/count,TFFmax,TFFmin,LbTFF,UbTFF,"TFF-b",0)
    CALL OVERLAY(73,TFFin,TFFinsum/count,TFFinmax,TFFinmin,LbTFF,UbTFF,"TFFin",0)
    CALL PLOTTING(92,VelF,VelFsum/count,VelFmax,VelFmin,LbVelFF,UbVelFF,"VelF-b",2)
    CALL OVERLAY(82,VelFF,VelFFsum/count,VelFFmax,VelFFmin,LbVelFF,UbVelFF,"VelFF",2)

    IF Key Input Then
      GET KEY Z
      IF Z=32 Then
        ! Key = 32 Is The Space Bar
        CALL SETAXIS
        IF zz <> 9 then LET I = Plen
      END IF
      IF Z=113 Then
        ! Key = 113 Is The Letter 'Q' For Quitting
        CALL WRITEFILE
        LET End = 1
        CALL SETSTAT
        LET count = 0
      END IF
      IF End = 1 THEN
        IF Z=115 Then
          ! Key = 115 Is The Letter 'S' For Starting
          CALL SETSTAT
          LET Count = 0
          LET End = 0
          LET Tymestart = Time
        END IF
      END IF
    END IF

    LET I = I+1
    IF I>Plen Then
      LET I=0
      CALL DRAWGRAPHS
    END IF
END SUB

SUB PLOTTING(nu,plotvar,ave,high,low,lowbd,upbd,tit$,mu)
```

```
    WINDOW #nu
    LET plotvardis=round(plotvar,rnu+1)
    LET avedis=round(ave,rnu)
    LET lowdis=round(low,rnu)
    LET highdis=round(high,rnu)
    SET COLOR 5
    BOX AREA .1*plen,.99*plen,upbd-(upbd-lowbd)*.04,upbd-(upbd-lowbd)*.16
    SET COLOR 1
    SET TEXT justify "right","top"
    PLOT TEXT,AT .278*plen,upbd: tit$
    PLOT TEXT,AT .456*plen,upbd: str$(plotvardis)
    PLOT TEXT,AT .634*plen,upbd: str$(avedis)
    PLOT TEXT,AT .812*plen,upbd: str$(lowdis)
    PLOT TEXT,AT .990*plen,upbd: str$(highdis)
    PLOT LINES:i,plotvar;
 END SUB

 SUB OVERLAY(nu,plotvar,ave,high,low,lowbd,upbd,tit$,rnu)
    WINDOW #nu
    LET plotvardis=round(plotvar,rnu+1)
    LET avedis=round(ave,rnu)
    LET lowdis=round(low,rnu)
    LET highdis=round(high,rnu)
    SET COLOR 5
    BOX AREA .1*plen,.99*plen,lowbd+(upbd-lowbd)*.04,lowbd+(upbd-lowbd)*.16
    SET COLOR 1
    SET TEXT justify "right","bottom"
    PLOT TEXT,AT .278*plen,lowbd: tit$
    PLOT TEXT,AT .456*plen,lowbd: str$(plotvardis)
    PLOT TEXT,AT .634*plen,lowbd: str$(avedis)
    PLOT TEXT,AT .812*plen,lowbd: str$(lowdis)
    PLOT TEXT,AT .990*plen,lowbd: str$(highdis)
    SET COLOR 3
    PLOT LINES:i,plotvar;
    SET COLOR 1
 END SUB

 SUB InitializeDA
    CALL Com_open (#1, 1, 4800, "")    ! Open Comm Line At 4800 Baud
    LET First = 0
    CALL Reset
    LET First = 1
    LET Zero = Ord("0")

    ! Text Screen
    OPEN #12:Screen 0,1,.615,1

    ! Mdot Screen
    OPEN #22:Screen .502,1,0,.15

    ! Evap Load1 Fresh Food Screen
    OPEN #32:Screen .502,1,.1525,.3025

    ! Evap Load2 Freezer Screen
    OPEN #42:Screen 0,.498,.1525,.3025

    ! Super Super Heat8 Screen
```

```
    OPEN #52:Screen 0,.498,0,.15

    ! Evap TF Screen
    OPEN #62:Screen 0,.498,.305,.455
    ! Evap TFin Screen
    OPEN #63:Screen 0,.498,.305,.455

    ! Super TFF Screen
    OPEN #72:Screen .502,1,.305,.455
    ! Super TFFin Screen
    OPEN #73:Screen .502,1,.305,.455

    ! Super Vel FF Screen
    OPEN #82:Screen .502,1,.4575,.6075
    ! Super Vel F Screen
    OPEN #92:Screen .502,1,.4575,.6075

    ! Evap Sub Cool Screen
    OPEN #53:Screen 0,.498,.4575,.6075

    CALL SETSTAT

    CALL SETAXIS

    CALL DRAWGRAPHS

    LET Format$ =  "RUNNING for ###.# mins      Press 'Q' to stop or 'space' to change graph limits"
    LET Format1$ = "####  ###.#    ###  ###  ###     #######  ####.#    ####  ####  ####"
    LET Format2$ = "####  ###.#    ###  ###  ###     #######  ####.#   ####.#"
    LET Format3$ = "######## ##  ##### ###.#  #### ##/##    ### ##.# ##.# ##.# ##.#"

    LET End = 1
    LET I=0
    LET Count = 0
  END SUB

  SUB WRITEFILE
    !Set Up The Data File On The Floppy.  Use Tabs (CHR$(9)) To Separate The
    !Data Points.
    !First, Get The Date And Time For The Name Of The File.
    LET ThisTime$ = Time$
    IF val(thistime$[1:2]) > 12 then
      LET thistime$[1:2]=str$(0)&str$(val(thistime$[1:2])-12)
    END IF
    LET thistime$=thistime$[1:2]&thistime$[4:5]
    LET thisdate$=Date$[5:8]
    LET OutputFileName$ = "f"&thisdate$&ThisTime$
    OPEN #2: NAME OutputFileName$, CREATE NEWOLD, ORGANIZATION TEXT
    ERASE #2
    SET #2: MARGIN MAXNUM
    LET T$ = CHR$(9)

    !Print Out A Row Of Column Titles.
    PRINT #2: "Tamb";T$;"Mdot";T$;"FLoad";T$;"FFLoad";T$;
    PRINT #2: "Tchil";T$;"Ppum";T$;"Tpum";T$;
    PRINT #2: "TFin";T$;"DTF";T$;"TF";T$;
    PRINT #2: "TFFin";T$;"DTFF";T$;"TFF";T$;
```

```
PRINT #2: "VelF";T$;"VelFF";T$;
PRINT #2: "CFMF";T$;"CFMFF";T$;
PRINT #2: "MdotF";T$;"MdotFF";T$;
PRINT #2: "P1";T$;"P2";T$;"P3";T$;"P4";T$;"P5";T$;"P6";T$;"P7";T$;"P8";T$;
PRINT #2: "T1";T$;"T2";T$;"T3";T$;"T4";T$;"T5";T$;"T6";T$;"T7";T$;"T8";T$;
PRINT #2: "SH8";T$;"SC1"

PRINT #2: Tambsum/count;T$;Mdotsum/count;T$;FLoadsum/count;T$;FFLoadsum/count;T$;
PRINT #2: Tchilsum/count;T$;Ppumsum/count;T$;Tpumsum/count;T$;
PRINT #2: TFinsum/count;T$;DTFsum/count;T$;TFsum/count;T$;
PRINT #2: TFFinsum/count;T$;DTFFsum/count;T$;TFFsum/count;T$;
PRINT #2: VelFsum/count;T$;VelFFsum/count;T$;
PRINT #2: CFMFsum/count;T$;CFMFFsum/count;T$;
PRINT #2: MdotFsum/count;T$;MdotFFsum/count;T$;
PRINT #2: Psum(1)/count;T$;Psum(2)/count;T$;Psum(3)/count;T$;Psum(4)/count;T$;
PRINT #2: Psum(5)/count;T$;Psum(6)/count;T$;Psum(7)/count;T$;Psum(8)/count;T$;
PRINT #2: Tsum(1)/count;T$;Tsum(2)/count;T$;Tsum(3)/count;T$;Tsum(4)/count;T$;
PRINT #2: Tsum(5)/count;T$;Tsum(6)/count;T$;Tsum(7)/count;T$;Tsum(8)/count;T$;
PRINT #2: SHsum/count;T$;SC1sum/count

PRINT #2: Tambmin;T$;Mdotmin;T$;FLoadmin;T$;FFLoadmin;T$;
PRINT #2: Tchilmin;T$;Ppummin;T$;Tpummin;T$;
PRINT #2: TFinmin;T$;DTFmin;T$;TFmin;T$;
PRINT #2: TFFinmin;T$;DTFFmin;T$;TFFmin;T$;
PRINT #2: VelFmin;T$;VelFFmin;T$;
PRINT #2: CFMFmin;T$;CFMFFmin;T$;
PRINT #2: MdotFmin;T$;MdotFFmin;T$;
PRINT #2: Pmin(1);T$;Pmin(2);T$;Pmin(3);T$;Pmin(4);T$;
PRINT #2: Pmin(5);T$;Pmin(6);T$;Pmin(7);T$;Pmin(8);T$;
PRINT #2: Tmin(1);T$;Tmin(2);T$;Tmin(3);T$;Tmin(4);T$;
PRINT #2: Tmin(5);T$;Tmin(6);T$;Tmin(7);T$;Tmin(8);T$;
PRINT #2: SHmin;T$;SC1min

PRINT #2: Tambmax;T$;Mdotmax;T$;FLoadmax;T$;FFLoadmax;T$;
PRINT #2: Tchilmax;T$;Ppummax;T$;Tpummax;T$;
PRINT #2: TFinmax;T$;DTFmax;T$;TFmax;T$;
PRINT #2: TFFinmax;T$;DTFFmax;T$;TFFmax;T$;
PRINT #2: VelFmax;T$;VelFFmax;T$;
PRINT #2: CFMFmax;T$;CFMFFmax;T$;
PRINT #2: MdotFmax;T$;MdotFFmax;T$;
PRINT #2: Pmax(1);T$;Pmax(2);T$;Pmax(3);T$;Pmax(4);T$;
PRINT #2: Pmax(5);T$;Pmax(6);T$;Pmax(7);T$;Pmax(8);T$;
PRINT #2: Tmax(1);T$;Tmax(2);T$;Tmax(3);T$;Tmax(4);T$;
PRINT #2: Tmax(5);T$;Tmax(6);T$;Tmax(7);T$;Tmax(8);T$;
PRINT #2: SHmax;T$;SC1max

PRINT #2: Tambstdev;T$;Mdotstdev;T$;FLoadstdev;T$;FFLoadstdev;T$;
PRINT #2: Tchilstdev;T$;Ppumstdev;T$;Tpumstdev;T$;
PRINT #2: TFinstdev;T$;DTFstdev;T$;TFstdev;T$;
PRINT #2: TFFinstdev;T$;DTFFstdev;T$;TFFstdev;T$;
PRINT #2: VelFstdev;T$;VelFFstdev;T$;
PRINT #2: CFMFstdev;T$;CFMFFstdev;T$;
PRINT #2: MdotFstdev;T$;MdotFFstdev;T$;
PRINT #2: Pstdev(1);T$;Pstdev(2);T$;Pstdev(3);T$;Pstdev(4);T$;
PRINT #2: Pstdev(5);T$;Pstdev(6);T$;Pstdev(7);T$;Pstdev(8);T$;
PRINT #2: Tstdev(1);T$;Tstdev(2);T$;Tstdev(3);T$;Tstdev(4);T$;
PRINT #2: Tstdev(5);T$;Tstdev(6);T$;Tstdev(7);T$;Tstdev(8);T$;
```

```
    PRINT #2: SHstdev;T$;SC1stdev

    PRINT #2: "Runtime=";T$;Runtime
    CLOSE #2
  END SUB

  SUB SETSTAT
    CALL SETNUM(SHmin,SHmax,SHsum,SHsumsq)
    CALL SETNUM(SH7min,SH7max,SH7sum,SH7sumsq)
    CALL SETNUM(SC1min,SC1max,SC1sum,SC1sumsq)
    CALL SETNUM(Mdotmin,Mdotmax,Mdotsum,Mdotsumsq)
    CALL SETNUM(FLoadmin,FLoadmax,FLoadsum,FLoadsumsq)
    CALL SETNUM(FFLoadmin,FFLoadmax,FFLoadsum,FFLoadsumsq)
    CALL SETNUM(Tambmin,Tambmax,Tambsum,Tambsumsq)
    CALL SETNUM(Tchilmin,Tchilmax,Tchilsum,Tchilsumsq)
    CALL SETNUM(Tpummin,Tpummax,Tpumsum,Tpumsumsq)
    CALL SETNUM(TFinmin,TFinmax,TFinsum,TFinsumsq)
    CALL SETNUM(DTFmin,DTFmax,DTFsum,DTFsumsq)
    CALL SETNUM(TFmin,TFmax,TFsum,TFsumsq)
    CALL SETNUM(TFFinmin,TFFinmax,TFFinsum,TFFinsumsq)
    CALL SETNUM(DTFFmin,DTFFmax,DTFFsum,DTFFsumsq)
    CALL SETNUM(TFFmin,TFFmax,TFFsum,TFFsumsq)
    CALL SETNUM(Ppummin,Ppummax,Ppumsum,Ppumsumsq)
    CALL SETNUM(VelFmin,VelFmax,VelFsum,VelFsumsq)
    CALL SETNUM(VelFFmin,VelFFmax,VelFFsum,VelFFsumsq)
    CALL SETNUM(CFMFmin,CFMFmax,CFMFsum,CFMFsumsq)
    CALL SETNUM(CFMFFmin,CFMFFmax,CFMFFsum,CFMFFsumsq)
    CALL SETNUM(MdotFmin,MdotFmax,MdotFsum,MdotFsumsq)
    CALL SETNUM(MdotFFmin,MdotFFmax,MdotFFsum,MdotFFsumsq)
    FOR nn = 1 To 8
      CALL SETNUM(Pmin(nn),Pmax(nn),Psum(nn),Psumsq(nn))
      CALL SETNUM(Tmin(nn),Tmax(nn),Tsum(nn),Tsumsq(nn))
    NEXT nn
  END SUB

  SUB SETNUM(Minset,Maxset,Sumset,Sumsqset)
    LET Minset = 9999
    LET Maxset = -9999
    LET Sumset = 0
    LET Sumsqset = 0
  END SUB

  SUB Minmaxstat(In,Min,Max,Sum,Sumsq,Stdev)
    IF In < Min Then LET Min = In
    IF In > Max Then LET Max = In
    LET Sum = Sum + In
    LET Sumsq = Sumsq + In^2
    IF Count > 1 Then
      IF (Sumsq-Sum^2/Count) > 0 Then
        LET Stdev = Sqr((Sumsq-Sum^2/Count)/(Count-1))
      END IF
    ELSE
      LET Stdev = 0
    END IF
  END SUB

  SUB SETAXIS
```

```
    WINDOW #12
    CLEAR
    PRINT "Use Default axis settings (Y or N)"
    INPUT defaxis$
    IF defaxis$="y" then
      LET Lbmdot=130
      LET Ubmdot=170
      LET Lbload1=110
      LET Ubload1=210
      LET Lbload2=110
      LET Ubload2=210
      LET Lbsh=-5
      LET Ubsh=35
      LET Lbsc=0
      LET Ubsc=35
      LET LbTF=-12
      LET UbTF=-2
      LET LbTFF=0
      LET UbTFF=10
      LET Plen=100
      LET LbVelFF=.3
      LET UbVelFF=1.3
    ELSE
      PRINT "enter 0 to skip to time base"
      PRINT "enter 9 to reset stats"
      PRINT "enter # of graph you wish to change (1 - 8) top to bottom/left to right"
      INPUT zz
      LET ans$ = "y"
      DO while zz >= 1 and zz <=8 and ans$ = "y"
        IF zz = 1 then CALL ASK("Subcooling (C)",Lbsc,Ubsc)
        IF zz = 2 then CALL ASK("VelF and VelFF (m/s)",LbVelFF,UbVelFF)
        IF zz = 3 then CALL ASK("TF and TFin (C)",LbTF,UbTF)
        IF zz = 4 then CALL ASK("TFF and TFFin (C)",LbTFF,UbTFF)
        IF zz = 5 then CALL ASK("FLoad (W)",Lbload2,Ubload2)
        IF zz = 7 then CALL ASK("Superheat (C)",Lbsh,Ubsh)
        IF zz = 6 then CALL ASK("FFLoad (W)",Lbload1,Ubload1)
        IF zz = 8 then CALL ASK("mdot (g/min)",Lbmdot,Ubmdot)
      LOOP
      IF zz = 9 then
        CALL SETSTAT
        LET count = 0
      ELSE
        ! 60 Points Is 5 Minutes At 6 Sec Sample Interval
        PRINT "Enter Time Base For Graphs In Minutes"
        INPUT Plen
        LET Plen = Plen*10
      END IF
    END IF
    CLEAR
END SUB

SUB ASK(var$,Lbask,Ubask)
    PRINT "Enter Target "&var$
    INPUT Tar
    PRINT "Enter "&var$&" Range"
    INPUT Ran
    LET Lbask=Tar-Ran
```

```
    LET Ubask=Tar+Ran
    PRINT "Enter Y to change another graph axis"
    INPUT ans$
    IF ans$="y" then
      PRINT "input # of graph you wish to change"
      INPUT zz
    END IF
 END SUB

 SUB DRAWGRAPHS
    CALL DRAWWIN(22,Lbmdot,Ubmdot)
    CALL DRAWWIN(32,Lbload1,Ubload1)
    CALL DRAWWIN(42,Lbload2,Ubload2)
    CALL DRAWWIN(53,Lbsc,Ubsc)
    CALL DRAWWIN(52,Lbsh,Ubsh)
    CALL DRAWWINOL(63,LbTF,UbTF)
    CALL DRAWWIN(62,LbTF,UbTF)
    CALL DRAWWINOL(73,LbTFF,UbTFF)
    CALL DRAWWIN(72,LbTFF,UbTFF)
    CALL DRAWWINOL(92,LbVelFF,UbVelFF)
    CALL DRAWWIN(82,LbVelFF,UbVelFF)
 END SUB

 SUB DRAWWINOL(ii,Lb,Ub)
    WINDOW #ii
    CLEAR
    SET WINDOW 0,Plen,Lb,Ub
 END SUB

 SUB DRAWWIN(ii,Lb,Ub)
    WINDOW #ii
    CLEAR
    SET WINDOW 0,Plen,Lb,Ub
    BOX LINES 0,Plen,Lb,Ub
    SET TEXT JUSTIFY "Left","Top"
    PLOT TEXT, AT 0,Ub: " "&Str$(Ub)
    SET TEXT JUSTIFY "Left","Bottom"
    PLOT TEXT, AT 0,Lb: " "&Str$(Lb)
 END SUB

 SUB Store
    DECLARE DEF AirmV,AirT
    IF Value > 0.0 And Sign = -1 Then LET Value = -Value
    IF Chan > 29 And Chan < 60 THEN
      IF Chan = 41 THEN        !We Have T Across The Freezer Evaporator
        LET TFin = Data(40)
        LET DmVF = Value/4
        LET MVFin = AirmV(TFin)
        LET MVFout = MVFin - DmVF
        LET TFout = AirT(MVFout)
        LET Data(41) = TFin-TFout
      ELSE IF Chan = 44 THEN    !We Have T Across The Fresh Food Evaporator
        LET TFFin = Data(43)
        LET DmVFF = Value/4
        LET MVFFin = AirmV(TFFin)
        LET MVFFout = MVFFin - DmVFF
        LET TFFout = AirT(MVFFout)
```

```
      LET Data(44) = TFFin-TFFout
    ELSE IF Chan = 51 THEN    !We Have Pressure At Station 3, Before The Expansion Valve
      LET Data(Chan)=((Value/248.8*1000)-4)*3447.325/16
    ELSE IF Chan = 53 THEN    !We Have Power Added To The Freezer Cabinet
      LET Data(Chan) = Value*100  !100 Watts / 1 Volt
    ELSE IF Chan = 54 THEN    !We Have The Power Added To The Fresh Food Cabinet
      LET Data(Chan) = Value*100-2.4   !100 Watts / 1 Volt
    ELSE IF Chan = 55 THEN    !We Have Pressure At The Outlet Of The Gear Pump
      LET Data(Chan)=((Value/248.8*1000)-4)*3447.325/16
    ELSE IF Chan = 56 THEN    !We Have Pressure At Station 1, After The Heater
      LET Data(Chan)=((Value/248.3*1000)-4)*3447.325/16
    ELSE IF Chan = 57 THEN    !We Have Pressure At Station 4, After The Expansion Valve
      LET Data(Chan)=(((Value/247.9*1000)-4)*689.465/16)  ! -6
    ELSE IF Chan = 58 THEN    !We Have Pressure At Station 8, Outlet Of The Box
      LET Data(Chan)=((Value/247.9*1000)-4)*689.465/16
    ELSE IF Chan = 59 THEN    !We Have Mass-flow Rate (grams/min)
      LET Data(Chan)=((Value/248.2*1000)-4)*250/16
    ELSE                      !We Have A Normal Temperature Reading
      LET Data(Chan)=Value
    END IF
  END IF
  IF Chan = 59 THEN CALL Calcs  !Condition And Print Out The Data
END SUB

DEF AirmV(T)
  !These functions are curve fits to the Omega Thermocouple catalog data
  !Obtained from Chris Siambekos, May 20, 1991
  !The temperature is expected in F, but it enters the funciton in
  !C, so make the conversion right away.
  LET TdegF = T*1.8 + 32
  LET AirmV = -.6714962203 + .020615284491*TdegF + 1.2885171534e-5*TdegF^2
END DEF

DEF AirT(mV)
  !These functions are curve fits to the Omega Thermocouple catalog data
  !Obtained from Chris Siambekos, May 20, 1991.
  !These curve fits give the temperature in F, so convert the answer
  !back to C for the main program.
  LET AirTdegF = 31.975298884 + 46.414499129*mV - 1.0666818645*mV^2
  LET AirT = (AirTdegF - 32)/1.8
END DEF

DEF SuperH(P)
  !Sat curve fit for R12 - 100 to 1200 kPa
  !LET SuperH = -53.884 + 0.29242*P - 5.5215e-4*P^2 + 6.8217e-7*P^3 - 4.3900e-10*P^4 + 1.1227e-13*P^5
  !
  !Sat curve fit for R22 - 100 to 2200 kPa
  LET SuperH = -56.594 + .19361*P - 2.2834e-4*P^2 +1.6844e-7*P^3 - 6.3072e-11*P^4 + 9.2334e-15*P^5
  !
  !SuperH Curve Fits Only Valid To 3000 KPa For 65% R22/R123 Mixture Only
  !With An Interaction Parameter Of 0.003
  !  LET SuperH= -24.965+0.20306*P-2.1368e-4*P^2+1.2916e-7*P^3-3.8151e-11*P^4+4.3107e-15*P^5
  !
  !SuperH Curve Fits Only Valid To 3000 KPa For 80% R22/R141b Mixture Only
  !With An Interaction Parameter Of 0.00
  !  LET SuperH= -27.242+0.19863*P-2.0925e-4*P^2+1.2659e-7*P^3-3.7407e-11*P^4+4.2277e-15*P^5
END DEF
```

```
DEF SubC(P)
  !Sat curve fit for R12 - 100 to 1200 kPa
  !LET SubC = -53.884 + 0.29242*P - 5.5215e-4*P^2 + 6.8217e-7*P^3 - 4.3900e-10*P^4 + 1.1227e-13*P^5
  !
  !Sat curve fit for R22 - 100 to 2200 kPa
  LET SubC = -56.594 + .19361*P - 2.2834e-4*P^2 +1.6844e-7*P^3 - 6.3072e-11*P^4 + 9.2334e-15*P^5
  !
  !SubC Curve Fits Only Valid To 3000 KPa For 65% R22/R123 Mixture Only
  !With An Interaction Parameter Of 0.003
  !  LET SubC= -55.133+0.20731*P-2.1378e-4*P^2+1.2900e-7*P^3-3.8065e-11*P^4+4.2989e-15*P^5
  !
  !SubC Curve Fits Only Valid To 3000 KPa For 80% R22/R141b Mixture Only
  !With An Interaction Parameter Of 0.00
  !  LET SubC= -56.463+0.20316*P-2.0997e-4*P^2+1.2675e-7*P^3-3.7407e-11*P^4+4.2252e-15*P^5
END DEF

DEF Phoair(T)
  LET T=T+273.15
  LET Phoair = -4.666*T+2561.188
END DEF

DEF Cpair(T)
  LET T=T+273.15
  LET Cpair = (.001/50)*T+1.001
END DEF

SUB Process(S$)              ! Enter The Character String
  FOR N = 1 To Len(S$)
    LET A$ = S$[N:N]         ! Look At Each Character
    IF A$ = Chr$(32) Then LET A$ = "~"
    IF A$ = Chr$(10) Then CALL Reset
    IF Pdec = 1 Then LET Mult = 0.1*Mult
    IF A$  = "." Then LET Pdec = 1
    IF A$ >= "0" And A$ <= "9" Then CALL Numval(A$)
    IF A$ >= "A" And A$ <= "Z" Then LET Units = 1
    IF A$  = "+" Then LET Sign =  1.0
    IF A$  = "-" Then LET Sign =  -1.0
  NEXT N
END SUB

SUB Numval (A$)              ! Analyse The Numerical Data
  LET Va = Ord(A$) - Zero
  IF Chan >= 9  And Pdec = 0 Then LET Value = (Value*10.0 + Va)
  IF Chan >= 9  And Pdec = 1 Then LET Value = Value + Mult*Va
  IF Chan > 0 And Chan < 9 Then LET Chan = Chan*10 + Va
  IF Chan = 0 Then LET Chan = Va
END SUB

SUB Reset                    ! Reset Upon Obtaining LF
  IF Value > 0.0 And Sign = -1 Then LET Value = -Value
  IF Chan <> 0 And First = 0 Then CALL Store
  IF First = 1 Then LET First = 0
  LET Chan  = 0
  LET Sign  = 1.0
  LET Pdec  = 0
  LET Mult  = 1.0
```

```
   LET Units = 0
   LET Value = 0.0
END SUB
END
```

APPENDIX J: CARNAHAN-STARLING-DESANTIS EQUATION OF STATE

This appendix briefly describes the equation of state subroutines used in this experiment. A brief discussion is included on the interaction parameter required by the equation of state subroutines.

All thermodynamic properties for this experiment were calculated with the National Institute of Standards and Technology (NIST) Carnahan-Starling-DeSantis (CSD) equation of state (EOS) subroutines. The CSD-EOS, based on the hard sphere fluid, was developed by Morrison and McLinden[1] for halogenated hydrocarbon refrigerants and their mixtures. The EOS models the thermophysical behavior of the fluid with the ability to predict unmeasured properties when there is limited experimental data available. The EOS is a modification of the hard sphere fluid first proposed by DeSantis *et al.*[2] The CSD-EOS has also been applied to other classes of fluids, such as hydrocarbons and simple inorganic molecules. The model was coded in a FORTRAN subroutine library.

For mixture evaluation, the program required the mixture concentration and the interaction parameter for the pair. The interaction parameter for the pair attempts to account for differences in polarizability of the two species, the deformation of the two electron clouds, and the closest distance of approach. The interaction parameters for the two mixtures were obtained directly from the USEPA.[3] Table J.1 shows the interaction parameters recommended.

Table J.1: Interaction parameters for the experimental mixtures

pair	interaction parameter	recommended by	date
R22/R123	0.003	Bare	7/8/91
R22/R141b	0.000	Gage	10/9/91

The computer subroutines were run on the Convex main frame computer due to their iterative nature and overall length. The routines were converted to run on the micro computer with little success. Table J.2 lists the available refrigerant coefficients for the version used for the data reduction. Figure J.1 shows all the available interaction parameters for the CSD EOS at the time of use.[4]

Table J.2: Refrigerants in CSD EOS subroutines

IR1 or IR2	working fluid	Normal Boiling Point (°C)	molecular weight (kg/kmol)
1	R11	23.82	137.370
2	R12	-29.79	120.910
3	R13	-81.40	104.460
4	R13b1	-57.75	148.910
5	R14	-127.90	88.000
6	R22	-40.76	86.470
7	R23	-82.10	70.010
8	R113	47.57	187.380
9	R114	3.80	170.920
10	R142b	-9.80	100.490
11	R152a	-25.00	66.050
12	R141b	31.8	116.95
13	R123	27.17 *	152.930
14	R143a	-47.22 *	84.040
15	Isobutane	-0.50	58.124
16	R124	-13.19 *	136.480
17	R125	-48.42 *	120.020
18	R134a	-26.16	102.030
19	R32	-51.70	52.024
20	Methane	-161.50	16.043
21	R216a	35.70 *	220.930
22	R216b	34.77 *	220.930

* NBP calculated from CSD equation of state, all other NBP's from ASHRAE Handbook of Fundamentals

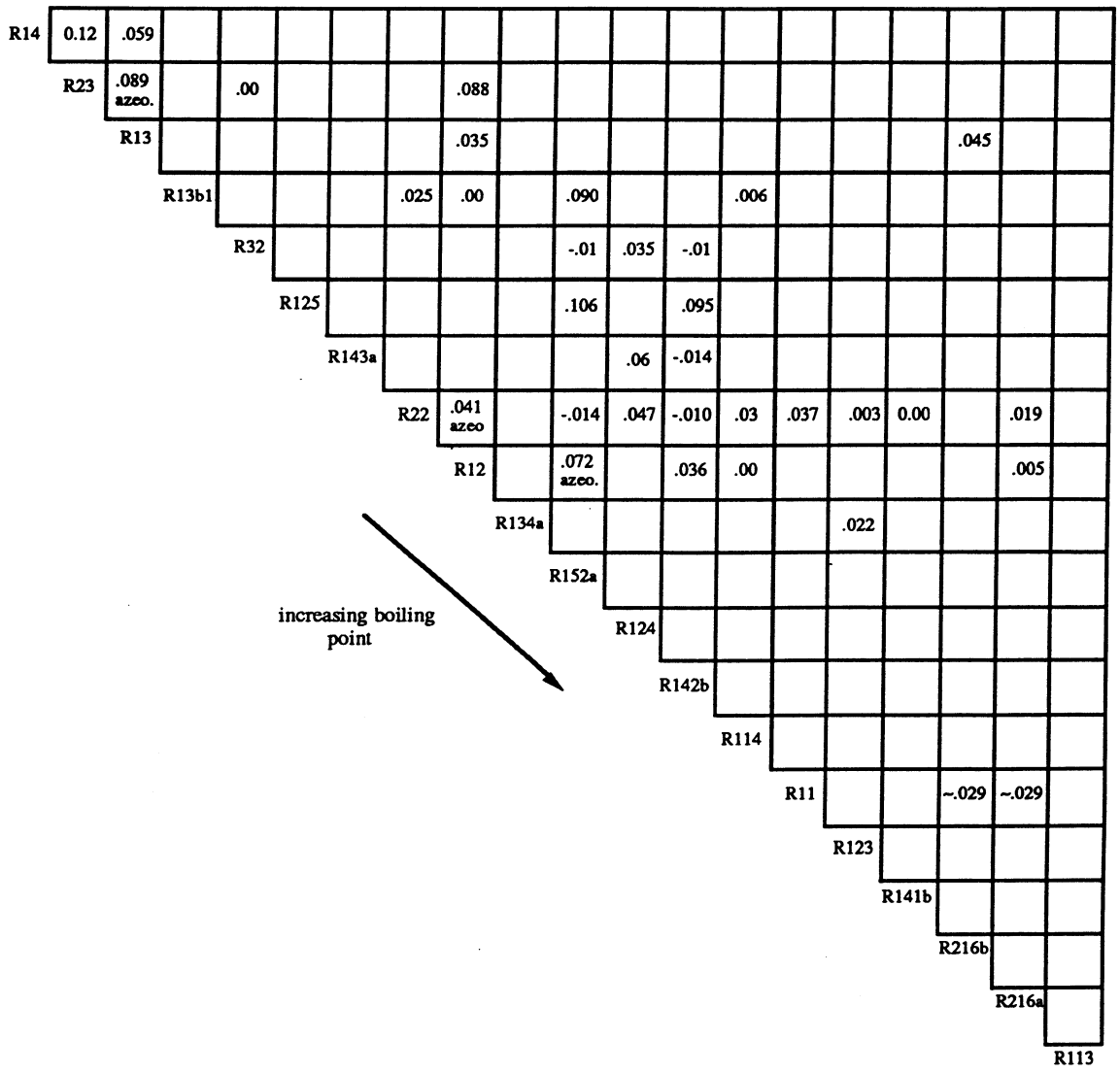

Figure J.1: Interaction parameters for use with the CSD EOS

---

[1] Morrison, G., M. O. McLinden, "Application of a Hard Sphere Equation of State to Refrigerants and Refrigerant Mixtures", National Bureau of Standards, Report # NBS/TN-1226, August, 1986.

[2] DeSantis, R., F. Gironi and L. Marrelli, *Ind. Eng. Chem., Fundam.*, 15, 183, 1976.

[3] Personal communication with J. Bare and C. Gage, United States Environmental Protection Agency, Research Triangle Park, North Carolina, 1991.

[4] Morrison, G., M. O. McLinden, "Application of a Hard Sphere Equation of State to Refrigerants and Refrigerant Mixtures", National Bureau of Standards, Report # NBS/TN-1226, August, 1986.

APPENDIX K: INTERCOOLING IMPACT ON SYSTEM IRREVERSIBILITY

The thermodynamic advantage of NARM intercooling can be explained in two ways. Previous arguments have been physically based. These arguments stated that the thermodynamic advantage of intercooling arises from achieving a lower average evaporating temperature with no decrease in evaporating pressure. Another interesting way to examining intercooling is based on irreversibility analysis and the Second Law of Thermodynamics. Irreversibility is the difference between reversible work and the actual work between two state points. Practically calculated it is the dead-state temperature times the difference of the exiting and entering entropies minus the difference of the exiting and entering enthalpies. (Adiabatic devices would not have the enthalpy difference as part of the irreversibility equation.) The dead-state temperature used for the calculations below is the ambient temperature; therefore, the heat transfer irreversibility associated with the heat transfer from the system to the environment is included.

Figure K.1 shows the component irreversibilities for the simulated R22/R123 systems shown in Figure K.2. Case 00 has the greatest expansion device irreversibility fraction for any of the cases. Addition of intercooling will shift this irreversibility from the expansion device to other components which, in some cases, can be reduced if system pinch-points are relieved. The large expansion irreversibility for case 00 is due to the expansion process being entirely contained in the saturation dome. With intercooling, the expansion will occur from the subcooled liquid region to a lower quality state point in the two-phase region. Since the start of the expansion process is moved from the saturated liquid line to the subcooled liquid region and the ending state point is at a lower quality, the entropy change of the process is greatly reduced. Recall that the entropy change for a liquid is much less than the entropy change for a vapor between the same pressure levels. Both case 00 and case 10 have the same total irreversibility, hence the same COP. The addition of low-temperature intercooler does not relieve any system pinch-points. For case 10, the irreversibility gain in the low-temperature evaporator and the created heat transfer irreversibility from the addition of an intercooler is exactly offset by the decrease in the expansion valve irreversibility.

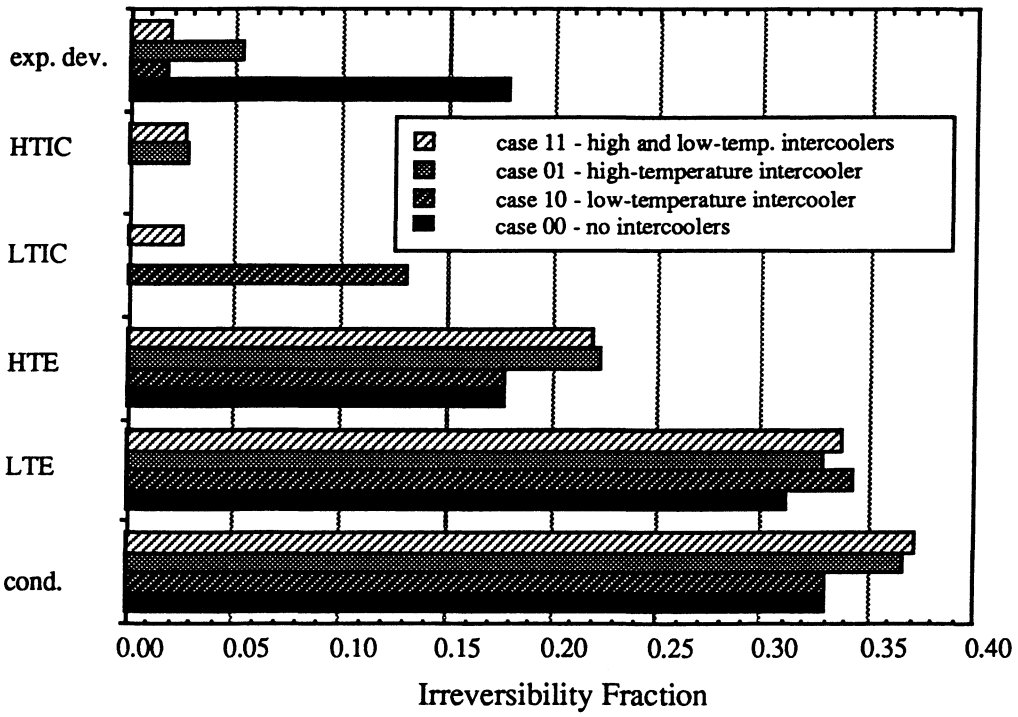

Figure K.1: Irreversibility fraction by component for a 65% R22/35% R123 refrigerant mixture with a 50%/50% load split

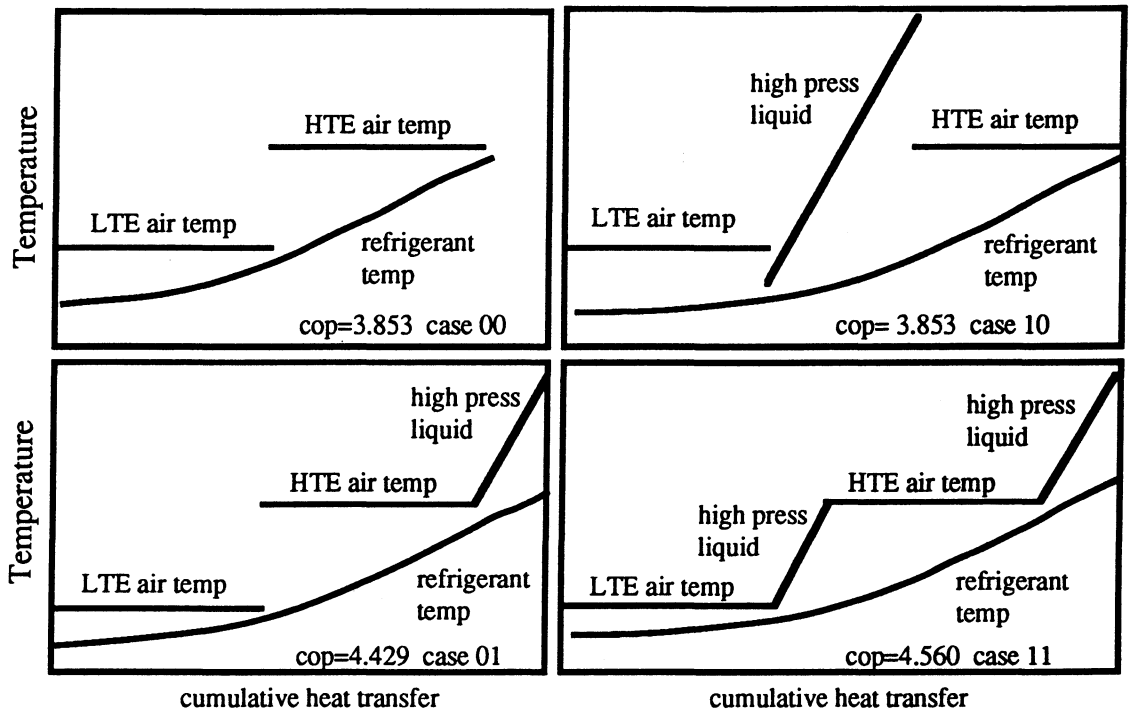

Figure K.2: System simulation for 65% R22/35% R123 for a 50% load split between the two evaporators, plotting temperature versus cumulative heat transfer

Table K.1 shows the actual irreversibility for the four cases. Notice that the total irreversibility is inversely related to the COP of the system. One must not confuse the irreversibility fraction with the actual irreversibility amounts. Case 00 and case 10 have the same total irreversibility so the comparison of the irreversibility fractions in Figure K.1 is proportionally equivalent to the results in Table K.1. Figure K.1 only shows how the irreversibility distribution is changed in the system as intercoolers are added.

Table K.1- Irreversibility for 65% R22/R123 systems in kJ/kg

case	COP	total irrev.	condenser irrev.	LTE irrev.	HTE irrev.	LTIC irrev.	HTIC irrev.	exp. dev. irrev.
00	3.85	41.95	13.87	13.07	7.48	0.00	0.00	7.53
10	3.85	41.95	13.87	14.41	7.48	5.48	0.00	0.71
01	4.46	36.85	13.49	12.13	8.22	0.00	1.03	1.97
11	4.56	36.14	13.44	12.25	7.91	0.92	0.95	0.67

The lowering of system irreversibility in case 01 by addition of a high-temperature intercooler occurs because the irreversibility gain by the addition of a high-temperature intercooler is much less than the irreversibility reduction for the expansion device. Looking at Table K.1, the major difference between case 10 and 01 is the irreversibility gain for the low-temperature intercooler versus the high-temperature intercooler. The load for the low-temperature intercooler was approximately twice that of the high-temperature intercooler, but the irreversibility associated with the low-temperature intercooler is over five times that of the high-temperature intercooler. Even though the high-temperature intercooler is penalized by having heat exchange at a higher quality, the closer mean temperatures of the fluid streams of the intercooler and the overall higher mean temperature of the heat transfer process account for the significant difference in the results. There is less irreversibility associated with heat transfer processes occurring closer to the dead-state temperature.

The key to the success of the NARMs research effort is to ensure that the COP penalty associated with an increase in irreversibilities for system components is less than the COP gain associated with a reduction of the heat transfer irreversibilities for the evaporators by better matching the fluid temperatures.

APPENDIX L: OPTIMIZATION RESULTS

system	configuration	p (kPa)	velf (m/s)	velff (m/s)	lli (W)	lhi (W)	sh (°C)
R12 BC	1E SLH/SH,50/50	130.7	1.60	NA	NA	53.9	60.9
R12 #1	1E,50/50	125.8	1.08	NA	NA	NA	NA
R12 #2	1E,SH,50/50	125.1	1.07	NA	NA	NA	NA
R12 #3	1E,SLH/SH,40/60	126.4	0.98	NA	NA	57.0	65.1
R12 #4	1E,SLH/SH,50/50	122.7	1.04	NA	NA	57.7	66.2
R12 #5	1E,SLH/SH,60/40	119.7	1.06	NA	NA	58.1	66.9
R12 #6	1E,SLH/SH,HEF,50/50	127.9	1.23	NA	NA	56.3	64.5
R12 #7	2E,50/50	133.4	1.06	0.47	NA	NA	NA
R12 #8	2E,SH,50/50	132.0	1.02	0.63	NA	NA	20.7
R12 #9	2E,SLH/SH,50/50	131.2	1.02	0.51	NA	55.2	63.7
R12 #10	2E,SLH/SH,HEF,50/50	135.7	1.24	0.63	NA	55.0	63.0
R134a #1	1E,50/50	109.2	1.09	NA	NA	NA	NA
R134a #2	1E,SH,50/50	108.6	1.08	NA	NA	NA	NA
R134a #3	1E,SLH/SH,40/60	109.5	1.00	NA	NA	61.5	66.2
R134a #4	1E,SLH/SH,50/50	105.6	1.03	NA	NA	62.1	67.0
R134a #5	1E,SLH/SH,60/40	104.0	1.12	NA	NA	65.3	66.7
R134a #6	1E,SLH/SH,HEF,50/50	109.9	1.19	NA	NA	61.4	66.0
R134a #7	2E,50/50	116.5	1.07	0.48	NA	NA	NA
R134a #8	2E,SH,50/50	114.8	1.03	0.62	NA	NA	22.8
R134a #9	2E,SLH/SH,50/50	113.8	1.01	0.49	NA	60.7	65.0
R134a #10	2E,SLH/SH,HEF,50/50	118.2	1.21	0.68	NA	59.9	64.3
R22/R123 #1	2E,50/50	105.8	0.82	0.62	NA	NA	NA
R22/R123 #2	2E,LI,50/50	132.6	0.74	0.78	95.2	NA	NA
R22/R123 #3	2E,HI,50/50	143.5	0.90	0.56	NA	76.5	NA
R22/R123 #4	2E,HI/LI,40/60	157.4	0.85	0.67	29.6	63.9	NA
R22/R123 #5	2E,HI/LI,50/50	148.6	0.91	0.60	26.2	68.9	NA
R22/R123 #6	2E,HI/LI,60/40	139.5	0.91	0.56	24.4	70.9	NA
R22/R123 #7	2E,HI/LI,HEF,50/50	151.8	1.01	0.72	25.6	68.2	NA
R22/R141b #1	2E,50/50	120.2	0.85	0.72	NA	NA	NA
R22/R141b #2	2E,LI,50/50	135.1	0.87	0.81	87.7	NA	NA
R22/R141b #3	2E,HI,50/50	142.8	0.88	0.54	NA	80.3	NA
R22/R141b #4	2E,HI/LI,40/60	150.3	0.87	0.65	29.2	55.2	NA
R22/R141b #5	2E,HI/LI,50/50	143.1	0.93	0.60	35.8	54.1	NA
R22/R141b #6	2E,HI/LI,60/40	137.1	0.94	0.59	34.9	59.4	NA
R22/R141b #7	2E,HI/LI,HEF,50/50	147.6	1.06	0.68	31.4	58.3	NA

system	obj. fn. ($)	obj. fn. uncert.	COP	COP w fan	G (kg/m^2-s)	$\dot{m}$ (g/s)	q"f (kW/m^2)	q"ff (kW/m^2)
R12 BC	858.57	8.11	1.40	1.16	30.5	1.49	0.80	NA
R12 #1	863.70	5.96	1.29	1.15	41.9	2.05	0.67	NA
R12 #2	863.73	5.56	1.28	1.15	41.9	2.05	0.68	NA
R12 #3	812.73	5.51	1.38	1.24	30.0	1.47	0.65	NA
R12 #4	825.78	5.44	1.36	1.22	29.9	1.47	0.68	NA
R12 #5	837.68	5.77	1.34	1.20	29.9	1.47	0.67	NA
R12 #6	813.31	5.16	1.39	1.25	30.0	1.47	0.65	NA
R12 #7	840.26	3.13	1.33	1.20	41.6	2.04	0.45	2.95
R12 #8	832.39	3.00	1.35	1.22	37.1	1.82	0.45	1.51
R12 #9	804.94	3.18	1.41	1.27	30.1	1.47	0.46	3.14
R12 #10	804.04	3.17	1.43	1.29	30.0	1.47	0.43	3.58
R134a #1	884.05	6.25	1.25	1.13	33.1	1.62	0.65	NA
R134a #2	884.06	5.80	1.25	1.12	33.1	1.62	0.67	NA
R134a #3	809.23	5.55	1.39	1.25	22.9	1.12	0.66	NA
R134a #4	822.23	5.45	1.36	1.22	22.9	1.12	0.68	NA
R134a #5	835.11	5.93	1.35	1.20	23.0	1.13	0.69	NA
R134a #6	810.11	5.00	1.39	1.26	22.9	1.12	0.65	NA
R134a #7	859.39	3.33	1.30	1.17	32.8	1.61	0.44	2.97
R134a #8	843.42	3.08	1.33	1.20	28.7	1.41	0.46	1.14
R134a #9	801.57	3.27	1.41	1.28	23.0	1.13	0.45	3.05
R134a #10	800.95	3.34	1.44	1.30	22.9	1.12	0.42	3.82
R22/R123 #1	922.42	6.99	1.21	1.11	27.9	1.37	0.29	0.92
R22/R123 #2	837.42	6.44	1.35	1.23	27.4	1.34	0.58	0.37
R22/R123 #3	806.95	6.35	1.41	1.28	27.2	1.33	0.34	1.20
R22/R123 #4	771.87	5.88	1.49	1.34	27.0	1.32	0.32	0.86
R22/R123 #5	794.91	6.22	1.44	1.30	27.1	1.33	0.37	1.05
R22/R123 #6	821.67	7.22	1.39	1.25	27.3	1.34	0.37	1.24
R22/R123 #7	795.27	5.76	1.46	1.32	27.1	1.33	0.34	1.14
R22/R141b #1	939.68	9.80	1.19	1.09	25.4	1.25	0.29	0.72
R22/R141b #2	892.52	5.97	1.26	1.15	25.2	1.24	0.47	0.42
R22/R141b #3	863.80	10.24	1.30	1.18	25.1	1.23	0.31	1.79
R22/R141b #4	842.34	8.85	1.34	1.22	25.0	1.23	0.28	1.27
R22/R141b #5	863.60	9.76	1.30	1.18	25.1	1.23	0.34	1.37
R22/R141b #6	884.91	11.27	1.27	1.15	25.2	1.24	0.36	1.68
R22/R141b #7	862.77	9.81	1.33	1.21	25.0	1.23	0.30	1.54

system	$\alpha_{r\,f}$ (W/m^2-K)	$\alpha_{r\,ff}$ (W/m^2-K)	$\alpha_{a\,f}$ (W/m^2-K)	$\alpha_{a\,ff}$ (W/m^2-K)	R_{rf} (%)	R_{rff} (%)	kWhr/yr	comp. pow. (W)
R12 BC	403.1	NA	22.3	NA	34.2	NA	603.9	143.0
R12 #1	482.0	NA	16.2	NA	24.0	NA	608.1	155.6
R12 #2	483.3	NA	16.3	NA	24.1	NA	608.5	156.1
R12 #3	384.8	NA	15.3	NA	27.2	NA	565.7	145.1
R12 #4	386.2	NA	16.1	NA	28.1	NA	575.8	147.4
R12 #5	384.3	NA	16.1	NA	28.3	NA	584.3	149.3
R12 #6	385.4	NA	17.1	NA	29.4	NA	561.1	144.2
R12 #7	465.6	716.9	18.7	19.2	27.3	20.1	583.1	150.3
R12 #8	428.7	545.8	18.3	19.7	28.6	25.3	575.6	148.4
R12 #9	369.1	689.6	18.4	20.2	31.9	21.6	553.1	142.3
R12 #10	368.0	754.4	19.8	22.8	33.5	22.1	541.7	139.6
R134a #1	483.7	NA	16.1	NA	23.8	NA	622.9	159.6
R134a #2	485.2	NA	16.3	NA	24.0	NA	623.4	160.1
R134a #3	378.0	NA	15.5	NA	27.8	NA	562.6	144.1
R134a #4	378.5	NA	16.0	NA	28.4	NA	572.7	146.6
R134a #5	379.7	NA	16.7	NA	29.3	NA	582.4	147.8
R134a #6	377.9	NA	16.8	NA	29.4	NA	558.1	143.9
R134a #7	468.7	713.1	18.5	19.4	27.0	20.3	597.0	154.0
R134a #8	425.6	506.3	18.4	18.0	28.9	25.0	582.8	150.3
R134a #9	362.1	661.3	18.2	19.6	32.0	21.8	549.8	141.4
R134a #10	360.6	771.2	19.1	24.0	33.2	22.6	538.3	138.7
R22/R123 #1	153.8	216.2	12.9	16.8	44.1	42.2	633.8	165.9
R22/R123 #2	188.0	173.2	16.6	14.1	45.3	43.3	569.7	147.7
R22/R123 #3	154.4	199.1	15.1	17.0	47.8	44.5	549.2	141.5
R22/R123 #4	156.4	179.8	15.7	16.5	48.5	46.2	522.3	134.3
R22/R123 #5	161.5	190.2	15.7	17.2	47.7	46.0	540.0	138.8
R22/R123 #6	159.5	200.5	14.3	18.2	45.7	46.1	558.8	143.7
R22/R123 #7	157.0	193.0	15.9	20.1	48.7	49.4	529.2	137.1
R22/R141b #1	59.8	87.7	13.3	17.5	67.6	65.2	644.9	168.0
R22/R141b #2	74.1	60.2	17.1	15.4	68.4	70.6	611.1	158.2
R22/R141b #3	56.2	196.4	14.1	18.5	70.2	46.9	591.9	153.6
R22/R141b #4	48.7	153.5	14.7	18.4	73.9	53.0	576.7	149.5
R22/R141b #5	57.3	158.2	15.1	18.5	71.2	52.4	592.9	153.5
R22/R141b #6	61.8	178.5	14.4	20.2	68.6	51.5	607.8	157.0
R22/R141b #7	52.5	172.7	15.2	20.9	73.2	53.1	580.4	151.0

system	fan_f pow. (W)	fan_{ff} pow. (W)	yr pow. cost ($)	tot. pow. cost ($)	fan cost ($)	mass (kg)	mass $ratio_f$	mass $ratio_{ff}$
R12 BC	18.80	NA	45.29	815.27	6.99	1.04	1.00	NA
R12 #1	7.45	NA	45.61	820.96	6.99	1.03	1.20	NA
R12 #2	7.02	NA	45.64	821.46	6.99	1.00	1.18	NA
R12 #3	5.80	NA	42.43	763.66	6.99	1.32	1.23	NA
R12 #4	6.46	NA	43.19	777.34	6.99	1.29	1.18	NA
R12 #5	6.96	NA	43.82	788.79	6.99	1.31	1.20	NA
R12 #6	5.42	NA	42.08	757.47	13.98	1.31	1.23	NA
R12 #7	5.49	0.17	43.73	787.19	13.98	0.87	0.89	0.14
R12 #8	4.86	0.54	43.17	777.07	13.98	0.98	0.88	0.27
R12 #9	4.89	0.21	41.49	746.75	13.98	1.11	0.88	0.13
R12 #10	4.33	0.18	40.62	731.25	27.96	1.13	0.92	0.11
R134a #1	7.63	NA	46.72	840.87	6.99	1.05	1.23	NA
R134a #2	7.33	NA	46.75	841.56	6.99	1.02	1.19	NA
R134a #3	5.98	NA	42.20	759.54	6.99	1.35	1.22	NA
R134a #4	6.32	NA	42.95	773.18	6.99	1.32	1.19	NA
R134a #5	7.91	NA	43.68	786.30	6.99	1.30	1.17	NA
R134a #6	4.92	NA	41.86	753.41	13.98	1.35	1.23	NA
R134a #7	5.68	0.18	44.77	805.89	13.98	0.89	0.91	0.14
R134a #8	4.94	0.59	43.71	786.76	13.98	1.05	0.88	0.35
R134a #9	4.80	0.18	41.23	742.20	13.98	1.16	0.89	0.13
R134a #10	4.16	0.23	40.37	726.73	27.96	1.20	0.96	0.11
R22/R123 #1	3.76	0.69	47.53	855.60	13.98	1.54	1.37	0.44
R22/R123 #2	1.62	2.73	42.73	769.06	13.98	1.61	0.69	1.09
R22/R123 #3	4.32	0.43	41.19	741.40	13.98	1.47	1.16	0.33
R22/R123 #4	3.22	1.03	39.17	705.12	13.98	1.53	0.99	0.56
R22/R123 #5	4.24	0.58	40.50	729.01	13.98	1.48	1.09	0.38
R22/R123 #6	4.93	0.37	41.91	754.41	13.98	1.55	1.31	0.26
R22/R123 #7	2.97	0.46	39.69	714.41	27.96	1.53	1.18	0.35
R22/R141b #1	4.29	1.27	48.36	870.55	13.98	1.66	1.38	0.56
R22/R141b #2	3.02	2.65	45.83	824.99	13.98	1.57	0.85	0.95
R22/R141b #3	4.47	0.31	44.39	799.03	13.98	1.43	1.30	0.22
R22/R141b #4	3.84	0.73	43.25	778.50	13.98	1.39	1.16	0.38
R22/R141b #5	4.75	0.49	44.47	800.47	13.98	1.36	1.20	0.29
R22/R141b #6	5.56	0.36	45.58	820.47	13.98	1.42	1.34	0.19
R22/R141b #7	3.84	0.33	43.53	783.54	27.96	1.46	1.33	0.26

system	len_f (m)	$pass\#_f$	len_{ff} (m)	$pass\#_{ff}$	len LI (m)	len HI (m)	$cost_f$ ($)	$cost_{ff}$ ($)
R12 BC	10.1	18.9	NA	NA	NA	2.4	12.12	NA
R12 #1	12.1	22.7	NA	NA	NA	NA	13.26	NA
R12 #2	11.8	22.2	NA	NA	NA	NA	13.10	NA
R12 #3	12.4	23.2	NA	NA	NA	3.4	13.40	NA
R12 #4	11.8	22.2	NA	NA	NA	3.6	13.11	NA
R12 #5	12.0	22.5	NA	NA	NA	3.7	13.21	NA
R12 #6	12.4	23.2	NA	NA	NA	3.3	13.41	NA
R12 #7	8.9	16.7	1.4	2.6	NA	NA	11.47	7.29
R12 #8	8.9	16.6	2.7	5.0	NA	NA	11.46	8.01
R12 #9	8.8	16.5	1.3	2.4	NA	3.2	11.42	7.24
R12 #10	9.3	17.4	1.1	2.1	NA	3.2	11.68	7.15
R134a #1	12.3	23.1	NA	NA	NA	NA	13.40	NA
R134a #2	12.0	22.4	NA	NA	NA	NA	13.18	NA
R134a #3	12.3	23.0	NA	NA	NA	3.9	13.36	NA
R134a #4	11.9	22.4	NA	NA	NA	3.9	13.16	NA
R134a #5	11.7	22.0	NA	NA	NA	3.9	13.05	NA
R134a #6	12.4	23.2	NA	NA	NA	3.8	13.41	NA
R134a #7	9.2	17.2	1.4	2.5	NA	NA	11.62	7.28
R134a #8	8.8	16.5	3.5	6.6	NA	NA	11.42	8.49
R134a #9	8.9	16.8	1.3	2.5	NA	3.7	11.50	7.26
R134a #10	9.7	18.1	1.1	2.0	NA	3.7	11.90	7.11
R22/R123 #1	13.8	25.8	4.4	8.2	NA	NA	14.19	8.97
R22/R123 #2	6.9	13.0	10.9	20.5	1.2	NA	10.37	12.62
R22/R123 #3	11.7	21.9	3.3	6.3	NA	2.4	13.03	8.39
R22/R123 #4	10.0	18.7	5.6	10.5	1.3	1.3	12.08	9.64
R22/R123 #5	10.9	20.5	3.8	7.2	1.5	1.4	12.60	8.65
R22/R123 #6	13.1	24.6	2.6	4.9	1.4	1.3	13.83	7.97
R22/R123 #7	11.9	22.2	3.5	6.6	1.4	1.5	13.12	8.49
R22/R141b #1	13.9	26.1	5.6	10.5	NA	NA	14.26	9.64
R22/R141b #2	8.5	15.9	9.5	17.9	0.6	NA	11.25	11.83
R22/R141b #3	13.0	24.4	2.2	4.2	NA	1.8	13.77	7.77
R22/R141b #4	11.7	21.9	3.8	7.1	0.4	0.6	13.02	8.64
R22/R141b #5	12.0	22.5	2.9	5.5	0.6	0.5	13.21	8.17
R22/R141b #6	13.5	25.3	1.9	3.6	0.8	0.6	14.02	7.59
R22/R141b #7	13.4	25.1	2.6	4.9	0.6	0.7	13.98	7.98

system	$cost_{LI}$ ($)	$cost_{HI}$ ($)	tot. hxer cost ($)	tot. OV (cm^3)	OV $ratio_f$	OV $ratio_{ff}$	tot. OV ratio	OV_f (cm^3)	OV_{ff} (cm^3)
R12 BC	NA	3.81	15.93	13111.9	1.06	NA	1.06	12918.9	NA
R12 #1	NA	NA	13.26	14471.2	1.27	NA	1.27	14471.2	NA
R12 #2	NA	NA	13.10	14262.9	1.24	NA	1.24	14262.9	NA
R12 #3	NA	5.43	18.83	14947.8	1.30	NA	1.30	14673.1	NA
R12 #4	NA	5.72	18.83	14555.5	1.24	NA	1.24	14266.0	NA
R12 #5	NA	5.81	19.03	14708.1	1.27	NA	1.27	14413.8	NA
R12 #6	NA	5.20	18.62	14950.0	1.30	NA	1.30	14686.6	NA
R12 #7	NA	NA	18.76	13074.4	0.94	0.14	1.08	9398.0	3676.4
R12 #8	NA	NA	19.48	14057.8	0.93	0.28	1.22	9386.0	4671.8
R12 #9	NA	5.05	23.70	13194.8	0.93	0.14	1.06	9327.3	3612.1
R12 #10	NA	5.11	23.94	13433.3	0.98	0.12	1.09	9682.5	3492.0
R134a #1	NA	NA	13.40	14661.2	1.30	NA	1.30	14661.2	NA
R134a #2	NA	NA	13.18	14361.0	1.26	NA	1.26	14361.0	NA
R134a #3	NA	6.15	19.51	14920.1	1.29	NA	1.29	14608.8	NA
R134a #4	NA	6.13	19.29	14649.3	1.26	NA	1.26	14338.9	NA
R134a #5	NA	6.22	19.27	14503.8	1.23	NA	1.23	14189.0	NA
R134a #6	NA	6.01	19.42	14990.0	1.30	NA	1.30	14686.0	NA
R134a #7	NA	NA	18.90	13265.4	0.96	0.14	1.11	9598.0	3667.4
R134a #8	NA	NA	19.91	14648.1	0.93	0.37	1.30	9331.9	5316.2
R134a #9	NA	5.84	24.60	13374.3	0.94	0.14	1.08	9438.6	3640.3
R134a #10	NA	5.92	24.93	13722.0	1.02	0.11	1.13	9983.3	3439.3
R22/R123 #1	NA	NA	23.16	19089.0	1.45	0.46	1.91	13112.5	5976.5
R22/R123 #2	1.92	NA	24.91	18949.8	0.73	1.15	1.88	7891.8	10960.6
R22/R123 #3	NA	3.87	25.29	16905.0	1.23	0.35	1.58	11529.8	5179.4
R22/R123 #4	2.03	2.06	25.81	17339.0	1.05	0.59	1.64	10232.2	6900.1
R22/R123 #5	2.40	2.28	25.93	16716.1	1.15	0.40	1.55	10933.9	5545.3
R22/R123 #6	2.23	2.12	26.15	17449.4	1.38	0.27	1.65	12618.0	4611.2
R22/R123 #7	2.20	2.36	26.16	17199.0	1.25	0.37	1.62	11650.3	5318.2
R22/R141b #1	NA	NA	23.90	20099.0	1.46	0.59	2.05	13208.9	6890.1
R22/R141b #2	0.88	NA	23.96	19026.6	0.89	1.00	1.90	9091.3	9890.6
R22/R141b #3	NA	2.80	24.34	17018.5	1.37	0.24	1.61	12532.8	4344.3
R22/R141b #4	0.61	0.98	23.25	17113.4	1.23	0.40	1.63	11511.7	5521.1
R22/R141b #5	0.89	0.86	23.13	16734.8	1.26	0.31	1.57	11767.4	4878.5
R22/R141b #6	1.34	0.94	23.89	17089.0	1.42	0.20	1.62	12877.0	4096.5
R22/R141b #7	0.96	1.07	23.98	17546.8	1.41	0.28	1.68	12819.4	4624.7

system	OV_{LI} (cm^3)	OV_{HI} (cm^3)	tot. OV cost ($)	x1	x2	x3	x4	x5	x6	x7	x8	x9
R12 BC	NA	193.0	20.39	0.00	-0.29	-0.29	0.18	1.00	1.00	1.00	1.22	1.84
R12 #1	NA	NA	22.50	0.00	0.00	0.00	0.40	1.00	1.00	1.00	1.00	1.39
R12 #2	NA	NA	22.18	0.00	0.00	0.00	0.41	1.00	1.00	1.00	1.00	1.39
R12 #3	NA	274.8	23.24	0.00	-0.31	-0.31	0.17	1.00	1.00	1.00	1.24	1.88
R12 #4	NA	289.5	22.63	0.00	-0.31	-0.31	0.17	1.00	1.00	1.00	1.24	1.90
R12 #5	NA	294.3	22.87	0.00	-0.32	-0.32	0.17	1.00	1.00	1.00	1.24	1.91
R12 #6	NA	263.4	23.24	0.00	-0.31	-0.31	0.17	1.00	1.00	1.00	1.23	1.87
R12 #7	NA	NA	20.33	0.00	0.00	0.00	0.40	0.70	0.70	1.00	1.00	1.38
R12 #8	NA	NA	21.86	0.00	0.00	0.00	0.40	0.74	0.74	1.07	1.07	1.53
R12 #9	NA	255.4	20.52	0.00	-0.30	-0.30	0.17	0.59	0.59	1.00	1.23	1.86
R12 #10	NA	258.7	20.89	0.00	-0.30	-0.30	0.17	0.58	0.58	1.00	1.23	1.84
R134a #1	NA	NA	22.80	0.00	0.00	0.00	0.43	1.00	1.00	1.00	1.00	1.36
R134a #2	NA	NA	22.33	0.00	0.00	0.00	0.43	1.00	1.00	1.00	1.00	1.36
R134a #3	NA	311.3	23.20	0.00	-0.34	-0.34	0.18	1.00	1.00	1.00	1.25	1.88
R134a #4	NA	310.3	22.78	0.00	-0.34	-0.34	0.18	1.00	1.00	1.00	1.26	1.89
R134a #5	NA	314.9	22.55	0.00	-0.36	-0.36	0.17	0.99	0.99	0.99	1.25	1.89
R134a #6	NA	304.0	23.31	0.00	-0.34	-0.34	0.18	1.00	1.00	1.00	1.25	1.88
R134a #7	NA	NA	20.63	0.00	0.00	0.00	0.42	0.71	0.71	1.00	1.00	1.35
R134a #8	NA	NA	22.77	0.00	0.00	0.00	0.42	0.75	0.75	1.08	1.08	1.53
R134a #9	NA	295.4	20.79	0.00	-0.33	-0.33	0.18	0.59	0.59	1.00	1.25	1.86
R134a #10	NA	299.5	21.34	0.00	-0.33	-0.33	0.17	0.59	0.59	1.00	1.25	1.85
R22/R123 #1	NA	NA	29.68	0.00	0.00	0.00	0.42	0.74	0.74	1.00	1.00	1.48
R22/R123 #2	97.4	NA	29.46	0.00	0.00	-0.39	0.05	0.41	0.73	1.00	1.00	1.43
R22/R123 #3	NA	195.8	26.28	0.00	-0.32	-0.32	0.11	0.47	0.47	0.79	1.00	1.42
R22/R123 #4	102.5	104.2	26.96	0.00	-0.27	-0.39	0.03	0.33	0.44	0.82	1.00	1.40
R22/R123 #5	121.2	115.6	25.99	0.00	-0.29	-0.40	0.03	0.40	0.50	0.81	1.00	1.41
R22/R123 #6	112.7	107.5	27.13	0.00	-0.29	-0.40	0.04	0.48	0.56	0.81	1.00	1.42
R22/R123 #7	111.3	119.3	26.74	0.00	-0.28	-0.39	0.03	0.41	0.50	0.81	1.00	1.41
R22/R141b #1	NA	NA	31.25	0.00	0.00	0.00	0.40	0.73	0.73	1.00	1.00	1.53
R22/R141b #2	44.7	NA	29.58	0.00	0.00	-0.37	0.07	0.43	0.73	1.00	1.00	1.50
R22/R141b #3	NA	141.5	26.46	0.00	-0.34	-0.34	0.09	0.45	0.45	0.79	1.00	1.49
R22/R141b #4	31.0	49.5	26.61	0.00	-0.23	-0.36	0.07	0.36	0.47	0.85	1.00	1.48
R22/R141b #5	45.2	43.6	26.02	0.00	-0.23	-0.38	0.05	0.42	0.55	0.86	1.00	1.49
R22/R141b #6	67.9	47.6	26.57	0.00	-0.25	-0.40	0.04	0.48	0.60	0.85	1.00	1.50
R22/R141b #7	48.7	54.0	27.28	0.00	-0.25	-0.38	0.05	0.42	0.53	0.85	1.00	1.48

system	h1 (kJ/kg)	h2 (kJ/kg)	h3 (kJ/kg)	h4 (kJ/kg)	h5 (kJ/kg)	h6 (kJ/kg)	h7 (kJ/kg)	h8 (kJ/kg)	h9 (kJ/kg)
R12 BC	80.0	43.9	43.9	43.9	177.9	177.9	177.9	214.0	309.8
R12 #1	80.0	80.0	80.0	80.0	177.5	177.5	177.5	177.5	253.4
R12 #2	80.0	80.0	80.0	80.0	177.4	177.4	177.4	177.4	253.5
R12 #3	80.0	41.2	41.2	41.2	177.3	177.3	177.3	216.1	314.9
R12 #4	80.0	40.6	40.6	40.6	177.1	177.1	177.1	216.4	317.0
R12 #5	80.0	40.3	40.3	40.3	176.8	176.8	176.8	216.5	318.5
R12 #6	80.0	41.7	41.7	41.7	177.7	177.7	177.7	215.9	314.0
R12 #7	80.0	80.0	80.0	80.0	129.1	129.1	178.2	178.2	251.9
R12 #8	80.0	80.0	80.0	80.0	134.9	134.9	189.9	189.9	271.5
R12 #9	80.0	42.5	42.5	42.5	110.4	110.4	178.3	215.8	312.4
R12 #10	80.0	42.6	42.6	42.6	110.5	110.5	178.5	215.8	310.6
R134a #1	111.8	111.8	111.8	111.8	235.1	235.1	235.1	235.1	333.6
R134a #2	111.8	111.8	111.8	111.8	235.0	235.0	235.0	235.0	333.7
R134a #3	111.8	57.0	57.0	57.0	235.1	235.1	235.1	289.9	418.3
R134a #4	111.8	56.5	56.5	56.5	234.6	234.6	234.6	290.0	420.6
R134a #5	111.8	53.8	53.8	53.8	231.4	231.4	231.4	289.4	420.7
R134a #6	111.8	57.1	57.1	57.1	235.1	235.1	235.1	289.8	417.8
R134a #7	111.8	111.8	111.8	111.8	173.9	173.9	236.1	236.1	331.8
R134a #8	111.8	111.8	111.8	111.8	182.8	182.8	253.9	253.9	360.7
R134a #9	111.8	57.8	57.8	57.8	146.7	146.7	235.6	289.6	415.3
R134a #10	111.8	58.5	58.5	58.5	147.5	147.5	236.4	289.6	413.0
R22/R123 #1	93.0	93.0	93.0	93.0	166.0	166.0	239.0	239.0	360.2
R22/R123 #2	93.0	93.0	22.1	22.1	96.6	167.4	241.9	241.9	351.9
R22/R123 #3	93.0	35.6	35.6	35.6	110.6	110.6	185.6	242.9	349.0
R22/R123 #4	93.0	44.6	22.2	22.2	82.7	105.1	195.8	244.2	345.7
R22/R123 #5	93.0	41.2	21.4	21.4	96.7	116.4	191.6	243.4	347.8
R22/R123 #6	93.0	39.9	21.7	21.7	111.4	129.7	189.5	242.6	350.0
R22/R123 #7	93.0	41.6	22.3	22.3	97.7	116.9	192.3	243.7	347.0
R22/R141b #1	96.4	96.4	96.4	96.4	176.6	176.6	256.8	256.8	391.4
R22/R141b #2	96.4	96.4	25.5	25.5	106.4	177.3	258.2	258.2	386.3
R22/R141b #3	96.4	31.1	31.1	31.1	112.4	112.4	193.7	259.0	383.8
R22/R141b #4	96.4	51.4	27.6	27.6	92.8	116.7	214.6	259.6	381.6
R22/R141b #5	96.4	52.5	23.4	23.4	104.7	133.8	215.0	259.0	383.7
R22/R141b #6	96.4	48.3	20.0	20.0	117.2	145.5	210.3	258.4	385.6
R22/R141b #7	96.4	48.9	23.3	23.3	104.9	130.5	212.0	259.6	382.7

system	T1 (°C)	T2 (°C)	T3 (°C)	T4 (°C)	T5 (°C)	T6 (°C)	T7 (°C)	T8 (°C)	T9 (°C)
R12 BC	44.0	7.5	7.5	-23.6	-23.6	-23.6	-23.6	37.2	186.7
R12 #1	44.0	44.0	44.0	-24.6	-24.6	-24.6	-24.6	-24.6	110.1
R12 #2	44.0	44.0	44.0	-24.7	-24.7	-24.7	-24.7	-24.7	110.3
R12 #3	44.0	4.7	4.7	-24.5	-24.5	-24.5	-24.5	40.6	193.6
R12 #4	44.0	4.1	4.1	-25.2	-25.2	-25.2	-25.2	41.0	196.3
R12 #5	44.0	3.7	3.7	-25.8	-25.8	-25.8	-25.8	41.1	198.3
R12 #6	44.0	5.2	5.2	-24.2	-24.2	-24.2	-24.2	40.4	192.3
R12 #7	44.0	44.0	44.0	-23.1	-23.1	-23.1	-23.1	-23.1	108.2
R12 #8	44.0	44.0	44.0	-23.4	-23.4	-23.4	-2.7	-2.7	134.9
R12 #9	44.0	6.0	6.0	-23.5	-23.5	-23.5	-23.0	40.2	190.2
R12 #10	44.0	6.2	6.2	-22.7	-22.7	-22.7	-22.5	40.3	187.8
R134a #1	44.0	44.0	44.0	-24.5	-24.5	-24.5	-24.5	-24.5	100.0
R134a #2	44.0	44.0	44.0	-24.6	-24.6	-24.6	-24.6	-24.6	100.1
R134a #3	44.0	5.0	5.0	-24.4	-24.4	-24.4	-24.4	41.8	176.9
R134a #4	44.0	4.6	4.6	-25.2	-25.2	-25.2	-25.2	41.8	179.0
R134a #5	44.0	2.5	2.5	-25.6	-25.6	-25.6	-25.6	41.2	179.1
R134a #6	44.0	5.1	5.1	-24.4	-24.4	-24.4	-24.4	41.6	176.5
R134a #7	44.0	44.0	44.0	-23.0	-23.0	-23.0	-23.0	-23.0	98.3
R134a #8	44.0	44.0	44.0	-23.4	-23.4	-23.4	-0.6	-0.6	125.3
R134a #9	44.0	5.6	5.6	-23.6	-23.6	-23.6	-23.6	41.5	174.3
R134a #10	44.0	6.1	6.1	-22.7	-22.7	-22.7	-22.6	41.6	172.4
R22/R123 #1	44.0	44.0	44.0	-30.4	-19.1	-19.1	-3.9	-3.9	171.5
R22/R123 #2	44.0	44.0	-20.6	-29.0	-25.0	-14.2	1.4	1.4	161.9
R22/R123 #3	44.0	-7.6	-7.6	-26.6	-21.8	-21.8	-8.5	3.2	158.6
R22/R123 #4	44.0	1.0	-20.5	-24.9	-22.0	-20.1	-4.2	5.5	154.8
R22/R123 #5	44.0	-2.3	-21.3	-26.3	-22.3	-20.3	-6.4	4.1	157.2
R22/R123 #6	44.0	-3.5	-21.0	-27.8	-22.3	-20.0	-8.1	2.6	159.8
R22/R123 #7	44.0	-1.9	-20.4	-25.8	-21.7	-19.7	-5.8	4.6	156.3
R22/R141b #1	44.0	44.0	44.0	-30.8	-23.0	-23.0	-4.7	-4.7	182.8
R22/R141b #2	44.0	44.0	-16.8	-30.4	-27.7	-20.4	-2.0	-2.0	177.2
R22/R141b #3	44.0	-11.7	-11.7	-29.0	-26.0	-26.0	-16.0	-0.7	174.5
R22/R141b #4	44.0	6.4	-14.9	-27.8	-25.8	-24.6	-10.1	0.5	172.0
R22/R141b #5	44.0	7.4	-18.7	-29.1	-26.4	-24.5	-11.0	-0.7	174.4
R22/R141b #6	44.0	3.7	-21.9	-30.2	-26.7	-24.4	-13.0	-1.7	176.4
R22/R141b #7	44.0	4.3	-18.8	-28.3	-25.7	-24.0	-11.1	0.3	173.2

system	LCC ($)	cons. cost ($)	man$ ($)	% diff LCC	% diff man$	% diff ene$
R12 BC	1364.02	548.76	235.52	0.00	0.00	0.00
R12 #1	1369.15	548.20	235.28	0.38	-0.10	0.70
R12 #2	1369.18	547.72	235.07	0.38	-0.19	0.76
R12 #3	1318.18	554.51	237.99	-3.36	1.05	-6.33
R12 #4	1331.23	553.90	237.72	-2.40	0.94	-4.65
R12 #5	1343.13	554.34	237.91	-1.53	1.02	-3.25
R12 #6	1318.76	561.29	240.90	-3.32	2.28	-7.09
R12 #7	1345.71	558.52	239.71	-1.34	1.78	-3.44
R12 #8	1337.84	560.76	240.67	-1.92	2.19	-4.68
R12 #9	1310.39	563.65	241.91	-3.93	2.71	-8.40
R12 #10	1309.49	578.24	248.17	-4.00	5.37	-10.31
R134a #1	1389.50	548.63	235.46	1.87	-0.02	3.14
R134a #2	1389.50	547.94	235.17	1.87	-0.15	3.23
R134a #3	1314.68	555.14	238.26	-3.62	1.16	-6.84
R134a #4	1327.68	554.51	237.98	-2.66	1.05	-5.16
R134a #5	1340.56	554.26	237.88	-1.72	1.00	-3.55
R134a #6	1315.56	562.16	241.27	-3.55	2.44	-7.59
R134a #7	1364.84	558.95	239.89	0.06	1.86	-1.15
R134a #8	1348.87	562.11	241.25	-1.11	2.43	-3.50
R134a #9	1307.02	564.82	242.41	-4.18	2.93	-8.96
R134a #10	1306.40	579.67	248.79	-4.22	5.63	-10.86
R22/R123 #1	1427.87	572.27	245.61	4.68	4.28	4.95
R22/R123 #2	1342.87	573.80	246.27	-1.55	4.56	-5.67
R22/R123 #3	1312.40	571.00	245.06	-3.79	4.05	-9.06
R22/R123 #4	1277.32	572.20	245.58	-6.36	4.27	-13.51
R22/R123 #5	1300.36	571.35	245.21	-4.67	4.12	-10.58
R22/R123 #6	1327.12	572.71	245.80	-2.71	4.36	-7.46
R22/R123 #7	1300.72	586.31	251.63	-4.64	6.84	-12.37
R22/R141b #1	1445.13	574.58	246.60	5.95	4.71	6.78
R22/R141b #2	1397.97	572.98	245.91	2.49	4.41	1.19
R22/R141b #3	1369.25	570.23	244.73	0.38	3.91	-1.99
R22/R141b #4	1347.79	569.28	244.33	-1.19	3.74	-4.51
R22/R141b #5	1369.05	568.58	244.02	0.37	3.61	-1.81
R22/R141b #6	1390.36	569.89	244.59	1.93	3.85	0.64
R22/R141b #7	1368.22	584.68	250.93	0.31	6.54	-3.89